



Universiteit
Leiden
The Netherlands

The synthesis and biological applications of photo-activated ruthenium anticancer drugs

Lameijer, L.N.

Citation

Lameijer, L. N. (2017, December 14). *The synthesis and biological applications of photo-activated ruthenium anticancer drugs*. Retrieved from <https://hdl.handle.net/1887/58398>

Version: Not Applicable (or Unknown)

License: [Licence agreement concerning inclusion of doctoral thesis in the Institutional Repository of the University of Leiden](#)

Downloaded from: <https://hdl.handle.net/1887/58398>

Note: To cite this publication please use the final published version (if applicable).

Cover Page



Universiteit Leiden



The handle <http://hdl.handle.net/1887/58398> holds various files of this Leiden University dissertation.

Author: Lameijer, L.N.

Title: The synthesis and biological applications of photo-activated ruthenium anticancer drugs

Issue Date: 2017-12-14

The synthesis and biological applications of photo-activated ruthenium anticancer drugs

PROEFSCHRIFT

ter verkrijging van
de graad van Doctor aan de Universiteit Leiden,
op gezag van Rector Magnificus Prof. mr. C.J.J.M Stolker
volgens besluit van het College voor Promoties
te verdedigen op donderdag 14 december 2017
klokke 12.30 uur

door

Lucien Nathanaël Lameijer

geboren te Nieuweschans in 1985

Samenstelling Promotiecommissie

Promotor

Prof. Dr. E. Bouwman

Co-promotor

Dr. S. Bonnet

Overige Leden

Prof. Dr. H.S. Overkleeft

Prof. Dr. G.A. van der Marel

Dr. W.C. Szymanski (University of Groningen)

Dr. G. Gasser (Chimie ParisTech, France)

ISBN: 978-94-6299-802-5

Cover: Elian Kloppenburg

Banner image: Samantha Hopkins

Printed by Ridderprint

“It is not down in any map; true places never are”
Herman Melville, Moby Dick

Table of contents

Chapter 1	7
General introduction	
Chapter 2	25
The synthesis of <i>O</i> -1 to <i>O</i> -6 substituted positional isomers of D-glucose-thioether ligands and their ruthenium polypyridyl conjugates	
Chapter 3	55
D- versus L-glucose conjugation: Mitochondrial targeting of a light-activated, dual-mode of action ruthenium-based anticancer prodrug	
Chapter 4	73
Photodynamic therapy or photoactivated chemotherapy? Effects of the bidentate ligand on the photophysical properties, cellular uptake, and (photo)cytotoxicity of glycoconjugates based upon the $[\text{Ru}(\text{tpy})(\text{NN})(\text{L})]^{2+}$ scaffold	
Chapter 5	97
$[\text{Ru}(\text{phbpy})(\text{N-N})(\text{dmsO-}\kappa\text{S})]^{+}$: A new photo-active chiral cyclometalated analogue of the $\text{Ru}(\text{tpy})(\text{N-N})(\text{dmsO-}\kappa\text{S})^{2+}$ scaffold	
Chapter 6	123
Efficient red light-activation of a NAMPT inhibitor under hypoxia using water-soluble ruthenium complexes	
Chapter 7	141
Summary, conclusions & outlook	

Appendix I	151
General procedures	
Appendix II	157
Supporting information for Chapter 3	
Appendix III	169
Supporting information for Chapter 4	
Appendix IV	173
Supporting information for Chapter 5	
Appendix V	177
Supporting information for Chapter 6	
Samenvatting	187
Curriculum Vitae	193
List of publications	195

Chapter 1:

General introduction

1.1 Introduction: Transition metals in medicine

Since the discovery of arsenic based salvarasan (Figure 1.1a) as a first chemotherapeutic agent against syphilis, the field of bioinorganic (medicinal) chemistry has made a great leap forward. Imaging agents containing Gd^{III} ions have proven to be useful in MRI diagnostic studies due to their unique magnetic properties, resulting from their large number of unpaired electrons and long electron-spin relaxation times.^[1] The complexes Dotarem® and Omniscan® have shown to be indispensable in modern tumor detection and imaging of blood vessels in the brain, spine or liver.^[2] Furthermore, the application of metal complexes of the metastable isotope ^{99m}Tc have shown their value in radiotherapy for diagnostic imaging. Examples of such compounds are Cardiolite® and Ceretec®, which are clinically used for the evaluation of stroke and myocardial perfusion imaging, respectively.^[1] However, one of the greatest accomplishments in the field of bioinorganic medicinal chemistry has been the discovery of cisplatin. Nowadays, this drug and its derivatives carboplatin and oxaliplatin (Figure 1.2) are the most widely used drugs against cancer.^[1]

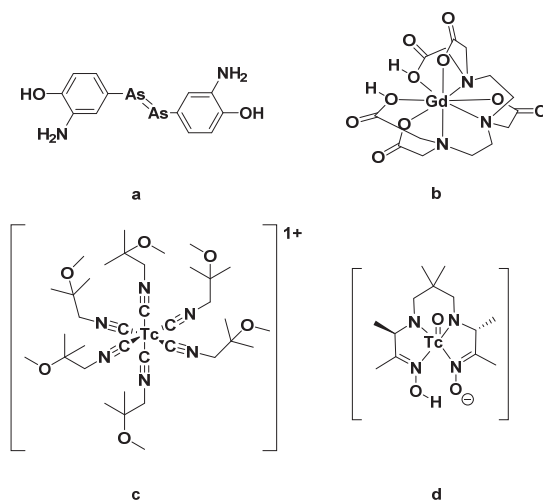


Figure 1.1. (a) Salvarasan, (b) Dotarem®, (c) Cardiolite® and (d) Ceretec®.

1.2 Cancer

Cancer is a group of diseases defined by unregulated cell growth and the invasion and migration of cells to neighboring tissue.^[3] Cancer starts at a genomic level where deleterious mutations to DNA that are not repaired by DNA repair mechanisms such as nucleotide excision repair (NER), and that are passed on to daughter generations, can lead to the formation of oncogenes. These genes, which are involved in regulation of cell growth, cell differentiation or cell death can together with mutated tumor suppressor genes, lead to the formation of cancer.^[3] With a mortality rate of 171 per 100,000 men and women per year (2008-2012) this disease is one of the leading causes of death in the United States.^[4] Current treatments against cancer are roughly divided in four types:

surgery, radiotherapy, immunotherapy and chemotherapy.^[5] In chemotherapy, platinum-based medicines are used in 50% of the cases.^[6] The next section will focus on the discovery of cisplatin and the further study of transition metal based chemotherapeutics.

1.2.1 Pt-based anticancer drugs

Barnett Rosenberg observed that *E. Coli* bacteria showed unusual growth behavior when grown in an ammonium chloride buffer while a current was applied. It was found that this effect could be ascribed to the platinum hydrolysis byproducts formed by the 'inert' platina electrodes. Further investigations showed that the inhibition of cell division was caused by the most active species *cis*-[PtCl₄(NH₃)₂] and *cis*-[PtCl₂(NH₃)₂]. These species were further considered for anticancer studies. After successful testing against a cancer cell line in mice and a further decade of clinical testing, cisplatin received FDA approval in 1978 and is now one of the most successful drugs used against cancer.^[7]

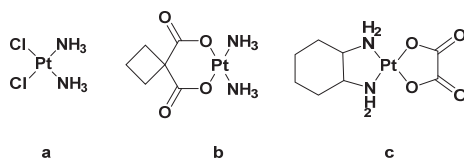


Figure 1.2. Chemical structures of (a) cisplatin, (b) carboplatin and (c) oxalipatin.

The cytotoxic effect of the drug is attributed to the interaction of the aquated species *cis*-[Pt(NH₃)₂(H₂O)₂]²⁺ with nuclear DNA resulting in a cascade of biological processes, leading to apoptosis of the cell.^[8] After intravenous administration the drug enters the bloodstream and stays mostly intact due to the relatively high concentration of chloride anions in the blood plasma (100 mM), preventing hydrolysis of the complex. However, after diffusion of the complex through the cell membrane, or upon cellular uptake mediated by a copper transporter, the complex hydrolysis inside the cell due to the low concentration of chloride ions in the cytoplasm (~4 mM), forming a positively charged reactive species that cannot pass lipid bilayers.^[8] This species either forms a monofunctional DNA adduct *via* N7 of guanine, or a bifunctional DNA adduct which cause a major distortion of the DNA, thereby preventing transcription. This DNA platination either triggers repair mechanisms such as nucleotide excision repair (NER) to repair DNA, which, when upregulated, leads to drug resistance, or to programmed cell death such as apoptosis and subsequent tumor elimination.^[9] Some cancers are intrinsically resistant against cisplatin, while others develop this resistance after prolonged exposure. Such drug resistance has been also attributed to increased levels of the 'scavenger' tripeptide glutathione or metallothionein, which leads to a decreased intracellular accumulation of cisplatin and increased tolerance of the DNA adducts.^[9] Although the side-effects of cisplatin and drug resistance can be circumvented using different analogues such as oxalipatin and carboplatin, the overall disadvantages of these type of drugs have

stimulated the scientific community to investigate alternative compounds based on other transition metals.^[10]

1.2.2 Ru-based anticancer drugs

Among the other transition metals, metal complexes of ruthenium have shown promising activity against cancer.^[11] Ruthenium is located in group 8 of the periodic table and proved its potential value for use in anticancer drugs when Dwyer and coworkers found that tris(3,4,7,8-tetramethyl-1,10-phenanthroline)ruthenium(II) dichloride showed some inhibitory effects on the growth of Landschütz ascites tumor in mice.^[12] For the past twenty years, complexes of this metal have demonstrated to have great potential both *in vitro* and *in vivo*.^[13] Two of the most studied ruthenium drugs are NAMI-A ([H₂Im][trans-RuCl₄(DMSO)(Im)]) (Im = imidazole, DMSO = dimethylsulfoxide) and KP1019 (*trans*-[tetrachloridobis(1*H*-indazolium)ruthenate(III)]. NAMI-A (Figure 1.3a) has low potency against primary tumors *in vitro*, but it has shown to be very effective against tumor metastasis *in vivo*.^[14] KP1019 (Figure 1.3b) on the other hand, has shown great promise *in vitro* against several cancer cell lines^[15] and entered Phase I clinical trials.^[15] However, poor water-solubility of this compound halted further investigation. Currently the more water-soluble sodium derivative of KP1019, KP1339 (Figure 1.3c) is under investigation in a phase I clinical trial too.^[16] Many other potent ruthenium-based anticancer drugs and their modes of action are described in the literature, but this is reviewed elsewhere.^[17]

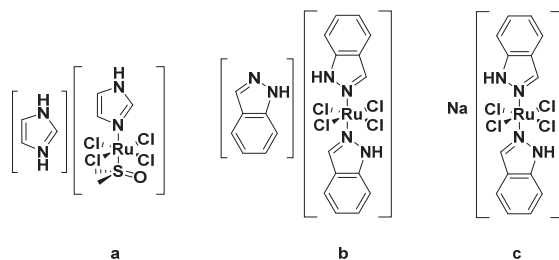


Figure 1.3. NAMI-A (a), KP-1019 (b) and KP-1339 (c).

1.3 Light and medicine

Next to their anticancer properties ruthenium(II) derivatives are excellent candidates for phototherapy. Their ability to absorb light in the visible region (400 – 700 nm) of the electromagnetic spectrum due to very strong metal-to-ligand charge transfer (MLCT) bands is often accompanied by photochemical processes such as photoreduction,^[18] oxidation,^[18] luminescence,^[19] isomerization^[20] or substitution.^[21] The outcome of the competition between these different photochemical processes can be fine-tuned: by modulating the ligands bound to ruthenium, phosphorescence can be enhanced or diminished, as well as the generation of singlet oxygen (¹O₂). Exploiting the latter phenomenon to selectively damage cancer tissue is referred to as photodynamic therapy

(PDT) and allows spatial and temporal control over toxicity of the drug. It has been proposed for the treatment of easily accessible tumors (e.g. skin, neck, head and mouth) but also of more difficult tumors such as prostate, pancreatic and brain tumours using interstitial PDT (I-PDT).^[22] Two types of PDT are generally distinguished, both of which are catalytic processes.^[23] In PDT Type I the photosensitizer is excited by the absorption of a photon and after inter-system crossing, reacts from the generated triplet state with molecular dioxygen directly via an electron-transfer mechanism (Figure 1.4) to a superoxide. In PDT type II, the photosensitizer reaches an excited state, which is followed by inter-system-crossing to a triplet state from which the photosensitizer reacts with molecular dioxygen ($^3\text{O}_2$) via triplet-triplet annihilation (TTA). This leads to the generation of singlet dioxygen ($^1\text{O}_2$), which is highly reactive and can oxidize a whole range of substrates, including biomolecules such as lipids in the cell membrane, cofactors, or proteins. Such irreversible damage typically leads to cell death, tumor elimination and a response from the immune system.^[24]

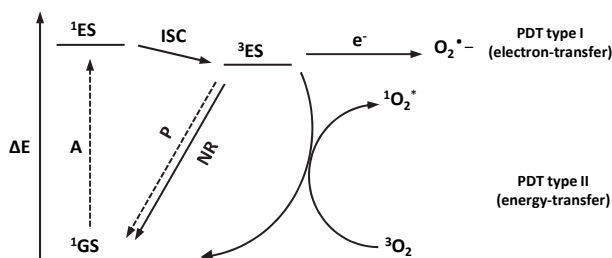


Figure 1.4. Jablonski diagram of photophysical pathways in photodynamic therapy type I and II with molecular oxygen. Dashed lines indicate processes involving photons. Abbreviations: GS (ground state), A (absorption), ES (excited state), ISC (inter-system crossing), P (phosphorescence), NR (non-radiative decay).

1.3.1 PDT with ruthenium(II) polypyridyl drugs

Ruthenium(II) photosensitizers have many advantages over classical PDT photosensitizers such as Foscan[®] and Photofrin[®]: they have increased water-solubility, long-lived triplet states, low toxicity in the dark and poor photobleaching.^[24] The group of Gasser has demonstrated the merit of using ruthenium compound by combining targeted delivery and $^1\text{O}_2$ generation. Complexes based upon the $[\text{Ru}(\text{bpy})_2(\text{dppz})]^{2+}$ (bpy = 2,2'-bipyridine, dppz = dipyrido[3,2- α :2',3'-c]phenazine) scaffold were designed with minor modifications on the planar dipyridophenazine ring. It was found that this complex (Figure 1.5a) had a remarkable activity against HeLa cancer cells when an amine was introduced. The cytotoxicity before light-activation, which is typically expressed as the effective concentration EC_{50} (the concentration at which 50% of the cells are dead compared to untreated control), was much lower than the cytotoxicity after light irradiation. Photoindices (PI), which are defined as the ratio $\text{EC}_{50\text{dark}}/\text{EC}_{50\text{light}}$, can reach up to 150. Due to its luminescent properties visualization and localization of this compound in HeLa cell was

possible; it was found to accumulate in the nucleus. This was further confirmed by fractionation experiments and high-resolution continuum source atomic absorption spectrometry (HR-CS AAS).^[25] Using a different approach, the group of Turro demonstrated that $[\text{Ru}(\text{bpy})(\text{dppn})(\text{CH}_3\text{CN})_2]^{2+}$ (Figure 1.5b) was able to both photosubstitute one monodentate ligand and generate $^1\text{O}_2$, leading to submicromolar photocytotoxicity in HeLa cells.^[26] However, the most promising candidate among the ruthenium(II) polypyridyl drugs was recently reported by the group of McFarland: The compound, $[\text{Ru}(\text{dmb})_2(\text{IP-TT})]^{2+}$ ($\text{dmb} = 4,4'$ -dimethyl-2,2'-bipyridine, $\text{IP-TT} = 2-(2',2'':5'',2''''\text{-terthiophene})\text{-imidazo}[4,5-f][1,10]\text{phenanthroline}$) also referred to as TLD1433 (Figure 1.5c), demonstrated to have great potential in both colon and glioma cancer cells, reaching PI values over 10000.^[27] This drug is currently under investigation in Phase I clinical trials (NCT03053635).

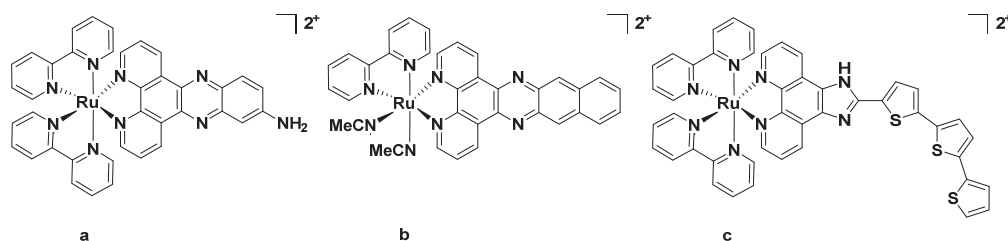


Figure 1.5. Representative examples of ruthenium(II) polypyridyl PDT drugs from the groups of (a) Gasser,^[28] (b) Turro,^[29] and (c) McFarland.^[24]

1.3.2 Tumor hypoxia and PDT

Due to rapid cell proliferation and structural and functional abnormalities in tumor blood vessels, certain regions in solid tumors are poorly oxygenated.^[30] This phenomenon was first observed by Grey et. al.^[31] and has a serious impact on the effectiveness of conventional treatments such as radiation therapy.^[32] For PDT type II a similar problem arises since the therapy is dioxygen-dependent (unlike PDT type I, which occurs via electron-transfer). In addition, PDT often results in additional hypoxia by consumption of the oxygen on the tumor site while simultaneously inducing damage to the tumor vasculature, preventing the consumed dioxygen to be renewed.^[22a, 33]

1.3.3 Photo-Chemotherapy (PCT) or Photo-Activated Chemotherapy (PACT)

The oxygen-dependence of PDT provides an incentive to develop anticancer agents that operate via a different, dioxygen-independent mode of action.^[11] Instead of generating $^1\text{O}_2$, these light-sensitive prodrugs become cytotoxic after photoisomerization,^[34] photoreduction,^[35] photocleavage,^[36] or photosubstitution.^[37] The last two mechanisms are often referred to as photo-uncaging and 'Photo-Activated ChemoTherapy' (PACT) when they are used in combination with cytotoxic anticancer drugs. In PACT the prodrug is not active (caged) in the dark, whereas light-activation leads to bond cleavage (uncaging) of the prodrug, releasing both the (cytotoxic) carrier and/or a drug payload.^[38]

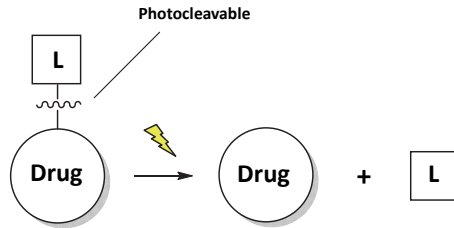


Figure 1.6. Principle of PACT.^[36, 38] Upon irradiation bond cleavage leads to release of a metal-based or ligand-based drug.

Several organic and inorganic systems for photo-release of cytotoxic drugs have been used by the scientific community. These prodrugs either work independently or in combination with a drug delivery system such as nanoparticles. In 2010, Lin et. al demonstrated an amino-coumarin system that, attached to a mesoporous nanoparticle, released chloroambucil using visible light (420 nm) and induced cytotoxicity in HeLa cells.^[39] More recently, Nani et. al. have further demonstrated that a cyanine-based photocaging agent can be combined with an antibody-drug conjugate, allowing release with near-infrared light (NIR) of a microtubule polymerization inhibitor combretastatin A4. Cytotoxicity was induced both *in vitro* and *in vivo*.^[40]

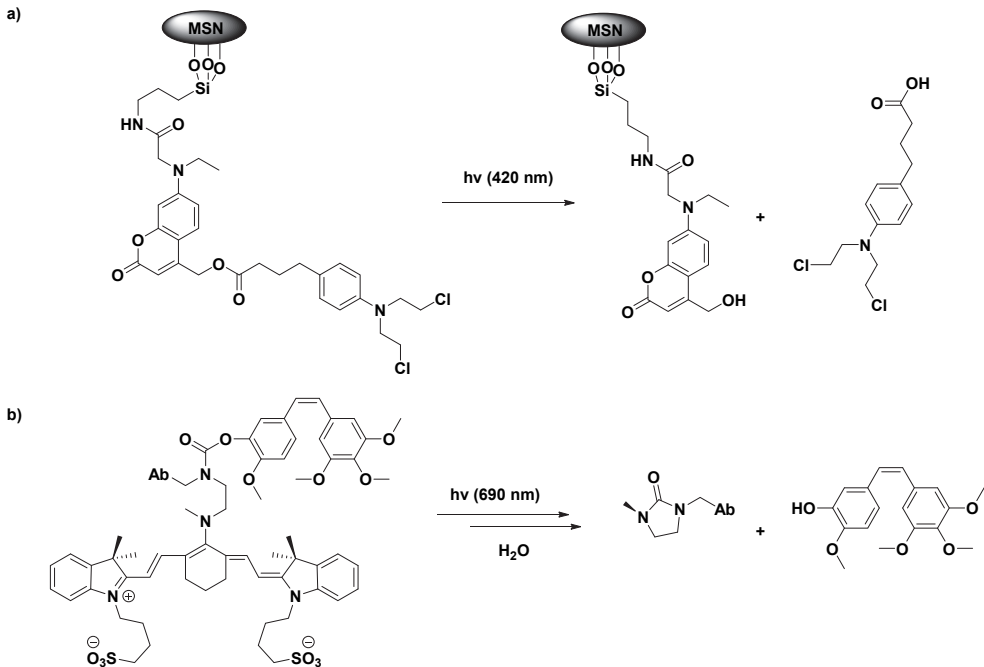


Figure 1.7. a). Mesoporous nanoparticles (MSN) covalently attached to amino coumarin based photocaged chloroambucil. b). Antibody-targeted cyanine-based photocaging system, releasing combretastatin A4 after irradiation with NIR light. Photo-oxidation, hydrolysis and cyclization steps have been omitted for clarity.

In the field of bioinorganic chemistry, examples of photocaging systems have been reported by the group of Gasser who have demonstrated the targeted delivery of rhenium-bombesin conjugates caged with *o*-nitrophenyl-based photo-linkers. Uncaging with low doses of UV-light led to the release of a tricarbonyl *N,N*-bis(quinolinoyl) rhenium (I) complex, achieving a ten-fold higher cytotoxicity towards HeLa cells than without irradiation.^[36] A ruthenium-based photocaging system utilizing nanoparticles has been reported by Frascioni et. al in 2013. Paclitaxel loaded mesoporous nanoparticles were ‘capped’ with $[\text{Ru}(\text{tpy})(\text{dppz})(\text{L})]^{2+}$ (tpy = 2,2':6',2''-terpyridine) complexes, releasing the anticancer drug after photo-activation with visible light (465 nm), which led to a marked decrease in cell viability in MDA-MB-231 and MDA-MB-248 cells.^[41] The research described in this thesis will focus on the latter types of systems, where ruthenium(II) polypyridyl drugs are used either as a PACT drug or PACT carrier using photosubstitution to release a cytotoxic drug or to induce cytotoxicity by themselves.

1.3.4 Ruthenium-based PACT

The mechanism of photosubstitution of ruthenium(II) (polypyridyl) compounds is generally thought to occur as follows: after absorption of a photon the metal-to-ligand charge-transfer state ($^1\text{MLCT}$) is populated via photon absorption by the ground state (^1GS), which is immediately followed by inter-system-crossing to the $^3\text{MLCT}$ state. This state can decay to the ground state *via* radiative or non-radiative processes, or populate the triplet metal-centered state (^3MC) via thermal internal conversion (IC). Due to the antibonding character of the orbitals ($d\sigma$) in this state, population of this state leads to elongation of a metal-ligand bond and ligand dissociation.^[29, 42] Since ruthenium(II) is a d^6 metal with an octahedral configuration, ligands such as tpy can reduce the coordination angles, leading to distorted pseudo-octahedral geometries in which the nitrogen lone pairs of the polypyridyl ligands have less overlap with the orbitals of the ruthenium center.^[43] This leads to smaller ligand field splitting compared to, for example, complexes such as $[\text{Ru}(\text{bpy})_3]^{2+}$. This octahedral distortion leads to an ^3MC excited state that is lower in energy, and thus more easily thermally populated from the $^3\text{MLCT}$.

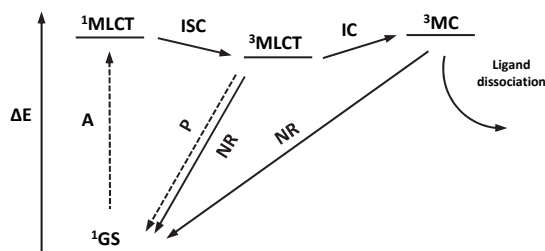


Figure 1.8. Jablonski diagram of proposed physical pathways of photosubstitution reactions in Ru(II) polypyridyl complexes. Dashed arrows represent pathways involving a photon. Abbreviations: GS (ground state), A (absorption), ISC (inter-system crossing), P (phosphorescence), NR (non-radiative decay), IC (internal conversion), MC (metal centered).

One of the first groups to find an application of these ruthenium complexes in chemical biology and phototherapy was that of Etchenique, who delivered a proof-of-concept that the biologically active ligand 4-aminopyridine (4AP) could be released from the complex $[\text{Ru}(\text{bpy})_2(4\text{AP})_2]\text{Cl}_2$.^[44] After irradiation with white light ($>500\text{ nm}$) in water, this complex selectively photosubstitutes one of the 4AP monodentate ligands for water, releasing free 4AP which induces an action potential in leech neurons.^[44] A similar demonstration leading to phototoxicity in cancer cells was first provided by the group of Turro, who demonstrated that photorelease in HeLa cells of 5-cyanouracil (5CNU), a known anticancer drug, by irradiation with white light ($>400\text{ nm}$) of $[\text{Ru}(\text{tpy})(5\text{CNU})_3]^{2+}$, leads to cell death.^[45] Turro also demonstrated that the released ruthenium species $[\text{Ru}(\text{tpy})(\text{H}_2\text{O})_2]^{2+}$ is able to bind to DNA, implying that this species may contribute to the observed cellular toxicity.^[45] A more recent example from 2012 by Howerton et. al. has demonstrated that the strained complex $[\text{Ru}(\text{bpy})_2(\text{dmbpy})]^{2+}$ (bpy = bipyridine, dmbpy = 6,6'-dimethyl-2,2'-dipyridyl) ejects a dmbpy ligand upon white light irradiation ($>450\text{ nm}$), generating the ruthenium species $[\text{Ru}(\text{bpy})_2(\text{H}_2\text{O})_2]^{2+}$ which was also found to be able to bind to DNA. The observed cytotoxicity in A549 tumor spheroids was attributed to the generation of this species.

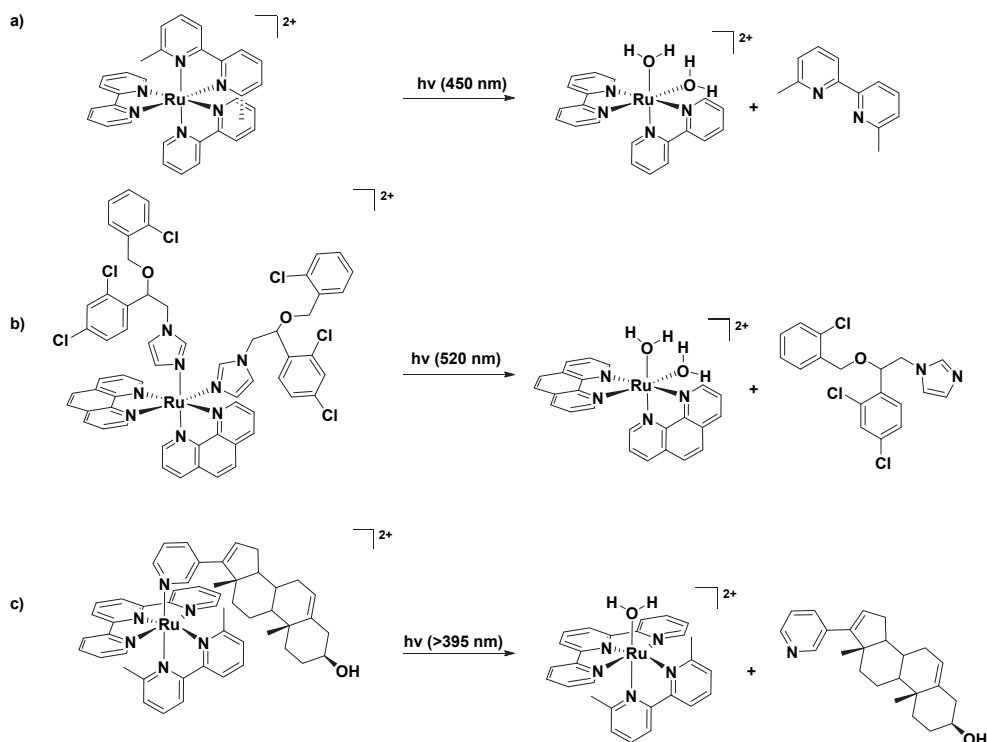


Figure 1.9. Representative ruthenium-based PACT drugs by the group of (a) Bonnet/Glazer,^[46] (b) Renfrew^[47] and (c) Kodanko.^[48]

This claim, however, was recently refuted by Cuello-Garibo and coworkers followed by Azar et. al.^[46a, 49] who independently demonstrated that the expelled ligand (dmbpy) was cytotoxic. Nevertheless, Howerton's work demonstrated that these complexes can be used to kill cancer cells using visible light *via* a dioxygen-independent mechanism, i.e., the release of the cytotoxic ligand dmbpy. More examples of ruthenium-based anticancer PACT drugs have been described by the group of Kodanko,^[48] Renfrew^[47] and Bonnet^[50] with some noteworthy examples of PACT drugs shown in Figure 1.9.

1.4 Selective treatment of cancer

Conventional anticancer drugs, such as cisplatin, generally affect both malignant and healthy cells, thereby reducing the maximum dosage which can be administered to a patient.^[51] One approach to improve selectivity and reduce the side effects for patients is to conjugate the anticancer drugs to a 'homing beacon' that specifically targets receptors that are overexpressed in cancer cells. This 'Trojan horse' approach has been successfully demonstrated by the clinically approved brentuximab vedotin in Hodgkin lymphoma and Trastuzumab emtansine in HER2-positive metastatic breast cancer. Other examples encompass folate receptor targeted therapy,^[52] a receptor that is overexpressed in ovarian cancers, the use of liposomes, such as demonstrated for lipoplatin,^[53] and the focus of the next section, glucose transporter (GLUT) targeted therapy.^[54]

1.4.1 Targeting GLUT

Tumorigenesis is hallmarked by some crucial alterations to cellular metabolism. One of the best characterized metabolic phenotypes in cancer is the increase of aerobic glycolysis for the generation of adenosine triphosphate (ATP), also known as the "Warburg effect".^[55] Even in the presence of normal concentrations of dioxygen in cancer cells, D-glucose is converted to lactic acid rather than using oxidative phosphorylation for the generation of ATP. It has been suggested that this phenomenon occurs for a powerful growth advantage and is necessary for the evolution of invasive human cancers.^[56] One of the consequences of this phenomenon is the overexpression of glucose transporters (GLUTs)^[57] in proliferating tumor cells: a family of thirteen different proteins (GLUT 1 – 12 and HMIT) responsible for the energy-independent uptake of monosaccharides and polyols in mammalian cells.^[58] GLUT1 and GLUT3 are predominantly overexpressed in most cancers, making it an important cancer hallmark and potential target in targeted chemotherapy.^[54, 56]

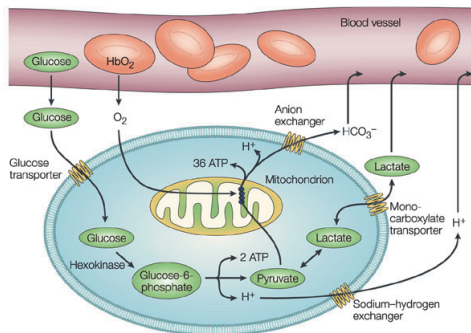


Figure 1.10. Glucose metabolism in healthy mammalian cells. Figure taken from Gatenby et. al.^[56]

The field of diagnosis imaging has exploited the Warburg effect for positron emission tomography (PET) using ^{18}F fluorodeoxyglucose (^{18}F FDG) (Figure 1.11a). This compound is a radioactive labeled derivative of D-glucose, which is taken *via* GLUT1 and subsequently trapped by hexokinase mediated phosphorylation allowing for tumor visualization.^[56] This hallmark has further been explored as a potential target in the field of medicinal chemistry by Wiessler and coworkers.^[59] Due to the heavy adverse side-effects of the widely used ifosfamide alkylating agent as antitumor drug, an alternative was found in its D-glucose derivative glufosfamide (Figure 1.11b). Compared to its aglycon, this compound was found to be less cytotoxic and could be administered in higher doses without affecting healthy cells.^[59] Other examples of glycoconjugated anticancer drugs have been reported by Mandai and Mikuni and coworkers in 2008.^[60] They revealed that the α -galactosyl conjugate of docetaxel (Figure 1.11c) widely used against breast, ovarian, prostate and non-small lung cancer, showed similar cytotoxic activity against P388 Murine Leukemia Cells compared to its aglycon. It was envisioned that this derivative is more water-soluble and therefore co-administration of solubilizing agents is not necessary.^[60]

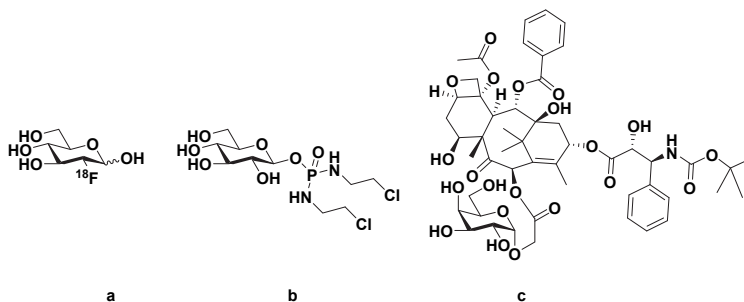


Figure 1.11. Overview of GLUT transported D-glucose and D-galactose conjugates. a). ^{18}F FDG b). Glufosfamide; c). 1- α -D-galactose conjugated docetaxel.

1.4.2 Substrate specificity

The selective targeting of cancer cells using glycoconjugates calls for a study of substrate specificity. As of date, both the structures of human GLUT1 and GLUT3 have been

elucidated.^[61] Whereas GLUT1 was co-crystallized in the presence of *n*-nonyl- β -D-glucopyranoside, GLUT3 tolerated both the α and β -anomer of D-glucose^[61] suggesting that 1-*O*- β -modifications, such as for glufosfamide (Figure 1.11b), are generally allowed. Both 2-(N-(7-nitrobenz-2-oxa-1,3-diazol-4-yl)amino)-2-deoxyglucose (NBDG) and FDG are modified on the 2-position of D-glucose, indicating that modification of this position is tolerated. Reports of glycoconjugates with modifications on the *O*-3, *O*-4 and *O*-6 position of D-glucose and their uptake by GLUT1 are abundant in literature, with the overall conclusion that, unless very bulky groups are installed, most positional modifications are tolerated.^[54] However a recent example by Park et. al. has shown that the overall charge of β -glycosidic cyanine based bioprobes might influence the uptake by GLUT1.^[62]

This raises the question whether this strategy can also be applied for metal complexes for radiotherapy or as potential theranostics. In the field of bioinorganic chemistry the group of Schubiger pioneered this strategy in 2001 with the synthesis of rhenium and ^{99m}Tc glycoconjugates.^[63] This work was followed with a whole mechanistic study and uptake study reported in 2005,^[64] which demonstrated that *O*-1, *O*-2 (Figure 1.12a), *O*-3 and *O*-6 glycoconjugates of ^{99m}Tc drugs were not taken up via GLUT1 in HT29 cells. No differences in uptake were observed in the presence of the GLUT1 inhibitor cytochalasin B and D-glucose.^[64] This is in great contrast to the recent findings of Patra et. al.^[65] who have demonstrated that *O*-2 glycoconjugates (Figure 1.12b) of a platinum-based drug (malonatoplatin) were taken up in an increased manner in A549 cells, compared to other positional isomers. The uptake in healthy RWPE2 cells, however, was similar among conjugates, implying that the higher expression of GLUT in A549 cancer cells has a strong effect on the uptake. This was further supported by using a DU145-GLUT1-knock-down cell-line that showed that the glycoconjugate was less toxic when GLUT-1 was not present. A recent example by Florindo et. al. has suggested that uptake of cyclopentadienyl-ruthenium(II) glycoconjugates is possible. The cell cytotoxicity induced by their glycoconjugate (Figure 1.12c) could be reduced in the presence of D-glucose.^[66] However, there is currently no general consensus as to which modifications of D-glucose are allowed in order to allow transport of antitumor drugs via GLUT1 or GLUT3 for ruthenium(II) drugs.

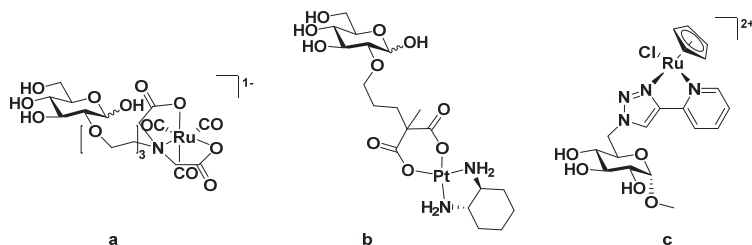


Figure 1.12. Representative glycoconjugates for GLUT targeting from the group of (a) Schubiger,^[64] (b) Lippard^[65b] and Fernandes.^[66]

1.5 Thesis goal and outline

The aim of the work described in this thesis was to investigate whether complexes based upon the $[\text{Ru}(\text{tpy})(\text{N-N})(\text{L})]^{n+}$ scaffold can be used either: (i) as a PACT prodrug where a toxic mono-aquated ruthenium complex is caged by a non-toxic ligand and liberated upon light irradiation; or (ii) as a PACT carrier for photocaging, where a thioether, nitrile or pyridine-based organic drug is caged by a non-toxic ruthenium fragment, and released upon light irradiation; (iii) or as a PDT prodrug, where reactive oxygen species (ROS) are generated upon blue, green or red light irradiation of the metal complex.

In Chapter 2 new synthetic routes are described towards methylthioether-functionalized positional isomers of D-glucose and their ruthenium polypyridyl conjugates. Due to the coordinating properties of the sulfur donor atoms in these ligands different protecting and deprotecting group strategies had to be employed compared to that for example of Lippard et. al.,^[65b] since the common benzyl and benzylidene protecting group cannot be efficiently removed in the presence of a thioether using palladium on carbon or a Birch reduction. The proposed routes for the most challenging 2-O and 4-O functionalized isomers are improvements over current strategies as they can potentially be used for ligands bearing sulfur (or nitrogen) donor atoms.

In Chapter 3 a new strategy is presented to analyze the effects of glycoconjugation on ruthenium anticancer prodrugs of the type $[\text{Ru}(\text{tpy})(\text{dppn})(\text{L})]^{2+}$. Two enantiomers of glycoconjugated prodrugs are presented which are both activated with blue light. Light irradiation makes them strongly cytotoxic, which is demonstrated to be a consequence of their localization in the mitochondria where they efficiently generate ROS. Interestingly, both enantiomers of the drugs showed similar uptake, which rules out GLUT-mediated transport, whereas the different dark cytotoxicity found for both enantiomers is most likely attributed to a post-uptake process such as hydrolysis by a β -glucosidase.

In Chapter 4 the influence of the bidentate ligand in sixteen complexes based upon the $[\text{Ru}(\text{tpy})(\text{N-N})(\text{L})]^{2+}$ scaffold is described in relation to their photoreactivity, phosphorescence, singlet oxygen generation, and photosubstitution quantum yield. By comparing the (photo)cytotoxicity, solubility and uptake of these complexes in two different cancer cell lines (A549 and MCF-7), insight is provided on the potential of these compounds as light-activated prodrugs. Whereas most of these complexes are not (photo)cytotoxic and are therefore excellent candidates as PACT carriers, three complexes were found to be cytotoxic after blue light irradiation, and thus represent interesting PACT drugs. Depending on the treatment protocol the compounds $[\text{Ru}(\text{tpy})(\text{dppz})(\text{L})]^{2+}$ were found to act as a potential PACT drug, while $[\text{Ru}(\text{tpy})(\text{dppn})(\text{L})]^{2+}$ complexes were found to act as very efficient PDT sensitizers even when using a strict treatment protocol.

Chapter 5 describes the synthesis of a series of chiral cyclometalated ruthenium complexes based upon the $[\text{Ru}(\text{phpy})(\text{N-N})(\text{dmsO-kS})]^{2+}$ scaffold, where Hphpy is 6'-phenyl-2,2'-bipyridine. Cyclometalation appears to reduce the charge and polarity of terpyridine analogues while their absorption is shifted towards the red region of the spectrum. Three of these complexes with N-N = bpy, phen, and dpq, are much less photoreactive than the terpyridine analogues described in Chapter 4, while the more conjugated dppz and dppn complexes are photochemically completely inactive. We demonstrate that these complexes are chiral by synthesizing and separating two diastereoisomers bound to a chiral, enantiomerically pure sulfoxide monodentate ligand. We finally show their potential as (green) light-activated anticancer drugs against A549 and MCF-7 cancer cells.

In Chapter 6 we demonstrate that both the $[\text{Ru}(\text{tpy})(\text{dmbpy})(\text{L})]^{2+}$ and $[\text{Ru}(\text{tpy})(\text{biq})(\text{L})]^{2+}$ scaffold can be used to cage L = STF-31, a pyridine-containing cytotoxic inhibitor of nicotinamide phosphoribosyltransferase (NAMPT). We show that both scaffolds can be uncaged using deeper tissue-penetrating red light, but that only $[\text{Ru}(\text{tpy})(\text{biq})(\text{L})]^{2+}$ is thermally stable enough to be used *in vitro* as a prodrug. By studying photoactivation under hypoxia (1% O₂), we demonstrate for the first time that PACT works independently of the dioxygen concentration in cells, whereas traditional dioxygen-dependent PDT would not work under the same conditions.

Finally, a summary of the findings in this thesis are presented in Chapter 7, followed by an outlook for ruthenium-based photoactivated prodrugs.

References

- [1] Z. J. Guo, P. J. Sadler, *Angew Chem Int Ed* **1999**, *38*, 1513-1531.
- [2] P. Caravan, J. J. Ellison, T. J. McMurry, R. B. Lauffer, *Chem Rev* **1999**, *99*, 2293-2352.
- [3] L. Pecorino, *Molecular biology of cancer: mechanisms, targets, and therapeutics*, Oxford university press, **2012**.
- [4] R. L. Siegel, K. D. Miller, A. Jemal, *CA Cancer J Clin* **2016**, *66*, 7-30.
- [5] K. D. Miller, R. L. Siegel, C. C. Lin, A. B. Mariotto, J. L. Kramer, J. H. Rowland, K. D. Stein, R. Alteri, A. Jemal, *CA Cancer J Clin* **2016**, *66*, 271-289.
- [6] S. Dhar, S. J. Lippard, *P Natl Acad Sci USA* **2009**, *106*, 22199-22204.
- [7] a). S. M. Cohen, S. J. Lippard, *Prog Nucleic Acid Res Mol Biol* **2001**, *67*, 93-130; b). R. A. Alderden, M. D. Hall, T. W. Hambley, *J Chem Educ* **2006**, *83*, 728-734.
- [8] S. Dasari, P. B. Tchounwou, *Eur J Pharmacol* **2014**, *740*, 364-378.
- [9] L. R. Kelland, S. Y. Sharp, C. F. O'Neill, F. I. Raynaud, P. J. Beale, I. R. Judson, *J Inorg Biochem* **1999**, *77*, 111-115.
- [10] P. C. Bruijninx, P. J. Sadler, *Curr Opin Chem Biol* **2008**, *12*, 197-206.

- [11] P. C. Bruijninx, P. J. Sadler, *Adv Inorg Chem* **2009**, *61*, 1-62.
- [12] F. P. Dwyer, E. Mayhew, E. M. F. Roe, A. Shulman, *Brit J Cancer* **1965**, *19*, 195-199.
- [13] A. Bergamo, C. Gaiddon, J. H. Schellens, J. H. Beijnen, G. Sava, *J Inorg Biochem* **2012**, *106*, 90-99.
- [14] A. Bergamo, S. Zorzet, B. Gava, A. Sorc, E. Alessio, E. Iengo, G. Sava, *Anticancer Drugs* **2000**, *11*, 665-672.
- [15] C. G. Hartinger, S. Zorbas-Seifried, M. A. Jakupec, B. Kynast, H. Zorbas, B. K. Keppler, *J Inorg Biochem* **2006**, *100*, 891-904.
- [16] A. K. Bytzek, G. Koellensperger, B. K. Keppler, G. H. C, *J Inorg Biochem* **2016**, *160*, 250-255.
- [17] J. Liu, L. N. Ji, W. J. Mei, *Prog Chem* **2004**, *16*, 969-974.
- [18] C. K. Prier, D. A. Rankic, D. W. MacMillan, *Chem Rev* **2013**, *113*, 5322-5363.
- [19] K. Nakamaru, *Bull Chem Soc Jpn* **1982**, *55*, 2697-2705.
- [20] H. Yamazaki, T. Hakamata, M. Komi, M. Yagi, *J Am Chem Soc* **2011**, *133*, 8846-8849.
- [21] R. E. Goldbach, I. Rodriguez-Garcia, J. H. van Lenthe, M. A. Siegler, S. Bonnet, *Chem Eur J* **2011**, *17*, 9924-9929.
- [22] a). D. E. Dolmans, D. Fukumura, R. K. Jain, *Nat Rev Cancer* **2003**, *3*, 380-387; b). J. F. Lovell, T. W. Liu, J. Chen, G. Zheng, *Chem Rev* **2010**, *110*, 2839-2857; c). G. Shafirstein, D. Bellnier, E. Oakley, S. Hamilton, M. Potasek, K. Beeson, E. Parilov, *Cancers* **2017**, *9*.
- [23] A. P. Castano, T. N. Demidova, M. R. Hamblin, *Photodiagnosis Photodyn Ther* **2004**, *1*, 279-293.
- [24] G. Shi, S. Monro, R. Hennigar, J. Colpitts, J. Fong, K. Kasimova, H. M. Yin, R. DeCoste, C. Spencer, L. Chamberlain, A. Mandel, L. Lilge, S. A. McFarland, *Coord Chem Rev* **2015**, *282*, 127-138.
- [25] C. Mari, V. Pierroz, R. Rubbiani, M. Patra, J. Hess, B. Spingler, L. Oehninger, J. Schur, I. Ott, L. Salassa, S. Ferrari, G. Gasser, *Chem Eur J* **2014**, *20*, 14421-14436.
- [26] B. A. Albani, B. Pena, N. A. Leed, N. A. de Paula, C. Pavani, M. S. Baptista, K. R. Dunbar, C. Turro, *J Am Chem Soc* **2014**, *136*, 17095-17101.
- [27] J. Fong, K. Kasimova, Y. Arenas, P. Kaspler, S. Lazic, A. Mandel, L. Lilge, *Photobiol Sci* **2015**, *14*, 2014-2023.
- [28] C. Mari, V. Pierroz, S. Ferrari, G. Gasser, *Chem Sci* **2015**, *6*, 2660-2686.
- [29] J. D. Knoll, B. A. Albani, C. Turro, *Acc Chem Res* **2015**, *48*, 2280-2287.
- [30] D. M. Gilkes, G. L. Semenza, D. Wirtz, *Nat Rev Cancer* **2014**, *14*, 430-439.
- [31] R. H. Thomlinson, L. H. Gray, *Brit J Cancer* **1955**, *9*, 539-549.
- [32] L. H. Gray, A. D. Conger, M. Ebert, S. Hornsey, O. C. Scott, *Br J Radiol* **1953**, *26*, 638-648.
- [33] B. W. Henderson, V. H. Fingar, *Cancer Res* **1987**, *47*, 3110-3114.
- [34] M. M. Lerch, M. J. Hansen, G. M. van Dam, W. Szymanski, B. L. Feringa, *Angew Chem Int Ed* **2016**, *55*, 10978-10999.

- [35] N. J. Farrer, J. A. Woods, V. P. Munk, F. S. Mackay, P. J. Sadler, *Chem Res Toxicol* **2010**, *23*, 413-421.
- [36] A. Leonidova, V. Pierroz, R. Rubbiani, Y. J. Lan, A. G. Schmitz, A. Kaech, R. K. O. Sigel, S. Ferrari, G. Gasser, *Chem Sci* **2014**, *5*, 4044-4056.
- [37] N. J. Farrer, J. A. Woods, L. Salassa, Y. Zhao, K. S. Robinson, G. Clarkson, F. S. Mackay, P. J. Sadler, *Angew Chem Int Ed* **2010**, *49*, 8905-8908.
- [38] J. Olejniczak, C. J. Carling, A. Almutairi, *J Control Release* **2015**, *219*, 18-30.
- [39] Q. Lin, Q. Huang, C. Li, C. Bao, Z. Liu, F. Li, L. Zhu, *J Am Chem Soc* **2010**, *132*, 10645-10647.
- [40] R. R. Nani, A. P. Gorka, T. Nagaya, H. Kobayashi, M. J. Schnermann, *Angew Chem Int Ed* **2015**, *54*, 13635-13638.
- [41] M. Frasconi, Z. Liu, J. Lei, Y. Wu, E. Strelakova, D. Malin, M. W. Ambrogio, X. Chen, Y. Y. Botros, V. L. Cryns, J.-P. Sauvage, J. F. Stoddart, *J Am Chem Soc* **2013**, *135*, 11603-11613.
- [42] a). J. D. Knoll, B. A. Albani, C. B. Durr, C. Turro, *J Phys Chem A* **2014**, *118*, 10603-10610; b). P. C. Ford, *Chem Sci* **2016**, *7*, 2964-2986.
- [43] A. J. Gottle, F. Alary, M. Boggio-Pasqua, I. M. Dixon, J. L. Heully, A. Bahreman, S. H. Askes, S. Bonnet, *Inorg Chem* **2016**, *55*, 4448-4456.
- [44] L. Zayat, C. Calero, P. Albores, L. Baraldo, R. Etchenique, *J Am Chem Soc* **2003**, *125*, 882-883.
- [45] M. A. Sgambellone, A. David, R. N. Garner, K. R. Dunbar, C. Turro, *J Am Chem Soc* **2013**, *135*, 11274-11282.
- [46] a). J. A. Cuello-Garibo, M. S. Meijer, S. Bonnet, *Chem Commun* **2017**, *53*, 6768-6771; b). B. S. Howerton, D. K. Heidary, E. C. Glazer, *J Am Chem Soc* **2012**, *134*, 8324-8327.
- [47] N. Karaoun, A. K. Renfrew, *Chem Commun* **2015**, *51*, 14038-14041.
- [48] A. Li, R. Yadav, J. K. White, M. K. Herroon, B. P. Callahan, I. Podgorski, C. Turro, E. E. Scott, J. J. Kodanko, *Chem Commun* **2017**, *53*, 3673-3676.
- [49] D. F. Azar, H. Audi, S. Farhat, M. El-Sibai, R. J. Abi-Habib, R. S. Khnayzer, *Dalton Trans* **2017**, *46*, 11529-11532.
- [50] V. H. S. van Rixel, B. Siewert, S. L. Hopkins, S. H. C. Askes, A. Busemann, M. A. Siegler, S. Bonnet, *Chem Sci* **2016**, *7*, 4922-4929.
- [51] K. Cho, X. Wang, S. Nie, Z. G. Chen, D. M. Shin, *Clin Cancer Res* **2008**, *14*, 1310-1316.
- [52] R. T. Morris, R. N. Joyrich, R. W. Naumann, N. P. Shah, A. H. Maurer, H. W. Strauss, J. M. Uszler, J. T. Symanowski, P. R. Ellis, W. A. Harb, *Ann Oncol* **2014**, *25*, 852-858.
- [53] T. Boulikas, *Expert Opin Investig Drugs* **2009**, *18*, 1197-1218.
- [54] E. C. Calvaresi, P. J. Hergenrother, *Chem Sci* **2013**, *4*, 2319-2333.
- [55] O. Warburg, F. Wind, E. Negelein, *Klin Wochenschr* **1926**, *5*, 829-832.
- [56] R. A. Gatenby, R. J. Gillies, *Nat Rev Cancer* **2004**, *4*, 891-899.
- [57] M. L. Macheda, S. Rogers, J. D. Best, *J Cell Physiol* **2005**, *202*, 654-662.

- [58] M. Mueckler, B. Thorens, *Mol Aspects Med* **2013**, *34*, 121-138.
- [59] J. Pohl, B. Bertram, P. Hilgard, M. R. Nowrousian, J. Stuben, M. Wiessler, *Cancer Chemother Pharmacol* **1995**, *35*, 364-370.
- [60] K. Mikuni, K. Nakanishi, K. Hara, K. Hara, W. Iwatani, T. Amano, K. Nakamura, Y. Tsuchiya, H. Okumoto, T. Mandai, *Biol Pharm Bull* **2008**, *31*, 1155-1158.
- [61] a). D. Deng, C. Xu, P. Sun, J. Wu, C. Yan, M. Hu, N. Yan, *Nature* **2014**, *510*, 121-125; b). D. Deng, P. Sun, C. Yan, M. Ke, X. Jiang, L. Xiong, W. Ren, K. Hirata, M. Yamamoto, S. Fan, N. Yan, *Nature* **2015**, *526*, 391-396.
- [62] J. Park, J. I. Um, A. Jo, J. Lee, D. W. Jung, D. R. Williams, S. B. Park, *Chem Commun* **2014**, *50*, 9251-9254.
- [63] J. Petrig, R. Schibli, C. Dumas, R. Alberto, P. A. Schubiger, *Chem Eur J* **2001**, *7*, 1868-1873.
- [64] R. Schibli, C. Dumas, J. Petrig, L. Spadola, L. Scapozza, E. Garcia-Garayoa, P. A. Schubiger, *Bioconjugate Chem* **2005**, *16*, 105-112.
- [65] a). M. Patra, T. C. Johnstone, K. Suntharalingam, S. J. Lippard, *Angew Chem Int Ed* **2016**, *55*, 2550-2554; b). M. Patra, S. G. Awuah, S. J. Lippard, *J Am Chem Soc* **2016**, *138*, 12541-12551.
- [66] P. R. Florindo, D. M. Pereira, P. M. Borralho, P. J. Costa, M. F. Piedade, C. M. Rodrigues, A. C. Fernandes, *Dalton Trans* **2016**, *45*, 11926-11930.

Chapter 2:

The synthesis of *O*-1 to *O*-6 substituted positional isomers of D-glucose-thioether ligands and their ruthenium polypyridyl conjugates

2

This chapter will be submitted for publication: L. N. Lameijer, S. Bonnet.; *Manuscript in preparation.*

2.1 Introduction

Carbohydrates are a class of biomolecules ubiquitously present in nature, comprising monosaccharides, oligosaccharides and polysaccharides, of which monosaccharides cannot be hydrolyzed further into smaller units. These molecules are recognized as important building blocks in the cell wall of bacteria (peptidoglycan),^[1] in plants (pectins),^[2] in the exoskeleton of insects (chitin),^[3] in cell recognition processes (lectins),^[4] or in the backbone of RNA and DNA.^[5] Among them, D-glucose is the most well-known monosaccharide as it serves as the primary source of chemical energy in eukaryotic cells for the production of ATP.^[6] Otto Warburg found that cancer cells have an increased glycolysis rate for the production of ATP compared to normal cells.^[7] As a consequence, glucose transporters (GLUTs) 1 and 3 are overexpressed in cancer cells.^[8] In recent years there has been a growing interest in using this effect to selectively deliver molecules of interest to cancer cells. In the field of diagnostic imaging the well-known radiotracer 2-deoxy-2-[¹⁸F]fluoroglucose (2-FDG) selectively accumulates in cancer cells since its metabolic breakdown is hampered by the replacement of a hydroxyl group on the 2-position of D-glucose by fluoride.^[9] This clinically approved agent allows PET imaging of tumors anywhere in the whole body. In the field of medicinal chemistry, glufosfamide has shown some success as a safer alternative for ifosfamide, an alkylating agent used in cancer treatment. The therapeutic efficiency of glufosfamide is thought to be higher due to its increased water solubility and preferred uptake in malignant cells versus normal cells.^[10] Recently Palay et. al. have demonstrated that a series of glucose conjugates of platinum-based medicines are taken up *via* GLUT1.^[11] This result is in contrast to the observation of Schubiger, who found that none of their radiodiagnostic glycoconjugates based on ^{99m}Tc were taken up via glucose transporters.^[12] For ruthenium(II) polypyridyl-based drugs this effect has not been thoroughly investigated. We have therefore designed a series of glycoconjugates of every positional isomers of D-glucose, containing different lengths of ethylene glycol-based spacers bearing one or two coordinating methylthioether groups. New routes towards these positional isomers were developed that are compatible with sulfur based ligands, since the existing routes use palladium-based catalysts that are deactivated by donor atoms.^[13] As traces of palladium also often interfere with the biological activity of pharmaceuticals,^[14] we herein describe a palladium-free synthesis for every PEGylated positional isomer of D-glucose-thioether ligands, and their coordination to ruthenium(II) polypyridyl complexes to afford eleven ruthenium-glycoconjugates (see structures in Figure 2.1) aimed at studying the structure-uptake relationship in cancer cells.

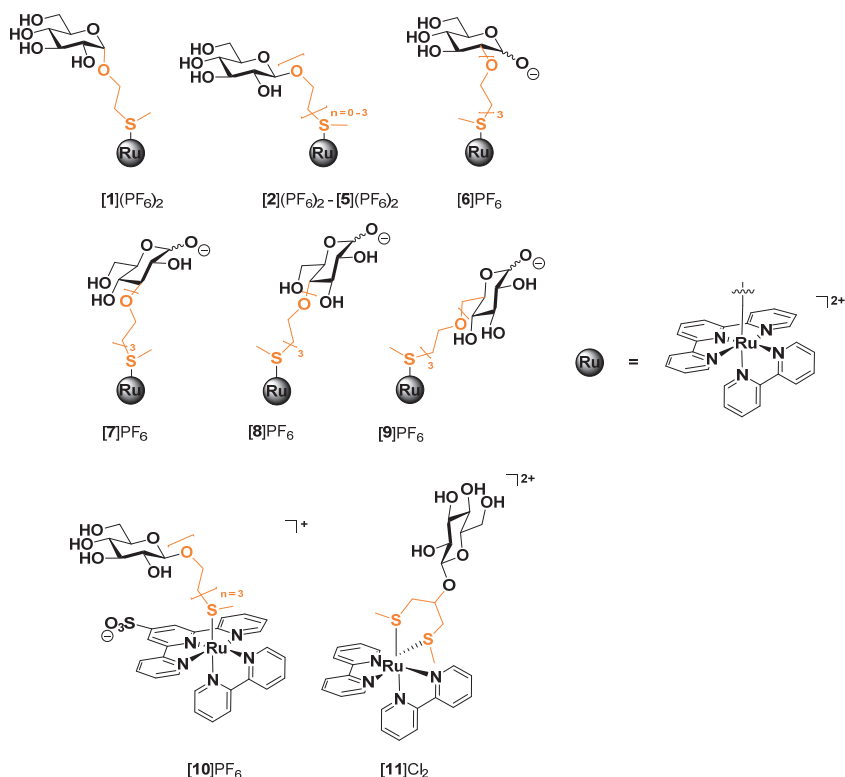
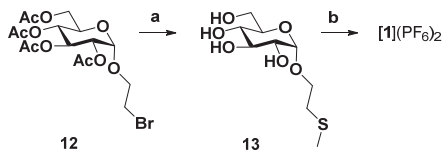


Figure 2.1. Schematic overview of O-1 to O-6 positional D-glucose ruthenium(II) polypyridyl conjugates presented in this study.

2.2 Results and discussion

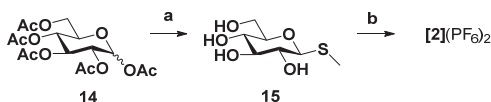
2.2.1 1-O substitution

Five hydroxyl groups are available for modification in D-glucose, of which the 1-O position is modified *via* chemical glycosylation.^[15] Recently Patra *et. al.* have demonstrated that the spacer length exerts influence over GLUT mediated uptake of platinum complexes in cells,^[11] however there is currently no established understanding of this effect in cationic ruthenium(II) polypyridyl compounds. Therefore oligoethyleneglycol spacers $[\text{OCH}_2\text{CH}_2]_n$ with varying length ($n = 0 - 3$) were introduced in glycoconjugates **[1](PF₆)₂ - [5](PF₆)₂** (Figure 2.1). The first complex in this series (**[1](PF₆)₂**) was synthesized starting from precursor **12** (Scheme 2.1).^[16] This building block and NaSMe were used in a $\text{S}_{\text{N}}2$ reaction ensuring the installment of the thioether group, affording **13**. This ligand was then reacted with $[\text{Ru}(\text{tpy})(\text{bpy})\text{Cl}]\text{Cl}$, affording glycoconjugate **[1](PF₆)₂**.



Scheme 2.1. a). *i.* NaOMe in DMF, rt, 16 h *ii.* NaOMe in MeOH, 66% over two steps; b). [Ru(tpy)(bpy)Cl]Cl in H₂O, 80 °C, 16 h, 39%.

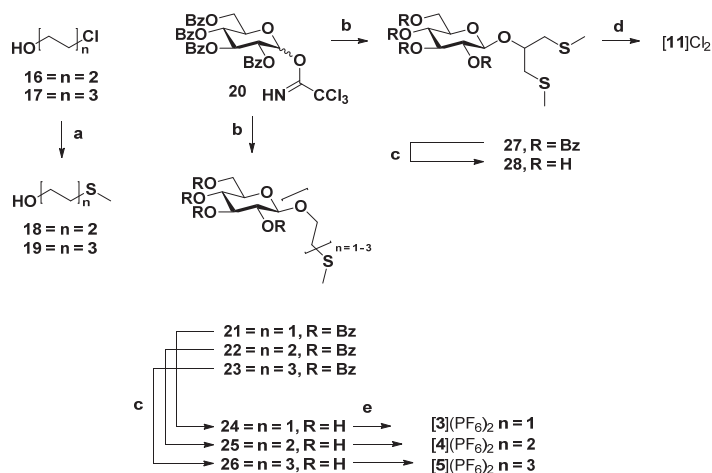
For complex **[2](PF₆)₂**, a three-step one-pot synthesis starting from *per*-acetylated glucose (**14**) was adapted from Valerio *et. al.*,^[17] which afforded the *trans* glucopyranoside as the only diastereoisomer. Treatment of this compound with sodium methoxide in methanol afforded fully deprotected **15** in 55% overall yield. Subsequent reaction of this ligand with [Ru(tpy)(bpy)Cl]Cl then gave **[2](PF₆)**.



Scheme 2.2. a). *i.* I₂, Et₃SiH in DCM, rt., 10 min; *ii.* Thiourea in MeCN, 80 °C, 30 min; *iii.* MeI, Et₃N, rt., 10 min.; *iv.* cat. NaOMe in MeOH, rt., overnight. 57% over four steps; d). [Ru(tpy)(bpy)Cl]Cl in H₂O, 80 °C, 48 h, 28%.

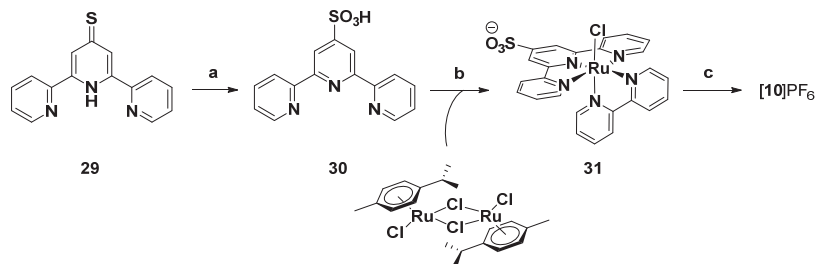
A different approach was employed for the installment of the ethylene glycol-based linkers ($n = 1 - 3$) for complexes **[3](PF₆)₂**-**[5](PF₆)₂** and **[11](PF₆)₂** (Scheme 2.3). The disarmed Schmidt donor **20** (Scheme 2.3) was chosen due to its straightforward synthesis and robustness. The benzoyl protecting group in this building block was favored over the more common acetyl group, due to the lower reactivity – and therefore higher stability – of the benzoyl imidate.^[18] Furthermore, the benzoyl group was chosen to reduce the possible formation of orthoesters, a common side reaction when using acetyl-bearing donors.^[19] Commercially available 2-(methylthio)ethanol was used as acceptor and condensed with donor **20** (Scheme 2.3), affording **21** which after de-*O*-benzoylation acquired deprotected **24**. Compounds **25**, **26** and **28** were acquired in a similar fashion using acceptor **18**, **19** and 1,3-bis(methylthio)propan-2-ol respectively. The synthesis of their ruthenium complexes was found to be straightforward, by reacting excess ligand with the ruthenium species [Ru(tpy)(bpy)Cl]Cl or [Ru(bpy)₂Cl₂]. Their purification however, was found arduous due to the increased water-solubility of these compounds. Although hydrophilicity is a highly desired property in medicinal chemistry, it also decreases the number of available work-up techniques. Common workup methods for metal complexes such as extraction and precipitation were not applicable, since both the ligand and product are water-soluble. Also, the lability of these compounds on C-18 columns prevented reverse-phase chromatographic purification. The most reproducible approach was by purification over silica using a mixture of acetone, water and aqueous KPF₆, followed by a methanol Sephadex LH-20 size exclusion purification to remove excess salt

and minor impurities. This method afforded ruthenium polypyridyl derivatives **[3]**(PF₆)₂-**[5]**(PF₆)₂ and **[11]**Cl₂ in moderate to good yield (28 – 66%).



Scheme 2.3. a). 2-(2-chloroethoxy)ethanol, NaSMe in THF, reflux, 6 h, 94%; b). 2-(methylthio)ethanol, 1,3-bis(methylthio)propanol, **18** or **19**, cat. TMSOTf in DCM, 4Å molsieves, rt, 4 h, 81% for **21**, 66% for **22**, 85% for **23**, 90% for **27**; c). NaOMe in MeOH, rt, 88% for **24**, 86% for **25**, 91% for **26**, 70% for **28**; d). [Ru(bpy)₂Cl]₂ in H₂O, 80 °C, 59% for **[11]**Cl₂; e). [Ru(tpy)(bpy)Cl]Cl in H₂O, 80 °C, 39% for **[3]**(PF₆)₂, 66% for **[4]**(PF₆)₂, 65% for **[5]**(PF₆)₂.

Park and coworkers have demonstrated that glucose bioprobes with a formal charge of +1 are taken up preferentially over neutral and negatively charged probes.^[20] To allow future study of the effect on the overall charge for ruthenium(II) polypyridyl drugs on uptake and toxicity, a derivative of [Ru(tpy)(bpy)Cl]Cl bearing a negative charge on the spectator terpyridine ligand was also synthesized. Compound **31** (Scheme 2.4) was prepared starting from thione **29**,^[21] which was oxidized using *in situ* generated per-acetic acid followed by hydrogenation using 10% palladium on carbon to reverse partial overoxidation to its *N*-oxide, affording ligand **30**. A one-pot synthesis using (*p*-cymene)ruthenium(II) chloride dimer, **30** and bpy provided complex **31**. Reaction of ligand **26** (Scheme 2.3) with this complex then gave complex **[10]**(PF₆)₂.

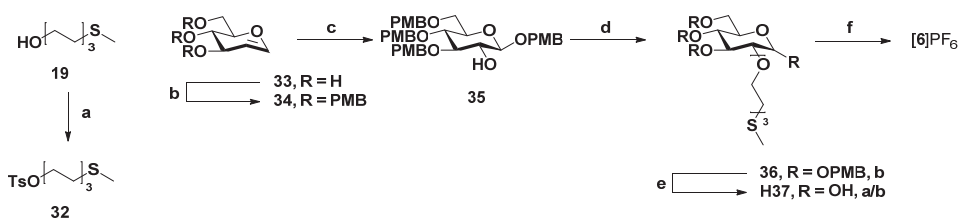


Scheme 2.4. a). i. H₂O₂ in AcOH, 70 °C, 6 hr.; ii. H₂, Pd/C, 40 °C, overnight, 24% over two steps; b). bpy in MeOH, 60 °C, 72%; c). **25**, in H₂O, 80 °C, 16 h, 38%.

2.2.2 2-O substitution

Demonstrations of the covalent modification of the 2-O position of D-glucose with an alkyl-based linker have been given by Dumas *et. al* and Patray and coworkers.^[11, 22] Both groups chose a similar approach starting from methyl 3,5,6-tri-O-benzyl- α/β -D-glucopyranoside followed by installment of the linker and subsequent deprotection of the protection groups using dihydrogen and palladium on carbon. Sulfur based linkers however, poisoned the palladium catalysts which made removal of the benzyl protecting groups impossible following this approach.^[13, 23] Other methods to remove benzyl groups, such as Birch reductions, have been reported to cleave thioethers.^[24] Therefore all described approaches for the functionalization of the O-2 position in D-glucose with a metal-binding moiety, including the glucopyranoside approach described by Schubiger or Lippard, or the approach *via* a benzylorthoacetate intermediate described by Miao *et. al.*^[25] were found unsuitable for thioether-containing compounds.

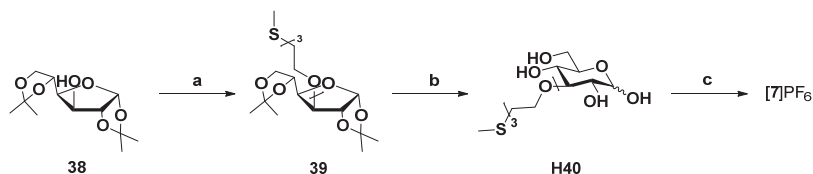
We therefore devised a new protecting group strategy improving the 10-step, 5% yield procedure published by Lippard *et al.*,^[11] and employing the α -oxirane method developed by the group of Danishefsky^[26] and attempted by Dumas *et. al* (Scheme 2.5).^[22] Using this method, D-glucal was protected using the *p*-methoxy benzyl (PMB) group, affording **34**. Treatment of this compound with freshly prepared dimethyldioxirane (DMDO) afforded its corresponding 1,2-anhydrosugar which was then condensed with *p*-methoxy benzyl alcohol (PMB-OH) in the presence of anhydrous ZnCl₂ in THF, afforded β -substituted **35** while simultaneously liberating the 2-O position. This compound was then treated with tosylate **32** (Scheme 2.5) for the installment of the thioether moiety. This conversion proceeded smoothly, which is in contrast to the observation of Schubiger *et al* who had to divert to the furanoside approach due to difficulties encountered during the installment of their iminodiacetic acid based spacer.^[22] With compound **36** in hand, a recently described method^[27] employing a catalytic amount of 37% hydrochloric acid in hexafluoroisopropanol (HFIP) was used to remove all four PMB groups simultaneously. After quenching the reaction using Et₃N an intermediate species was observed (*m/z* = 463.4 found, 463.2 calculated) corresponding to the desired product **H37** and a PMB group. This same intermediate was also observed in the presence of a mild reducing agent such as Et₃SiH. However, when this intermediate was treated with MeNH₂ in MeOH,^[28] the methyl thioether could be liberated, acquiring hemiacetal **H37** in five steps (18% overall yield). After reaction of this compound with [Ru(tpy)(bpy)(H₂O)](PF₆)₂ glycoconjugate [Ru(tpy)(bpy)(**37**)]PF₆, ([**6**]PF₆) was acquired instead of [Ru(tpy)(bpy)(**H37**)](PF₆)₂. This is most likely due to the relatively protic nature of the anomeric proton, resulting in deprotonation during purification on Sephadex and replacement of one of the PF₆ counterions by the 'charged' deprotonated glucose species as interpreted by elemental analysis. On mass however, only the +2 species is observed, indicating that reprotonation occurs in solution. This behavior was observed for all hemiacetal glucose derivatives.



Scheme 2.5. a). **19**, TsCl, Et₃N in DCM, 0 °C to rt, 16 h, 92%; b). PMB-Cl, NaH in DMF, 0 °C to rt, 16 h, 84%; c). *i.* DMDO (0.088M in acetone) in DCM, 0 °C to rt, 3 h; *ii.* PMB-OH, ZnCl₂ in THF, -78 °C to rt, 16 h, 39% over two steps; d). **32**, NaH in DMF, 0 °C to rt, 6 h, 80%; e). *i.* cat. HCl in HFIP/DCM, 5 min; *ii.* MeNH₂ in MeOH/H₂O, 60 °C, 30 min, 67%; f). [Ru(tpy)(bpy)(H₂O)](PF₆)₂ in acetone/H₂O, 80 °C, 24 h, 36%.

2.2.3 3-O substitution

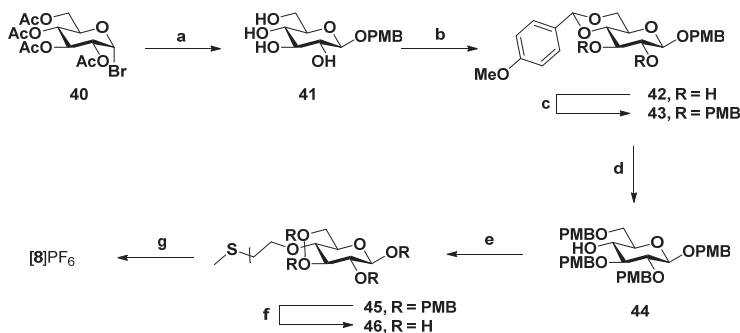
The most straightforward thioether functionalization in these series of ligands was the modification of the 3-*O* position of D-glucose. Starting from diacetone glucose **38** (Scheme 2.6),^[29] the thioether moiety was installed using **32** (Scheme 2.5), affording compound **39**, which was subsequently hydrolyzed using Amberlite® IR-120 H⁺, affording **H40** in 42% overall yield. Glycoconjugation of **H40** with [Ru(tpy)(bpy)Cl]Cl gave [Ru(tpy)(bpy)(40)]PF₆ (**[7]**PF₆).



Scheme 2.6. a). **32**, NaH in DMF, 0 °C to rt, 16 h, 91%; b). Amberlite IR-120 H⁺ in H₂O, 60 °C, 24 h, 46%; c). [Ru(tpy)(bpy)Cl]Cl in H₂O, 80 °C, 16 h, 37%.

2.2.4 4-O substitution

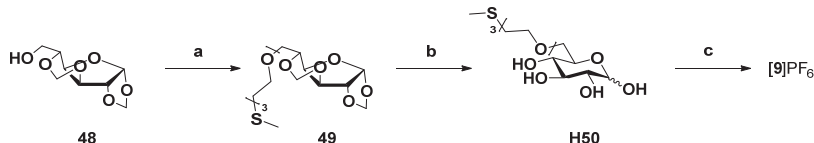
The 4-*O* position of D-glucose was modified starting from acetobromo- α -D-glucose **40** (Scheme 2.7). Using a procedure first described by Kaji et. al., this building block was converted *in situ* to its anomeric iodide, followed by a Koenigs-Knorr type glycosylation with *p*-methoxy benzyl alcohol as an acceptor and Ag₂CO₃ as a base.^[30] De-*O*-acetylation furnished intermediate **41**, followed by 4,6-*O*-benzylideneation and installment of PMB groups affording fully protected **43**. With this building block in hand, a reductive opening using NaCNBH₃ and TFA, liberated the 4-*O* position, which could then be alkylated *via* a Williamson etherification using **32** described in the previous sections, affording **45**. Global deprotection was achieved by treatment with HFIP/HCl, which gave thioether ligand **H46** in 11% overall yield. The subsequent reaction of **H46** with [Ru(tpy)(bpy)(H₂O)](PF₆)₂, afforded glycoconjugate [Ru(tpy)(bpy)(46)]PF₆ (**[8]**PF₆). The synthesis of **H46** was also attempted via an alternative approach using α -methyl glucose following a similar protecting group strategy. However, this proved to be unsuccessful due to the inertness of the anomeric methyl acetal towards acid.



Scheme 2.7. a). *i.* PMB-OH, I_2 , Ag_2CO_3 in Et_2O , rt, 24 h; *ii.* NaOMe in MeOH, rt, 4 h, 72% over two steps; b). $\alpha,\alpha,4$ -Trimethoxytoluene, cat. p -TsOH. H_2O in DMF, 60 °C, 16 h, 89%; c). PMB-Cl, NaH in DMF, 0 °C to rt, 78%; d). NaCNBH₃, TFA in DMF, 0 °C to rt, 16 h, 95%; e). **32**, NaH in DMF, 0 °C to rt, 6 h, 78%; f). cat. HCl in HFIP/DCM, 30 min, 29%; g). [Ru(tpy)(bpy)Cl]Cl in H_2O , 80 °C, 64%.

2.2.5 6-O substitution

Finally, the 6-*O* position of D-glucose was easily modified starting from dimethyl glucose **48** (Scheme 2.8),^[31] which could be converted to **49** using a Williamson etherification with tosylate **31**, followed by acid hydrolysis using dilute hydrochloric acid affording methyl thioether **H50** in 55% over two steps. Glycoconjugation with [Ru(tpy)(bpy)Cl]Cl afforded [Ru(tpy)(bpy)(50)]PF₆ (**[9]PF₆**).



Scheme 2.8. a). **31**, NaH in DMF, 0 °C to rt, 3 h, 78%; b). 2M HCl in H_2O , 60 °C, 1 h, 70%; c). [Ru(tpy)(bpy)Cl]Cl in H_2O , 80 °C, 16 h, 17%.

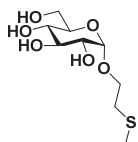
2.3 Conclusion

In this work, we have presented efficient and robust routes to all positional isomers of D-glucose bearing a thioether ligand bound to a light-cleavable ruthenium(II) polypyridyl complex. The general protecting-deprotecting group strategy presented in this work is compatible with compounds bearing donor atoms such as sulfur, as no transition metals catalysts were used until final coordination to the functional ruthenium compound. These routes could possibly be extended to application with other functionalized ligands, such as carboxylates, amines, or pyridines. The study of this library of ruthenium(II) glycoconjugates might shed light on the influence of the stereochemistry of glucose functionalization on GLUT-mediated uptake and the metabolism of the ruthenium-glucose conjugates by enzymes such as hexokinase II.

2.4 Experimental

2.4.1 General

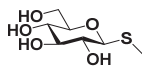
Reagents were purchased from Sigma-Aldrich and used without further purification. 2,2':6',2''-Terpyridine (tpy) was ordered from ABCR GmbH & Co. Dry solvents were collected from a Pure Solve MD5 solvent dispenser from Demaco. For all inorganic reactions solvents were deoxygenated by bubbling dinitrogen through the solution for 30 minutes. All organic reactions were carried out under a dinitrogen atmosphere at rt. Flash chromatography was performed on silica gel (Screening devices B.V.) with a particle size of 40 - 64 μM and a pore size of 60 \AA . TLC analysis was conducted on TLC aluminium foils with silica gel matrix (Supelco, silica gel 60, 56524) with detection by UV-absorption (254 nm), by spraying with 10% H_2SO_4 in ethanol or with a solution of $\text{NH}_4\text{Mo}_7\text{O}_{24}\cdot 4\text{H}_2\text{O}$ 25 g/L, $\text{NH}_4\text{CeSO}_4\cdot\text{H}_2\text{O}$ 10 g/L, 10% H_2SO_4 in H_2O , followed by charring at $\sim 250^\circ\text{C}$ on a heating plate. Optical rotation measurements were performed on a Propol automated polarimeter (sodium D-line, $\lambda = 589\text{ nm}$) with a concentration of 10 mg/mL ($c = 1$) unless stated otherwise. Infrared spectra were recorded on a Perkin Elmer UATR (Single Reflection Diamond) Spectrum Two device (4000-700 cm^{-1} ; resolution 4 cm^{-1}). ^1H NMR and ^{13}C NMR were recorded in CD_3OD and CDCl_3 with chemical shift (δ) relative to the solvent peak on a Bruker AV 400 or AV 500. High resolution mass spectra were recorded by direct injection (2 μl of 2 μM solution in water/acetonitrile; 50/50; v/v and 0.1% formic acid) in a mass spectrometer (Thermo Finnigan LTQ Orbitrap) equipped with an electrospray 250°C with resolution $R = 60,000$ at m/z 400 (mass range $m/z = 150 - 2000$) and dioctylphthalate ($m/z = 391.28428$) as a lock mass. The high-resolution mass spectrometer was calibrated prior to measurements with a calibration mixture (Thermo Finnigan). Combustion analysis for glycoconjugates [1](PF_6)₂ - [5](PF_6)₂, [6] PF_6 - [10] PF_6 , and [11](PF_6)₂ was performed at Mikrolab Kolbe Germany.



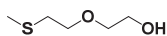
(2-Methylthio)ethyl- α -D-glucopyranoside, 13: 2,3,4,6-Tetra-*O*-acetyl-(2-bromo)ethyl- α -D-glucopyranoside^[16] (135 mg, 0.297 mmol) was dissolved in dry DMF (3 mL) and to this solution was added fresh NaSMe (23 mg, 0.33 mmol). The reaction was stirred overnight after which it was diluted with

EtOAc (25 mL), washed with water (2x), aq. NaHCO_3 (2x), and dried (Na_2SO_4). Concentration *in vacuo* was followed by purification of the residue by silica column chromatography (10% MeOH in DCM), affording the title compound (50.0 mg, 0.197 mmol, 66% over two steps) as a colorless oil. $R_f = 0.84$ (20% MeOH in DCM); IR (neat): 3350, 2918, 1639, 1426, 1018; ^1H NMR (400 MHz, CD_3OD) $\delta = 4.80$ (d, $J = 3.8$ Hz, 1H, H-1), 3.91 – 3.75 (m, 2H, *CHH* H-6, *CHH* OCH_2), 3.69 – 3.58 (m, 4H, H-4, H-5, *CHH* H-6, *CHH* OCH_2), 3.37 (dd, $J = 9.7, 3.8$ Hz, 1H, H-2), 3.25 (d, $J = 9.3$ Hz, 1H, H-3), 2.73 (td, $J = 6.9, 1.8$ Hz, 2H, OCH_2SMe), 2.12 (s, 3H, OCH_2SMe). ^{13}C NMR (101 MHz, CD_3OD) $\delta = 100.3$ (C-1),

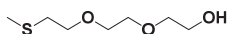
75.1 (C-4), 73.9 (C-5), 73.5 (C-2), 71.8 (C-3), 68.4 (OCH₂), 62.7 (C-6), 34.3 (OCH₂SMe), 15.8 (OCH₂SMe); HRMS: m/z calcd for [C₉H₁₈O₆S + Na]⁺: 277.07163; found: 277.07108.



Methylthio-β-D-glucopyranoside, 15: α/β-D-Glucose pentaacetate (4.99 g, 12.4 mmol) was dissolved in anhydrous DCM (20 mL) and to this solution was added I₂ (4.84 g, 19.0 mmol) and Et₃SiH (2.90 mL, 18.2 mmol) this mixture was allowed to stir for 10 minutes after which it was diluted with DCM (100 mL) and washed with aqueous saturated Na₂S₂O₃ (1x) and Na₂CO₃ (1x). Layers were separated, the organic layer was dried (Na₂SO₄) and concentrated *in vacuo*. The crude was coevaporated with toluene (3x) and redissolved in dry MeCN (20 mL), followed by the addition of thiourea (1.46 g, 19.2 mmol). The mixture was then heated for 30 minutes at 80 °C, concentrated *in vacuo*, followed by purification of the residue over silica (0 to 50% Et₂O in PE) yielding methyl 2,3,4,6-tetra-O-acetyl-1-thio-β-D-glucopyranoside as a yellow foam (2.71 g, 7.24 mmol). This compound was then dissolved in dry MeOH (70 mL) followed by the addition of a catalytic amount of NaOMe, which after stirring overnight was quenched upon the addition of Amberlite IR-120 H⁺. Filtration was followed by concentration *in vacuo*, yielding the title compound as a colourless oil (1.48 g, 7.04 mmol, 57% over four steps). *R*_f = 0.63 (20% MeOH in DCM); IR (neat): 3336, 2923, 2881, 1425, 1017; ¹H NMR (400 MHz, CD₃OD) δ = 4.35 (d, *J* = 9.6 Hz, 1H, H-1), 3.93 (d, *J* = 11.8 Hz, 1H, CHH H-6), 3.77 – 3.68 (m, 1H, CHH H-6), 3.48 – 3.35 (m, 3H, H-3, H-4, H-5), 3.31 (t, *J* = 9.1 Hz, 1H, H-2), 2.26 (s, 3H, SMe). ¹³C NMR (101 MHz, CD₃OD) δ = 87.1 (C-1), 81.8 (C-3), 79.3 (C-4), 73.5 (C-2), 71.3 (C-5), 62.7 (C-6), 12.0 (SMe). HRMS: m/z calcd for [C₇H₁₄O₅S + Na]⁺: 233.04542; found: 233.04442.

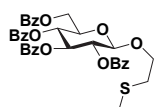


2-(Methylthio)ethoxyethanol, 18: To a flame-dried round-bottom flask was added freshly prepared NaSMe^[32] (1.21 g, 15.5 mmol) under argon. Deoxygenated THF (50 mL) was added, followed by the addition of 2-(2-(2-chloroethoxy)ethanol (1.50 mL, 14.2 mmol). This solution was heated at 60 °C for 6 h, after which it was allowed to cool to room temperature. The mixture was diluted with EtOAc (100 mL) and washed with aqueous NaHCO₃ (2x) and water (1x). Layers were separated, the organic layer was dried (Na₂SO₄) and concentrated *in vacuo* affording a slightly yellowish oil (1.89 g, 13.9 mmol, 89%). IR (neat): 3480, 2907, 2866, 1611, 1512; ¹H NMR (400 MHz, CDCl₃) δ = 3.68 (m, 2H, CH₂), 3.62 (t, *J* = 6.7 Hz, 2H, CH₂), 3.54 (d, *J* = 5.1 Hz, 2H, CH₂), 2.94 – 2.81 (s, 1H, OH), 2.66 (t, *J* = 6.6 Hz, 2H, -SCH₂), 2.10 (s, 3H, CH₃). ¹³C NMR (100 MHz, CDCl₃) δ = 72.1 (CH₂), 69.9 (CH₂), 61.5 (CH₂), 33.6 (SCH₂), 15.8 (SCH₃); HRMS: m/z calcd for [C₅H₁₂O₂S + Na]⁺: 159.04502; found: 159.04566.



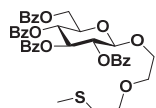
2-[2-(2-(Methylthio)ethoxy)ethoxy]ethanol, 19: The procedure was followed as described for **18** using NaSMe^[32] (4.23 g, 60.4 mmol) and 2-(2-(2-chloroethoxy)ethoxy)ethanol (10.0 g, 59.3 mmol). **19** was afforded as a colourless oil (9.25

g, 51.0 mmol, 85%). IR (neat): 3427, 2915, 2869, 1105, 1063; ^1H NMR: (400 MHz, CDCl_3) δ = 3.61 – 3.42 (m, 10H, 5 x CH_2), 3.09 (s, 1H, -OH), 2.60 – 2.50 (m, 2H, 1 x CH_2), 2.03 – 1.94 (s, 3H, CH_3). ^{13}C NMR: (100 MHz, CDCl_3) δ = 72.4 ($-\text{CH}_2$), 70.2 (CH_2), 70.1 (CH_2), 70.0 (CH_2), 61.3 (CH_2) 33.13 ($-\text{SCH}_2$), 15.7 ($-\text{SCH}_3$). HRMS: m/z calcd for $[\text{C}_7\text{H}_{16}\text{O}_3\text{S} + \text{Na}]^+$: 203.07124; found: 203.07134.



(2-Methylthio)ethyl 2,3,4,6-tetra-O-benzoyl- β -D-glucopyranoside, 21:

2,3,4,6-Tetra-O-benzoyl- β -D-glucopyranosyl trichloroacetimidate^[33] (370 mg, 0.364 mmol) and 2-(methylthio)ethanol (100 μL , 1.15 mmol) were coevaporated three times with anhydrous toluene after which they were dissolved in anhydrous DCM (36 mL). Freshly activated 4 Å molsieves were added, and the mixture was allowed to stir for 15 minutes after which a catalytic amount of TMSOTf (20.0 μL , 111 μmol) was added. After stirring for 4 h at room temperature, the reaction was quenched upon the addition of Et_3N (100 μL , 0.714 mmol) and concentrated *in vacuo* followed by purification of the residue over silica (10% to 50% EtOAc in PE), affording the title compound as a clear oil (270 mg, 0.410 mmol, 81%). R_f = 0.74 (30% EtOAc in PE); IR (neat): 3064, 2922, 2853, 1720, 1258; ^1H NMR (400 MHz, CDCl_3) δ = 8.07 – 8.02 (m, 2H, H_{arom}), 8.00 – 7.96 (m, 2H, H_{arom}), 7.94 – 7.90 (m, 2H, H_{arom}), 7.87 – 7.81 (m, 2H, H_{arom}), 7.60 – 7.25 (m, 12H, H_{arom}), 5.93 (t, J = 9.7 Hz, 1H, H-3), 5.70 (t, J = 9.7 Hz, 1H, H-4), 5.56 (dd, J = 9.8, 7.8 Hz, 1H, H-2), 4.93 (d, J = 7.8 Hz, 1H, H-1), 4.67 (dd, J = 12.2, 3.2 Hz, 1H, CHH H-6), 4.52 (dd, J = 12.1, 5.4 Hz, 1H, CHH H-6), 4.19 (ddd, J = 8.6, 5.4, 3.2 Hz, 1H, H-5), 4.09 (dt, J = 10.2, 6.7 Hz, 1H, CHH OCH_2), 3.78 (dt, J = 10.3, 7.3 Hz, 1H, CHH OCH_2), 2.67 (t, J = 6.9 Hz, 2H, CH_2SMe), 2.01 (s, 3H, CH_2SMe). ^{13}C NMR (101 MHz, CDCl_3) δ = 166.2 (C=O Bz), 165.9 (C=O Bz), 165.3 (C=O Bz), 165.2 (C=O Bz), 133.6 (C_H Arom), 133.4 (C_H Arom), 133.3 (C_H Arom), 129.9 (C_H Arom), 129.9 (C_H Arom), 129.9 (C_H Arom), 129.8 (C_H Arom), 129.7 (C_q Arom), 129.4 (C_q Arom), 128.9 (C_q Arom), 128.8 (C_q Arom), 128.5 (C_H Arom), 128.5 (C_H Arom), 128.5 (C_H Arom), 128.4 (C_H Arom), 101.4 (C-1), 73.0 (C-3), 72.4 (C-5), 71.9 (C-2), 69.8 (C-4), 69.8 (OCH_2) 63.2 (C-6), 33.4 (CH_2SMe), 16.1 (CH_2SMe); HRMS: m/z calcd for $[\text{C}_{37}\text{H}_{34}\text{O}_{10}\text{S} + \text{NH}_4]^+$: 688.22109; found: 688.22223.

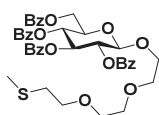


[2-(2-(Methylthio)ethoxy)]ethyl 2,3,4,6-tetra-O-benzoyl- β -D-glucopyranoside, 22:

The general procedure described for **21** was followed, with 2,3,4,6-tetra-O-benzoyl- β -D-glucopyranosyl trichloroacetimidate (6.00 g, 8.14 mmol) and 2-(2-(methylthio)ethoxy)ethanol (1.24 g, 9.10 mmol). Purification of the residue by silica column purification (0 – 25% EtOAc in PE) afforded the title compound as a clear oil (3.86 g, 5.40 mmol, 66%). R_f = 0.34 (33% EtOAc in PE); IR (neat): 3064, 2919, 1722, 1602, 1249; ^1H NMR (400 MHz, CDCl_3) δ = 8.05 – 8.01 (m, 2H, H_{arom}), 8.00 – 7.96 (m, 2H, H_{arom}), 7.93 – 7.88 (m, 2H, H_{arom}), 7.86 – 7.81 (m, 2H, H_{arom}), 7.58 – 7.24 (m, 12H, H_{arom}), 5.92 (t, J = 9.7 Hz, 1H, H-3), 5.69 (t, J = 9.7 Hz, 1H, H-4), 5.54 (dd, J = 9.9, 7.7 Hz, 1H, H-2), 4.99 (d, J = 7.8 Hz, 1H, H-1), 4.65 (dd, J = 12.1, 3.2 Hz, 1H,

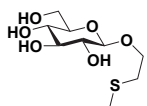
CHH H-6), 4.51 (dd, $J = 12.1, 5.1$ Hz, 1H, CHH H-6), 4.18 (ddd, $J = 10.1, 5.2, 3.1$ Hz, 1H, H-5), 4.00 (dt, $J = 11.4, 4.1$ Hz, 1H, CHH OCH₂), 3.81 (ddd, $J = 11.1, 6.9, 3.8$ Hz, 1H, CHH OCH₂), 3.58 (dt, $J = 6.7, 3.7$ Hz, 2H, OCH₂), 3.48 (t, $J = 6.7$ Hz, 2H, OCH₂), 2.44 (t, $J = 6.7$ Hz, 2H, CH₂SMe), 2.03 (s, 3H, CH₂SMe). ¹³C NMR (101 MHz, CDCl₃) $\delta = 166.3$ (C=O Bz), 165.9 (C=O Bz), 165.3 (C=O Bz), 165.2 (C=O Bz), 133.6 (C_H Arom), 133.4 (C_H Arom), 133.3 (C_H Arom), 129.9 (C_H Arom), 129.9 (C_H Arom), 129.9 (C_H Arom), 129.9 (C_H Arom), 129.7 (C_q Arom), 129.4 (C_q Arom), 128.9 (C_q Arom), 128.9 (C_q Arom), 128.5 (C_H Arom), 128.5 (C_H Arom), 128.4 (C_H Arom), 101.4 (C-1), 73.0 (C-3), 72.3 (C-5), 72.0 (C-2), 70.6 (OCH₂), 70.2 (OCH₂), 69.8 (C-4), 69.4 (OCH₂), 63.2 (C-6), 33.5 (CH₂SMe), 16.1 (CH₂SMe); HRMS: m/z calcd for [C₃₉H₃₈O₁₁S+ NH₄]⁺: 732.24731; found: 732.24836.

2



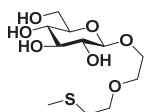
2-[2-(2-(Methylthio)ethoxy)ethoxy]ethyl 2,3,4,6-tetra-O-benzoyl- β -D-glucopyranoside, 23: The general procedure described for **21** was followed, with 2,3,4,6-tetra-O-benzoyl- β -D-glucopyranosyl trichloroacetimidate^[33] (2.65 g, 3.58 mmol) and **19** (792 mg, 4.39 mmol).

Purification of the residue over silica (10% to 50% EtOAc in PE) afforded the title compound as a clear oil (2.32 g, 3.06 mmol, 85%). $R_f = 0.16$ (20% EtOAc in PE); $[\alpha]_D^{20}$ (CHCl₃): +18.0; IR (neat): 3063, 2918, 2869, 1722, 1451; ¹H-NMR: (400 MHz, CDCl₃) $\delta = 8.03$ (d, $J = 8.6$ Hz, 2H, H_{arom}), 7.97 (d, $J = 8.6$ Hz, 2H, H_{arom}), 7.90 (d, $J = 8.7$ Hz, 2H, 2H, H_{arom}), 7.83 (d, $J = 8.6$ Hz, 2H, H_{arom}), 7.58 – 7.43 (m, 3H, H_{arom}), 7.43 – 7.29 (m, 7H, H_{arom}), 7.29 – 7.21 (m, 2H, H_{arom}), 5.93 (t, $J = 9.7$ Hz, 1H, H-3), 5.70 (t, $J = 9.7$ Hz, 1H, H-4), 5.55 (dd, $J = 9.7, 7.8$ Hz, 1H, H-2), 5.01 (d, $J = 7.8$ Hz, 1H, H-1), 4.66 (dd, $J = 12.1, 3.1$ Hz, 1H, CHH H-6), 4.51 (dd, $J = 12.1, 5.1$ Hz, 1H, CHH H-6), 4.20 (ddd, $J = 9.9, 5.1, 3.1$ Hz, 1H, H-5), 4.03 – 3.95 (m, 1H, CHH –OCH₂), 3.83 (m, 1H, CHH –OCH₂), 3.69 – 3.56 (m, 2H, -OCH₂), 3.55 (t, $J = 6.9$ Hz, 2H, -OCH₂), 3.50 – 3.42 (m, 2H, -OCH₂), 3.37 (t, $J = 4.6$ Hz, 2H, -OCH₂), 2.64 (t, $J = 6.9$ Hz, 2H, -CH₂SMe), 2.11 (s, 3H, -SCH₃). ¹³C NMR: (101 MHz, CD₃OD) $\delta = 166.1$ (C=O Bz), 165.8 (C=O Bz), 165.2 (C=O Bz), 165.1 (C=O Bz), 133.5 (CH Arom), 133.3 (CH Arom), 133.2 (CH Arom), 129.8 (CH Arom), 129.8 (CH Arom), 129.6 (C_q Arom), 129.4 (C_q Arom), 128.8 (C_q Arom), 128.4 (CH Arom), 128.4 (CH Arom), 101.3 (C-1), 73.0 (C-3), 72.2 (C-5) 72.0 (C-2), 70.7 (OCH₂), 70.5 (OCH₂), 70.2 (OCH₂), 69.8 (C-4), 69.4 (OCH₂), 63.2 (OCH₂), 33.4 (CH₂SMe), 16.0 (CH₂SMe). HRMS: m/z calcd for [C₄₁H₄₂O₁₂S + Na]⁺: 781.22892; found: 781.22795.

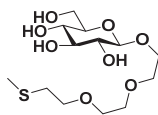


(2-Methylthio)ethyl- β -D-glucopyranoside, 24: The protected glucoside **23** (240 mg, 0.410 mmol) was dissolved in MeOH (6 mL) after which a catalytic amount of NaOMe was added. The solution was allowed to stir for 16 h, after which Amberlite IR-120 H⁺ was added, until neutral pH. The resin was filtered off and the mixture was concentrated *in vacuo*. Purification of the residue over silica (0 to 10% MeOH in DCM) afforded the title compound as a colorless oil (80.0 mg, 0.315 mmol, 88%). $R_f = 0.15$ (5% MeOH in DCM); IR (neat): 3351, 2919, 2881, 1072, 1016; ¹H NMR (400 MHz, CD₃OD) $\delta = 4.30$ (d, $J = 7.8$ Hz, 1H, H-1), 4.03 (dt, $J = 10.1, 7.1$ Hz, 1H, CHH OCH₂), 3.87 (dd,

$J = 11.9, 1.8$ Hz, 1H, CHH H-6), 3.74 (dt, $J = 10.1, 7.1$ Hz, 1H, CHH OCH₂), 3.69 – 3.64 (m, 1H, CHH H-6), 3.39 – 3.33 (m, 1H, H-4), 3.29 – 3.26 (m, 2H, H-3, H-5), 3.21 – 3.15 (m, 1H, H-2), 2.73 (t, $J = 7.1$ Hz, 2H, CH₂SMe), 2.13 (s, 3H, CH₂SMe). ¹³C NMR (101 MHz, CD₃OD) $\delta = 104.4$ (C-1), 77.9 (C-3), 77.9 (C-4), 75.0 (C-2), 71.6 (C-5), 70.0 (OCH₂), 62.7 (C-6), 34.3 (CH₂SMe), 15.7 (CH₂SMe); HRMS m/z calcd for [C₉H₁₈O₆S + Na]⁺: 277.07136; found: 277.07160.



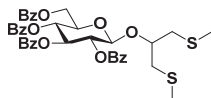
[2-(2-(Methylthio)ethoxy)]-ethyl- β -D-glucopyranoside, 25: The procedure as described for **24** was followed, using protected glycoside **22** (560 mg, 0.780 mmol) and THF/MeOH (10 mL, 1:1). Purification of the crude over silica (0 to 20% acetone in DCM) afforded the title compound as a white solid (200 mg, 0.670 mmol, 86%). $R_f = 0.19$ (10% acetone in DCM); IR (neat): 3304, 2919, 1075, 1354, 1028; ¹H NMR (400 MHz, CD₃OD) $\delta = 4.31$ (d, $J = 7.8$ Hz, 1H, H-1), 4.05 – 3.96 (m, 1H, CHH OCH₂), 3.87 (dd, $J = 11.9, 1.8$ Hz, 1H, CHH H-6), 3.78 – 3.62 (m, 6H, CHH H-6, CHH OCH₂, 2 x OCH₂), 3.40 – 3.25 (m, 3H, H-3, H-4, H-5), 3.19 (dd, $J = 9.3, 7.5$ Hz, 1H, H-2), 2.68 (t, $J = 6.8$ Hz, 2H, CH₂SMe), 2.13 (s, 3H, CH₂SMe). ¹³C NMR (101 MHz, CD₃OD) $\delta = 104.4$ (C-1), 78.0 (C-3), 78.0 (C-4), 75.1 (C-2), 71.6 (C-5), 71.5 (OCH₂), 71.2 (OCH₂), 69.7 (OCH₂), 62.8 (C-6), 34.2 (CH₂SMe), 15.8 (CH₂SMe). HRMS: m/z calcd for [C₁₁H₂₂O₇S + Na]⁺: 321.09784; found: 321.09760.



2-[2-(2-(Methylthio)ethoxy)ethoxy]ethyl β -D-glucopyranoside, 26: The protected glycoside **23** (973 mg, 1.28 mmol) was dissolved in MeOH (10 mL) after which a catalytic amount of NaOMe was added. The solution was allowed to stir for 16 h, after which Amberlite IR-120 H⁺ was added,

until reaching neutral pH. The resin was filtered off and the mixture was concentrated *in vacuo*. Purification of the residue over silica (0 - 10% MeOH in DCM) afforded the title compound as a colorless oil (400 mg, 1.17 mmol, 91%). $R_f = 0.29$ (10% MeOH in DCM):

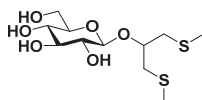
$[\alpha]_D^{20}$ (MeOH): -10.0; IR: 3371, 2915, 2874, 1073, 1031; ¹H NMR (400 MHz, CDCl₃) $\delta = 4.35$ (d, $J = 7.8$ Hz, 1H, H-1), 4.06 (ddd, $J = 10.2, 5.0, 3.0$ Hz, 1H, CHH OCH₂), 3.90 (dd, $J = 11.9, 1.7$ Hz, 1H, CHH OCH₂), 3.82 – 3.65 (m, 10H, CHH OCH₂, H-5, H-6, 3 x CH₂ OCH₂), 3.45 – 3.37 (m, 1H, H-3), 3.37 – 3.28 (m, 1H, H-4), 3.24 (dd, $J = 9.1, 7.8$ Hz, 1H, H-2), 2.72 (t, $J = 6.8$ Hz, 2H, -OCH₂), 2.17 (s, 3H, -SCH₃). ¹³C NMR (101 MHz, CD₃OD) $\delta = 104.4$ (C-1), 77.9 (C-3), 75.0 (C-4), 71.6 (OCH₂), 71.5 (C-5), 71.5 (2 x OCH₂), 71.1 (OCH₂), 69.6 (OCH₂), 62.7 (C-6), 34.2 (CH₂SMe), 15.9 (CH₂SMe). HRMS m/z calcd for [C₁₃H₃₀O₈S + Na]⁺: 365.12406; found: 365.12376



[1,3-Bis(methylthio)]-propyl-2,3,4,6-tetra-O-benzoyl- β -D-glucopyranoside, 27: The general procedure described for **21** was followed, with 2,3,4,6-tetra-O-benzoyl- β -D-glucopyranosyl

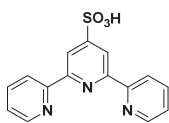
trichloroacetimidate (5.00 g, 6.75 mmol) and 1,3-bis(methylthio)propanol (830 μ L, 6.09

mmol). Purification of the residue by silica column purification (0 – 20% EtOAc in PE) afforded the title compound as a clear oil (3.95 g, 5.40 mmol, 90%). $R_f = 0.55$ (20% EtOAc in PE); IR (neat): 2919, 2853, 1722, 1601, 1259; $^1\text{H NMR}$ (400 MHz, CDCl_3) $\delta = 8.07 - 8.00$ (m, 2H, H_{arom}), 7.99 – 7.94 (m, 2H, H_{arom}), 7.91 (d, $J = 7.8$ Hz, 2H, H_{arom}), 7.85 – 7.79 (m, 2H, H_{arom}), 7.60 – 7.24 (m, 12H, H_{arom}), 5.91 (t, $J = 9.7$ Hz, 1H, H-3), 5.65 (t, $J = 9.7$ Hz, 1H, H-4), 5.52 (dd, $J = 10.1, 7.7$ Hz, 1H, H-2), 5.09 (d, $J = 7.9$ Hz, 1H, H-1), 4.67 (dd, $J = 12.1, 3.1$ Hz, 1H, CHH H-6), 4.48 (dd, $J = 12.2, 5.6$ Hz, 1H, CHH H-6), 4.18 (ddd, $J = 9.3, 5.7, 3.0$ Hz, 1H, H-5), 4.04 – 3.91 (m, 1H, $\text{CH}(\text{CH}_2\text{SMe})_2$), 2.86 (dd, $J = 13.8, 4.4$ Hz, 1H, CHH $\text{CH}(\text{CH}_2\text{SMe})_2$), 2.81 – 2.71 (m, 2H, $\text{CH}_2 \text{CH}(\text{CH}_2\text{SMe})_2$), 2.61 (td, $J = 13.5, 7.4$ Hz, 1H, CHH $\text{CH}(\text{CH}_2\text{SMe})_2$), 2.06 (s, 3H, SMe), 1.90 (s, 3H, SMe). $^{13}\text{C NMR}$ (101 MHz, CDCl_3) $\delta = 166.2$ (C=O Bz), 165.9 (C=O Bz), 165.4 (C=O Bz), 165.3 (C=O Bz), 133.6 (C_H Arom), 133.4 (C_H Arom), 133.4 (C_H Arom), 133.3 (C_H Arom), 130.0 (C_H Arom), 129.9 (C_H Arom), 129.9 (C_H Arom), 129.9 (C_H Arom), 129.6 (C_q Arom), 129.5 (C_q Arom), 128.9 (C_q Arom), 128.8 (C_q Arom), 128.6 (C_H Arom), 128.4 (C_H Arom), 101.7 (C-1), 80.2 ($\text{CH}(\text{CH}_2\text{SMe})_2$), 73.0 (C-3), 72.4 (C-5), 72.1 (C-2), 69.9 (C-4), 63.2 (C-6), 38.4 ($\text{CH}_2 \text{CH}(\text{CH}_2\text{SMe})_2$), 37.8 ($\text{CH}_2 \text{CH}(\text{CH}_2\text{SMe})_2$), 16.7 (2 x SMe); HRMS m/z calcd for $[\text{C}_{39}\text{H}_{38}\text{O}_{10}\text{S}_2 + \text{NH}_4]^+$: 748.22446; found: 748.22543.



[1,3-bis(methylthio)]-propyl- β -D-glucopyranoside, 28: The procedure as described for **22** was followed, using protected glycoside **27** (3.20 g, 4.38 mmol) and DCM/MeOH (50 mL, 1:50).

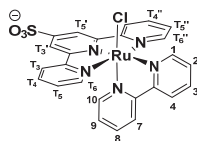
Purification of the residue over silica (0 to 10% MeOH in DCM) afforded **28** as a white foam (960 mg, 3.05 mmol, 70%). $R_f = 0.24$ (100% EtOAc); IR (neat): 3368, 2916, 1424, 1071, 1016; $^1\text{H NMR}$ (400 MHz, CD_3OD) $\delta = 4.45$ (d, $J = 7.8$ Hz, 1H, H-1), 4.06 (p, $J = 5.8$ Hz, 1H, $\text{CH}(\text{CH}_2\text{SMe})_2$), 3.90 – 3.83 (m, 1H, CHH H-6), 3.70 – 3.63 (m, 1H, CHH H-6), 3.41 – 3.33 (m, 1H, H-3), 3.33 – 3.26 (m, 2H, H-4, H-5), 3.24 – 3.14 (m, 1H, H-2), 2.94 – 2.83 (m, 3H, CHH, $\text{CH}_2 \text{CH}(\text{CH}_2\text{SMe})_2$), 2.79 (dd, $J = 13.8, 5.6$ Hz, 1H, CHH $\text{CH}(\text{CH}_2\text{SMe})_2$), 2.15 (s, 6H, 2 x SMe). $^{13}\text{C NMR}$ (101 MHz, CD_3OD) $\delta = 104.1$ (C-1), 79.4 ($\text{CH}(\text{CH}_2\text{SMe})_2$), 77.9 (C-3), 77.9 (C-4), 75.2 (C-2), 71.5 (C-5), 62.7 (C-6), 39.0 ($\text{CH}_2 \text{CH}(\text{CH}_2\text{SMe})_2$), 37.9 ($\text{CH}_2 \text{CH}(\text{CH}_2\text{SMe})_2$), 16.6 (SMe), 16.4 (SMe); HRMS m/z calcd for $[\text{C}_{11}\text{H}_{22}\text{O}_6\text{S}_2 + \text{Na}]^+$: 337.07500; found: 337.07520



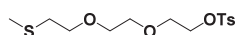
[2,2':6',2''-Terpyridine]-4'-sulfonic acid, 30 (HS-tpy): [2,2':6',2''-terpyridine]-4'(1'H)-thione^[34] (534 mg, 2.01 mmol) was suspended in acetic acid (6 mL) and to this mixture was added 30% H_2O_2 (1 mL). The resulting purple mixture was heated at 70 °C for 12 h, and concentrated

in vacuo. The crude was then redissolved in H_2O , followed by the addition of 10% Pd/C (32 mg) and purged with H_2 (5 min). After stirring overnight at 40 °C under a H_2 atmosphere, the reaction was filtered over Celite®, concentrated and purified over silica (0 to 10% MeOH in DCM), affording the title compound as a bright yellow powder. $R_f = 0.37$ (20% MeOH in DCM); IR (neat): 3391, 3064, 1622, 1398, 1189; $^1\text{H NMR}$ (400 MHz, D_2O) $\delta = 8.09$ (dd, $J = 4.9, 1.9$ Hz, 2H, T_3, T_3''), 7.84 (s, 2H, T_3', T_5'), 7.61 (d, $J = 7.4$ Hz, 2H, T_6, T_6''), 7.54 (td,

$J = 7.7, 1.9$ Hz, 2H, T_4, T_4''), 7.15 (ddd, $J = 7.4, 5.0, 1.4$ Hz, 2H, T_5, T_5''). ^{13}C NMR (101 MHz, D_2O) $\delta = 154.9$ (C_q Arom), 152.7 (C_q Arom), 152.7 (C_q Arom), 148.1 (T_3, T_3''), 138.1 (T_4, T_4''), 124.9 (T_5, T_5''), 121.8 (T_6, T_6''), 116.5 (T_3, T_3''); HRMS m/z calcd for $[\text{C}_{15}\text{H}_{11}\text{N}_3\text{O}_3\text{S} + \text{H}]^+$: 314.05939; found: 314.05999.



[Ru(S-tpy)(bpy)(Cl)], **31**: Compound **30** (134 mg, 0.426 mmol) was dissolved in MeOH (10 mL) and to this solution was added 100 mg washed Amberlite® Na^+ . After stirring for 5 minutes at rt, the ion exchange resin was filtered off and the filtrate was concentrated *in vacuo*, affording a pinkish solid. This compound was then together with *p*-cymene dimer, redissolved in deoxygenated MeOH (5 mL) and heated to 60 °C. A solution of bpy in MeOH (2.3 mL) was then added dropwise over 10 minutes from which the color of the solution changed from purple to red. After stirring for 2 h under nitrogen, the solution was allowed to cool to rt, after which Et_2O (20 mL) was added. The resulting precipitate was filtered and washed with Et_2O (3x) affording a brown powder (185 mg, 0.306 mmol, 72%). $R_f = 0.29$ (10% MeOH in DCM); HRMS: m/z calcd for $[\text{M}]^+$: 605.99351; found: 605.99462.



2-(2-(2-(methylthio)ethoxy)ethoxy)ethyl

4-

methylbenzenesulfonate, **32**: Compound **19** (715 mg, 3.97 mmol)

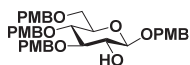
was dissolved in dry DCM (40 mL) and cooled to 0 °C. To this solution were added Et_3N (850 μl , 6.09 mmol) and Ts-Cl (1.12 g, 5.87 mmol). The reaction was allowed to stir overnight after which it was diluted with DCM (100 mL) and transferred to a separatory funnel. After washing with water (1x) and brine (1x), layers were separated, the organic layer was dried (Na_2SO_4) and concentrated *in vacuo*. Purification of the residue by silica column chromatography (0 to 50% EtOAc in PE) afforded the title compound as a colorless oil (1.22 g, 3.64 mmol, 92%). $R_f = 0.78$ (50% EtOAc in PE); IR (neat): 2917, 2868, 1598, 1353, 1174; ^1H NMR (400 MHz, CDCl_3) $\delta = 7.73$ (d, $J = 8.3$ Hz, 2H, H_{arom}), 7.30 (d, $J = 8.1$ Hz, 2H, H_{arom}), 4.18 – 4.02 (m, 2H, CH_2), 3.65 – 3.61 (m, 2H, CH_2), 3.57 (t, $J = 6.8$ Hz, 2H, CH_2), 3.51 (m, 4H, 2 x CH_2), 2.60 (t, $J = 6.8$ Hz, 2H, CH_2), 2.39 (s, 3H, CH_3 Tosyl), 2.07 (s, 3H, CH_3). ^{13}C NMR (100 MHz, CDCl_3) $\delta = 144.7$ (C_q Arom), 132.7 (C_q Arom), 129.7 (C_H Arom), 127.7 (C_H Arom), 70.5 (CH_2), 70.4 (CH_2), 70.0 (CH_2), 69.2 (CH_2), 68.5 (CH_2), 33.2 (SCH_2), 21.5 (CH_3 Tosyl), 15.8 (SCH_3); HRMS: m/z calcd for $[\text{C}_{14}\text{H}_{22}\text{O}_5\text{S}_2 + \text{Na}]^+$: 357.08009; found: 357.08003.



3,4,6-Tri-O-(4-methoxybenzyl)-D-glucal, **34**: To a cooled solution (0 °C) of D-

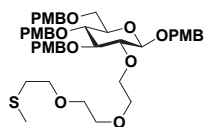
glucal in dry DMF (230 mL) was slowly added NaH (60% dispersion in mineral oil, 3.10 g, 77.5 mmol) followed by the addition of 4-methoxybenzyl chloride (10.1 mL, 74.5 mmol). After stirring overnight under a dinitrogen atmosphere, H_2O (10 mL) was added and the mixture was allowed to stir for another 10 minutes. The mixture was further diluted with EtOAc (200 mL) and transferred to a separatory funnel, washed with

water (3x) and brine (3x). The organic layer was dried over Na_2SO_4 and concentrated *in vacuo*. Purification by silica column chromatography (0 to 15% EtOAc in PE) afforded **34** (9.82 g, 19.4 mmol, 84%) as a clear oil that solidified upon standing over a longer time. R_f = 0.66 (10% EtOAc in PE); IR (neat): 2999, 2863, 2907, 1647, 1512; ^1H NMR (400 MHz, CDCl_3) δ = 7.16 (d, J = 8.3 Hz, 4H, H_{arom}), 7.04 (d, J = 8.5 Hz, 2H, H_{arom}), 6.75 (dd, J = 11.9, 8.1 Hz, 6H, H_{arom}), 6.31 (d, J = 6.2 Hz, 1H, H-1), 4.74 (dd, J = 6.2, 3.2 Hz, 1H, H-2), 4.64 (d, J = 10.9 Hz, 1H, CHH PMB), 4.52 – 4.35 (m, 5H, CHH PMB, 2 x CH_2 PMB), 4.07 (dd, J = 6.5, 2.2 Hz, 1H, H-3), 3.92 (dt, J = 8.6, 4.1 Hz, 1H, H-5), 3.70 (s, 3H, CH_3 PMB), 3.69 (s, 4H, CH_3 PMB, H-4), 3.69 (s, 3H, CH_3 PMB), 3.66 – 3.58 (m, 2H, CH_2 H-6). ^{13}C NMR (101 MHz, CDCl_3) δ = 159.3 (C_{H} Arom), 159.3 (C_{H} Arom), 159.3 (C_{H} Arom), 144.7 (C-1), 130.6 (C_{q} Arom), 130.4 (C_{q} Arom), 130.1 (C_{q} Arom), 129.7 (C_{H} Arom), 129.6 (C_{H} Arom), 129.5 (C_{H} Arom), 113.9 (C_{H} Arom), 113.9 (C_{H} Arom), 100.2 (C-2), 76.9 (C-5), 75.6 (C-2), 74.2 (C-4), 73.5 (CH_2 PMB), 73.2 (CH_2 PMB), 70.3 (CH_2 PMB), 68.3 (C-6), 55.4 (3 x CH_3 PMB); HRMS m/z calcd for $[\text{C}_{30}\text{H}_{34}\text{O}_7 + \text{NH}_4]^+$: 524.26428; found: 524.26551



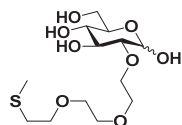
(4-Methoxybenzyl)-3,4,6-Tri-O-(4-methoxybenzyl)- β -D-glucopyranoside, **35:**

To a solution of protected glycoside **35** (821 mg, 1.62 mmol) in dry DCM (8 mL) under a dinitrogen atmosphere, were added freshly activated 4Å molsieves. After stirring for 15 minutes, the mixture was allowed to cool to 0 °C and freshly prepared dimethyldioxirane in acetone (20 mL, 88 mM) was slowly added. The mixture was stirred for 3 h and allowed to reach rt, after which it was filtered over Celite® and concentrated *in vacuo*. The crude was then, together with 4-methoxyl benzyl alcohol (335 mg, 2.42 mmol) redissolved in dry THF under a dinitrogen atmosphere, followed by the addition of freshly activated 4Å molsieves. After stirring for 15 minutes, the mixture was cooled down to -78 °C and a cooled solution (10 °C) of ZnCl_2 in THF (2.43 mL, 1M) was added dropwise over ten minutes. The mixture was allowed to stir overnight at rt after which it was filtered over Celite®, concentrated *in vacuo* and purified by silica column chromatography (0 to 20% EtOAc in PE) to afford **35** (413 mg, 0.625 mmol, 39% over two steps) as a colorless oil. R_f = 0.48 (40% EtOAc in PE); IR (neat): 3480, 3000, 2907, 1611, 1511; ^1H NMR (400 MHz, CDCl_3) δ = 7.30 (dd, J = 8.5, 4.8 Hz, 6H, H_{arom}), 7.08 (d, J = 8.6 Hz, 2H, H_{arom}), 6.98 – 6.77 (m, 8H, H_{arom}), 4.87 (dd, J = 15.4, 11.2 Hz, 2H, CH_2 PMB), 4.76 (dd, J = 10.7, 6.4 Hz, 2H, CH_2 PMB), 4.63 – 4.42 (m, 4H, 2 x CH_2 PMB), 4.32 (d, J = 7.3 Hz, 1H, H-1), 3.80 (s, 6H, 2 x CH_3 PMB), 3.79 (s, 3H, CH_3 PMB), 3.79 (s, 3H, CH_3 PMB), 3.70 (m, 2H, H-6), 3.62 – 3.50 (m, 3H, H-2, H-3, H-4), 3.45 (dd, J = 9.9, 4.1 Hz, 1H, H-5), 2.41 (s, 1H, OH). ^{13}C NMR (101 MHz, CDCl_3) δ = 159.5 (C_{q} Arom), 159.3 (C_{q} Arom), 159.3 (C_{q} Arom), 130.9 (C_{q} Arom), 130.4 (C_{q} Arom), 130.3 (C_{q} Arom), 130.0 (C_{H} Arom), 129.7 (C_{H} Arom), 129.7 (C_{H} Arom), 129.6 (C_{H} Arom), 129.3 (C_{q} Arom), 114.0 (C_{H} Arom), 113.9 (C_{H} Arom), 113.9 (C_{H} Arom), 101.5 (C-1), 84.3 (C-2), 77.4 (C-3), 75.3 (C-4), 74.9 (CH_2 PMB), 74.7 (C-5), 73.2 (CH_2 PMB), 70.8 (CH_2 PMB), 68.5 (C-6), 55.4 (4 x CH_3 PMB); HRMS m/z calcd for $[\text{C}_{38}\text{H}_{44}\text{O}_{10} + \text{NH}_4]^+$: 678.32727; found: 678.33019.



(4-Methoxybenzyl)-2-O-(2-[2-(2-(methylthio)ethoxy)ethoxy]ethyl)-3,4,6-Tetra-O-(4-methoxybenzyl)-β-D-glucopyranoside, **36:**

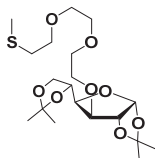
35 (333 mg, 0.504 mmol) was dissolved in dry DMF (5 mL) and cooled to 0 °C. To this solution was added NaH (60% dispersion in mineral oil, 26 mg, 0.65 mmol) portionwise followed by the addition of tosylate **31** (185 mg, 0.554 mmol). After stirring for 6 h at rt under a dry atmosphere, MeOH was added (1 mL). The mixture was then diluted with EtOAc (50 mL), transferred to a separatory funnel and washed with water (3x) and brine (3x). The organic layer was dried (Na₂SO₄) and concentrated *in vacuo*. Purification of the residue by column chromatography (0 to 30% EtOAc in PE) afforded the title compound **36** as milky oil (334 mg, 0.405 mmol, 80%). *R_f* = 0.39 (40% EtOAc in PE); IR (neat): 2999, 2864, 2835, 1612, 1512; ¹H NMR (400 MHz, CDCl₃) δ = 7.39 – 7.18 (m, 6H, H_{arom}), 7.07 (dd, *J* = 8.7, 4.8 Hz, 2H, H_{arom}), 6.92 – 6.75 (m, 8H, H_{arom}), 4.96 – 4.80 (m, 2H, CH₂ PMB), 4.78 – 4.66 (m, 2H, CH₂ PMB), 4.62 – 4.37 (m, 5H, CH₂ PMB, H-1), 4.06 (dt, *J* = 9.9, 4.6 Hz, 1H, CHH OCH₂), 3.85 (q, *J* = 5.2 Hz, 1H, CHH OCH₂), 3.81 (s, 3H, CH₃ PMB), 3.80 (s, 3H, CH₃ PMB), 3.79 (s, 3H, CH₃ PMB), 3.79 (s, 3H, CH₃ PMB), 3.74 – 3.66 (m, 2H, H-6), 3.66 – 3.53 (m, 9H, H-3, 4 x OCH₂), 3.49 (t, *J* = 9.2 Hz, 1H, H-4), 3.40 (ddd, *J* = 9.7, 5.1, 2.2 Hz, 1H, H-5), 3.29 (t, *J* = 8.3 Hz, 1H, H-2), 2.62 (t, *J* = 7.0 Hz, 2H, CH₂SMe), 2.10 (s, 3H, CH₂SMe). ¹³C NMR (101 MHz, CDCl₃) δ = 159.3 (C_q arom), 159.3 (C_q arom), 159.3 (C_q arom), 159.3 (C_q arom), 131.1 (C_q arom), 130.5 (C_q arom), 130.4 (C_q arom), 129.8 (C_H arom), 129.7 (C_H arom), 129.7 (C_H arom), 129.6 (C_H arom), 113.8 (C_H arom), 102.1 (C-1), 84.4 (C-4), 83.3 (C-2), 77.6 (C-4), 75.3 (CH₂ PMB), 74.9 (C-5), 74.7 (CH₂ PMB), 73.2 (CH₂ PMB), 72.1 (OCH₂), 70.9 (OCH₂), 70.9 (CH₂ PMB), 70.6 (OCH₂), 70.5 (OCH₂), 70.4 (OCH₂), 68.7 (C-6), 55.4 (4 x CH₃ PMB), 33.4 (CH₂SMe), 16.1 (CH₂SMe); HRMS *m/z* calcd for [C₄₅H₅₈O₁₂S + NH₄]⁺: 840.39872; found: 840.40019.



2-O-(2-[2-(2-(methylthio)ethoxy)ethoxy]ethyl)-α/β-D-glucopyranoside, **H37:**

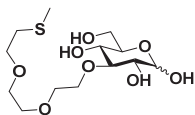
Compound **36** (241 mg, 0.293 mmol) was dissolved in a mixture of DCM/HFIP (3 mL) and to this solution were added 5 drops of 37% HCl in H₂O. The color immediately changed to dark red, and after stirring for 5 minutes the mixture was quenched upon the addition of Et₃N (500 μL, 3.57 mmol). The mixture was then concentrated *in vacuo* and redissolved in H₂O (5.8 mL), followed by the addition of a solution of MeNH₂ in MeOH (145 μL, 2M). After heating the reaction mixture for 30 minutes at 60 °C, solvents were removed under reduced pressure and the resulting residue was purified by silica column chromatography (0 to 20% MeOH in DCM) to afford fully deprotected hemiacetal **H37** (67 mg, 0.196 mmol, 67%) as a clear oil. *R_f* = 0.54 (25% MeOH in DCM); IR (neat): 3411, 2917, 2865, 1115, 1042; ¹H NMR (400 MHz, CD₃OD) δ = 5.29 (d, *J* = 3.5 Hz, 1H, H-1α), 4.53 (d, *J* = 7.8 Hz, 1H, H-1β), 4.04 (dt, *J* = 11.3, 4.4 Hz, 1H, CHH H-6), 3.89 – 3.70 (m, 8H), 3.70 – 3.59 (m, 19H), 3.42 – 3.32 (m, 1H, H-3β), 3.30 – 3.20 (m, 2H), 3.03 – 2.86 (m, 1H, H-2β), 2.68 (t, *J* = 6.8 Hz, 4H, 2 x CH₂SMe), 2.13 (s, 6H, 2 x

CH_2SMe). ^{13}C NMR (101 MHz, CD_3OD) δ = 98.1 (C-1 β), 91.8 (C-1 α), 85.1 (C-1 β), 82.4, 77.9, 77.5, 73.9, 72.8, 72.6, 71.9, 71.9, 71.6, 71.6, 71.5, 71.5, 71.4, 71.2, 71.1, 71.0, 62.8 (C-6 α), 62.7 (C-6 β), 34.2 (2 x CH_2SMe), 15.9 (2 x CH_2SMe); HRMS m/z calcd for $[\text{C}_{13}\text{H}_{26}\text{O}_8\text{S} + \text{Na}]^+$: 365.12406; found: 365.12513.



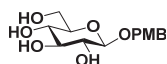
1,2:5,6-di-O-isopropylidene-3-O-(2-[2-(2-(methylthio)ethoxy)ethoxy]ethyl)- α -D-glucopyranose, **38:**

To a cooled solution of diacetone glucose (200 mg, 0.768 mmol) in dry DMF (8 mL) was added 60% NaH in mineral oil (80.0 mg, 2.00 mmol). After stirring for 5 min, tosylate **32** was added and the mixture was overnight. After quenching the reaction with MeOH (1 mL), Et_2O (50 mL) was added and the reaction was transferred to a separatory funnel. After washing with water (1x), aq. NaHCO_3 (1x) and brine (1x), layers were separated and the organic layer was dried (Na_2SO_4) and concentrated *in vacuo*. Purification of the residue over silica (0–50% EtOAc in PE) gave **38** as a clear oil. (294 mg, 0.700 mmol, 91%). R_f = 0.73 (50% EtOAc in PE); IR (neat): 2985, 2871, 1456, 1371, 1058; ^1H NMR (400 MHz, CDCl_3) δ = 5.87 (d, J = 3.8 Hz, 1H, H-1), 4.57 (d, J = 3.6 Hz, 1H, H-2), 4.31 (dt, J = 7.8, 5.9 Hz, 1H, H-5), 4.14–4.10 (m, 1H, H-3), 4.09–4.05 (m, 1H, CHH H-6), 3.99 (dd, J = 8.6, 5.8 Hz, 1H, CHH H-6), 3.92 (d, J = 3.1 Hz, 1H, H-4), 3.79–3.71 (m, 2H, OCH_2), 3.68–3.60 (m, 8H, 4 x OCH_2), 2.69 (t, J = 6.9 Hz, 2H, CH_2SMe), 2.14 (s, 3H, CH_2SMe), 1.49 (d, J = 2.7 Hz, 3H, CH_3 isopropylidene), 1.42 (s, 3H, CH_3 isopropylidene), 1.34 (s, 3H, CH_3 isopropylidene), 1.31 (d, J = 3.6 Hz, 3H, CH_3 isopropylidene). ^{13}C NMR (101 MHz, CDCl_3) δ = 111.9 (C_q isopropylidene), 109.0 (C_q isopropylidene), 105.4 (C-1), 82.8 (C-2), 82.7 (C-4), 81.2 (C-3), 72.7 (C-5), 70.8 (OCH_2), 70.7 (OCH_2), 70.6 (OCH_2), 70.5 (OCH_2), 70.28, 67.3 (C-6), 33.5 (CH_2SMe), 27.0 (CH_3 isopropylidene), 27.0 (CH_3 isopropylidene), 26.4 (CH_3 isopropylidene), 25.6 (CH_3 isopropylidene), 16.2 (CH_2SMe); HRMS m/z calcd for $[\text{C}_{19}\text{H}_{34}\text{O}_8\text{S} + \text{NH}_4]^+$: 440.23126; found: 440.23203.

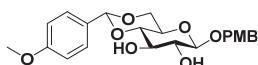


3-O-(2-[2-(2-(methylthio)ethoxy)ethoxy]ethyl)- α/β -D-glucopyranoside, **H40:**

To a suspension of compound **38** in H_2O , was added Amberlite[®] IR-120 H^+ and this mixture was stirred for 24 h at 60 $^\circ\text{C}$ after which it was filtered and concentrated *in vacuo*. Purification of the residue over silica (0 to 10% MeOH in DCM) afforded the title compound **H40** as a clear oil (α/β = 1:1, 81 mg, 0.24 mmol, 46%). R_f = 0.32 (10% MeOH in DCM); IR (neat): 3369, 2918, 2873, 1104, 1077; ^1H NMR (400 MHz, CD_3OD) δ = 5.08 (d, J = 3.6 Hz, 1H, H-1 α), 4.47 (d, J = 7.7 Hz, 1H, H-1 β), 4.24–3.13 (m, 40H), 2.67 (t, J = 6.9 Hz, 4H, 2 x CH_2SMe), 2.11 (s, 6H, 2 x CH_2SMe). ^{13}C NMR (101 MHz, CD_3OD) δ = 98.1 (C-1 β), 94.0 (C-1 α), 87.6, 84.5, 77.8, 76.1, 73.7, 73.1, 73.0, 72.2, 72.1, 71.6, 71.4, 71.4, 71.3, 71.1, 62.8 (C-6 β), 62.6 (C-6 α), 34.2 (2x OCH_2SMe), 15.9 (2x OCH_2SMe); HRMS m/z calcd for $[\text{C}_{13}\text{H}_{26}\text{O}_8\text{S} + \text{Na}]^+$: 365.12406; found: 365.12434.

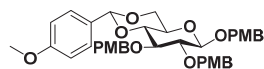


(4-Methoxybenzyl)-β-D-glucopyranoside, 41: To a solution of 2,3,4,6-tetra-*O*-acetyl-α-D-glucopyranosyl bromide (3.00 g, 7.30 mmol) and 4-methoxybenzyl alcohol (5.04 g, 36.5 mmol) in dry Et₂O (75 mL) were added freshly activated 4Å molsieves. The resulting mixture was allowed to stir for ten minutes, after which Ag₂CO₃ (6.00 g, 21.8 mmol) and I₂ (1.85 g, 7.30 mmol) were added. After stirring an additional 24 h under a dinitrogen atmosphere at rt in the dark, the reaction mixture was filtered over Celite®, diluted with EtOAc (200 mL), washed with 1M Na₂S₂O₃ (3x), aq. NaHCO₃ (3x) and brine (3x). The organic layer was dried (Na₂SO₄) and concentrated *in vacuo*. Purification of the residue by silica column chromatography (20% EtOAc in DCM) afforded (4-methoxybenzyl)-2,3,4,6-tetra-*O*-acetyl-β-D-glucopyranoside (2.39 g), which was then redissolved in dry MeOH (70 mL) followed by the addition of a catalytic amount of NaOMe. The resulting mixture was allowed to stir for 4 h, after which Amberlite® IR-120 H⁺ was added until neutral pH, filtered and concentrated *in vacuo*, affording the title compound **41** as a clear oil (1.57 g, 5.23 mmol, 72% over two steps). *R*_f = 0.57 (20% MeOH in DCM); IR (neat): 3335, 2924, 1612, 1027, 819; ¹H NMR (400 MHz, CD₃OD) δ = 7.32 (d, *J* = 8.6 Hz, 2H, H_{arom}), 6.95 – 6.71 (m, 2H, H_{arom}), 4.85 (d, *J* = 18.0 Hz, 1H, CHH PMB), 4.58 (d, *J* = 11.3 Hz, 1H, CHH PMB), 4.31 (d, *J* = 7.8 Hz, 1H, H-1), 3.89 (dd, *J* = 12.0, 2.2 Hz, 1H, CHH H-6), 3.68 (dd, *J* = 12.0, 5.5 Hz, 1H, CHH H-6), 3.42 – 3.14 (m, 4H, H-2, H-3, H-4, H-5). ¹³C NMR (101 MHz, CD₃OD) δ = 160.8 (C_q Arom), 130.9 (C_H Arom), 130.9 (C_q Arom), 114.6 (C_H Arom), 102.9 (C-1), 78.0 (C-3), 78.0 (C-4), 75.1 (C-2), 71.7 (C-5), 71.4 (CH₂ PMB), 62.8 (C-6), 55.7 (CH₃ PMB). HRMS *m/z* calcd for [C₁₄H₂₀O₇ + Na]⁺: 365.12406; found: 365.12513.



(4-Methoxybenzyl)-4,6-*O*-(4-methoxybenzylidene)-β-D-glucopyranoside, 42: To a solution of **41** (309 mg, 1.03 mmol) in dry DMF (5 mL) were added 4-methoxybenzaldehyde dimethyl acetal (135 μL, 0.793 mmol) and *p*-TsOH.H₂O (10 mg, 0.05 mmol). The resulting reaction mixture was heated at 60 °C for 16, after which it was concentrated *in vacuo*. Saturated aqueous NaHCO₃ (50 mL) was added, and the mixture was further diluted with EtOAc (200 mL) and transferred to a separatory funnel. After washing with aq. NaHCO₃ (3x), water (3x) and brine (3x), layers were separated, the organic layer was dried (Na₂SO₄) and concentrated *in vacuo*. Compound **43** (382 mg, 0.910 mmol, 89%) was obtained after silica column chromatography (0 to 10% MeOH in DCM) as a white powder. *R*_f = 0.48 (10% MeOH in DCM); IR (neat): 3480, 2869, 1612, 1516, 1244; ¹H NMR (400 MHz, CD₃CN) δ = 7.39 (d, *J* = 8.8 Hz, 2H, H_{arom}), 7.31 (d, *J* = 8.7 Hz, 2H, H_{arom}), 7.00 – 6.86 (m, 4H, H_{arom}), 5.50 (s, 1H, CH PMB acetal), 4.76 (d, *J* = 11.5 Hz, 1H, CHH PMB), 4.55 (d, *J* = 11.5 Hz, 1H, CHH PMB), 4.43 (d, *J* = 7.8 Hz, 1H, H-1), 4.24 (dd, *J* = 10.3, 4.6 Hz, 1H, CHH H-6), 3.78 (s, 6H, 2 x CH₃ OMe) 3.72 (t, *J* = 9.9 Hz, 1H, CHH H-6), 3.62 – 3.50 (m, 1H, H-3), 3.49 – 3.33 (m, 2H, H-4, H-5), 3.26 (td, *J* = 8.1, 3.7 Hz, 1H, H-2). ¹³C NMR (101 MHz, CD₃CN) δ = 161.1 (C_q Arom), 160.4 (C_q Arom), 131.3 (C_q Arom), 130.7 (C_H Arom), 128.6 (C_H Arom), 114.6 (C_H Arom), 114.4 (C_H Arom), 103.4 (C-1), 102.1 (CH PMB acetal), 81.6 (C-4), 75.6 (C-2), 74.3 (C-3), 71.4 (CH₂

PMB), 69.3 (C-6), 67.2 (C-5), 55.9 (2 x CH₃ PMB). HRMS *m/z* calcd for [C₂₂H₂₆O₈ + H]⁺: 419.17004; found: 419.17101.



(4-Methoxybenzyl)-2,3-di-O-(4-methoxybenzyl)-4,6-O-(4-methoxybenzylidene)-β-D-glucopyranoside, 43:

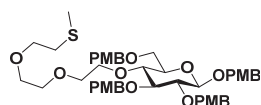
To a cooled solution (0 °C) of *p*-methoxy benzylidene protected **42** (377 mg, 0.900 mmol) in dry DMF (9 mL) was slowly added NaH (60% dispersion in mineral oil, 80.0 mg, 2.00 mmol) followed by the addition of 4-methoxybenzyl chloride (255 μL, 1.89 mmol). After stirring for 5 h under a dinitrogen atmosphere, the reaction was quenched upon the addition of MeOH (3 mL). The mixture was further diluted with Et₂O (200 mL) and transferred to a separatory funnel, washed with water (1x), aq. NaHCO₃ (1x) and brine (1x). The organic layer was dried over Na₂SO₄ and concentrated *in vacuo*. Purification by silica column chromatography (0 to 20% EtOAc in PE) yielded the title compound **43** as a clear oil (447 mg, 0.680 mmol, 76%). *R_f* = 0.74 (40% EtOAc in PE); IR (neat): 3480, 2869, 1612, 1516, 1244; ¹H NMR (400 MHz, CDCl₃) δ = 7.43 (d, *J* = 8.9 Hz, 2H, H_{arom}), 7.36 – 7.18 (m, 5H, H_{arom}), 7.00 – 6.78 (m, 6H, H_{arom}), 5.54 (s, 1H, CH benzylidene), 4.89 (d, *J* = 11.4 Hz, 1H, *CHH* PMB), 4.82 (dd, *J* = 10.8, 5.6 Hz, 2H, CH₂ PMB), 4.71 (dd, *J* = 16.0, 10.7 Hz, 2H, CH₂ PMB), 4.65 – 4.57 (m, 2H, *CHH* PMB, H-1), 4.37 (dd, *J* = 10.5, 5.0 Hz, 1H, *CHH* H-6), 3.82 (s, 6H, 2 x CH₃ PMB), 3.82 (s, 3H, CH₃ PMB), 3.80 (s, 3H, CH₃ PMB), 3.69 (p, *J* = 9.1 Hz, 2H, H-3, H-4), 3.49 (t, *J* = 7.9 Hz, 1H, H-2), 3.40 (td, *J* = 9.5, 5.0 Hz, 1H, H-5). ¹³C NMR (101 MHz, CDCl₃) δ = 160.1 (C_q Arom), 159.5 (C_q Arom), 159.3 (C_q Arom), 159.3 (C_q Arom), 130.8 (C_q Arom), 130.6 (C_q Arom), 129.9 (C_H Arom), 129.8 (C_H Arom), 129.8 (C_H Arom), 129.3 (C_q Arom), 127.4 (C_H Arom), 113.9 (C_H Arom), 113.8 (C_H Arom), 113.7 (C_H Arom), 103.0 (C-1), 101.2 (CH PMB acetal), 81.9 (C-2), 81.5 (C-3), 80.7 (C-4), 75.1 (CH₂ PMB), 74.9 (CH₂ PMB), 71.4 (CH₂ PMB), 68.9 (C-6), 66.2 (C-5), 55.4 (3 x CH₃ PMB), 55.3 (CH₃ PMB acetal); HRMS *m/z* calcd for [C₃₈H₄₂O₁₀ + Na]⁺: 681.26702; found: 681.26706.



(4-Methoxybenzyl)-2,3,6-tri-O-(4-methoxybenzyl)-β-D-glucopyranoside, 44:

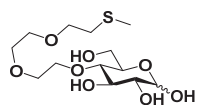
Fully protected glycoside **43** (400 mg, 0.610 mmol) was dissolved in DMF (12 mL) and to this solution were added freshly activated 4Å molsieves and fresh NaCNBH₃ (385 mg, 6.13 mmol). After stirring for 15 minutes the solution was cooled to 0 °C and a precooled solution (0 °C) of trifluoroacetic acid (1.2 mL) in DMF (3 mL) on 4Å molsieves was then added dropwise over 15 minutes. The reaction mixture was maintained at rt for 48 h at rt and filtered over Celite®, diluted with EtOAc (100 mL) and transferred to a separatory funnel. After washing with water (1x), aq. NaHCO₃ (1x) and brine (1x), the organic layer was dried (Na₂SO₄) and concentrated *in vacuo*. Purification of the residue by column chromatography over silica (0 to 30% EtOAc in PE) afforded **44** (385 mg, 0.580 mmol, 95%) as a clear oil. *R_f* = 0.48 (40% EtOAc in PE); IR (neat): 3480, 3000, 2907, 1612, 1512; ¹H NMR (400 MHz, CD₃Cl₃) δ = 7.42 – 7.16 (m, 8H, H_{arom}), 6.87 (tdd, *J* = 8.9, 4.7, 2.6 Hz, 8H, H_{arom}), 4.92 – 4.82 (m, 3H, *CHH* PMB, CH₂ PMB),

4.67 – 4.53 (m, 5H, CHH PMB, 2 x CH₂ PMB), 4.49 (d, *J* = 7.2 Hz, 1H, H-1), 3.82 (s, 3H, CH₃ PMB), 3.81 (s, 3H, CH₃ PMB), 3.81 (s, 3H, CH₃ PMB), 3.80 (s, 3H, CH₃ PMB), 3.79 – 3.66 (m, 2H, H-6), 3.59 – 3.51 (m, 1H, H-5), 3.48 – 3.36 (m, 3H, H-2, H-3, H-4). ¹³C NMR (101 MHz, CDCl₃) δ = 159.4 (C_q Arom), 152.7 (C_q Arom), 152.5 (C_q Arom), 130.7 (C_H Arom), 130.0 (C_H Arom), 129.9 (C_H Arom), 129.8 (C_H Arom), 129.5 (C_H Arom), 114.1 (C_H Arom), 113.9 (C_H Arom), 102.5 (C-1), 83.8 (C-4), 81.6 (C-2), 75.0 (CH₂ PMB), 74.5 (CH₂ PMB), 74.2 (C-3), 73.4 (CH₂ PMB), 71.7 (C-5), 71.1 (CH₂ PMB), 70.2 (C-6), 55.4 (4 x CH₃ PMB); HRMS *m/z* calcd for [C₃₈H₄₄O₁₀ + NH₄]⁺: 678.32727; found: 678.33206.



(4-Methoxybenzyl)-2-O-(2-[2-(2-(methylthio)ethoxy)ethoxy]ethyl)-3,6-tri-O-(4-methoxybenzyl)-β-D-glucopyranoside, 45: Compound **44** (300 mg, 0.454 mmol)

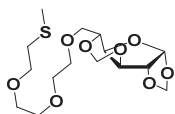
was dissolved in dry DMF and cooled to (0 °C) after which 60% NaH in mineral oil (31 mg, 0.77 mmol) was added. This mixture was allowed to stir for 5 min, after which tosylate **32** (177 mg, 0.530 mmol) was added dropwise. The reaction was allowed to stir for 6 h, after which it was quenched upon the addition of MeOH (2 mL), diluted with Et₂O and transferred to a separatory funnel. After washing with aq. NaHCO₃ (1x), water (1x) and brine (1x), layers were separated, the organic layer dried (Na₂SO₄) and concentrated *in vacuo*. Purification of the residue by column chromatography (0 to 40% EtOAc in PE) afforded the title compound **45** as a clear oil (291 mg, 0.354 mmol, 78%). *R_f* = 0.38 (40% EtOAc in PE); IR (neat): 2998, 2907, 2836, 1612, 1513; ¹H NMR (400 MHz, CDCl₃) δ = 7.36 – 7.18 (m, 8H, H_{arom}), 6.94 – 6.79 (m, 8H, H_{arom}), 4.97 – 4.50 (m, 8H, 4 x CH₂ PMB), 4.46 (d, *J* = 7.8 Hz, 1H, H-1), 3.95 (dt, *J* = 9.8, 4.5 Hz, 1H, CHH OCH₂), 3.81 – 3.74 (m, 1H, CHH H-6), 3.76 – 3.63 (m, 3H, CHH H-6, 2 x CHH OCH₂), 3.65 – 3.50 (m, 8H, H-5, CHH OCH₂, 3 x OCH₂), 3.46 – 3.38 (m, 3H, H-2, H-3, H-4), 2.66 (t, *J* = 6.9 Hz, 2H, CH₂SMe), 2.12 (s, 3H, CH₂SMe). ¹³C NMR (101 MHz, CDCl₃) δ = 159.7 (C_q Arom), 159.4 (C_q Arom), 131.1 (C_q Arom), 130.8 (C_q Arom), 130.6 (C_q Arom), 130.0 (C_H Arom), 129.8 (C_H Arom), 129.5 (C_H Arom), 113.9 (C_H Arom), 113.8 (C_H Arom), 102.5 (C-1), 84.3 (C-5), 82.0 (C-2), 78.7 (C-3), 75.4 (CH₂ PMB), 75.0 (C-4), 74.6 (CH₂ PMB), 73.2 (CH₂ PMB), 72.2 (OCH₂), 71.0 (CH₂ PMB), 70.9 (OCH₂), 70.7 (OCH₂), 70.6 (OCH₂), 70.4 (CH₂SMe), 68.8 (C-6), 33.5 (4 x CH₃ PMB), 16.2 (CH₂SMe). HRMS *m/z* calcd for [C₄₅H₅₈O₁₂S + NH₄]⁺: 840.39872; found: 840.40276.



4-O-(2-[2-(2-(methylthio)ethoxy)ethoxy]ethyl)-α/β-D-glucopyranoside, H46: Compound **45** (108 mg, 0.131 mmol) was

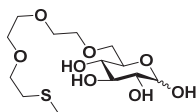
dissolved in a mixture of DCM/HFIP (1:1, 2 mL) and to this solution was added a catalytic amount of 37% HCl (4 drops). The mixture slowly turned red to deep purple in 30 minutes, after which it was quenched with Et₃N (0.5 mL) and concentrated *in vacuo*. The crude was redissolved in MeOH, Amberlite IR-120 H⁺ was added and the mixture was stirred for 5 minutes, filtered and concentrated. Purification of the resulting residue over silica (0 to 15% MeOH in DCM) afforded the title compound **H46** as a clear oil

(13 mg, 0.038 mmol, 29%). $R_f = 0.57$ (20% MeOH in DCM); IR (neat): 3370, 2918, 2873, 1104, 1077; ^1H NMR (400 MHz, CD_3OD) $\delta = 5.09$ (d, $J = 3.7$ Hz, 1H, H-1 α), 4.45 (d, $J = 7.7$ Hz, 1H, H-1 β), 4.02 – 3.58 (m, 28H), 3.47 (t, $J = 8.9$ Hz, 1H, H-3 β), 3.29 – 3.19 (m, 2H), 3.13 (dd, $J = 9.2, 7.9$ Hz, 1H, H-2 β), 2.68 (t, $J = 6.8$ Hz, 4H, 2 x OCH_2SMe), 2.13 (s, 6H, 2 x OCH_2SMe). ^{13}C NMR (100 MHz, CD_3OD) $\delta = 98.2$ (C-1 β), 93.9 (C-1 α), 80.5, 80.3, 78.2, 77.0, 76.3, 75.0, 73.9, 72.9, 72.0, 71.7, 71.5, 71.2, 62.5 (C-1 β), 62.4 (C-1 α), 34.3 (2x OCH_2SMe), 15.9 (OCH_2SMe); HRMS m/z calcd for $[\text{C}_{13}\text{H}_{26}\text{O}_8\text{S} + \text{Na}]^+$: 365.12406; found: 365.12513.



1,2:3,5-bis(O-methylidene)-6-O-(2-[2-(2-

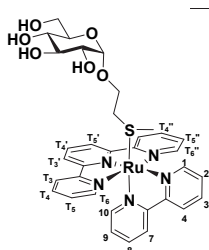
(methylthio)ethoxy)ethoxy]ethyl)- α -D-glucopyranose, **49:** To a cooled (0 $^\circ\text{C}$) solution of 1,2:3,5-bis(O-methylidene)- α -D-glucopyranose (206 mg, 1.00 mmol) in dry DMF (10 mL) was added 60% NaH in mineral oil (57 mg, 1.42 mmol). After 10 minutes, **19** (385 mg, 1.15 mmol) was added dropwise and the resulting mixture was stirred for 3 hr at rt, after which it was quenched upon the addition of MeOH (2 mL). The reaction mixture was extracted with Et_2O (50 mL), washed with aq. NaHCO_3 (2x), water (2x) and brine (2x). Layers were separated, the organic layer was dried (Na_2SO_4) and concentrated *in vacuo*. The resulting residue was then purified by silica column chromatography (0 to 60% EtOAc in PE) affording **49** as a colorless oil. $R_f = 0.57$ (50% EtOAc in PE); IR (neat): 2867, 1455, 1082, 1184, 1058; ^1H NMR (400 MHz, CDCl_3) $\delta = 6.03$ (d, $J = 3.8$ Hz, 1H, H-1), 5.12 (d, $J = 5.9$ Hz, 1H, CHH methylene), 5.08 (s, 1H, CH_2 methylene), 5.03 (s, 1H, CH_2 methylene), 4.78 (d, $J = 6.0$ Hz, 1H, CHH methylene), 4.46 (d, $J = 3.9$ Hz, 1H, H-2), 4.37 (d, $J = 3.0$ Hz, 1H, H-3), 4.14 (t, $J = 4.4$ Hz, 1H, H-5), 4.03 (d, $J = 2.7$ Hz, 1H, H-4), 3.85 (dd, $J = 10.5, 3.9$ Hz, 1H, CHH H-6), 3.75 (dd, $J = 10.5, 4.8$ Hz, 1H, CHH H-6), 3.64 (dd, $J = 11.8, 5.6$ Hz, 10H, 4 x OCH_2), 2.69 (t, $J = 6.9$ Hz, 2H, CH_2SMe), 2.14 (s, 3H, CH_2SMe). ^{13}C NMR (101 MHz, CDCl_3) $\delta = 104.4$ (C-1), 96.6 (CH_2 methylene), 88.2 (CH_2 methylene), 83.9 (C-2), 76.8 (C-3), 76.1 (C-4), 72.5 (C-6), 71.6 (C-5), 71.0 (OCH_2), 70.7 (OCH_2), 70.7 (OCH_2), 70.7 (OCH_2), 70.4 (OCH_2), 33.5 (OCH_2SMe), 16.2 (OCH_2SMe). HRMS m/z calcd for $[\text{C}_{15}\text{H}_{26}\text{O}_8\text{S} + \text{H}]^+$: 367.14211; found: 367.14295.



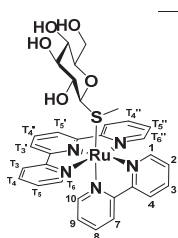
6-O-(2-[2-(2-(methylthio)ethoxy)ethoxy]ethyl)- α/β -D-
glucopyranoside, **H50:** Compound **49** was dissolved in 2M HCl (5 mL) and this mixture was heated at 100 $^\circ\text{C}$ for 1 h after which the reaction was neutralized with 1M NaOH (10 mL) and concentrated *in vacuo*.

Purification of the residu by silica column chromatography (0 to 20% MeOH in DCM) afforded **H50** as a colorless oil (101 mg, 0.295 mmol, 70%). $R_f = 0.50$ (20% MeOH in DCM); IR (neat): 3368, 2917, 2874, 1427, 1078; ^1H NMR (500 MHz, CD_3OD) $\delta = 5.13$ (d, $J = 3.7$ Hz, 1H, H-1 α), 4.52 (d, $J = 7.7$ Hz, 1H, H-1 β), 4.06 – 3.94 (m, 4H), 3.91 – 3.87 (m, 1H, CHH H-6 α/β), 3.86 – 3.77 (m, 2H), 3.75 – 3.64 (m, 20H, 10 x OCH_2), 3.49 – 3.38 (m, 3H), 3.41 (ddd, $J = 9.8, 8.8, 6.0$ Hz, 2H), 3.34 – 3.30 (m, 1H), 3.25 – 3.22 (m, 2H), 2.72 (t, $J = 6.8$ Hz, 4H, 2 x CH_2SMe), 2.16 (s, 6H, 2 x CH_2SMe). ^{13}C NMR (126 MHz, CD_3OD) $\delta = 98.1$ (C-1 β), 94.0 (C-

1 α), 87.6, 84.4, 77.8, 76.1, 73.6, 73.0 (OCH₂), 73.0 (OCH₂), 73.0, 72.1 (OCH₂), 72.1 (OCH₂), 71.6 (OCH₂), 71.6 (OCH₂), 71.4 (OCH₂), 71.4 (OCH₂), 71.3, 71.1 (OCH₂), 71.1 (OCH₂), 62.8 (C-6 α / β), 62.7 (C-6 α / β), 34.2 (2 x CH₂SMe), 15.9 (2 x CH₂SMe). HRMS *m/z* calcd for [C₁₃H₂₆O₈S + Na]⁺: 365.12406; found: 365.12519.

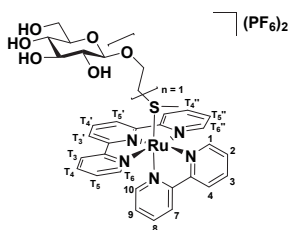


[Ru(tpy)(bpy)(13)](PF₆)₂, [1](PF₆)₂: [Ru(tpy)(bpy)Cl]Cl (63 mg, 0.112 mmol) and **13** (93 mg, 0.366 mmol) were dissolved in deoxygenated H₂O (18 mL) and this mixture was heated at 80 °C for 16 h, after which it was concentrated *in vacuo*. Purification of the residue by silica column chromatography (100/0/0 to 100/80/20 aceton/water/aq. KPF₆), followed by purification over Sephadex LH-20 (MeOH), afforded the title compound as a red solid (44 mg, 42.4 μ mol, 39%). *R_f* = 0.69 (100/80/20 aceton/water/aq. KPF₆); ¹H NMR (400 MHz, CD₃OD) δ = 9.85 (d, *J* = 5.7 Hz, 1H, 1), 8.81 (d, *J* = 8.0 Hz, 1H, 4), 8.77 (d, *J* = 8.2 Hz, 2H, T₃', T₅'), 8.62 (d, *J* = 8.1 Hz, 2H, T₆, T₆'), 8.58 (d, *J* = 7.8 Hz, 1H, 10), 8.44 – 8.34 (m, 2H, T₄', 3), 8.18 – 8.04 (m, 3H, T₅, T₅'', 2), 7.92 (td, *J* = 7.8, 1.6 Hz, 1H, 9), 7.79 (d, *J* = 5.6 Hz, 2H, T₃, T₃''), 7.45 (ddd, *J* = 7.3, 5.6, 1.4 Hz, 2H, T₄, T₄''), 7.34 – 7.26 (m, 1H, 7), 7.23 (ddd, *J* = 7.3, 5.7, 1.3 Hz, 1H, 8), 4.69 (d, *J* = 3.7 Hz, 1H, H-1), 3.79 – 3.68 (m, 2H, CHH H-6, CHH OCH₂), 3.64 – 3.34 (m, 5H, CHH H-6, CHH OCH₂, H-2, H-3, H-5), 3.29 – 3.20 (m, 1H, H-4), 2.12 – 1.91 (m, 2H, CH₂SMe), 1.39 (s, 3H, CH₂SMe). ¹³C NMR (101 MHz, CD₃OD) δ = 159.3 (C_q Arom), 158.7 (C_q Arom), 158.1 (C_q Arom), 157.9 (C_q Arom), 154.3 (C_H T₃, T₃''), 153.5 (C_H 1), 150.8 (C_H 7), 140.1 (C_H T₅, T₅''), 139.4 (C_H T₄'), 139.3 (C_H 9), 138.3 (C_H 3), 129.8 (C_H T₄, T₄''), 129.4 (C_H 2), 128.4 (C_H 8), 126.2 (C_H T₆), 126.2 (C_H T₆''), 125.9 (C_H 4), 125.5 (C_H T₃', T₅'), 125.1 (C_H 10), 100.2 (C-1), 75.1 (C-5), 74.3 (C-3), 73.1 (C-2), 71.7 (C-4), 64.8 (OCH₂), 62.8 (C-6), 35.9 (CH₂SMe), 14.8 (CH₂SMe); HRMS *m/z* calcd for [M]²⁺: 372.57485; found: 372.57558; Elemental analysis calcd (%) for [1](PF₆)₂·2MeOH: C, 39.35; H, 4.13; N, 6.37; found: 41.45; H, 4.18; N, 6.35.



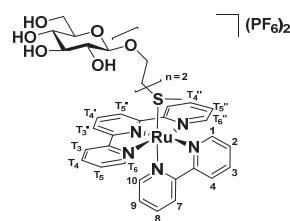
[Ru(tpy)(bpy)(15)](PF₆)₂, [2](PF₆)₂: The title compound was synthesized analogous according to the procedure described for [1](PF₆)₂ using [Ru(tpy)(bpy)Cl]Cl (200 mg, 0.357 mmol) and **15** (100 mg, 0.476 mmol) in H₂O (60 mL) affording [2](PF₆)₂, as an orange powder (98.4 mg, 99.3 μ mol, 28%). *R_f* = 0.15 (100/80/20 acetone/water/aq. KPF₆); ¹H NMR (400 MHz, CD₃OD) δ = 10.01 (d, *J* = 4.1 Hz, 1H, 1), 8.82 (dt, *J* = 8.2, 1.1 Hz, 1H, 4), 8.76 (ddd, *J* = 8.2, 4.3, 0.9 Hz, 2H, T₃', T₅'), 8.66 – 8.56 (m, 3H, T₆, T₆'', 10), 8.43 – 8.36 (m, 2H, T₄', 3), 8.13 – 8.02 (m, 3H, T₅, T₅'', 2), 7.93 (ddd, *J* = 8.2, 7.0, 2.1 Hz, 1H, 9), 7.86 (ddd, *J* = 5.5, 1.5, 0.7 Hz, 1H, T₃), 7.80 (ddd, *J* = 5.5, 1.5, 0.7 Hz, 1H, T₃''), 7.44 (ddt, *J* = 7.8, 5.5, 1.3 Hz, 2H, T₄, T₄''), 7.27 – 7.18 (m, 2H, 7, 8), 3.52 (d, *J* = 9.1 Hz, 1H, H-1), 3.43 (t, *J* = 3.6 Hz, 2H, H-6), 3.02 – 2.90 (m, 3H, H-2, H-3, H-4), 2.48 (d, *J* = 8.7 Hz, 1H, H-5), 1.39 (s, 3H, SMe). ¹³C NMR (101

MHz, CD₃OD) δ = 163.4 (C_q Arom), 160.7 (C_q Arom), 160.0 (C_q Arom), 159.8 (C_q Arom), 158.9 (C_q Arom), 158.2 (C_q Arom), 158.0 (C_q Arom), 154.5 (C_H T₃), 154.3 (C_H T₃''), 153.8 (C_H 1), 150.4 (C_H 7), 140.2 (C_H T₅), 140.1 (C_H T₅''), 139.6 (C_H T₄'), 139.5 (C_H 9), 138.2 (C_H 3), 129.7 (C_H T₄), 129.6 (C_H T₄''), 129.0 (C_H 2), 128.5 (C_H 8), 126.1 (C_H 4), 126.0 (C_H T₆), 125.9 (C_H T₆'') 125.3 (C_H T₃', T₅'), 125.1 (C_H 10), 85.7 (C-1), 82.7 (C-5), 78.6 (C-2), 71.3 (C-3), 70.0 (C-4), 61.8 (C-6), 9.0 (*SMe*). HRMS *m/z* calcd for [M]²⁺: 350.56175; found: 350.56289. Elemental analysis calcd (%) for [2](PF₆)₂: C, 38.18; H, 3.30; N, 6.96; found: 38.93; H, 3.39; N, 7.19.



[Ru(tpy)(bpy)(24)](PF₆)₂, [3](PF₆)₂: The title compound was synthesized analogous according to the procedure described for [1](PF₆)₂ using [Ru(tpy)(bpy)Cl]Cl (101 mg, 0.180 mmol) and **24** (75.7 mg, 0.298 mmol) in H₂O (30 mL) affording the title compound as a hygroscopic orange powder (73.3 mg, 70.7 μ mol, 39%). *R_f* = 0.36 (100/10/20 acetone/water/aq. KPF₆); ¹H NMR (500 MHz, CD₃OD) δ = 9.85 (dd, *J* = 5.6, 0.7 Hz,

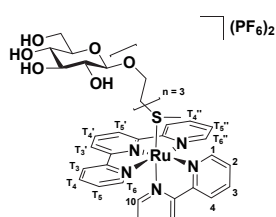
1H, 1), 8.81 (dd, *J* = 17.9, 8.2 Hz, 3H, 4, T₃', T₅'), 8.63 (d, *J* = 8.1 Hz, 2H, T₆, T₆''), 8.59 (d, *J* = 8.2 Hz, 1H, 10), 8.45 – 8.36 (m, 2H, T₄', 3), 8.14 – 8.04 (m, 3H, T₅, T₅'', 2), 7.93 (td, *J* = 7.8, 1.5 Hz, 1H, 9), 7.80 (td, *J* = 5.4, 0.8 Hz, 2H, T₃, T₃''), 7.45 (ddd, *J* = 7.6, 5.5, 1.3 Hz, 2H, T₄, T₄''), 7.30 (ddd, *J* = 5.7, 1.5, 0.7 Hz, 1H, 7), 7.23 (ddd, *J* = 7.2, 5.7, 1.3 Hz, 1H, 8), 4.15 (d, *J* = 7.8 Hz, 1H, H-1), 3.88 – 3.76 (m, 2H, CHH H-6, CHH OCH₂), 3.57 (ddd, *J* = 12.7, 11.5, 5.6 Hz, 2H, CHH H-6, CHH OCH₂), 3.26 (m, 1H, H-3), 3.23 – 3.17 (m, 2H, H-2, H-4), 3.09 (dd, *J* = 9.2, 7.8 Hz, 1H, H-5), 1.98 (t, *J* = 5.6 Hz, 2H, CH₂SMe), 1.39 (s, 3H, CH₃SMe). ¹³C NMR (126 MHz, CD₃OD) δ = 159.3 (C_q Arom), = 159.3 (C_q Arom), 158.8 (C_q Arom), 158.2 (C_q Arom), 158.0 (C_q Arom), 154.4 (C_H T₃), 154.4 (C_H T₃''), 153.6 (C_H 1), 150.8 (C_H 7), 140.1 (C_H T₅, T₅''), 139.5 (T₄'), 139.4 (C_H 9), 138.3 (C_H 3), 129.8 (C_H T₄, T₄''), 129.2 (C_H 2), 128.4 (C_H 8), 126.2 (T₆, T₆''), 125.9 (C_H 4), 125.5 (T₃', T₅'), 125.1 (C_H 10), 104.2 (C-1), 78.2 (C-3), 78.1 (C-4), 74.9 (C-2), 71.5 (C-5), 66.6 (OCH₂), 62.6 (C-6), 35.8 (CH₂SMe), 14.8 (CH₃SMe). HRMS *m/z* calcd for [M]²⁺: 372.57485; found: 372.57581; Elemental analysis calcd (%) for [3](PF₆)₂: C, 39.47; H, 3.60; N, 6.77; found: 40.57; H, 3.53; N, 7.00.



[Ru(tpy)(bpy)(25)](PF₆)₂, [4](PF₆)₂: The title compound was synthesized analogous according to the procedure described for [1](PF₆)₂ using [Ru(tpy)(bpy)Cl]Cl (94.2 mg, 0.168 mmol) and **25** (71.0 mg, 0.238 mmol) in H₂O (28 mL) affording the title compound as a hygroscopic orange powder (120 mg, 111 μ mol, 66%). *R_f* = 0.56 (50/30/20 acetone/water/aq. KPF₆); ¹H NMR (400 MHz, CD₃OD) δ = 9.83 (d, *J* = 5.7 Hz, 1H, 1), 8.79

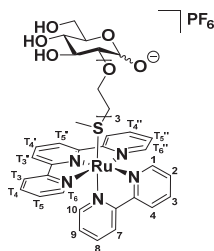
(dd, *J* = 14.9, 8.1 Hz, 3H, 4, T₃', T₅'), 8.60 (dd, *J* = 16.6, 8.1 Hz, 2H, T₆, T₆''), 8.43 – 8.34 (m, 2H, T₄', 3), 8.10 (m, 3H, T₅, T₅'', 2), 7.91 (td, *J* = 7.8, 1.5 Hz, 1H, 9), 7.80 (d, *J* = 4.7 Hz, 1H, T₃, T₃''), 7.51 – 7.41 (m, 2H, T₄, T₄''), 7.32 – 7.27 (m, 1H, 7), 7.23 (ddd, *J* = 7.2, 5.7, 1.3 Hz, 1H,

8), 4.27 (d, $J = 7.8$ Hz, 1H, H-1), 3.97 – 3.89 (m, 1H, CHH OCH₂), 3.85 (dd, $J = 11.8, 1.7$ Hz, 1H, CHH H-6), 3.71 – 3.58 (m, 2H, CHH H-6, CHH OCH₂), 3.54 (dd, $J = 5.4, 3.8$ Hz, 2H, OCH₂), 3.46 (t, $J = 5.5$ Hz, 2H, OCH₂), 3.35 (m, $J = 2.4$ Hz, 1H, H-3), 3.28 – 3.22 (m, 3H, H-4, H-5), 3.12 (dd, $J = 9.0, 7.8$ Hz, 1H,), 1.96 – 1.88 (m, 2H, CH₂SMe), 1.40 (s, 3H, CH₂SMe). ¹³C NMR (101 MHz, CD₃OD) $\delta = 159.3$ (C_q Arom), 158.7 (C_q Arom), 158.1 (C_q Arom), 157.9 (C_q Arom), 154.4 (C_H T₃, T₃'), 153.4 (C_H 1), 150.8 (C_H 7), 140.1 (T₅, T₅'), 139.5 (C_H T₄'), 139.3 (C_H 9), 138.3 (C_H 3), 129.8 (C_H T₄, T₄'), 129.3 (C_H 2), 128.4 (C_H 8), 126.2 (C_H T₆), 125.9 (C_H T₆'), 125.5 (C_H 4), 125.1 (C_H T₃', T₅'), 104.4 (C-1), 78.1 (C-3), 78.0 (C-4), 75.1 (C-2), 71.6 (C-5), 71.4 (OCH₂), 69.7 (OCH₂), 68.2 (OCH₂), 62.7 (C-6), 35.6 (CH₂SMe), 15.2 (CH₂SMe). HRMS m/z calcd for [M]²⁺: 394.58796; found: 394.58870; Elemental analysis calcd (%) for [4](PF₆)₂: C, 40.08; H, 3.83; N, 6.49; found: 40.78; H, 3.97; N, 6.34.



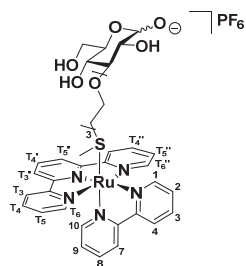
[Ru(tpy)(bpy)(26)](PF₆)₂, [5](PF₆)₂: The title compound was synthesized analogous according to the procedure described for [1](PF₆)₂ using [Ru(tpy)(bpy)Cl]Cl (102 mg, 0.182 mmol) and **26** (100 mg, 0.292 mmol) in H₂O (30 mL) affording the title compound as a red solid (130 mg, 116 μ mol, 65%). $R_f = 0.35$ (100/80/20 acetone/water/aq. KPF₆); ¹H NMR (400 MHz, CD₃OD) $\delta = 9.83$ (d, $J = 5.8$ Hz, 1H, 1), 8.81 (dd, $J = 12.6, 7.9$ Hz,

3H, 4, T₃', T₅'), 8.62 (dd, $J = 17.9, 8.1$ Hz, 3H, T₆, T₆'', 10), 8.46 – 8.35 (m, 2H, T₄', 3), 8.10 (t, $J = 8.3$ Hz, 3H, T₅, T₅'', 2), 7.93 (t, $J = 7.9$ Hz, 1H, 9), 7.80 (d, $J = 5.8$ Hz, 2H, T₃, T₃''), 7.47 (t, $J = 6.6$ Hz, 2H, T₄, T₄''), 7.30 (d, $J = 5.8$ Hz, 1H, 7), 7.23 (t, $J = 6.6$ Hz, 1H, 8), 4.26 (d, $J = 7.8$ Hz, 1H, H-1), 4.06 – 3.91 (m, 1H, CHH OCH₂), 3.86 (d, $J = 11.8$ Hz, 1H, CHH H-6), 3.73 – 3.39 (m, 10H, CHH H-6, CHH OCH₂, 4 x OCH₂), 3.35 (m, 1H, H-5), 3.26 (d, $J = 6.3$ Hz, 2H, H-3, H4), 3.10 (t, $J = 8.5$ Hz, 1H, H-2), 1.90 (d, $J = 5.6$ Hz, 2H, OCH₂SMe), 1.41 (s, 3H, OCH₂SMe). ¹³C NMR (101 MHz, CD₃OD) $\delta = 157.9$ (C_q Arom), 157.4 (C_q Arom), 156.8 (C_q Arom), 156.6 (C_q Arom), 153.1 (C_H T₃, T₃''), 152.1 (C_H 1), 149.5 (C_H 7), 138.8 (C_H T₅, T₅''), 138.2 (C_H 9), 138.0 (C_H T₄'), 136.9 (C_H 3), 128.5 (C_H T₄, T₄''), 127.9 (C_H 8), 127.1 (C_H 2), 124.9 (C_H T₆, T₆''), 124.6 (C_H 4), 124.1 (C_H T₃, T₅'), 123.8 (C_H 10), 103.1 (C-1), 76.6 (C-3, C-5), 73.7 (C-2), 70.3 (C-4), 70.0 (OCH₂), 69.9 (OCH₂), 69.8 (OCH₂), 68.3 (OCH₂), 67.0 (OCH₂), 61.3 (C-6), 34.1 (OCH₂SMe), 14.00 (OCH₂SMe). HRMS: m/z calcd for [M]²⁺: 416.60107; found: 416.60252; Elemental analysis calcd (%) for [5](PF₆)₂·3H₂O: C, 38.78; H, 4.37; N, 5.95; found: 39.27; H, 4.68; N, 5.95.

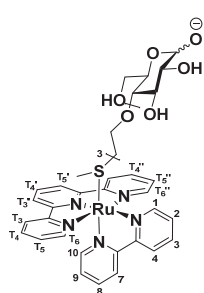


[Ru(tpy)(bpy)(37)]PF₆, [6]PF₆: [Ru(tpy)(bpy)(H₂O)](PF₆)₂ (35.9 mg, 45.0 μ mol) and **H37** (30.3 mg, 44.7 μ mol) were dissolved in a deoxygenated mixture of acetone/H₂O (4:1, 8 mL) and heated at 50 °C for 16 h, after which the reaction mixture was concentrated *in vacuo* and purified over Sephadex LH-20 (MeOH), affording the title compound as a red solid (18 mg, 18.4 μ mol, 41%). $R_f = 0.52$

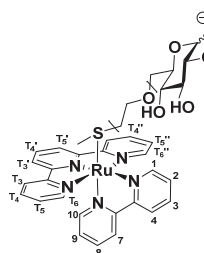
(acetone/water/aq. KPF₆ 100/80/20); ¹H NMR (500 MHz, CD₃OD) δ = 9.84 (d, *J* = 5.6 Hz, 1H, 1), 8.88 – 8.80 (m, 3H, 4, T₃', T₅'), 8.67 (d, *J* = 7.1 Hz, 2H, T₆, T₆'), 8.62 (d, *J* = 7.5 Hz, 1H, 10), 8.43 (q, *J* = 7.9 Hz, 2H, T₄', 3), 8.17 – 8.08 (m, 3H, T₅, T₅''), 7.95 (td, *J* = 7.8, 1.5 Hz, 1H, 9), 7.81 (d, *J* = 5.5 Hz, 2H, T₃, T₃''), 7.48 (ddd, *J* = 7.2, 5.5, 1.3 Hz, 2H, T₄, T₄''), 7.36 – 7.28 (m, 1H, 7), 7.24 (ddd, *J* = 7.2, 5.7, 1.3 Hz, 1H, 8), 5.23 (d, *J* = 3.5 Hz, 0.5H, H-1α), 4.45 (d, *J* = 7.8 Hz, 0.5H, H-1β), 3.99 (dt, *J* = 11.1, 4.6 Hz, 0.5H CHH OCH₂ α/β), 3.86 (dd, *J* = 11.8, 2.3 Hz, 0.5H, CHH H-6α), 3.81 – 3.55 (m, 7.5H, CHH H-6α, CH₂ H-6β, H-3α, H-5α, H-5β, CHH OCH₂ α/β, 1 x OCH₂ α/β, 2 x OCH₂ α+β), 3.51 – 3.47 (m, 2H, OCH₂), 3.45 (ddd, *J* = 6.4, 5.2, 1.6 Hz, 2H, OCH₂), 3.30 – 3.20 (m, 1.5H, H-3β, H-4β, H-4α), 3.16 (dd, *J* = 9.6, 3.5 Hz, 0.5H, H-2α), 2.91 (dd, *J* = 8.9, 7.8 Hz, 0.5H, H-2β), 1.97 – 1.89 (m, 2H, CH₂SMe), 1.43 (s, 1.5H, CH₂SMe α), 1.42 (s, 1.5H, CH₂SMe β). ¹³C NMR (126 MHz, CD₃OD) δ = 159.3 (C_q Arom), 158.8 (C_q Arom), 158.2 (C_q Arom), 158.0 (C_q Arom), 154.4 (C_H T₃, T₃''), 153.4 (C_H 1), 150.8 (C_H 7), 140.2 (C_H T₅, T₅''), 139.6 (C_H T₅, T₅''), 139.4 (C_H T₄', 9), 138.4 (C_H 3), 129.9 (C_H T₄, T₄''), 129.3 (C_H 2), 128.4 (C_H 8), 126.3 (C_H T₆, T₆''), 126.0 (C_H 4), 125.5 (C_H T₃', T₅'), 125.2 (C_H 10), 98.1 (C-1β), 91.8 (C-1α), 85.2 (C-2β), 82.5 (C-2α), 78.0, 77.6, 73.9, 72.9, 72.6, 71.8, 71.8, 71.6, 71.3, 71.3, 71.2, 70.9, 68.4, 68.3, 62.8 (C-6α/β), 62.7 (C-6α/β), 35.7 (CH₂SMe), 35.6 (CH₂SMe), 15.4 (CH₂SMe), 15.4 (CH₂SMe). HRMS: *m/z* calcd for [M]²⁺: 416.60107; found: 416.60278; Elemental analysis calcd (%) for [6]PF₆·3H₂O: C, 44.27; H, 4.89; N, 6.79; found: 44.70; H, 4.73; N, 6.49.



[Ru(tpy)(bpy)(40)]PF₆, [7]PF₆: The title compound was synthesized analogously according to the procedure described for [1](PF₆)₂ using [Ru(tpy)(bpy)Cl]Cl (59.1 mg, 0.105 mmol) and **H40** (40.0 mg, 0.117 mmol) in H₂O (18 mL) affording the title compound as a red solid (44.2 mg, 39.3 μmol, 37%); *R_f* = 0.55 (100/80/20 acetone/water/aq. KPF₆); ¹H NMR (500 MHz, CD₃OD) δ = 9.86 (d, *J* = 5.9 Hz, 1H, 1), 8.96 – 8.80 (m, 3H, 4, T₃', T₅'), 8.74 – 8.69 (m, 2H, T₆, T₆''), 8.67 – 8.62 (m, 1H, 10), 8.51 – 8.40 (m, 2H, T₄', 3), 8.15 (dtd, *J* = 9.6, 4.4, 2.4 Hz, 3H, T₅, T₅''), 8.01 – 7.93 (m, 1H, 9), 7.87 – 7.79 (m, 2H, T₃, T₃''), 7.55 – 7.46 (m, 2H, T₄, T₄''), 7.36 – 7.32 (m, 1H, 7), 7.27 (ddt, *J* = 7.3, 5.7, 1.5 Hz, 1H, 8), 5.10 (d, *J* = 3.6 Hz, 0.5H, H-1α), 4.51 (d, *J* = 7.6 Hz, 0.5H, H-1β), 4.29 – 3.08 (m, 15H), 1.96 (t, *J* = 5.4 Hz, 2H, 2 x CH₂SMe), 1.45 (s, 3H, 2 x CH₂SMe). ¹³C NMR (126 MHz, CD₃OD) δ = 159.3 (C_q Arom), 158.8 (C_q Arom), 158.2 (C_q Arom), 158.0 (C_q Arom), 154.4 (C_H T₃, T₃''), 153.4 (C_H 1), 150.8 (C_H 7), 140.2 (C_H T₅, T₅''), 139.6 (C_H T₄'), 139.4 (C_H 9), 138.3 (C_H 3), 129.9 (C_H T₄, T₄''), 129.3 (C_H 2), 128.4 (C_H 8), 126.3 (C_H T₆, T₆''), 126.0 (C_H 4), 125.5 (C_H T₃', T₅'), 125.2 (C_H 10), 98.2 (C-1β), 94.0 (C-1α), 87.6, 84.4, 77.8, 76.1, 73.7, 73.0, 73.0, 72.0, 72.0, 71.6, 71.4, 71.3, 71.2, 71.2, 71.1, 71.1, 68.4, 68.3, 62.6 (C-6α/β), 62.5 (C-6α/β), 35.7 (2 x CH₂SMe), 15.4 (2 x CH₂SMe); HRMS: *m/z* calcd for [M]²⁺: 416.60107; found: 416.60242; Elemental analysis calcd (%) for [7]PF₆·2H₂O: C, 45.02; H, 4.87; N, 6.91; found: C, 44.82; H, 4.61; N, 6.79.

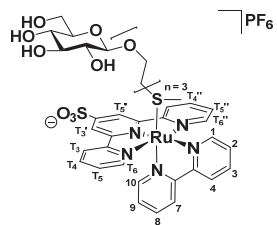


[Ru(tpy)(bpy)(46)]PF₆, [8]PF₆: [Ru(tpy)(bpy)(H₂O)](PF₆)₂ (25.8 mg, 32.0 μmol) and **H46** (11.0 mg, 32.1 μmol) were dissolved in a deoxygenated mixture of acetone/H₂O (4:1, 6 mL) and heated at 50 °C for 48 h, after which the reaction mixture was concentrated *in vacuo* and purified over Sephadex LH-20 (MeOH), affording the title compound as a red solid (23 mg, 23.5 μmol, 73%). *R_f* = 0.61 (100/80/20 acetone/water/aq. KPF₆); ¹H NMR (500 MHz, CD₃OD) δ = 9.85 (dd, *J* = 5.5, 1.1 Hz, 1H, 1), 8.86 (d, *J* = 8.3 Hz, 1H, 4), 8.83 (d, *J* = 8.1 Hz, 2H, T₃', T₅'), 8.69 – 8.66 (m, 2H, T₆, T₆'), 8.63 (dt, *J* = 8.2, 1.1 Hz, 1H, 10), 8.47 – 8.41 (m, 2H, T₄', 3), 8.13 (td, *J* = 7.8, 1.5 Hz, 3H, T₅, T₅'', 2), 7.96 (td, *J* = 7.9, 1.5 Hz, 1H, 9), 7.82 (dd, *J* = 5.7, 1.6 Hz, 2H, T₃, T₃''), 7.49 (ddt, *J* = 7.3, 5.4, 1.8 Hz, 2H, T₄, T₄''), 7.31 (ddd, *J* = 5.7, 1.6, 0.8 Hz, 1H, 7), 7.25 (ddd, *J* = 7.2, 5.7, 1.3 Hz, 1H, 8), 5.11 (d, *J* = 3.7 Hz, 0.5H, H-1α), 4.44 (d, *J* = 7.8 Hz, 0.5H, H-1β), 3.98 – 3.05 (m, 15H), 1.95 (t, *J* = 5.5 Hz, 2H, 2 x CH₂SMe), 1.43 (s, 1.5H, CH₂SMe), 1.43 (s, 1.5H, CH₂SMe). ¹³C NMR (126 MHz, CD₃OD) δ = 159.3 (C_q Arom), 158.8 (C_q Arom), 158.2 (C_q Arom), 158.0 (C_q Arom), 154.4 (C_H T₃), 154.4 (C_H T₃'), 153.4 (C_H 1), 150.8 (C_H 7), 140.2 (C_H T₅, T₅''), 139.6 (C_H T₄'), 139.4 (C_H 9), 138.3 (C_H 3), 129.9 (C_H T₄, T₄''), 129.3 (C_H 2), 128.4 (C_H 8), 126.3 (C_H T₆, T₆''), 125.9 (C_H 4), 125.5 (C_H T₃', T₅'), 125.2 (C_H 10), 98.3 (C-1β), 93.9 (C-1α), 80.6, 80.4, 78.1, 77.0, 76.3, 74.9, 73.8, 72.8, 72.0, 71.9, 71.3, 71.2, 71.2, 68.4, 68.4, 62.5 (C-6 α/β), 62.4 (C-6α/β), 35.7 (CH₂SMe), 35.6 (CH₂SMe), 15.3 (2x CH₂SMe); HRMS: *m/z* calcd for [M]²⁺: 416.60107; found: 416.60261; Elemental analysis calcd (%) for [8]PF₆·2.5H₂O: C, 44.62; H, 4.93; N, 6.85; found: 45.17; H, 5.16; N, 6.55.



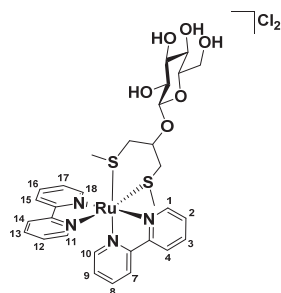
[Ru(tpy)(bpy)(50)]PF₆, [9]PF₆: The title compound was synthesized analogous according to the procedure described for [1](PF₆)₂ using [Ru(tpy)(bpy)Cl]Cl (58.8 mg, 0.105 mmol) and **H50** (42.0 mg, 123 μmol) in H₂O (18 mL) affording the title compound as a red solid (23.5 mg, 24.1 μmol, 23%). *R_f* = 0.36 (16/4/1 acetone/water/1M HCl); ¹H NMR (500 MHz, CD₃OD) δ = 9.86 (ddd, *J* = 5.6, 1.5, 0.7 Hz, 1H, 1), 8.89 – 8.87 (m, 1H, 4), 8.85 (d, *J* = 8.2 Hz, 2H, T₃', T₅'), 8.69 (dd, *J* = 8.2, 1.2 Hz, 2H, T₆, T₆''), 8.67 – 8.62 (m, 1H, 10), 8.50 – 8.41 (m, 2H, T₄', 3), 8.16 – 8.10 (m, 3H, T₅, T₅'', 2), 7.97 (td, *J* = 7.8, 1.5 Hz, 1H, 9), 7.84 (ddd, *J* = 5.6, 1.5, 0.7 Hz, 2H, T₃, T₃''), 7.50 (ddd, *J* = 7.2, 5.6, 1.4 Hz, 2H, T₄, T₄''), 7.33 (dq, *J* = 5.9, 0.9 Hz, 1H, 7), 7.26 (ddd, *J* = 7.2, 5.7, 1.3 Hz, 1H, 8), 5.10 (d, *J* = 3.6 Hz, 0.5H, H-1α), 4.50 (d, *J* = 7.6 Hz, 0.5H, H-1β), 3.99 – 3.08 (m, 15H), 1.96 (t, *J* = 5.5 Hz, 2H, 2 x CH₂SMe), 1.44 (s, 3H, 2 x CH₂SMe). ¹³C NMR (126 MHz, CD₃OD) δ = 159.3 (C_q Arom), 158.8 (C_q Arom), 158.2 (C_q Arom), 158.0 (C_q Arom), 154.4 (C_H T₃'), 153.4 (C_H 1), 150.8 (C_H 7), 140.2 (C_H T₅, T₅''), 139.6 (C_H T₄'), 139.4 (C_H 9), 138.3 (C_H 3), 129.9 (C_H T₄, T₄''), 129.3 (C_H 2), 128.4 (C_H 8), 126.3 (C_H T₆, T₆''), 126.0 (C_H 4), 125.6 (C_H T₃'), 125.5 (C_H T₅'), 125.1 (C_H 10), 98.2 (C-1β), 94.0 (C-1α), 87.6, 84.4, 77.8, 76.1, 73.7, 73.0, 73.0, 73.0, 72.0, 72.0, 71.3, 71.3,

71.2, 71.2, 71.1, 68.4, 68.3, 62.6 (C-6 α / β), 62.5 (C-6 α / β), 35.7 (2 x CH₂SMe), 15.4 (2 x CH₂SMe); HRMS: *m/z* calcd for [M]²⁺: 416.60107; found: 416.60264; Elemental analysis calcd (%) for [9]PF₆·2H₂O: C, 45.02; H, 4.87; N, 6.91; found: C, 44.88; H, 4.59; N, 6.78.



[Ru(S-tpy)(bpy)(26)]PF₆, [10]PF₆: A deoxygenated solution of **31** (40.0 mg, 0.0661 mmol) and **26** (48.0 mg, 0.140 mmol) in H₂O (11 mL) was heated at 80 °C for 16 h after which it was concentrated *in vacuo*. The resulting residue was then purified over silica (100/0/0 to 100/95/5 in acetone/water/aq. KPF₆), followed by purification over Sephadex LH-20 (MeOH) to afford the title compound as a red microcrystalline solid (18 mg, 24.4

μmol, 37%). *R_f* = 0.46 (100/80/20 acetone/water/aq. KPF₆); ¹H NMR (500 MHz, CD₃OD) δ = 9.84 (d, *J* = 5.9 Hz, 1H, 1), 9.03 (s, 2H, T₃', T₅'), 8.81 (d, *J* = 8.2 Hz, 1H, 4), 8.73 (d, *J* = 8.1 Hz, 2H, T₆, T₆'), 8.58 (d, *J* = 8.2 Hz, 1H, 10), 8.43 (t, *J* = 7.9 Hz, 1H, 3), 8.13 (dt, *J* = 13.2, 7.4 Hz, 3H, 2, T₄, T₄'), 7.95 (t, *J* = 7.7 Hz, 1H, 9), 7.81 (d, *J* = 5.9 Hz, 2H, T₃, T₃'), 7.60 – 7.43 (m, 2H, T₅, T₅'), 7.25 (dt, *J* = 12.7, 6.0 Hz, 2H, 8, 7), 4.30 (d, *J* = 7.8 Hz, 1H, H-1), 4.00 (dd, *J* = 10.6, 5.3 Hz, 1H, CHH OCH₂), 3.86 (d, *J* = 12.0 Hz, 1H, CHH H-6), 3.67 (m, 4H, CHH H-6, CHH OCH₂, 2 x OCH₂), 3.57 (dd, *J* = 5.7, 3.4 Hz, 2H, OCH₂), 3.48 (dd, *J* = 5.8, 3.4 Hz, 2H, OCH₂), 3.44 (t, *J* = 5.5 Hz, 2H, OCH₂), 3.41 – 3.36 (m, 1H, H-3), 3.29 (m, 2H, H-4, H-5), 3.14 (t, *J* = 8.5 Hz, 1H, H-2), 1.91 (t, *J* = 5.5 Hz, 2H, CH₂SMe), 1.41 (s, 3H, CH₂SMe). ¹³C NMR (126 MHz, CD₃OD) δ = 159.2 (C_q Arom), 158.7 (C_q Arom), 157.9 (C_q Arom), 157.7 (C_q Arom), 154.8 (C_q Arom), 154.2 (C_H T₃, T₃'), 153.2 (C_H 1), 150.6 (C_H 7), 140.4 (C_H T₄, T₄'), 139.8 (C_H 3), 139.6 (C_H 9), 130.2 (C_H T₅, T₅'), 129.3 (C_H 8) 128.5 (C_H 2), 126.7 (C_H T₆, T₆'), 125.9 (C_H 4), 125.1 (C_H 10), 121.7 (C_H T₃', T₅'), 104.2 (C-1), 77.8 (C-3, C-5), 74.9 (C-2), 71.4 (C-5), 71.1 (OCH₂), 71.0 (OCH₂), 69.7 (OCH₂), 68.0 (OCH₂), 62.5 (C-6), 35.2 (CH₂SMe), 15.2 (CH₂SMe). HRMS: *m/z* calcd for [M]⁺: 912.15167; found: 912.15427; Elemental analysis calcd (%) for [10]PF₆·0.5KPF₆·5H₂O: C, 36.84; H, 4.39; N, 5.65; found: 36.83; H, 4.40; N, 5.36.



Δ/Λ-[Ru(tpy)(bpy)(28)](PF₆)₂, [11]Cl₂: [Ru(bpy)₂Cl₂] (73.0 mg, 0.151 mmol) and **28** (46.0 mg, 0.146 mmol) were dissolved in deoxygenated H₂O (10 mL) and this mixture was heated at 80 °C for 16 h, after which the mixture was concentrated *in vacuo*. Purification by Sephadex LH-20 (MeOH) afforded the title compound as an inseparable mixture of diastereomers (69.0 mg, 0.0864 mmol, 59%). *R_f* = 0.28 (16/4/1 acetone/water/1M HCl); ¹H NMR (500 MHz, CD₃OD) δ = 10.02 (dd, *J* = 5.7, 1.4 Hz, 1H), 9.86 (dd, *J* = 5.7, 1.4 Hz, 1H), 9.50 (dd, *J* = 5.7, 1.4 Hz, 1H), 9.42 (dd, *J* = 5.7, 1.3 Hz, 1H), 8.81 (d, *J* = 8.2 Hz, 2H), 8.79 – 8.76 (m, 2H), 8.69 – 8.62 (m, 4H), 8.45 – 8.36 (m, 4H), 8.12 (tt, *J* = 8.0, 1.8 Hz, 4H), 8.06 (dddd, *J* = 13.5, 7.3, 5.6, 1.4 Hz, 5H), 7.63 (td, *J* = 5.7, 1.4 Hz, 2H), 7.57 (ddd, *J* = 7.5, 5.7, 1.4 Hz, 2H), 7.49 – 7.42 (m, 4H), 4.65 (d, *J* =

7.8 Hz, 1H), 4.58 (d, $J = 7.8$ Hz, 1H), 3.92 (ddd, $J = 19.8, 11.8, 1.9$ Hz, 2H), 3.78 – 3.70 (m, 1H), 3.62 (dd, $J = 11.9, 6.4$ Hz, 1H), 3.50 – 3.35 (m, 10H), 3.30 (t, $J = 8.2$ Hz, 1H), 3.27 – 3.20 (m, 2H), 3.13 (dd, $J = 14.0, 6.4$ Hz, 1H), 3.02 (dd, $J = 13.9, 7.1$ Hz, 1H), 2.92 (dd, $J = 13.1, 2.1$ Hz, 1H), 2.80 (dd, $J = 13.1, 1.7$ Hz, 1H), 1.53 (s, 3H), 1.50 (s, 3H), 1.25 (s, 3H), 1.23 (s, 3H). ^{13}C NMR (126 MHz, CD_3OD) $\delta = 159.1, 159.1, 159.0, 158.9, 158.1, 158.0, 157.9, 155.4, 155.0, 154.9, 154.8, 152.0, 152.0, 151.9, 151.9, 140.3, 140.2, 130.8, 130.0, 129.9, 129.5, 129.3, 129.0, 129.0, 128.9, 126.2, 126.1, 126.0, 125.6, 125.6, 125.5, 125.4, 104.2, 103.6, 78.4, 78.3, 78.3, 78.2, 75.3, 75.3, 75.2, 71.6, 71.6, 62.7, 40.5, 38.6, 38.4, 37.4, 18.5, 18.1, 16.1, 16.0$; HRMS: m/z calcd for $[\text{M}]^{2+}$: 364.06326; found: 364.06459; Elemental analysis calcd (%) for $[\mathbf{11}]\text{Cl}_2 \cdot 3\text{H}_2\text{O}$: C, 43.66; H, 5.20; N, 6.57; found: 43.34; H, 5.35; N, 6.29.

References

- [1] K. H. Schleifer, O. Kandler, *Bacteriol Rev* **1972**, *36*, 407-477.
- [2] K. H. Caffall, D. Mohnen, *Carbohydr Res* **2009**, *344*, 1879-1900.
- [3] H. Merzendorfer, L. Zimoch, *J Exp Biol* **2003**, *206*, 4393-4412.
- [4] B. K. Brandley, R. L. Schnaar, *J Leukocyte Biol* **1986**, *40*, 97-111.
- [5] J. D. Watson, F. H. Crick, *Nature* **1953**, *171*, 737-738.
- [6] S. Tornroth-Horsefield, R. Neutze, *P Natl Acad Sci USA* **2008**, *105*, 19565-19566.
- [7] M. G. Vander Heiden, L. C. Cantley, C. B. Thompson, *Science* **2009**, *324*, 1029-1033.
- [8] L. Szablewski, *Biochim Biophys Acta* **2013**, *1835*, 164-169.
- [9] J. S. Fowler, T. Ido, *Semin Nucl Med* **2002**, *32*, 6-12.
- [10] E. C. Calvaresi, P. J. Hergenrother, *Chem Sci* **2013**, *4*, 2319-2333.
- [11] M. Patra, S. G. Awuah, S. J. Lippard, *J Am Chem Soc* **2016**, *138*, 12541-12551.
- [12] J. Petrig, R. Schibli, C. Dumas, R. Alberto, P. A. Schubiger, *Chem Eur J* **2001**, *7*, 1868-1873.
- [13] N. T. Kulishkin, A. V. Mashkina, *React Kinet Catal L* **1991**, *45*, 41-47.
- [14] J. C. Hermann, Y. Chen, C. Wartchow, J. Menke, L. Gao, S. K. Gleason, N. E. Haynes, N. Scott, A. Petersen, S. Gabriel, B. Vu, K. M. George, A. Narayanan, S. H. Li, H. Qian, N. Beatini, L. Niu, Q. F. Gan, *ACS Med Chem Lett* **2013**, *4*, 197-200.
- [15] S. van der Vorm, T. Hansen, H. S. Overkleeft, G. A. van der Marel, J. D. C. Codee, *Chem Sci* **2017**, *8*, 1867-1875.
- [16] B. G. Davis, M. A. T. Maughan, M. P. Green, A. Ullman, J. B. Jones, *Tetrahedron: Asymmetry* **2000**, *11*, 245-262.
- [17] S. Valerio, A. Iadonisi, M. Adinolfi, A. Ravida, *J Org Chem* **2007**, *72*, 6097-6106.
- [18] B. Fraser-Reid, Z. Wu, U. E. Udodong, H. Ottosson, *J Org Chem* **1990**, *55*, 6068-6070.
- [19] Z. Yang, W. Lin, B. Yu, *Carbohydr Res* **2000**, *329*, 879-884.
- [20] J. Park, J. I. Um, A. Jo, J. Lee, D. W. Jung, D. R. Williams, S. B. Park, *Chem Commun* **2014**, *50*, 9251-9254.

- [21] C. W. Machan, M. Adelhardt, A. A. Sarjeant, C. L. Stern, J. Sutter, K. Meyer, C. A. Mirkin, *J Am Chem Soc* **2012**, *134*, 16921-16924.
- [22] C. Dumas, R. Schibli, P. A. Schubiger, *J Org Chem* **2003**, *68*, 512-518.
- [23] Y. Li, G. Manickam, A. Ghoshal, P. Subramaniam, *Synth Commun* **2006**, *36*, 925-928.
- [24] G. Grue-Sørensen, E. Kelstrup, A. Kjær, J. Ø. Madsen, *J Chem Soc, Perkin Trans 1* **1984**, 1091-1097.
- [25] Y. Miao, C. Rousseau, A. Mortreux, P. Martin, P. Zinck, *Polymer* **2011**, *52*, 5018-5026.
- [26] a). J. Gervay, S. Danishefsky, *J Org Chem* **1991**, *56*, 5448-5451; b). R. L. Halcomb, S. J. Danishefsky, *J Am Chem Soc* **1989**, *111*, 6661-6666.
- [27] A. G. Volbeda, H. A. Kistemaker, H. S. Overkleeft, G. A. van der Marel, D. V. Filippov, J. D. C. Codee, *J Org Chem* **2015**, *80*, 8796-8806.
- [28] J. T. Doi, G. W. Luehr, *Tetrahedron Lett* **1985**, *26*, 6143-6146.
- [29] a). F. Hu, Z. Chen, L. Zhang, Y. Shen, L. Wei, W. Min, *Angew Chem Int Ed* **2015**, *54*, 9821-9825; b). X. Xue, Z. Yin, X. Meng, Z. Li, *J Org Chem* **2013**, *78*, 9354-9365; c). T. K. M. Shing, Y. L. Zhong, *Tetrahedron* **2001**, *57*, 1573-1579.
- [30] E. Kaji, F. W. Lichtenthaler, Y. Osa, K. Takahashi, S. Zen, *Bull Chem Soc Jpn* **1995**, *68*, 2401-2408.
- [31] C. Morin, L. Ogier, *Carbohydr Res* **1998**, *310*, 277-282.
- [32] T. A. Wark, D. W. Stephan, *Organometallics* **1989**, *8*, 2836-2843.
- [33] U. Muhlhausen, R. Schirmacher, M. Piel, B. Lecher, M. Brieger, A. Piee-Staffa, B. Kaina, F. Rosch, *J Med Chem* **2006**, *49*, 263-272.
- [34] Q. Wang, P. Day, J. P. Griffiths, H. Nie, J. D. Wallis, *New J Chem* **2006**, *30*, 1790-1800.

Chapter 3:

D- versus L-glucose conjugation

Mitochondrial targeting of a light-activated, dual-mode of action ruthenium-based anticancer prodrug

Abstract: Light-activated ruthenium polypyridyl anticancer prodrugs often suffer from poor water solubility, poor selectivity, and/or ill-defined intracellular targets. Coordination of the D- or L-glucose thioether ligand **3** = 2-(2-(2-(methylthio)ethoxy)ethoxy)ethyl- β -glucopyranoside to the highly lipophilic ruthenium complex $[\text{Ru}(\text{tpy})(\text{dppn})(\text{OH}_2)]^{2+}$ (**[1]**²⁺, tpy = 2,2':6',2''-terpyridine, dppn = benzo[*l*]dipyrido-[3,2- α :2',3'-c]phenazine) solved all problems at once. The two enantiomers $[\text{Ru}(\text{tpy})(\text{dppn})(\mathbf{3})](\text{PF}_6)_2$ (**[D-2]**(PF₆)₂ and **[L-2]**(PF₆)₂) are soluble in water, which allowed for probing the influence of the chirality of the glucose moiety on uptake, toxicity, and intracellular localization of the prodrug without changing any other physical and/or chemical properties. Both compounds showed mild but different cytotoxicity in A549 (human lung carcinoma) and MCF-7 (human breast adenocarcinoma) cancer cells in the dark, whereas similarly high cytotoxicity was observed for both compounds after irradiation with low doses of visible light (3.1 J.cm⁻² at 455 nm). Irrespective of chirality the slightly emissive Ru complexes were found in the mitochondria, where two modes of action may contribute to light-induced cell death. On the one hand, the glucose-thioether ligand is photosubstituted by water, thus releasing **[1]**²⁺ that interacts with DNA at an exceptionally high 400:1 bp:Ru ratio. On the other hand, both **[2]**²⁺ and **[1]**²⁺ produce large amounts of singlet oxygen, leading to very efficient photocleavage of DNA.

This work was published as a full paper: L. N. Lameijer, S. L. Hopkins, T. G. Brevé, S. H. C. Askes, S. Bonnet, *Chem. Eur. J.* **2016**, *22*, 18484-18491.

3.1 Introduction

One of the major challenges in the development of new anticancer drugs is to improve selectivity. A common strategy to better differentiate normal proliferating cells from malignant cells is to develop drugs targeting specific hallmarks of cancer cells, such as aerobic glycolysis. As first described by Otto Warburg,^[1] cancer cells use glycolysis for their energy production and therefore have a higher demand for simple sugars such as D-glucose. As the cell membrane is impermeable to polar molecules specific membrane transporters control glucose uptake (GLUT and SGLT). These transporters are overexpressed in many cancer cell types, which not only aids D-glucose penetrating into the cell, but also provides a method to target imaging or therapeutic compounds to cancer cells.^[2] For example, 2-deoxy-2-(¹⁸F)fluoro-D-glucose (18-FDG) is a common radiotracer used in the clinics to image tumors *in vivo*.^[3] Conjugating D-glucose or other GLUT substrates to organic^[3-4] or inorganic^[5] anticancer compounds is a quickly expanding cancer-targeting strategy. Several methods have been proposed to assess the benefits of D-glucose functionalization of an anticancer drug. Enhanced uptake is usually demonstrated indirectly, for example by comparing glucose-functionalized drugs to their aglycon counterpart,^[6] or by competitive inhibition experiments with D-glucose.^[7] However, these methods usually ignore the difference in polarity and hydrophilicity between the glycoconjugates and aglycon analogues, which for many compounds can have major influence on drug uptake, localization, and/or mode-of-action. Comparing the biological effects of a glycoconjugate on different cell lines with different expressions of glucose transporters is another alternative.^[8] However, depending on the cell line different glucose transporters may be overexpressed,^[9] which complicates the interpretation of such experiments. Finally, adding glucose transporter inhibitors to switch off the uptake of glucose functionalized compounds, is also possible.^[10] However, synergies between biologically active compounds have been demonstrated on multiple occasions,^[11] and it may be difficult to distinguish impaired drug uptake due to the inhibitors, from the cytotoxicity of the inhibitor itself.^[12]

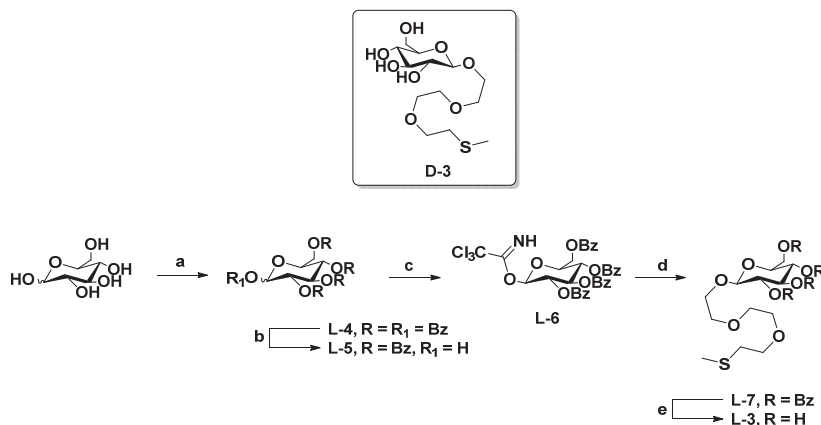
To solve these biases we herein propose a new approach consisting in directly comparing the activity of the D- and L-glucose conjugates of the same drug, here an achiral, highly lipophilic ruthenium compound [Ru(tpy)(dppn)(OH₂)]²⁺ (**1**)²⁺, Scheme 3.2, tpy = 2,2':6',2''-terpyridine, dppn = benzo[*i*]dipyrido-[3,2-*a*:2',3'-*c*]phenazine). Contrary to D-glucose, L-glucose is not a substrate for the glucose transport system.^[13] Our basic assumption was that a L-glucose-modified drug will have the same structural properties and therefore the same polarity and hydrophilicity as its D-glucose analogue but will not be recognized by cellular enzymes due to its different chirality. Therefore it might be possible to probe the biological effects of the D-glucose functional group without the experimental biases mentioned above. Compound **1**)²⁺ has another interesting property: it belongs to a family of metallodrugs that can be activated by visible light irradiation.^[14] Light-activatable

anticancer compounds have been proposed as a way to improve the selectivity of anticancer treatments by an external trigger that limit the toxicity of the treatment to the time and place of light irradiation.^[15] We thus designed the two light-activatable prodrugs $[\text{Ru}(\text{tpy})(\text{dppn})(\text{D-3})]^{2+}$ and $[\text{Ru}(\text{tpy})(\text{dppn})(\text{L-3})]^{2+}$ ($[\text{D-2}]^{2+}$ or $[\text{L-2}]^{2+}$, respectively), where **3** is a thioether ligand covalently linked to D- or L-glucose that binds to ruthenium *via* a thermally stable Ru-S coordination bond (Scheme 3.2). The synthesis, photochemistry, and biological evaluation of these enantiomeric ruthenium compounds is reported, and their cytotoxicity, cellular distribution, and mode-of-action, are discussed.

3.2 Results and Discussion

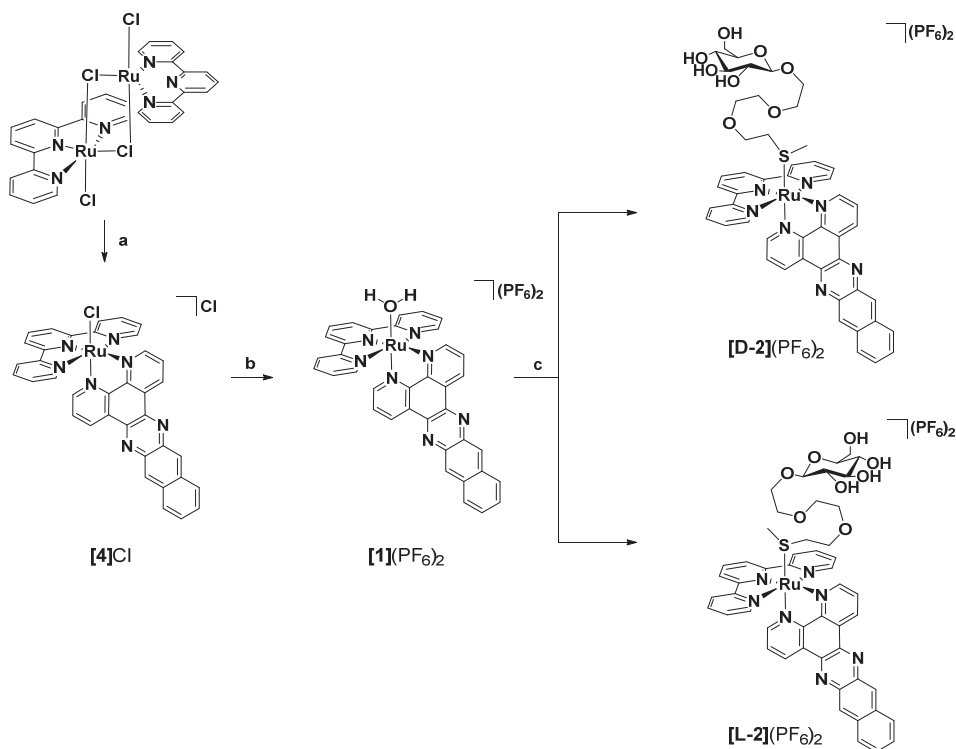
3.2.1 Synthesis

The thioether-glucose conjugates **D-3** (Chapter 2) and **L-3** (Scheme 3.1) were synthesized from D- and L-glucose, respectively, according to the Schmidt methodology.^[16] As expected both ligands were found to have the same physical and spectroscopic properties, except for their opposite sign of optical rotation (**D-3**: $[\alpha]_D^{20}$ -10.0 ($c = 1.00$ in MeOH) and **L-3**: $[\alpha]_D^{20}$ +11.8 ($c = 1.00$ in MeOH) and their different retention time on chiral HPLC (Figure S.II.13 and S.II.14).



Scheme 3.1 a). BzCl in pyridine, 0 °C – rt, 6 h, quant.; b). i. 33% HBr/AcOH in DCM, rt, overnight; ii. Ag₂CO₃ in acetone/water, rt, 3 h, 99% over two steps; c). trichloroacetonitrile, DBU in DCM, rt, overnight, 78%; d). 2-(2-(2-(methylthio)ethoxy)ethoxy)ethan-1-ol, DCM, cat. TMSOTf, rt, 3 h, 69%; e). cat. NaOMe in MeOH, rt, overnight, 85%.

In a second step, the ligands **D-3** or **L-3** were coordinated to ruthenium according to Scheme 3.2. Isolation of the aqua complex, **[1](PF₆)₂** was necessary, and further reaction with a three-fold excess of **D-3** or **L-3** under mild conditions (acetone, 50 °C) afforded the D- and L-glucose conjugates **[D-2](PF₆)₂** and **[L-2](PF₆)₂** in moderate yields (32% and 35% respectively). Unlike **[1](PF₆)₂** and $[\text{Ru}(\text{tpy})(\text{dppn})\text{Cl}]\text{Cl}$ (**[4]Cl**), which are virtually insoluble in water, **[D-2](PF₆)₂** and **[L-2](PF₆)₂** can be dissolved in water even in absence of DMSO.



Scheme 3.2 Synthesis of **[D-2](PF₆)₂** and **[L-2](PF₆)₂**. a). 2 eq. dppn in ethylene glycol, 5 hr, 100 °C, 75%; b). i. 1.0 eq. AgNO₃ in acetone/water (3:1), 50 °C; ii. NH₄PF₆, 84%; c). 2.66 eq. **D-3** or **L-3** in acetone, 50 °C, 24 h, 35% for **[D-2](PF₆)₂** and 32% for **[L-2](PF₆)₂**.

3.2.2 Photochemistry

The photoreactivity of the water-soluble thioether complex **[D-2](PF₆)₂** was tested in different conditions. Figure 3.1 shows the evolution of the UV-vis spectrum of **[D-2](PF₆)₂** upon blue light irradiation (450 nm) in pure water and under argon. The initial absorption maximum at 460 nm decreased while a new ¹MLCT band at 474 nm increased; a clear isosbestic point was also observed, showing that in such conditions a single photoproduct was obtained. According to mass spectrometry, the photoproduct was **[Ru(tpy)(dppn)(OH₂)]²⁺** (**[1]²⁺**, *m/z* = found 342.4, calculated 342.5). Photosubstitution of the thioether-glucose conjugate by water proceeds with a quantum yield of 0.00095 (± 0.00002) in deoxygenated water. Usually, such photosubstitution processes significantly reduce the emission of ruthenium polypyridyl complexes. Indeed, the phosphorescence of **[D-2](PF₆)₂** in PBS (pH = 7.4) and in air under 450 nm excitation was found to be very weak; the wavelength of the emission maximum was 648 nm, and a phosphorescence quantum yield Φ_p of 3.7×10^{-5} was measured. Under prolonged blue light irradiation in air, the wavelength of the emission band shifted from 648 nm to 690 nm, indicating the formation of the also weakly emissive photoproduct **[1]²⁺** ($\Phi_p = 3.2 \times 10^{-5}$). Near-infrared emission

spectroscopy was also performed under 450 nm excitation to check whether irradiating $[\text{D-2}]^{2+}$ in air would produce singlet oxygen. In water, PBS, or D_2O , no emission at 1270 nm was detected because of the very short lifetime of $^1\text{O}_2$ in aqueous solutions. However, in CD_3OD an intense emission peak at 1270 nm, characteristic of singlet oxygen, was observed upon blue light irradiation of $[\text{D-2}](\text{PF}_6)_2$ (Figure S.II.2). The quantum yield of singlet oxygen production (Φ_Δ) of $[\text{D-2}](\text{PF}_6)_2$ in methanol- d_4 was 0.71, *i.e.*, $[\text{D-2}](\text{PF}_6)_2$ generates $^1\text{O}_2$ very efficiently in air (Figure S.II.2). The photoproduct $[\text{Ru}(\text{tpy})(\text{dppn})(\text{CD}_3\text{OD})]^{2+}$, which was obtained after extensive blue light irradiation of $[\text{D-2}]^{2+}$ in CD_3OD , also generated singlet oxygen with a high quantum yield Φ_Δ of 0.43 (Table 3.1).

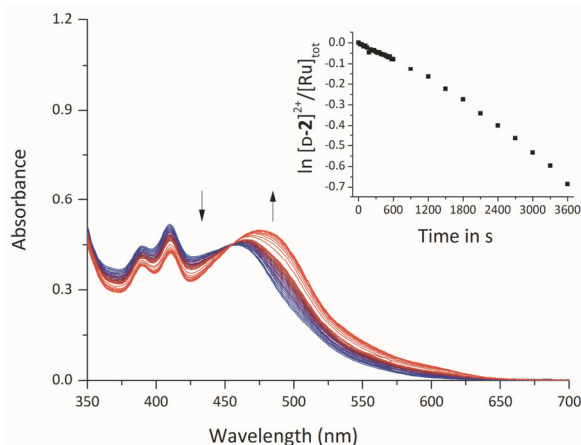


Figure 3.1 Electronic absorption spectra of $[\text{D-2}](\text{PF}_6)_2$ in deoxygenated H_2O irradiated at 450 nm for 60 min. Spectra were taken each 30 s for the first 10 min, followed by a spectrum every 5 min until 60 min. $T = 298 \text{ K}$, $[\text{Ru}]_{\text{tot}} = 4.23 \times 10^{-5} \text{ M}$, $\lambda_{\text{exc}} = 450 \text{ nm}$, photon flux = $1.77 \times 10^{-7} \text{ mol photons s}^{-1}$. Inset depicts the evolution of $\ln [\text{D-2}]/[\text{Ru}]_{\text{tot}}$ vs. irradiation time.

The results of photosubstitution of the thioether ligand **3** in $[\text{D-2}]^{2+}$ contrast with recent work from the Turro group, who demonstrated that the analogous complex $[\text{Ru}(\text{tpy})(\text{dppn})(\text{pyridine})]^{2+}$ did not undergo photosubstitution of the pyridine ligand in organic solvents. Instead, the complex was reported to efficiently produce $^1\text{O}_2$ ($\Phi_\Delta = 0.98$) due to the presence of low-lying $\pi\text{-}\pi^*$ excited states centered on the dppn ligand.^[17] Apparently, the nature of the monodentate ligand plays an important role in the photoreactivity of this family of dppn-based ruthenium complexes. Although photosubstitution, phosphorescence, and singlet oxygen generation often represent competing pathways in ruthenium photochemistry, when $[\text{D-2}]^{2+}$ is irradiated with blue light all processes may occur, depending on dioxygen concentration. In deoxygenated conditions photosubstitution of the thioether ligand to form the aqua complex is preferred, whereas in air efficient generation of $^1\text{O}_2$ becomes a competing pathway and is observed both before and after photosubstitution.

Table 3.1 Lowest energy absorption maxima, quantum yield for photosubstitution (Φ_{450}), $^1\text{O}_2$ production (Φ_Δ) and phosphorescence (Φ_p) at 298 K.

Complex	$\lambda_{\text{abs}}^{[a]}/\text{nm}$ ($\epsilon/\text{M}^{-1}\text{cm}^{-1}$)	$\Phi_{450}^{[a]}$	$\Phi_\Delta^{[b]}$	$\Phi_p^{[c]}$
$[\text{D-2}]^{2+}$	458 (11619)	0.00095 ± 0.00002	0.71	0.000037
$[\text{1}]^{2+}$	475 (12643)	-	0.43	0.000032

3.2.3 Cytotoxicity assay

The cytotoxic properties of $[\text{D-2}](\text{PF}_6)_2$ and of its enantiomer $[\text{L-2}](\text{PF}_6)_2$ were tested in the dark on two human cancer cell lines, A549 and MCF-7.^[9] In parallel, considering the dual photoreactivity of $[\text{D-2}](\text{PF}_6)_2$ the phototoxicity of $[\text{D-2}](\text{PF}_6)_2$ and $[\text{L-2}](\text{PF}_6)_2$ was also tested under a low dose of blue light (5 minutes at 454 ± 11 nm, 10.5 ± 0.7 mW \cdot cm $^{-2}$, 3.2 ± 0.2 J \cdot cm $^{-2}$). Cells were seeded at $t = 0$ (5×10^3 per well for A549 and 8×10^3 per well for MCF-7), treated with a concentration series of either $[\text{D-2}](\text{PF}_6)_2$ or $[\text{L-2}](\text{PF}_6)_2$ 24 h after seeding, irradiated or maintained in the dark after media refreshment 48 h after seeding, and cell viability was assayed using sulforhodamine B (SRB) 96 h after seeding. The dose-response curves and effective concentrations (EC_{50}) are reported in Figure 3.2 and Table 3.2, respectively. Images of A549 and MCF-7 treated cells (20 μM , $[\text{D-2}](\text{PF}_6)_2$) 96 h after seeding for dark and irradiated samples are shown in Figures S.II.11 and S.II.12. In the dark the cytotoxicity of $[\text{D-2}](\text{PF}_6)_2$ and $[\text{L-2}](\text{PF}_6)_2$ was significantly different, both for A549 and MCF-7 cells. For $[\text{D-2}](\text{PF}_6)_2$ the effective concentration was 2.6 and 1.9 fold lower for A549 and MCF-7 cells, respectively, than for $[\text{L-2}](\text{PF}_6)_2$ (Table 3.2). Upon light irradiation, both compounds were activated and showed similar high cytotoxicity, characterized by sub-micromolar effective concentrations (EC_{50}). According to these results, the chiral nature of the glucose functional group seems to have an effect on the dark cytotoxicity of the prodrug. In addition, upon light irradiation either the release of the photoproduct $[\text{1}]^{2+}$, or efficient singlet oxygen generation by the prodrug $[\text{D/L-2}]^{2+}$ and the activated drug $[\text{1}]^{2+}$, or both, result in a highly cytotoxic combination.^[18]

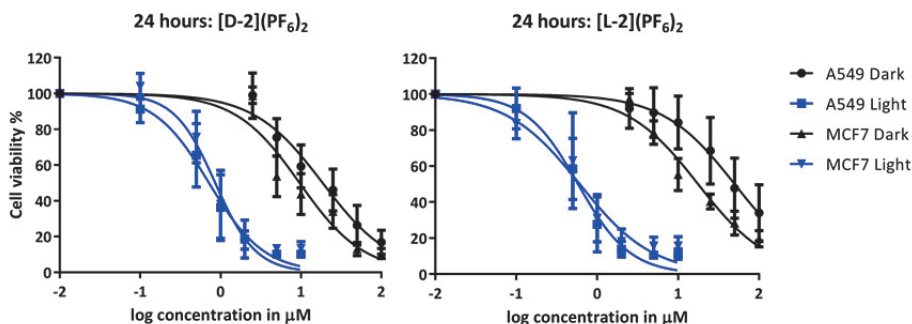


Figure 3.2. Cell viability of A549 and MCF-7 cells versus the logarithm of the concentration of $[\text{D-2}](\text{PF}_6)_2$ and $[\text{L-2}](\text{PF}_6)_2$ in the dark and the light. Data points are means of three independent experiments with \pm SD as error bars.

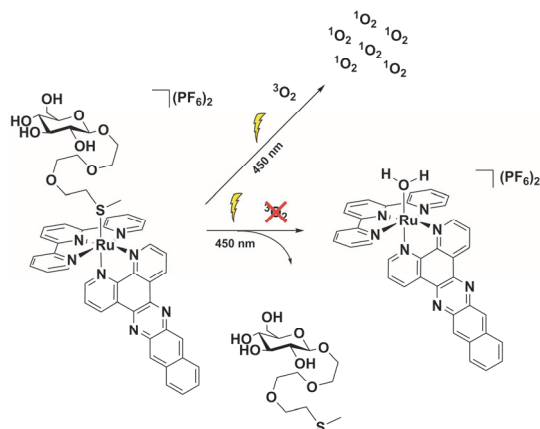


Figure 3.3 Schematic representation of the light-induced dual mode of action for the glycoconjugated compound $[\text{Ru}(\text{tpy})(\text{dppn})(\text{D-3})]^{2+}$ ($[\text{D-2}]^{2+}$), where D-3 is a thioether-glucose conjugate. For clarity the L enantiomers are left out.

Table 3.2 (Photo)cytotoxicity of $[\text{D-2}](\text{PF}_6)_2$ and $[\text{L-2}](\text{PF}_6)_2$ expressed as effective concentrations (EC_{50} in μM) in the dark and after blue light irradiation, and photocytotoxicity index (PI)^[c] versus A549 and MCF-7 cells before and after irradiation with blue light. Values are reported in μM with $\pm 95\%$ Confidence Intervals (CI).

Complex	A549					MCF-7				
	EC_{50} dark ^[a]	$\pm\text{CI}$	EC_{50} 455 nm ^[b]	$\pm\text{CI}$	PI	EC_{50} dark ^[a]	$\pm\text{CI}$	EC_{50} 455 nm ^[b]	$\pm\text{CI}$	PI
$[\text{D-2}](\text{PF}_6)_2$	19	+4.0	0.72	+0.16	26	9.6	+2.9	0.86	+0.21	11
		-3.3		-0.13			-2.3		-0.17	
$[\text{L-2}](\text{PF}_6)_2$	50	+17	0.58	+0.13	86	18	+3.8	0.61	+0.28	30
		-13		-0.11			-3.1		-0.19	

[a] Cells were incubated with complexes for 24 h. [b] Cells were incubated with the complex for 24 h, and the media was refreshed before blue light irradiation (5 min at 455 nm with $3.2 \pm 0.2 \text{ J}\cdot\text{cm}^{-2}$). [c] $\text{EC}_{50}(\text{dark})/\text{EC}_{50}(455 \text{ nm})$.

3.2.4 Cellular localization and in vitro imaging

Contrary to many ruthenium complexes capable of photo-substituting one of their ligands, $[\text{D-2}](\text{PF}_6)_2$ and $[\text{L-2}](\text{PF}_6)_2$ were found to be slightly emissive in cells, which allowed for performing uptake and localization studies (Figures 3.4 and S.II.5-S.II.10). Microscopy imaging was performed for A549 cells treated in the dark with $[\text{D-2}](\text{PF}_6)_2$ or $[\text{L-2}](\text{PF}_6)_2$ for 4, 6, and 24 h ($\lambda_{\text{exc}} = 488 \text{ nm}$, Figure S9). These images revealed that independent on incubation time, $[\text{D-2}](\text{PF}_6)_2$ and $[\text{L-2}](\text{PF}_6)_2$ displayed no significant difference in localization or emission intensity, and both complexes were clearly localized outside the nucleus (Figures S.II.5-S.II.6). Co-localization experiments using MitoTracker Deep Red (MTDR, $\lambda_{\text{exc}} = 639 \text{ nm}$) were attempted after 6 h incubation (Figure S.II.9). Due to the weaker emission of $[\text{1}]^{2+}$ compared to MTDR, and some absorption of MTDR at 488 nm, it was impossible to quantitatively co-localize the ruthenium compound and the dye unequivocally. However, the ruthenium compounds and MTDR, added separately, gave qualitatively very similar images using the 488 or 639 nm channels, respectively (Figure 3.4). This suggested that the ruthenium compound might localize in the mitochondria. To confirm that, an experiment was designed where cells were treated with $[\text{D-2}](\text{PF}_6)_2$ at 25

μM in the presence of MTDR. MTDR images were taken at 639 nm, showing normal mitochondrial morphology (Figure S.II.9B and S.II.9E). Then, new images were taken using the 488 nm channel (Figure S.II.9C and S.II.9F), followed by a second set of MTDR images (Figure S.II.9D and S.II.9G). The mitochondria of cells that had been irradiated at 488 nm were altered, showing bubble-like structures, compared to untreated cells. Thus, the combination of treatment with the complexes and 488 nm light irradiation led to modifications of the mitochondria structure. Mitochondria are known to have a highly negative inner membrane potential, which can be targeted by cationic, lipophilic compounds.^[18] Considering the positive charge and lipophilic nature of [D-2](PF₆)₂ and [L-2](PF₆)₂, and the experimental facts highlighted above, it is proposed that upon crossing the plasma membrane, both complexes target the mitochondria.

Due to the lack of uptake selectivity of [D-2](PF₆)₂ vs [L-2](PF₆)₂ and proposed localization in the mitochondria, a final imaging experiment with sodium azide (NaN₃) was realized. Sodium azide treatment is known to inhibit all energy-dependent uptake mechanisms. Cells treated with NaN₃ together with [D-2](PF₆)₂ or [L-2](PF₆)₂, did not show significant differences in uptake or localization (Figure S.II.8) compared to cells that were only treated the ruthenium compounds. Altogether, and although the cytotoxicity of both enantiomers does depend on the chirality of the glucose moiety, these results support a glucose transporter-independent, energy-independent^[19] uptake mechanism *in vitro*.

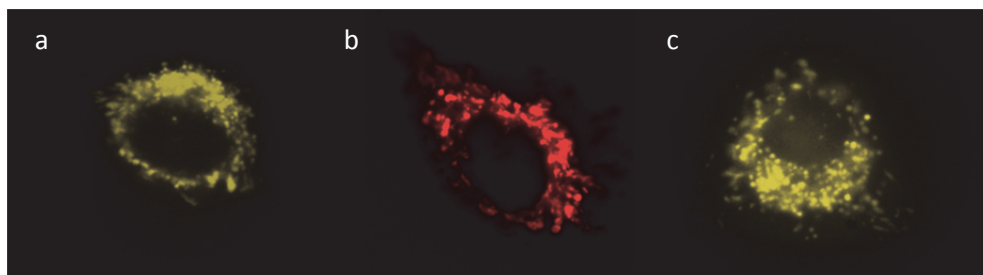


Figure 3.4 Microscopy images of A549 cell treated with (a) [D-2](PF₆)₂ ($\lambda_{\text{exc}} = 488 \text{ nm}$, $c = 25 \mu\text{M}$), (b) MitoTracker deep red ($\lambda_{\text{exc}} = 639 \text{ nm}$, $c_{\text{final}} = 1.1 \mu\text{M}$), and (c) [L-2](PF₆)₂ ($\lambda_{\text{exc}} = 488 \text{ nm}$, $c = 25 \mu\text{M}$).

3.2.5 Photochemistry with DNA

The mitochondria house double stranded, circular DNA, which is very interesting given the mitochondrial localization and the DNA light-switch capabilities of dppz analogues of [D-2](PF₆)₂.^[20] Therefore, the photochemistry of [D-2](PF₆)₂ with calf thymus DNA (CT-DNA) and pUC19 plasmid DNA was studied in more detail. As explained above, in PBS under blue light excitation (450 nm) in air the emission maximum of [D-2](PF₆)₂ shifted from 648 nm to 690 nm, which was attributed to the formation of [1]²⁺. In such conditions, there was no significant change in emission intensity over irradiation time (Figure 3.5a). However, under the same irradiation conditions, but in the presence of CT-DNA the emission not only shifted from 648 to 700 nm, but it also increased by 10-fold in intensity over 25 min of irradiation (Figure 3.5b). Under similar conditions, the presence of micelles

(Pluronic F-127), DOPC/DMPC liposomes, L-cysteine, L-histidine, L-glutathione, L-lysine, L-tryptophane and 5'-GMP (5 mM in PBS) did not enhance the emission after irradiation. These data not only confirm a specific DNA light-switch interaction of $[1]^{2+}$ with CT-DNA, but they also provide further support that the emission in cells to be the result of interactions with DNA.

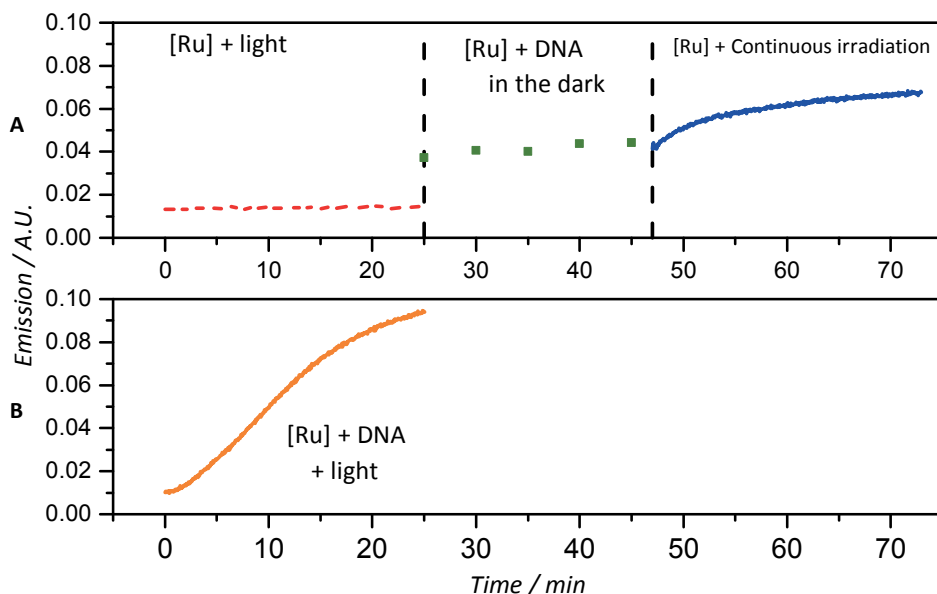


Figure 3.5 a) Emission spectrum of $[D-2](PF_6)_2$ in PBS without DNA (-), with CT-DNA (-) and during continuous irradiation (-). $\lambda_{em} = 707$ nm. b) Emission spectrum of $3.5 \mu M$ in PBS + CT-DNA during constant blue light irradiation (450 nm).

The emission study suggested different interaction of $[D-2]^{2+}$ and $[1]^{2+}$ with DNA. To further investigate this point interaction of $[D-2](PF_6)_2$ and pUC19 plasmid DNA was further analysed using agarose gel electrophoresis. pUC19 was supplied as a 2686 bp plasmid, of which $\sim 95\%$ was in the supercoiled (SC) form. A single nick in one of the SC strands, caused by 1O_2 for example, results in the open circular (OC) form, which migrates more slowly through the gel than the SC form. Staining and visualization of the DNA using ethidium bromide (EtBr), a known DNA intercalator, is sensitive to the ratio of DNA bp (base pairs) to metal complex (MC, Figure 3.6). Thus, $[D-2]^{2+}$ and EtBr compete for the same DNA binding sites. To determine the photobinding and photocleaving ability of $[D-2]^{2+}$, a 400:1 bp:MC (base pairs:metal complex) ratio was used. At such a low metal complex concentration ($\sim 5 \mu M$), $[D-2]^{2+}$ displayed minimal binding in the dark, and also allowed for DNA visualization using EtBr (Figure 3.6). With increasing light doses however ($\lambda_{exc} = 454$ nm, 1 min, $0.6 J \cdot cm^{-2}$, to 15 min, $9.5 J \cdot cm^{-2}$) two phenomena were observed. First, an increased volume of the OC form was observed at increased light doses, which is a sign of 1O_2 generation (Figure S.II.4). Second, migration retardation of the SC form was clearly observed. In our case, a limitation of DNA gel electrophoresis was that the specific mode of interaction (covalent modification vs. intercalation) could not be specified.

However, it did show that photo-induced association of $[1]^{2+}$ or $[D-2]^{2+}$ with the SC form was occurring. Taking into account both sets of DNA experiments, it is proposed that the photoproduct $[1]^{2+}$ is able to interact with mitochondrial DNA either *via* intercalation or *via* coordination, which results in increased emission of the metal complex and DNA photocleavage *via* formation of 1O_2 . Both DNA binding and DNA cleavage occur at very high bp:MC ratio compared to previously reported DNA switches,^[20-21] which highlight the exceptional photodynamic properties of $[1]^{2+}$.

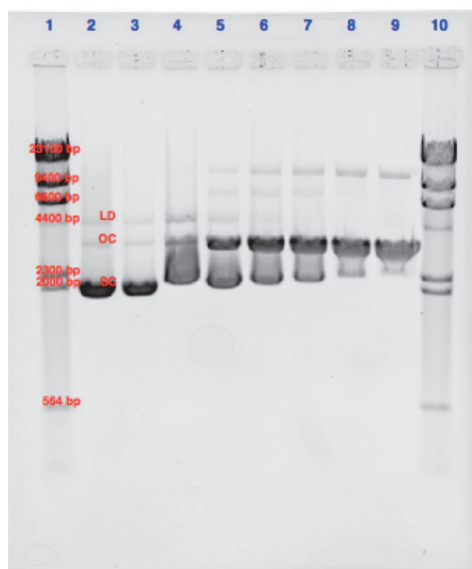


Figure 3.6. Agarose gel showing photoinduced binding and photocleavage of pUC19 plasmid DNA with $[D-2](PF_6)_2$ irradiated for 0-15 min with blue light (455 nm). LD = linear dimer, OC = open circular and SC = supercoiled. Lane 1 = λ MW marker, 2 = DNA control, 37 °C, dark, 3 = DNA control, 37 °C, irradiated, 4 = 400:1 BP:MC, 37 °C, dark, 5 – 9 = 1, 3, 5, 10 and 15 min irradiation, 10 = λ MW marker.

3.3 Conclusions

Glycoconjugation may have two functions in drug design. First, it dramatically improves the hydrophilicity of a compound, which improves drug-likeness for lipophilic compounds such as $[1]^{2+}$. By combining glycoconjugation with the light-induced uncaging properties of ruthenium-based polypyridyl compounds, one can recover the hydrophobic active molecule $[1]^{2+}$ inside the cell providing the glycoconjugated compound can still cross the cell membrane. For $[D-2](PF_6)_2$ and $[L-2](PF_6)_2$ this approach was very successful: the dpnn ligand is lipophilic enough to counter-balance the hydrophilicity of the glucose moiety, which allows passive uptake to take place. Upon irradiation with a low dose of visible light (454 nm, $3.2 \text{ J}\cdot\text{cm}^{-2}$) a very high cytotoxic activity characterized by submicromolar EC_{50} values was obtained. The significant phototoxic indices of these compounds may be a

consequence of two photochemical reactions occurring at least in the mitochondria. First, photosubstitution of the thioether-glucose ligand in $[\mathbf{D-2}]^{2+}$ by water occurs, which allows the photoproduct $[\mathbf{1}]^{2+}$ to interact better with biomolecules. In particular, mitochondrial DNA seems a likely target of the achiral photoproduct $[\mathbf{1}]^{2+}$, as it interacts with plasmid DNA at particularly high bp:Ru ratio. Second, both $[\mathbf{2}]^{2+}$ and $[\mathbf{1}]^{2+}$ efficiently generate $^1\text{O}_2$, which for adducts between mitochondrial DNA and $[\mathbf{1}]^{2+}$ leads to extensive DNA photocleavage. To our knowledge, these results represent the first practical demonstration that photosubstitution and singlet oxygen generation can combine *in vitro* into a dual mode-of-action resulting in highly efficient light-induced cancer cell death.

The second function of glycoconjugation is to introduce specific interactions between the (pro)drug and glucose-sensitive enzymes. Increased cytotoxicities measured for D-glucose-appended drugs, for example vs. their aglycon analogues, are often interpreted as a sign of glucose transporter-mediated uptake. A similar interpretation would have led us to conclude that the higher dark cytotoxicity of $[\mathbf{D-2}](\text{PF}_6)_2$ vs. $[\mathbf{L-2}](\text{PF}_6)_2$ was the result of glucose transporters being targeted by the D-glucose functional group in $[\mathbf{D-2}](\text{PF}_6)_2$. However, *in vitro* imaging showed no difference in uptake or cellular localization between the two enantiomers, and addition of sodium azide concluded to energy-independent drug uptake. These results demonstrate that GLUT or SGLT are not involved in the uptake of these compounds, and thus that other enzymes, such as for example efflux pumps and/or glucosidases,^[22] must be responsible for the twice higher cytotoxicity of $[\mathbf{D-2}](\text{PF}_6)_2$ in the dark, compared to $[\mathbf{L-2}](\text{PF}_6)_2$. This work has also unexpected consequences: although $[\mathbf{D-2}](\text{PF}_6)_2$, *i.e.*, the complex conjugated to the natural D-glucose moiety, would be expected to be the most interesting “targeting” enantiomer, $[\mathbf{L-2}](\text{PF}_6)_2$, *i.e.*, the complex conjugated to the non-natural L-glucose moiety, actually shows a higher phototoxic index because of its lower cytotoxicity in the dark. In the end, L-glucose derivatization showed a better pharmacological outcome than functionalization with D-glucose.

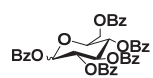
3.4 Experimental

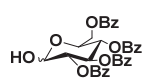
3.4.1 General

Reagents were purchased from Sigma-Aldrich and used without further purification. Benzo[*i*]dipyrido-[3,2-*a*:2',3'-*c*]phenazine (dppn) was synthesized according to a literature procedure.^[23] 2,2':6',2''-Terpyridine (tpy) was ordered from ABCR GmbH & Co. Dry solvents were collected from a Pure Solve MD5 dry solvent dispenser from Demaco. For all inorganic reactions solvents were deoxygenated by bubbling argon through the solution for 30 minutes. Flash chromatography was performed on silica gel (Screening devices B.V.) with a particle size of 40 - 64 μM and a pore size of 60 Å. TLC analysis was conducted on TLC aluminium foils with silica gel matrix (Supelco, silica gel 60, 56524) with detection by UV-absorption (254 nm), by spraying with 10% H_2SO_4 in ethanol or with a solution of

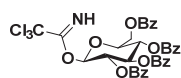
$\text{NH}_4\text{Mo}_7\text{O}_{24}\cdot 4\text{H}_2\text{O}$ 25 g/L, $\text{NH}_4\text{CeSO}_4\cdot \text{H}_2\text{O}$ 10 g/L, 10% H_2SO_4 in H_2O , followed by charring at ~ 250 °C on a heating plate. Optical rotation measurements were performed on a Propol automated polarimeter (sodium D-line, $\lambda = 589$ nm) with a concentration of 10 mg/mL ($c = 1$) unless stated otherwise. Infrared spectra were recorded on a Perkin Elmer UATR (Single Reflection Diamond) Spectrum Two device ($4000\text{--}700$ cm^{-1} ; resolution 4 cm^{-1}). ^1H NMR and ^{13}C NMR were recorded in $[\text{D}_6]\text{DMSO}$, CD_3OD and CDCl_3 with chemical shift (δ) relative to the solvent peak. High resolution mass spectra were recorded by direct injection (2 μL of 2 μM solution in water/acetonitrile; 50/50; v/v and 0.1% formic acid) in a mass spectrometer (Thermo Finnigan LTQ Orbitrap) equipped with an electrospray ion source in positive mode (source voltage 3.5 kV, sheath gas flow 10, capillary temperature 250 °C) with resolution $R = 60000$ at m/z 400 (mass range $m/z = 150 - 2000$) and dioctylphthalate ($m/z = 391.28428$) as a lock mass. The high-resolution mass spectrometer was calibrated prior to measurements with a calibration mixture (Thermo Finnigan). Elemental analysis was performed at Kolbe Mikrolab Germany.

3.4.2 Synthesis

 **1,2,3,4,6-Penta-O-benzoyl- α/β -L-glucopyranose, L-6:** To a solution of L-glucose^[24] (627 mg, 3.47 mmol) in pyridine (17.0 mL) at 0 °C, was slowly added benzoyl chloride (2.20 mL, 18.9 mmol). The suspension was allowed to stir for 6 h at room temperature, after which excess benzoyl chloride was neutralized upon the addition of water (10 mL), resulting in a clear solution. The solution was further diluted with EtOAc (~ 100 mL) and washed with 1 M HCl (2x), NaHCO_3 (aq.) (2x) and brine (2x). Layers were separated, and the organic layer was dried over Na_2SO_4 and subsequently concentrated *in vacuo*. Purification over silica (0 to 10% MeOH in DCM) afforded the title compound as a white solid (2.43 g, 3.47 mmol, quant. α/β ratio of 1:2). The analytical data are in agreement with those reported in literature^[25], but the sign of the specific rotation was found opposite. $[\alpha]_{\text{D}}^{20}$ (CHCl_3): +49.2 (α/β 1:2).

 **2,3,4,6-Tetra-O-benzoyl- α,β -L-glucopyranose, L-7:** To a cooled solution of L-6 (3.01 g, 4.30 mmol) in DCM (10 mL) was added 33% HBr in AcOH (2.50 mL, 10.2 mmol). The resulting yellow/orange solution was allowed to stir overnight, after which it was diluted with EtOAc (250 mL) followed by washing NaHCO_3 aq. (2x), H_2O (2x) and brine (2x). Layers were separated and the organic layer was dried over Na_2SO_4 and concentrated *in vacuo*. The crude was dissolved in acetone (15 mL) and water (0.40 mL) and Ag_2CO_3 (650 mg, 2.36 mmol) were added. The suspension was allowed to stir at room temperature for 3 h, after it was filtrated over Celite® and concentrated *in vacuo*, affording the title compound as a white foam (2.43 g, 4.26 mmol, 99%, α/β ratio of

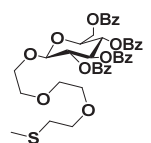
1:1). The analytical data are in agreement with those reported in literature^[26], but the sign of the specific rotation was found opposite. α -anomer: $[\alpha]_{\text{D}}^{20}(\text{CHCl}_3)$: -68.2°



2,3,4,6-Tetra-O-benzoyl-1- β -L-glucopyranosyl trichloroacetimidate, L-8:

To a solution of L-7 (2.19 g, 3.67 mmol) and in dry DCM was added DBU (0.60 mL, 4.02 mmol) and trichloroacetonitrile (13.0 mL, 130 mmol).

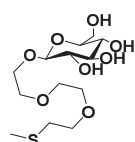
This solution was allowed to stir overnight, after which it was concentrated *in vacuo*. Purification of the crude over silica (33% EtOAc in PE) afforded the title compound as an off-white foam (2.12 g, 2.86 mmol, 78%, α/β ratio of 1:1). The analytical data are in agreement with those reported in literature,^[27] but the sign of the specific rotation was found opposite. α -anomer: $[\alpha]_{\text{D}}^{20}(\text{CHCl}_3)$: -62.0°



2-[2-(2-(Methylthio)ethoxy)ethoxy]ethyl 2,3,4,6-tetra-O-benzoyl- β -L-glucopyranoside, L-9:

This compound was prepared as described for 2-[2-(2-(Methylthio)ethoxy)ethoxy]ethyl 2,3,4,6-tetra-O-benzoyl- β -D-glucopyranoside (Chapter 2), but starting from L-8 (2.12 g, 2.86 mmol).

Yield: 1.49 g, 1.96 mmol, 69%. L-9 has the same spectroscopic properties as its enantiomer, however with the opposite sign of rotation. $[\alpha]_{\text{D}}^{20}(\text{CHCl}_3)$: -18.0 .

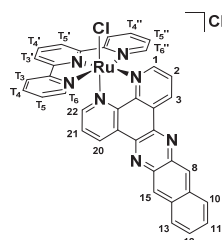


2-[2-(2-(Methylthio)ethoxy)ethoxy]ethyl β -L-glucopyranoside, L-3:

This compound was prepared as described for (2-Methylthio)ethyl- β -D-glucopyranoside (Chapter 2) but starting from L-9 (1.47 g, 1.99 mmol) Yield:

580 mg, 1.69 mmol, 85%. L-3 has the same spectroscopic properties as its

enantiomer, however with opposite sign of rotation. $[\alpha]_{\text{D}}^{20}(\text{MeOH})$: $+11.8$.



[Ru(tpy)(dppn)Cl]Cl, [4]Cl: Ruthenium dimer $[\{\text{Ru}(\text{tpy})\text{Cl}_2\}_2] \cdot \text{H}_2\text{O}$ ^[28]

(300 mg, 0.347 mmol) and dppn^[23] (231 mg, 0.695 mmol) were

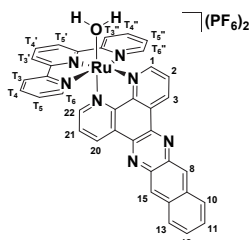
dissolved in a deoxygenated solution of ethylene glycol (17 mL) which was heated to 100 °C under an argon atmosphere for five h.

The resulting purple solution was then filtered over Celite®.

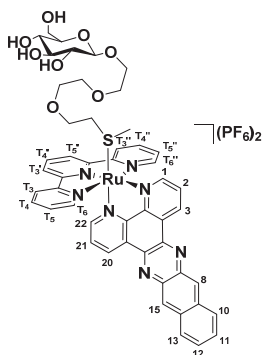
Addition of Et₂O to the filtrate resulted in a precipitate which was collected on a glass frit and thoroughly washed with water and

Et₂O, followed by drying under high vacuum which furnished the title compound as a purple powder (383 mg, 0.473 mmol, 75%). $R_f = 0.31$ (10% MeOH in DCM). ¹H NMR (400 MHz, [D₆]DMSO) $\delta = 10.42$ (d, $J = 4.7$ Hz, 1H, 1), 9.75 (d, $J = 8.0$ Hz, 1H, 3), 9.21 – 9.06 (m, 3H, 8, 22, 15), 8.90 (d, $J = 8.1$ Hz, 2H, T₃', T₅'), 8.75 (d, $J = 8.1$ Hz, 2H, T₆', T₆''), 8.56 (dd, $J = 8.1, 5.4$ Hz, 1H, 2), 8.38 (d, $J = 9.5$ Hz, 1H, T₃', T₃''), 8.30 (t, $J = 8.1$ Hz, 1H, T₄''), 7.99 (t, $J = 8.1$ Hz, 2H, T₅', T₅''), 7.83 (d, $J = 5.4$ Hz, 1H, 20), 7.78 – 7.65 (m, 4H, 10, 13, T₄', T₄''), 7.53 (dd, $J = 8.1, 5.5$ Hz, 1H, 21), 7.32 (t, $J = 6.7$ Hz, 2H, 11, 12); ¹³C NMR (100 MHz, DMSO) $\delta = 158.4$

(C_q), 157.6 (C_q), 154.0 (C_H 1), 153.80 (C_H 20), 152.6 (C_q), 152.5 (C_H 10, C_H 13), 150.5 (C_q), 141.5 (C_q), 141.0 (C_q), 137.9 (C_q), 137.8 (C_q), 137.2 (C_H T₅, C_H T₅''), 134.5 (C_q), 134.4 (C_q), 134.2 (C_H T₄'), 131.9 (C_H 3), 130.8 (C_H 8), 130.1 (C_q), 129.6 (C_q), 128.5 (C_H T₃), 128.5 (C_H T₃''), 127.9 (C_H 22), 127.8 (C_H 15), 127.3 (C_H T₄, T₄''), 127.2 (C_H 11, C_H 12), 126.5 (C_H 21), 123.7 (C_H 21), 122.80 (C_H T₃', C_H T₅'); HRMS m/z calcd for [C₃₇H₂₃N₇RuClRu - Cl]: 702.07415; found: 702.07439. Elemental analysis calcd (%) for C₃₇H₂₃N₇Ru.4H₂O: C 54.89, H 3.86, N 12.11; found: C 53.63, H 3.83, N 11.61.



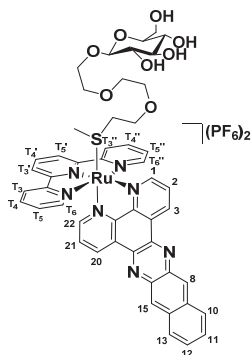
[Ru(tpy)(dppn)(H₂O)](PF₆)₂, [1](PF₆)₂: To a solution of [4]Cl (73.0 mg, 0.099 mmol) in acetone/water (10 mL, 3:1) was added AgNO₃ (39.0 mg, 0.230 mmol). This mixture was allowed to stir under argon at 50 °C for 16 h, after which it was filtered over Celite®. 2 mL of a saturated solution of NH₄PF₆ was added to the filtrate and the resulting brown precipitate was collected on a glass frit, followed by washing with H₂O (3x) and Et₂O (3x), affording [10](PF₆)₂ as a brown precipitate (60 mg, 0.083 mmol, 84%) which was used without further purification. *R_f* = 0.5 (100/80/20 acetone/water/sat. aq. KPF₆).



[Ru(tpy)(dppn)(d-3)](PF₆)₂, [D-2](PF₆)₂: [1](PF₆)₂ (60.0 mg, 0.0668 mmol) and ligand d-3 (61.0 mg, 0.178 mmol) were dissolved in deoxygenated acetone and stirred at 50 °C for 24 h under an argon atmosphere in the dark. The resulting brown/orange solution was concentrated *in vacuo* at 30 °C in the dark, followed by purification of the crude over silica (acetone/water/saturated aqueous KPF₆ 100:0:0 to 80:20:0 to 100:80:20) followed by further purification over Sephadex LH-20 (acetone). The orange fraction was collected and the volume was reduced to ~10%, followed by addition of Et₂O, resulting in

a precipitate which was collected by filtration over a Whatman® RC60 membrane filter and subsequently washed with EtOAc (3x), Et₂O (3x) and *n*-hexane (3x), affording the title compound as an orange powder (30 mg, 23 μmol, 35%). *R_f* = 0.36 (16:4:1 acetone/water/sat. KPF₆); ¹H NMR (400 MHz, [D₆]acetone) δ = 10.39 (d, J = 5.4 Hz, 1H, 1), 10.09 (d, J = 8.2 Hz, 1H, 3), 9.60 (d, J = 8.3 Hz, 1H, 22), 9.27 (s, 1H, 8), 9.15 (s, 1H, 15), 9.03 (d, J = 8.2 Hz, 2H, T₃', T₅'), 8.84 (d, J = 8.0 Hz, 2H, T₆, T₆''), 8.73 (dd, J = 8.3, 5.3 Hz, 1H, 2), 8.61 (t, J = 8.2 Hz, 1H, T₄'), 8.44 (dd, J = 18.7, 9.0 Hz, 2H, 11, 12), 8.19 (t, J = 7.9 Hz, 2H, T₅, T₅''), 8.13 (t, J = 3.7 Hz, 2H, T₄, T₄''), 8.06 (d, J = 5.4 Hz, 1H, 20), 7.84 – 7.76 (m, 3H, 21, 10, 13), 7.47 (t, J = 6.6 Hz, 2H, T₃, T₃''), 4.31 (d, J = 7.7 Hz, 1H, H-1), 4.23 (dd, J = 12.9, 3.5 Hz, 1H, CHH H-6), 3.99 – 3.92 (m, 1H, CHH OCH₂), 3.86 – 3.76 (m, 1H, CHH OCH₂), 3.71 – 3.51 (m, 12H, CHH H-6, 2 x CHH OCH₂, 3 x CH₂ OCH₂), 3.41 – 3.23 (m, 3H, H-3, H-4, H-5), 3.11 (td, J = 8.2, 3.5 Hz, 1H, H-2), 2.26 – 2.18 (m, 2H, CH₂ OCH₂SMe), 1.66 (s, 3H). ¹³C NMR (100

MHz, [D₆]acetone) δ = 159.0 (C_q), 158.5 (C_q), 155.0 (C_H 1), 153.2 (C_H 1, C_H T₃, C_H T₃''), 139.4 (C_H T₅, C_H T₅''), 138.3 (C_H T₄'), 136.0 (C_q), 135.0 (C_H 3) 134.7 (C_H 22), 132.5 (C_q), 131.4 (C_q), 129.5 (C_H T₄, C_H T₄''), 129.5 (C_H 11, C_H 12) 129.1 (C_H 8, C_H 15), 128.9 (C_H 11, C_H 5, C_H 8), 128.0 (H_{arom}), 126.1 (C_H T₆, C_H T₆''), 125.4 (C_H T₃', C_H T₅'), 104.2 (C-1), 78.0 (C-3), 77.5 (C-4), 74.8 (C-2), 71.7 (C-5), 71.0 (2 x CH₂ OCH₂), 70.9 (CH₂ OCH₂), 69.3 (CH₂ OCH₂), 68.2 (CH₂ OCH₂), 62.9 (C-6), 35.6 (CH₂ OCH₂SMe), 15.6 (OCH₂SMe); HRMS *m/z* calcd for [C₅₀H₄₉O₈N₇SRu – 2PF₆]: 504.61979; found: 504.61993. Elemental analysis calcd (%) for [D-2](PF₆)₂: C 46.23, H 3.80, N 7.55; found: C 46.26, H 3.81, N 7.53.



[Ru(tpy)(dppn)(L-3)](PF₆)₂, [L-2](PF₆)₂: This compound was synthesized and purified according to the procedure described for compound [D-2](PF₆)₂, starting from ligand L-3 (94.0 mg, 0.0964 mmol) instead of D-3. This procedure afforded [L-2](PF₆)₂ as an orange powder (40 mg, 0.031 mmol, 32%). ¹H NMR and HRMS matched those reported for [D-2](PF₆)₂. Elemental analysis for [L-2](PF₆)₂·H₂O: C 45.60, H 3.90, N 7.44; found: C 45.70, H 4.06, N 7.32.

3.4.3 Emission spectroscopy: Interaction with DNA

0.15 mL of a stock solution of [D-2](PF₆)₂ (14 μ M) was prepared in phosphate buffer and was diluted with PBS (0.30 mL) in a semi-micro cuvette (4.7 μ M), followed by 450 nm irradiation of the sample for 25 minutes (50 mW, 4 mm beam diameter, 8% of the sample simultaneously irradiated). During this period, emission spectra were continuously recorded. At the end of irradiation, [D-2](PF₆)₂ had been fully converted to the aqua complex [1](PF₆)₂. Then, 0.15 mL of a solution of sonicated calf thymus DNA was added to reach a final DNA concentration of 0.5 mg/mL, leading to a strong increase of the emission. The sample was left in the dark, while emission spectra were recorded at an interval of five minutes until *t* = 45 minutes; no major variation of the emission intensity was observed. After this period, the sample was irradiated continuously again, which led to a gradual increase of the emission intensity. In a parallel experiment, CT-DNA and [D-2](PF₆)₂ were mixed directly at *t* = 0 and the sample was irradiated at 450 nm for 25 min while recording emission spectra continuously. In such conditions the emission intensity increased in a sigmoidal curve, suggesting cleavage of the thioether-glucose conjugate and switched on emission following insertion of the dppn ligand between DNA based pairs.

3.4.4 Photochemistry

3.4.4.5 General procedure for photosubstitution quantum yield measurements

3.00 mL of a solution of [D-2](PF₆)₂ (4.23×10⁻⁵ M) in H₂O was deoxygenated for 15 minutes with dinitrogen gas, after which it was irradiated with a blue LED (447 nm, FWHM: 19 nm) with photon flux $\Phi = 1.77 \cdot 10^{-7}$ mol photons · s⁻¹ while the solution was kept at constant temperature (25 °C). During irradiation UV-vis spectra were recorded on a Varian Inc. Cary 50 UV-vis spectrometer with intervals of 30 seconds until t = 3600 seconds. ESI-MS spectra were recorded after the irradiation experiment to confirm the formation of the aqua species [Ru(tpy)(dppn)(OH₂)²⁺ (m/z = found 342.4, calculated 342.5). The quantum yield for the photosubstitution of the thioether ligand was calculated according to the method described earlier.^[29] Reference molar absorption coefficients used to calculate concentrations during irradiation are provided in Table 3.3.

Table 3.3 Reference wavelengths (λ_{ref}) and molar absorption coefficients (ϵ_{ref}) for photosubstitution quantum yield calculations.

Compound	λ_{ref} in nm	ϵ_{ref} (M ⁻¹ cm ⁻¹)
[1](PF ₆) ₂	490	10.8 × 10 ³
	430	12.4 × 10 ³
[D-2](PF ₆) ₂	490	10.5 × 10 ³
	430	7.4 × 10 ³

3.4.4.6 ¹O₂ and phosphorescence quantum yield measurements

See general appendix I.1.1 and Figure S.II.2.

3.4.5 Biology

Cytotoxicity studies were carried out as described in appendix 1.2.1. A detailed description of the DNA interaction studies and emission microscopy experiments are given in appendix II.2.

References

- [1] a). D. Deng, C. Xu, P. Sun, J. Wu, C. Yan, M. Hu, N. Yan, *Nature* **2014**, *510*, 121-125; b). K. O. Alfarouk, D. Verduzco, C. Rauch, A. K. Muddathir, H. H. B. Adil, G. O. Elhassan, M. E. Ibrahim, J. David Polo Orozco, R. A. Cardone, S. J. Reshkin, S. Harguindey, *Oncoscience* **2014**, *1*, 777-802.
- [2] a). M. M. Welling, R. Alberto, *Nucl Med Commun* **2010**, *31*, 239-248; b). C. L. Ferreira, S. R. Bayly, D. E. Green, T. Storr, C. A. Barta, J. Steele, M. J. Adam, C. Orvig, *Bioconjugate Chem* **2006**, *17*, 1321-1329.
- [3] E. C. Calvaresi, P. J. Hergenrother, *Chem Sci* **2013**, *4*, 2319-2333.
- [4] a). E. C. Calvaresi, C. Granchi, T. Tuccinardi, V. Di Bussolo, R. W. Huigens, 3rd, H. Y. Lee, R. Palchadhuri, M. Macchia, A. Martinelli, F. Minutolo, P. J. Hergenrother, *ChemBiochem* **2013**, *14*, 2263-2267; b). D. N. Pelageev, S. A. Dyshlovoy, N. D.

- Pokhilo, V. A. Denisenko, K. L. Borisova, G. Keller-von Amsberg, C. Bokemeyer, S. N. Fedorov, F. Honecker, V. P. Anufriev, *Eur J Med Chem* **2014**, *77*, 139-144.
- [5] a). U. Basu, I. Khan, A. Hussain, B. Gole, P. Kondaiah, A. R. Chakravarty, *Inorg Chem* **2014**, *53*, 2152-2162; b). W. H. Law, L. C. Lee, M. W. Louie, H. W. Liu, T. W. Ang, K. K. Lo, *Inorg Chem* **2013**, *52*, 13029-13041; c). P. Liu, Y. Lu, X. Gao, R. Liu, D. Zhang-Negrerie, Y. Shi, Y. Wang, S. Wang, Q. Gao, *Chem Commun* **2013**, *49*, 2421-2423; d). R. Schibli, C. Dumas, J. Petrig, L. Spadola, L. Scapozza, E. Garcia-Garayoa, P. A. Schubiger, *Bioconjugate Chem* **2005**, *16*, 105-112; e). M. L. Bowen, C. Orvig, *Chem Commun* **2008**, 5077-5091.
- [6] B. Banik, K. Somyajit, A. Hussain, G. Nagaraju, A. R. Chakravarty, *Dalton Trans* **2014**, *43*, 1321-1331.
- [7] J. Park, J. I. Um, A. Jo, J. Lee, D. W. Jung, D. R. Williams, S. B. Park, *Chem Commun* **2014**, *50*, 9251-9254.
- [8] M. Patra, T. C. Johnstone, K. Suntharalingam, S. J. Lippard, *Angew Chem Int Ed* **2016**, *55*, 2550-2554.
- [9] C. Barron, E. Tsiani, T. Tsakiridis, *BMC Proc* **2012**, *6*, P4.
- [10] J. Pohl, B. Bertram, P. Hilgard, M. R. Nowrousian, J. Stuben, M. Wiessler, *Cancer Chemother Pharmacol* **1995**, *35*, 364-370.
- [11] a). Y. Liu, Y. Cao, W. Zhang, S. Bergmeier, Y. Qian, H. Akbar, R. Colvin, J. Ding, L. Tong, S. Wu, J. Hines, X. Chen, *Mol Cancer Ther* **2012**, *11*, 1672-1682; b). W. K. Miskimins, H. J. Ahn, J. Y. Kim, S. Ryu, Y. S. Jung, J. Y. Choi, *PLoS One* **2014**, *9*, e85576; c). A. Dilip, G. Cheng, J. Joseph, S. Kunnimalaiyaan, B. Kalyanaraman, M. Kunnimalaiyaan, T. C. Gamblin, *Anticancer Drugs* **2013**, *24*, 881-888.
- [12] L. Venturelli, S. Nappini, M. Bulfoni, G. Gianfranceschi, S. Dal Zilio, G. Coceano, F. Del Ben, M. Turetta, G. Scoles, L. Vaccari, D. Cesselli, D. Cojoc, *Sci Rep* **2016**, *6*, 21629.
- [13] D. Deng, P. Sun, C. Yan, M. Ke, X. Jiang, L. Xiong, W. Ren, K. Hirata, M. Yamamoto, S. Fan, N. Yan, *Nature* **2015**, *526*, 391-396.
- [14] a). R. E. Goldbach, I. Rodriguez-Garcia, J. H. van Lenthe, M. A. Siegler, S. Bonnet, *Chem Eur J* **2011**, *17*, 9924-9929; b). B. S. Howerton, D. K. Heidary, E. C. Glazer, *J Am Chem Soc* **2012**, *134*, 8324-8327; c). T. Respondek, R. N. Garner, M. K. Herroon, I. Podgorski, C. Turro, J. J. Kodanko, *J Am Chem Soc* **2011**, *133*, 17164-17167; d). V. H. S. van Rixel, B. Siewert, S. L. Hopkins, S. H. C. Askes, A. Busemann, M. A. Siegler, S. Bonnet, *Chem Sci* **2016**, *7*, 4922-4929; e). M. A. Sgambellone, A. David, R. N. Garner, K. R. Dunbar, C. Turro, *J Am Chem Soc* **2013**, *135*, 11274-11282; f). L. Zayat, C. Calero, P. Albores, L. Baraldo, R. Etchenique, *J Am Chem Soc* **2003**, *125*, 882-883.
- [15] a). D. Crespy, K. Landfester, U. S. Schubert, A. Schiller, *Chem Commun* **2010**, *46*, 6651-6662; b). U. Schatzschneider, *Eur J Inorg Chem* **2010**, *2010*, 1451-1467; c). C. Mari, V. Pierroz, S. Ferrari, G. Gasser, *Chem Sci* **2015**, *6*, 2660-2686; d). N. J. Farrer, L. Salassa, P. J. Sadler, *Dalton Trans* **2009**, 10690-10701; e). A. Presa, R. F. Brissos, A. B. Caballero, I. Borilovic, L. Korrodi-Gregorio, R. Perez-Tomas, O. Roubeau, P. Gamez, *Angew Chem Int Ed* **2015**, *54*, 4561-4565.
- [16] X. Zhu, R. R. Schmidt, *Angew Chem Int Ed* **2009**, *48*, 1900-1934.

- [17] J. D. Knoll, B. A. Albani, C. Turro, *Chem Commun* **2015**, 51, 8777-8780.
- [18] H. Huang, B. Yu, P. Zhang, J. Huang, Y. Chen, G. Gasser, L. Ji, H. Chao, *Angew Chem Int Ed* **2015**, 54, 14049-14052.
- [19] A. C. Komor, J. K. Barton, *Chem Commun* **2013**, 49, 3617-3630.
- [20] a). A. E. Friedman, J.-C. Chambron, J.-P. Sauvage, N. J. Turro, J. K. Barton, *J Am Chem Soc* **1990**, 112, 4960-4962; b). H. Niyazi, J. P. Hall, K. O'Sullivan, G. Winter, T. Sorensen, J. M. Kelly, C. J. Cardin, *Nat Chem* **2012**, 4, 621-628.
- [21] a). H. Song, J. T. Kaiser, J. K. Barton, *Nat Chem* **2012**, 4, 615-620; b). Y. Sun, L. E. Joyce, N. M. Dickson, C. Turro, *Chem Commun* **2010**, 46, 2426-2428.
- [22] H. Seker, B. Bertram, A. Burkle, B. Kaina, J. Pohl, H. Koepsell, M. Wiesser, *Br J Cancer* **2000**, 82, 629-634.
- [23] A. J. McConnell, M. H. Lim, E. D. Olmon, H. Song, E. E. Dervan, J. K. Barton, *Inorg Chem* **2012**, 51, 12511-12520.
- [24] R. F. Martinez, Z. Liu, A. F. Glawar, A. Yoshihara, K. Izumori, G. W. Fleet, S. F. Jenkinson, *Angew Chem Int Ed* **2014**, 53, 1160-1162.
- [25] D. Sail, P. Kovac, *Carbohydr Res* **2012**, 357, 47-52.
- [26] A. E. Salinas, J. F. Sproviero, V. Deulofeu, *Carbohydr Res* **1987**, 170, 71-99.
- [27] I. A. Ivanova, A. J. Ross, M. A. J. Ferguson, A. V. Nikolaev, *J Chem Soc Dalton* **1999**, 1743-1754.
- [28] D. C. Marelus, S. Bhagan, D. J. Charboneau, K. M. Schroeder, J. M. Kamdar, A. R. McGettigan, B. J. Freeman, C. E. Moore, A. L. Rheingold, A. L. Cooksy, D. K. Smith, J. J. Paul, E. T. Papish, D. B. Grotjahn, *Eur J Inorg Chem* **2014**, 676-689.
- [29] A. Bahreman, J. A. Cuello-Garibo, S. Bonnet, *Dalton Trans* **2014**, 43, 4494-4505.

Chapter 4:

Photodynamic therapy or photoactivated chemotherapy?

Effects of the bidentate ligand on the photophysical properties, cellular uptake, and (photo)cytotoxicity of glycoconjugates based upon the $[\text{Ru}(\text{tpy})(\text{NN})(\text{L})]^{2+}$ scaffold

4

Abstract: Ruthenium polypyridyl complexes have received widespread attention as potential chemotherapeutics in photodynamic therapy (PDT) and in photochemotherapy (PACT). Herein we investigate a series of sixteen ruthenium polypyridyl complexes with general formula $[\text{Ru}(\text{tpy})(\text{N-N})(\text{L})]^{+2}$ (tpy = 2,2':6',2''-terpyridine, N-N = bpy (2,2'-bipyridine), phen (1,10-phenanthroline), dpq (pyrazino[2,3-f][1,10]phenanthroline), dppz (dipyrido[3,2- α :2',3'-c]phenazine, dppn (benzo[*j*]dipyrido[3,2- α :2',3'-c]phenazine), pmip (2-(4-methyl-phen-yl)-1*H*-imidazo[4,5-f][1,10]phenanthroline), pyimi ((*E*)-*N*-phenyl-1-(pyridin-2-yl)methanimine), or azpy (2-(phenylazo)pyridine), L = Cl or 2-(2-(2-(methylthio)ethoxy)ethoxy)ethyl- β -D-glucopyranoside) and their potential for either PDT or PACT. We demonstrate that although increased lipophilicity is generally related to increased uptake of these complexes, it does not necessarily lead to increased (photo)cytotoxicity. However, the non-toxic complexes are excellent candidates as PACT carriers.

This chapter will be submitted for publication: L. N. Lameijer, T. G. Brevé, V. H. S. van Rixel, S. H. C. Askes, M. Siegler, S. Bonnet.; *Manuscript in preparation.*

4.1 Introduction

Ruthenium based anti-cancer compounds have been investigated for several decades^[1] as potential alternatives to the clinically approved cisplatin. Cisplatin is associated with serious side effects such as renal toxicity, neurotoxicity, and hearing loss.^[2] The most thoroughly investigated ruthenium-based anti-cancer agents, NAMI-A and KP1019, both reached phase II clinical trials before being abandoned.^[3] More recently the tunable photophysical properties of ruthenium(II) polypyridyl complexes have been used to develop compounds combating bacterial resistance to antibiotics,^[4] or new photosensitizers for photodynamic therapy as an alternative to *e.g.* Photofrin.^[5] Recently, the group of McFarland have made a great step forward in this field, by entering Phase I clinical trials with a Ru(II)-thiophene-polypyridyl-based photosensitizer, TLD1433.^[6] Simultaneously, a great interest has been shown in the development of sterically strained ruthenium(II) complexes for the light-induced delivery of cytotoxic cargo.^[7] This last approach is often referred to as photo-activated chemotherapy (PACT).^[3b] The proof-of-concept for ruthenium-based PACT was first demonstrated by Etchenique's group, who showed that the photoinduced release of the potassium channel blocker 4-aminopyridine (4AP) from $[\text{Ru}(\text{bpy})_2(4\text{AP})_2]^{2+}$ upon visible light irradiation, lead to a response in leech neurons.^[8] Many other examples of ruthenium complexes used as photoactive agents releasing anticancer molecules have been developed by the group of Turro,^[9] Gasser,^[10] Glazer,^[11] Kodanko^[12], and Bonnet.^[13] Following up on our initial work using thioether monodentate ligands to cage cytotoxic aqua ruthenium complexes,^[13-14] we herein report a series of related chloride complexes **[1a]Cl**-**[8a]Cl** having the general formula $[\text{Ru}(\text{tpy})(\text{N-N})(\text{Cl})]\text{Cl}$ with N-N = bpy (2,2'-bipyridine), phen (1,10-phenanthroline), dpq (pyrazino[2,3-*f*][1,10]phenanthroline), dppz (dipyrido[3,2-*a*:2',3'-*c*]phenazine), dppn (benzo[*i*]dipyrido[3,2-*a*:2',3'-*c*]phenazine), pmip (2-(4-methyl-phen-yl)-1*H*-imidazo[4,5-*f*][1,10]phenanthroline), pymi ((*E*)-*N*-phenyl-1-(pyridin-2-yl)methanimine), or azpy (2-(phenylazo)pyridine), respectively, and of their water-soluble derivatives $[\text{Ru}(\text{tpy})(\text{N-N})(\text{L})](\text{PF}_6)_2$ (**[1b]**(PF₆)₂-**[8b]**(PF₆)₂), where R = (2-(2-(2-(methylthio)ethoxy)ethoxy)ethyl-β-D-glucopyranoside is a thioether-glucose conjugate (Figure 4.1).

On the one hand, $[\text{Ru}(\text{tpy})(\text{bpy})(\text{Cl})]\text{Cl}$ is known to be poorly cytotoxic to cancer cells.^[15] On the other hand, we recently demonstrated that $[\text{Ru}(\text{tpy})(\text{dppn})(\text{L})](\text{PF}_6)_2$ (**[5b]**(PF₆)₂, (Figure 4.1) has unique phototoxic properties based on a dual mode-of-action involving both photosubstitution of the thioether ligand and singlet oxygen generation. In this chapter, we compare the photophysical properties of all conjugates **[1b]**(PF₆)₂-**[8b]**(PF₆)₂ and of their chloride analogues **[1a]Cl**-**[8a]Cl** in water, and correlate them to the uptake and cytotoxicity in cancer cells. Critically, the glucose-containing ligand L ensures that all thioether-ruthenium complexes are soluble in water, allowing their photochemistry to be studied independently from the lipophilicity of the N-N spectator bidentate ligand.

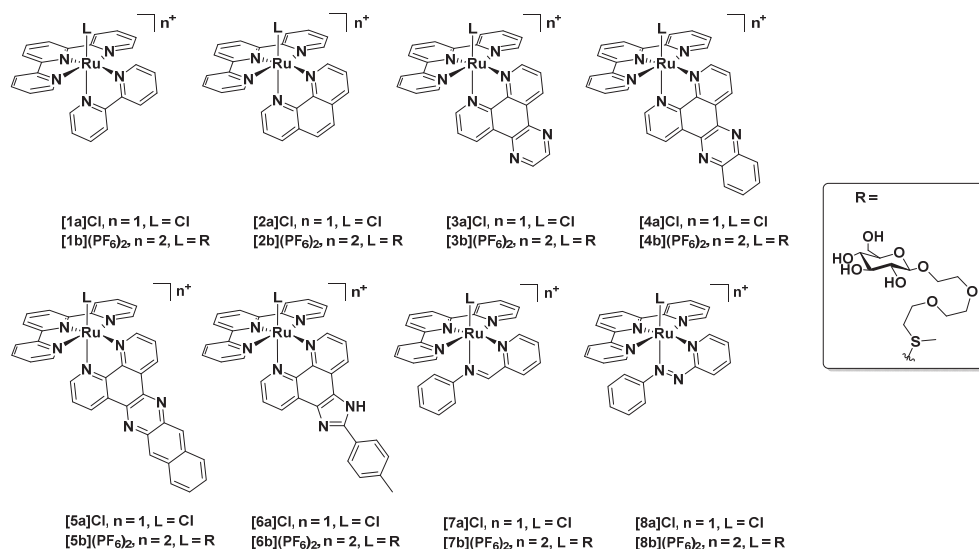


Figure 4.1. Chemical structure of the complexes used in this study. General formula [Ru(tpy)(N-N)(L)]ⁿ⁺, N-N = bpy, phen, dpq, dpbz, dpnn, pmip, pymi or azpy. L = Cl or L = R (2-(2-(2-(methylthio)ethoxy)ethoxy)ethyl-β-D-glucopyranoside).

4.2 Results

4.2.1 Synthesis

Chloride complexes [1a]Cl,^[16] [2a]Cl,^[17] [4a]Cl,^[18] [5a]Cl,^[13b] [7a]Cl,^[19] [8a]Cl,^[20] and the ligand 2-(2-(2-(methylthio)ethoxy)ethoxy)ethyl-β-D-glucopyranoside (**R**)^[13b] were synthesized as reported previously. Complex [1b](PF₆)₂ was synthesized as described in Chapter 2. Complexes [3a]Cl and [6a]Cl were synthesized by reacting [Ru(tpy)Cl₃] with the bidentate ligand dpq or pmip in the presence of triethylamine as a reducing agent. The chloride complexes [2a]Cl–[8a]Cl were then reacted with an excess of the thioether ligand **R** in the dark in water. Silica column purification of the crude complexes, followed by size exclusion chromatography, afforded the thioether-glucose ruthenium conjugates [2b](PF₆)₂ and [4b](PF₆)₂ as orange and red solids and [8b](PF₆)₂ as a purple solid. To ease purification of the pmip complex [6b](PF₆)₂ the synthesis was carried out similarly to the previously reported synthesis of [5b](PF₆)₂^[13b] by first converting the chloride precursor [5a]Cl to the aqua species [Ru(tpy)(pmip)(H₂O)](NO₃)₂ using AgNO₃, followed by reaction of the thioether ligand with the aqua complex. Similarly, the syntheses of [3b](PF₆)₂ and [7b](PF₆)₂ were carried out in the presence of AgPF₆ to ensure *in situ* conversion to the aqua species. All chloride complexes except [4a]Cl, [5a]Cl and [6a]Cl and all thioether complexes are soluble in water. As reported for the complex [Ru(tpy)(bpy)(Hmte)](PF₆)₂,^[21] all thioether complexes showed an upfield shift of the methylsulfide group to ~1.5 ppm in the ¹H NMR spectra, confirming coordination of the thioether donor atom to the ruthenium center. All new compounds were characterized

using NMR spectroscopy, thin layer chromatography, electronic absorption spectroscopy, high-resolution mass spectrometry, and elemental analysis.

4.2.2 Crystal structures

Attempts to crystallize the glycoconjugates **[1b]**(PF₆)₂ – **[8b]**(PF₆)₂ were unsuccessful and usually led to the formation of oils or colloidal suspensions. However, crystals suitable for X-ray diffraction analysis were obtained for **[5a]**Cl, and for **[3a]**PF₆ and **[4a]**PF₆ after salt metathesis of **[3a]**Cl and **[4a]**Cl using aqueous NH₄PF₆, followed by vapor diffusion of diethyl ether to a solution of **[3a]**PF₆ in acetone or acetone to a solution of **[4a]**PF₆ in ethyl acetate. Crystals suitable for X-ray diffraction for **[5a]**Cl were obtained by vapor diffusion of diisopropylether in acetonitrile. The three crystal structures showed the expected distorted octahedral geometry, with a reduced (< 180°) N-Ru-N angle for the coordinated terpyridine ligand (N1-Ru1-N3, 159.11 – 159.40°, Table 4.1). The bidentate ligands dpq, dpbz and dppn are all bound perpendicular to tpy, with a N4-Ru1-N5 bite angle of 79.26 – 80.2° (Table 4.1). The Ru1-Cl1 bond lengths were found to be similar with values ranging from 2.4015 to 2.4165 Å which are very close to reported values for related complexes. Selected bond lengths and angles are given in Table 4.1.^[22]

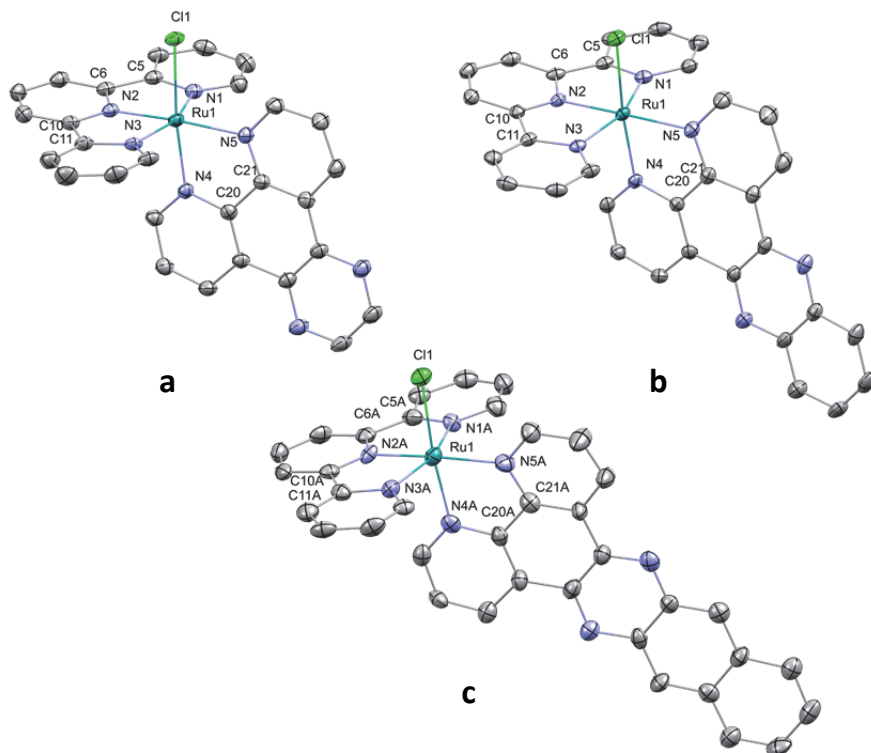


Figure 4.2. Displacement ellipsoid plots (50% probability level) of the complex cation **[3a]**PF₆, **[4a]**PF₆·(CH₃)₂CO and **[5a]**Cl. For **[5a]**Cl only one of the independent molecules is shown. Hydrogen atoms, counter-ions, and lattice solvent molecules, have been omitted for clarity.

Table 4.1 Selected bond distances (Å) and bond angles (°) for complexes **[3a]**PF₆, **[4a]**PF₆·(CH₃)₂CO and **[5a]**Cl.

	[3a] (PF ₆) ₂	[4a] (PF ₆) ₂	[5a] Cl ^[a]
Ru1 - Cl1	2.4062(5)	2.4015(7)	2.4165(17)
Ru1 - N1	2.069(2)	2.053(2)	2.048(5)
Ru1 - N2	1.9569(19)	1.957(2)	1.953(5)
Ru1 - N3	2.058(2)	2.064(2)	2.050(5)
Ru1 - N4	2.046(2)	2.044(2)	2.043(5)
Ru1 - N5	2.0917(19)	2.074(2)	2.073(5)
C5 - C6	1.472(3)	1.469(4)	1.469(9)
C5 - N1	1.369(3)	1.372(3)	1.389(8)
C6 - N2	1.355(3)	1.357(3)	1.340(7)
C10 - C11	1.478(3)	1.479(4)	1.484(8)
C10 - N2	1.355(3)	1.349(4)	1.340(7)
C11 - N3	1.371(3)	1.372(3)	1.384(7)
C20 - C21	1.446(3)	1.440(4)	1.459(8)
C20 - N4	1.370(3)	1.371(3)	1.370(7)
C21 - N5	1.364(3)	1.362(3)	1.379(8)
N1- Ru1 - N3	159.10(8)	159.58(9)	159.67(19)
N4 - Ru1- N5	79.45(8)	79.26(9)	80.2(2)

[a] Values for Ru1A.

4.2.3 Photophysical properties of the [Ru(tpy)(NN)(L)]^{nt} complexes

The photophysical properties of the chloride complexes **[1a]**Cl – **[8a]**Cl were first investigated in acetonitrile, in which the complexes are all soluble and do not hydrolyze. The chloride complexes **[1a]**Cl – **[8a]**Cl show metal-to ligand charge transfer (¹MLCT) bands varying between 501 and 523 nm corresponding to the, with molar absorptivities ranging from 9.1×10^3 to $12.8 \times 10^3 \text{ M}^{-1} \text{ cm}^{-1}$ (Table 4.2), comparable to reported values for ruthenium(II) polypyridyl complexes.^[7, 11, 14b, 23] All complexes have very low phosphorescence quantum yields under deoxygenated conditions ($\Phi_p < 10^{-4}$) except for **[2a]**Cl, **[5a]**Cl, and **[6a]**Cl that are weakly emissive ($\Phi_p = 10^{-3}$ to 10^{-4}). The ¹O₂ generation quantum yield in CD₃OD are low ($\Phi_\Delta \leq 0.05$), with the exception of **[6a]**Cl ($\Phi_\Delta = 8.2 \times 10^{-2}$), which is also the most emissive complex.

The hydrophilicity of the thioether analogues **[1b]**(PF₆)₂ – **[8b]**(PF₆)₂ allowed for studying photosubstitution quantum yields in water using electronic absorption spectroscopy. Monochromatic blue light (450 or 470 nm) was used to irradiate the complexes into their ¹MLCT absorption band. While all thioether complexes are thermally stable at room temperature, seven of the eight complexes, i.e., **[1b]**(PF₆)₂ to **[7b]**(PF₆)₂, showed light-induced exchange of their thioether ligand for H₂O. The ligand photosubstitution was characterized by clear isosbestic points in the UV-vis spectra (450 to 476 nm), as shown in Figure 4.3 For each of these reactions a bathochromic shift of the ¹MLCT band was observed, which is consistent with earlier reports on the formation of mono-aqua-ruthenium complexes in aqueous solution.^[14a] Most complexes have a photosubstitution quantum yield (Φ_{450}) of 0.5 – 2 percent, leading to photosubstitution reactivities ($\xi = \Phi_{450} \times \epsilon_{450}$, where ϵ_{450} is the molar absorption at 450 nm) in the order of ten to hundreds ($\xi = 11 - 256$). Changing the bidentate ligand therefore has a significant influence on the photosubstitution rates. Interestingly, the dppz complex **[4b]**²⁺ has the highest

photosubstitution quantum yield of the series, which is also ~20-fold higher ($\Phi_{450} = 0.020$) than that of the structurally similar dppn analogue $[5b]^{2+}$, which showed the lowest Φ_{450} (0.00095).^[13b] Furthermore, $[4b]^{2+}$ produced minimal amounts of 1O_2 ($\Phi_{\Delta} = 0.0010$) and is poorly emissive ($\Phi_p < 1 \times 10^{-5}$), which indicated that contrary to the dppn complex $[5b]^{2+}$ for which light irradiation leads to low-lying $^3\pi\pi^*$ excited states located on the spectator bidentate ligand.^[13b] With the dppz complex such $^3\pi\pi^*$ states are either too high in energy to be populated, or outcompeted by a rather quick conversion to the photodissociative metal-centered triplet state (3MC).

Another interesting observation concerned the difference in reactivity between $[7b]^{2+}$ and $[8b]^{2+}$. Whereas $[7b]^{2+}$ displayed ligand dissociation efficiency comparable to that of the bpy complex $[1b]^{2+}$, the azpy compound $[8b]^{2+}$ did not show any ligand photosubstitution, indicating a strong electronic effect of the azo ligand on the photoreactivity of its ruthenium complex. The 1MLCT absorption maximum for $[8b]^{2+}$ is significantly lower in energy (505 nm) than that of $[7b]^{2+}$ (472 nm), which points to the low energy of the azo-based π^* orbital of the azpy ligand, leading to a low-lying 3MLCT state for the complex. Since there is no steric strain in this complex to lower the 3MC state,^[23b] the 3MC - 3MLCT energy gap is very large in $[8b]^{2+}$, therefore preventing photosubstitution reactions to occur. It should be noted that $[8b]^{2+}$ is not emissive at all ($\Phi_p < 1 \times 10^{-5}$) and has a negligible 1O_2 generation quantum yield (0.007), and thus that non-radiative decay is the main deactivation pathway for this complex. Regarding 1O_2 generation, most of the other complexes produced small amounts of 1O_2 in CD_3OD ($\Phi_{\Delta} = 0.002 - 0.14$), with the exception of $[5b]^{2+}$ with a 1O_2 quantum yield of 0.71.^[13b] Interestingly, its chloride analogue $[5a]^+$ only has a 1O_2 quantum yield of 0.023 under the same conditions, emphasizing the critical influence of the monodentate ligand on the photochemical and photosensitizing properties of this family of complexes.

Table 4.2 Lowest-energy absorption maxima (λ_{max}), molar absorption coefficients at λ_{max} (ϵ_{max} in $M^{-1} cm^{-1}$) and λ_{450} (ϵ_{450} in $M^{-1} cm^{-1}$), photosubstitution quantum yields (Φ_{450}) at 298 K, 1O_2 quantum yields (Φ_{Δ}) at 293 K, photosubstitution reactivity ($\xi = \Phi_{450} \times \epsilon_{450}$), and phosphorescence quantum yield (Φ_p) at 293 K for complexes **[1a]Cl**-**[8a]Cl** and **[1b](PF₆)₂** - **[8b](PF₆)₂**.

Complex	λ_{max} in nm (ϵ_{max} in $M^{-1} cm^{-1}$) ^[a]	ϵ_{450} ($M^{-1} cm^{-1}$)	Φ_{450} ^[b]	ξ	Φ_{Δ} ^[c]	Φ_p ^[c]
[1a]Cl	504 (9.1×10^3)	4.6×10^3	-	-	0.055	$< 1 \times 10^{-5}$
[2a]Cl	501 (9.1×10^3)	6.5×10^3	-	-	0.048	8.5×10^{-4}
[3a]Cl	504 (9.1×10^3)	6.6×10^3	-	-	0.055	$< 1 \times 10^{-5}$
[4a]Cl	511 (9.6×10^3)	5.6×10^3	-	-	0.005	$< 1 \times 10^{-5}$
[5a]Cl	498 (12.0×10^3)	8.5×10^3	-	-	0.023	4.3×10^{-4}
[6a]Cl	501 (1.12×10^4)	6.8×10^3	-	-	0.082	3.2×10^{-3}
[7a]Cl	523 (13.0×10^3)	3.4×10^3	-	-	0.012	1.4×10^{-5}
[8a]Cl	508 (12.2×10^3)	3.9×10^3	-	-	< 0.001	1.8×10^{-5}
[1b](PF₆)₂	450 (7.0×10^3)	7.0×10^3	0.0084	59	0.020 (0.020)	$< 1 \times 10^{-5}$
[2b](PF₆)₂	448 (6.2×10^3)	6.2×10^3	0.0065	40	0.050 (0.080)	1.2×10^{-4}
[3b](PF₆)₂	448 (8.9×10^3)	8.9×10^3	0.0067	60	0.030 (0.010)	$< 1 \times 10^{-5}$
[4b](PF₆)₂	458 (13.1×10^3)	12.8×10^3	0.020	256	0.0010 (0.0030)	$< 1 \times 10^{-5}$
[5b](PF₆)₂	458 (11.6×10^3)	11.4×10^3	0.00095	11	0.71/(0.41)	$< 1 \times 10^{-5}$
[6b](PF₆)₂	460 (11.0×10^3)	10.4×10^3	0.0070	73	0.0020	$< 1 \times 10^{-5}$
[7b](PF₆)₂	472 (11.7×10^3)	11.7×10^3	0.0053	62	0.11 (0.14)	2.5×10^{-3}
[8b](PF₆)₂	505 (7.2×10^3)	2.7×10^3	-	-	0.0070(-)	$< 1 \times 10^{-5}$

[a]. In MeCN for **[1a]Cl** - **[8a]Cl** and in MilliQ H₂O for **[1b](PF₆)₂** - **[8b](PF₆)₂**. [b] in H₂O. $\lambda_{irr} = 450$ nm for **[1b](PF₆)₂** - **[6b](PF₆)₂** and 470 nm for **[7b](PF₆)₂**. [c] in CD₃OD.

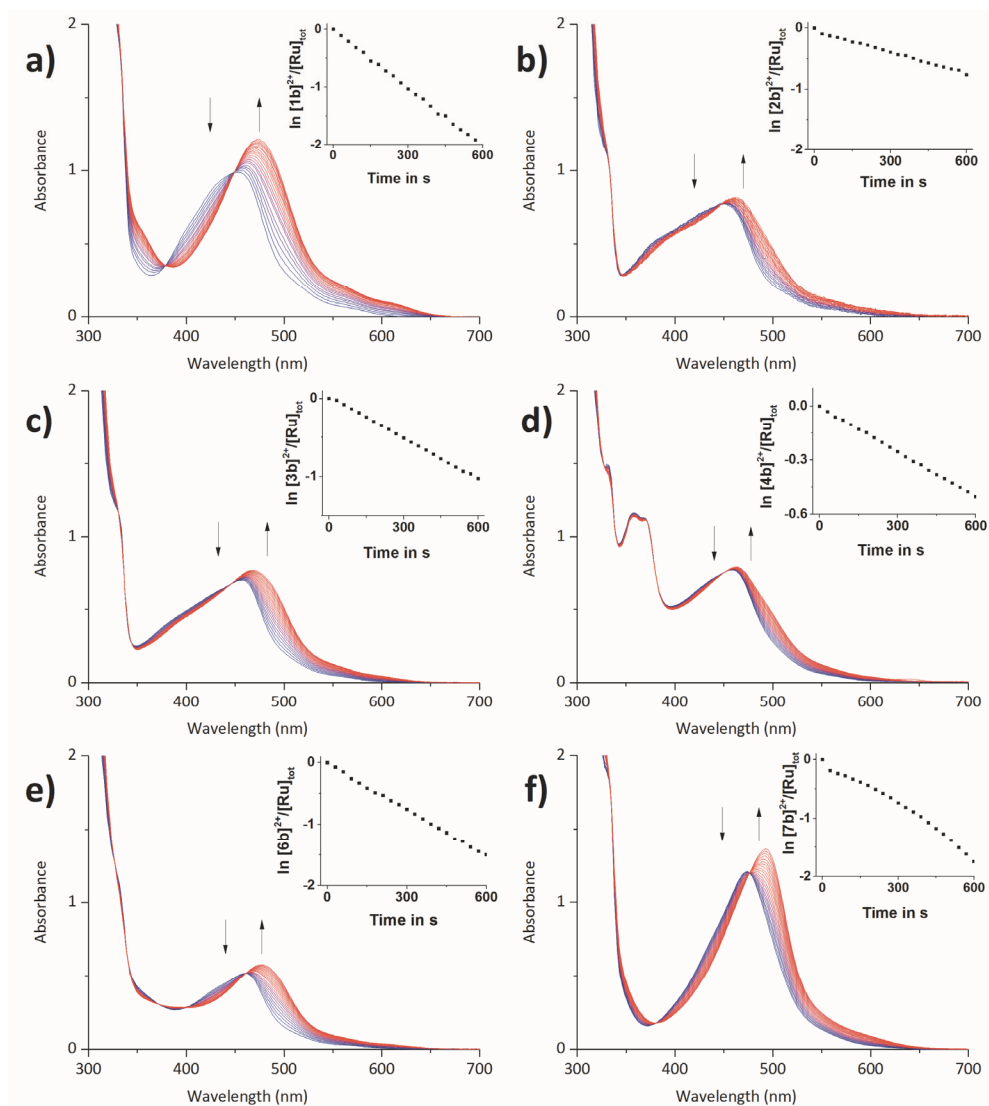


Figure 4.3. Electronic absorption spectra of **[1b]**(PF₆)₂ - **[4b]**(PF₆)₂, **[6b]**(PF₆)₂ and **[7b]**(PF₆)₂ in deoxygenated H₂O upon irradiation at 450 or 470 nm for 5 min at T = 298 K. Spectra measured every 30 s. a) **[1b]**(PF₆)₂, [Ru]_{tot} = 1.38 × 10⁻⁴ M, λ_{exc} = 450 nm, photon flux = 1.71 × 10⁻⁷ mol s⁻¹. b) **[2b]**(PF₆)₂, [Ru]_{tot} = 1.15 × 10⁻⁴ M, λ_{exc} = 450 nm, photon flux = 6.83 × 10⁻⁸ mol s⁻¹. c) **[3b]**(PF₆)₂, [Ru]_{tot} = 7.91 × 10⁻⁵ M, λ_{exc} = 450 nm, photon flux = 5.29 × 10⁻⁸ mol s⁻¹. d) **[4b]**(PF₆)₂, [Ru]_{tot} = 8.66 × 10⁻⁵ M, λ_{exc} = 450 nm, photon flux = 2.84 × 10⁻⁸ mol s⁻¹. e) **[6b]**(PF₆)₂, [Ru]_{tot} = 4.75 × 10⁻⁵ M, λ_{exc} = 450 nm, photon flux = 4.97 × 10⁻⁸ mol s⁻¹. f) **[7b]**(PF₆)₂, [Ru]_{tot} = 8.88 × 10⁻⁵ M, λ_{exc} = 470 nm, photon flux = 1.52 × 10⁻⁷ mol s⁻¹. Inset depicts the evolution of Ln [Ru]_{SRR}/[Ru]_{tot} vs. irradiation time in s, where [Ru]_{SRR} represents the concentration of ruthenium-thioether complex at time t, and [Ru]_{tot} the total ruthenium concentration.

4.2.4 Cytotoxicity

The cytotoxic properties of the chloride complexes **[1a]Cl** - **[8a]Cl** and their caged analogues **[1b](PF₆)₂** - **[8b](PF₆)₂** were evaluated against two different human cell lines: A549 (human lung carcinoma) and MCF-7 (human breast adenocarcinoma). Considering the photo-substitution properties of some of these complexes, their photocytotoxicity was also tested under blue light irradiation ($3.2 \pm 0.2 \text{ J}\cdot\text{cm}^{-2}$ at $454 \pm 11 \text{ nm}$) as described previously for **[5b](PF₆)₂**.^[13b] Cells were seeded at $t = 0$, treated after 24 h with a concentration gradient of each ruthenium complex, irradiated or maintained in the dark after replacing the media, and further incubated in the dark for 48 h. At $t = 96 \text{ h}$ cell viability was determined using the sulforhodamine B (SRB) assay.^[24] The effective concentrations (EC_{50}), defined as the concentration at which a 50% survival rate on cell viability is observed, are reported in Table 4.3. Most chloride complexes were found to be non-cytotoxic, with the exception of **[8a]Cl** that was found moderately cytotoxic ($EC_{50} = 28 \mu\text{M}$) against the MCF-7 cell line, in agreement with the value reported by Reedijk et al.^[25] The values for **[4a]Cl** ($59 \mu\text{M}$ and $34 \mu\text{M}$ against A549 and MCF-7, respectively) were found similar to that observed for $[\text{Ru}(\text{bpy})(\text{dppz})_2]^{2+}$ analogues reported by the group of Schatzschneider.^[26] Based on their results, it was expected that the structurally similar but more lipophilic dppn complex **[5a]Cl** would be cytotoxic, but no significant toxicity was observed for this complex. On the other hand, its EC_{50} could not be clearly determined due to the poor solubility of this complex in cell culture medium.^[13b] Interestingly however, **[5a]Cl** was found to be cytotoxic upon blue light irradiation, with EC_{50} values of $9.7 \mu\text{M}$ and $3.2 \mu\text{M}$ for A549 and MCF-7 cells, respectively, corresponding to photoindexes (PI) of more than 2.6 and 7.9, respectively. This result is unexpected, since the $^1\text{O}_2$ quantum yield of **[5a]Cl** (0.023) is much lower than that of its glycoconjugated analogue **[5b](PF₆)₂** (0.71). A possible explanation would be the partial conversion, after uptake, of the chloride complex to its aquated counterpart $[\text{Ru}(\text{tpy})(\text{dppn})(\text{H}_2\text{O})]^{2+}$ (Figure 4.4a), which has been demonstrated to be a good $^1\text{O}_2$ sensitizer as demonstrated by close analogue $[\text{Ru}(\text{tpy})(\text{dppn})(\text{CD}_3\text{OD})]^{2+}$ ($\Phi_{\Delta} = 0.43$).^[13b] An alternative explanation, would be that a different type of PDT is occurring, such as PDT type I, which is dependent upon the formation of radical species without intervention of molecular oxygen.^[27] Further studies would be needed to conclude on the biological mechanism of the photocytotoxicity of **[5a]Cl**.

None of the glycoconjugated complexes were found photocytotoxic except **[5b](PF₆)₂**, which was recently reported to enter passively into the cells and to destroy mitochondrial DNA by singlet oxygen generation.^[13b] In our standard treatment protocol, media is replaced before light irradiation. In such conditions, photocytotoxicity can solely rely on the molecules that have been taken up by the cells during incubation, which may be a problem for highly hydrophilic glucose-conjugates such as **[1b](PF₆)₂** - **[8b](PF₆)₂** (see below). For compound **[4b](PF₆)₂**, an adjustment of the protocol, consisting in irradiating the cells without media refreshing, led to a modest but clearly improved PI (2.4 and 2.6 for

MCF-7 and A549, respectively). With such a protocol the full dose of compound added to each well remains present during and after irradiation, and most importantly activation may occur outside the cell, and be followed by cellular uptake of the activated photoproduct. For **[4b]**(PF₆)₂, the observed phototoxicity might thus be explained by the formation of the aquated species [Ru(tpy)(dppz)(H₂O)]²⁺ outside the cell, followed by *in situ* conversion to the chloride species **[4a]**Cl due to the high chloride content in media (>100 mM), followed by cellular uptake (Figure 4.4b). This interpretation is supported by the EC₅₀ values found for **[4a]**Cl, which were not impressive but could clearly be measured (59 μM and 34 μM for A549 and MCF-7 respectively). Not refreshing the media before light activation did not lead to enhanced toxicity for **[1b]**(PF₆)₂ – **[3b]**(PF₆)₂ and for **[6b]**(PF₆)₂ – **[7b]**(PF₆)₂, showing that keeping high concentrations of the prodrug during and after light irradiation does not necessarily lead to enhanced phototoxicity. Overall, these results demonstrate that **[4b]**(PF₆)₂ is a moderately effective PACT agent,^[3b] whereas the dppn analogues **[5a]**Cl and **[5b]**(PF₆)₂ are catalytic PDT sensitizers which can be activated using a low dose of blue light. They also demonstrate that apparently minor differences in the treatment protocol of light-activated drugs may lead to very different interpretation of the cytotoxicity of light-activated compounds.

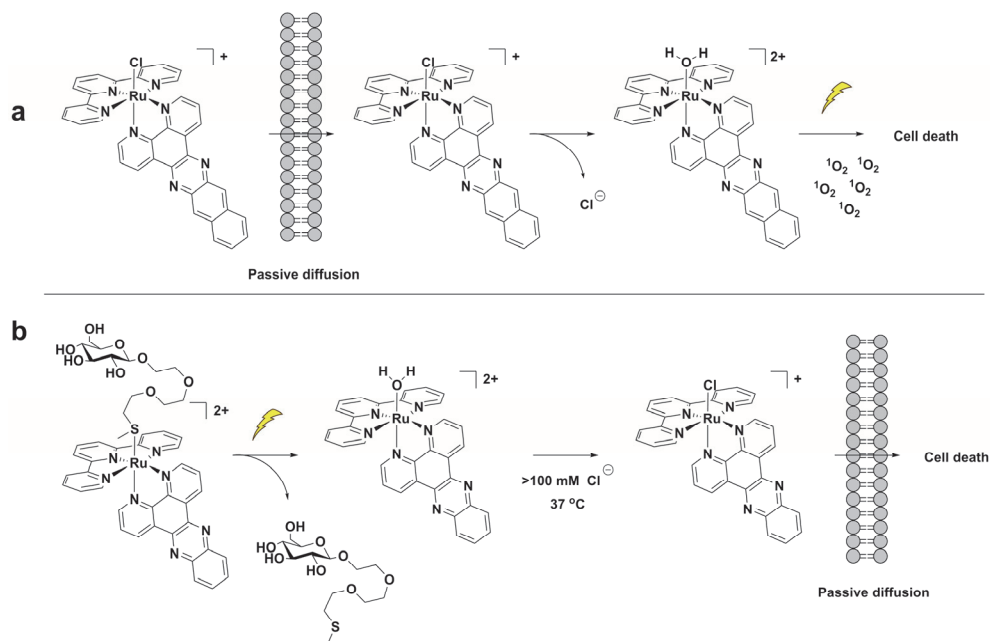


Figure 4.4. Proposed mechanisms for light-induced toxicity for a) **[5a]**Cl with media replacement, and b) **[4b]**(PF₆)₂ without media replacement. The lipid bilayer represents the cell membrane.

Table 4.3 Cytotoxicity of compounds [1a]Cl – [8a]Cl and [1b](PF₆)₂ – [8b](PF₆)₂ towards A549 and MCF-7 cells in the dark and upon blue light irradiation (454 nm, 3.2 J.cm⁻²). Cell-growing inhibition effective concentrations (EC₅₀) are reported in μM with 95% confidence interval (CI) in μM. Data is the mean over three independent experiments. Photocytotoxicity index (PI) = EC_{50dark}/EC_{50light}.

Complex ^[a]	Light Dose (J cm ⁻²)	A549 EC ₅₀	CI	PI	MCF-7 EC ₅₀	CI	PI
[1a]Cl	0	>100			>100		
	3.2	>100		-	>100		-
[2a]Cl	0	>100			64	+12	
	3.2	>100		-	52	-9.1 +15 -10	1.2
[3a]Cl	0	>100			>100		-
	3.2	>100		-	>100		-
[4a]Cl	0	59	+31 -21	1.3	34	+6.0 -5.1	1.1
	3.2	47	+19 -13		31	+4.8 -4.2	
[5a]Cl	0	>25			>25		
	3.2	9.7	+4.4 -2.6	>2.6	3.2	+1.3 -0.87	>7.9
[6a]Cl	0	>25			>25		-
	3.2	>25		-	>25		-
[7a]Cl	0	>100			>100		-
	3.2	>100		-	>100		-
[8a]Cl	0	>100			28	+4.9	
	3.2	-		-	-	-4.2	-
[1b](PF ₆) ₂	0	>100			>100		-
	3.2	>100		-	>100		-
[2b](PF ₆) ₂	0	>100			>100		-
	3.2	>100		-	>100		-
[3b](PF ₆) ₂	0	>100			>100		-
	3.2	>100		-	>100		-
[4b](PF ₆) ₂	0	>100			>100		-
	3.2	>100		-	>100		-
[4b](PF ₆) ₂ ^[b]	0	64	+17 -13	2.4	52	+12 -9.4	2.6
	3.2	27	+6.4 -5.2		20	+2.5 -2.2	
[5b](PF ₆) ₂ ^[c]	0	19	+4.0 -3.3	26	9.6	+2.9 -2.3	11
	3.2	0.72	+0.16 -0.13		0.86	+0.21 -0.17	
[6b](PF ₆) ₂	0	>100			>100		-
	3.2	>100		-	>100		-
[7b](PF ₆) ₂	0	>100			>100		-
	3.2	>100		-	>100		-
[8b](PF ₆) ₂	0	>100			>100		-
	3.2	>100		-	>100		-

[a] Normal protocol: Cells were incubated with compound for 24 h, followed by replacement of the media, kept in the dark, or irradiated with blue light (5 min at 454 nm, 10.5 mW.cm⁻², 3.2 J.cm⁻²). [b] As in normal protocol, without replacing media during treatment (cells are irradiated in the presence of compound). [c] Ref^[13b].

4.2.5 Log P_{o/w} and uptake

To acquire more insight on the effect of glycoconjugation on the solubility, cellular uptake, and toxicity of these complexes, the water-octanol partition coefficients (log P_{o/w}) were determined for all complexes according to reported standards (Figure 4.5b).^[28] As shown in Figure 4.5b (left) the chloride compounds with the smallest bidentate ligands, i.e., [1a]Cl – [3a]Cl, have similar log P_{o/w} values ranging from -0.81 to -1.1, while [7a]Cl and [8a]Cl

have log $P_{o/w}$ values of -1.60 to -1.80. For these five complexes the chloride counter anion provides appreciable water solubility. By contrast, the chloride compounds with the largest bidentate ligands, i.e., **[4a]Cl** – **[6a]Cl**, are much more hydrophobic with log $P_{o/w}$ values ranging from -0.10 to +1.0. Whereas one may expect that the dicationic nature of **[1b](PF₆)₂** – **[8b](PF₆)₂** and glycoconjugation should improve water solubility compared to their chloride analogues, we found that **[1b](PF₆)₂** – **[3b](PF₆)₂** had similar log $P_{o/w}$ values (-0.11 to -0.51, respectively) compared to their analogues **[1a]Cl** – **[3a]Cl**, while **[7b](PF₆)₂** and **[8b](PF₆)₂** were slightly more hydrophobic (log $P_{o/w}$ = -0.20 and -0.18, respectively) than **[7a]Cl** and **[8a]Cl**. This result points to the critical influence of the counterions, as the two hexafluoridophosphate anions of the glycoconjugate compounds increase lipophilicity, compared to chlorides. Furthermore, the chloride complexes are not stable in water, resulting in (partial) conversion to the **[Ru(tpy)(N-N)(H₂O)]Cl₂** species which are more soluble in water than the hexafluoridophosphate salts of the R-substituted ruthenium complexes. The most hydrophobic chloride complexes **[4a]Cl** – **[6a]Cl**, that were much more difficult to dissolve in water, profited most of glycoconjugation, as **[4b](PF₆)₂** – **[6b](PF₆)₂** indeed became water soluble (log $P_{o/w}$ = -0.84 to -0.50, respectively). Overall glycoconjugation allowed for investigating the photochemistry of *all* thioether complexes **[1b](PF₆)₂** – **[8b](PF₆)₂** in water.

In order to check whether the low toxicity of the thioether-glucose conjugates was not simply due to a low uptake, cellular uptake was studied for all sixteen complexes in A549 cells at a concentration of 25 μ M, using an incubation time of 24 h and measuring intracellular ruthenium concentrations by ICP-MS. Although no general correlation could be found between the log $P_{o/w}$ values for these complexes and their cellular uptake, very strong differences in metal uptake were observed depending on the ligands and counterions (Figure 4.5a). The most hydrophobic chloride compounds **[4a]Cl**, **[5a]Cl** and **[6a]Cl** displayed very high metal uptake (>1000 ng Ru per million cells), while their glycoconjugates **[4b](PF₆)₂**, **[5b](PF₆)₂** and **[6b](PF₆)₂** displayed cellular uptake that was much lower (10 - 20 ng Ru per million cells, e.g. 250 times lower for **[5b](PF₆)₂** compared to **[5a]Cl**). Of course, this lower uptake can partially be explained by the lower log $P_{o/w}$ values of the glycoconjugates, and at least for **[5b](PF₆)₂**, by the absence of GLUT-based active uptake.^[13b] However, **[4b](PF₆)₂** – **[6b](PF₆)₂** are also taken up in 10-fold higher amounts than **[1b](PF₆)₂** – **[3b](PF₆)₂**, which have comparable log $P_{o/w}$ values. These results may not necessarily represent the conditions experienced by these compounds at the cell membrane, for which it is more likely that the lipophilic PF₆⁻ counterions are already exchanged for the more abundant and more water soluble chloride or phosphate anions in the buffer, canceling the effect of the PF₆⁻ anion on lipophilicity.

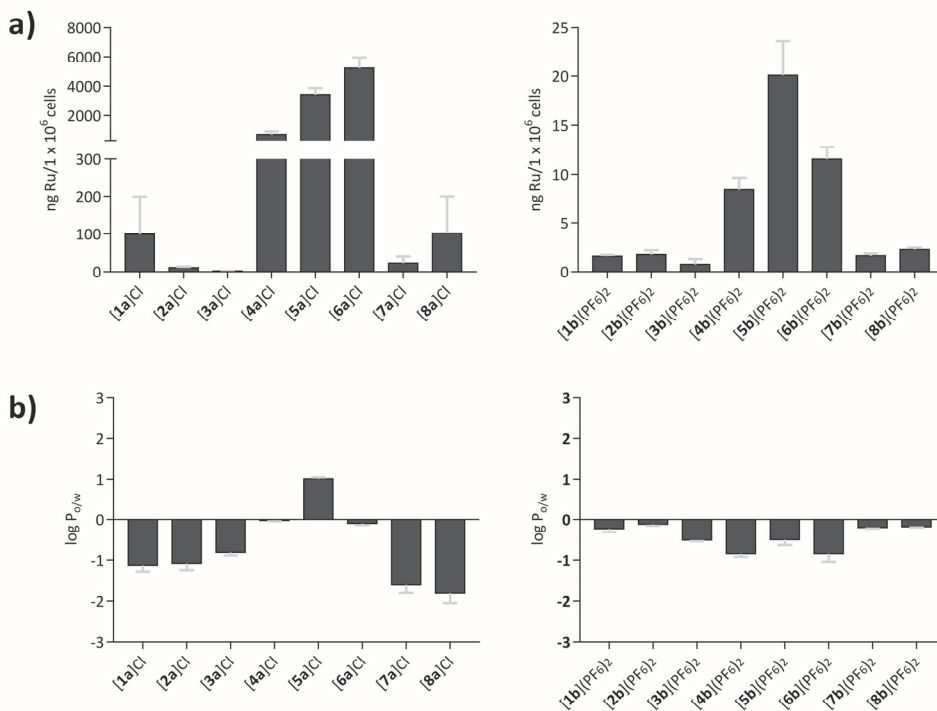


Figure 4.5. a). Intracellular uptake of 25 μM of [1a](PF₆)₂– [8a]Cl (left) and [1b] – [8b](PF₆)₂ (right) in A549 cells after 24 h. Values are reported \pm SD, n = 2. **b).** Log P_{o/w} values found for [1a]Cl – [8a]Cl (left) and [1b](PF₆)₂ – [8b](PF₆)₂ (right). Values are reported \pm SD, n = 3.

4.3 Discussion

Some of the chloride complexes [1a]Cl – [8a]Cl were thermally unstable in water and therefore no photodissociation quantum yields were determined, while their singlet oxygen properties were in general very low. The phototoxicity in the series of the most lipophilic compounds [4a]Cl–[6a]Cl cannot be explained by the trends observed in cell uptake and singlet oxygen generation. [6a]Cl has a higher singlet oxygen quantum yield (0.082) than [4a]Cl and [5a]Cl (0.005 and 0.023, respectively), but it is not phototoxic whereas [4a]Cl and [5a]Cl are. At the same time all three complexes are taken up in high amounts. In this series of complexes different intracellular localization or biological targets, coupled to unknown photoreactions of [5a]Cl, must explain the differences in phototoxicity between [6a]Cl on the one hand and [4a]Cl and [5a]Cl on the other hand. An opposite conclusion can be drawn for the glycoconjugates series [4b](PF₆)₂, [5b](PF₆)₂ and [6b](PF₆)₂. The only phototoxic agent of this series, [5b](PF₆)₂, has by far the highest singlet oxygen quantum yield (0.71 vs. 0.0010 and 0.0020), while all three compounds are taken up in similar amounts (10–20 ng Ru per million cells). Hence, [5b](PF₆)₂ is an excellent PDT agent, while a PACT mode of action cannot be ruled out considering the

phototoxic properties of [5a]Cl and its low singlet oxygen quantum yield. The phototoxicity observed for [4b](PF₆)₂ when the medium is not refreshed before irradiation, suggests that this compound may act as a cytotoxic PACT agent. Furthermore, [4b](PF₆)₂ showed the highest photosubstitution quantum yield (0.02) and no significant singlet oxygen production. When cell-culture media was replaced before light irradiation, the glycoconjugate compound was not taken up in high amounts, and given the poor photodynamic properties of the photoproduct ([4a]⁺ or [Ru(tpy)(dppz)(OH₂)]²⁺) not enough reactive oxygen species could be generated to kill the cells. This example demonstrates that the potential of [4b](PF₆)₂ as a PACT agent is determined by the treatment protocol, which should be taken into account in further PACT studies. Furthermore, this complex has been shown to act as a DNA light-switch in the presence of DNA, which might be useful for theranostic applications.^[29]

4.4 Conclusion

Overall, eight chloride terpyridine complexes [1a]Cl – [8a]Cl with eight different bidentate spectator chelating ligands, and their eight thioether-glucose conjugates, were synthesized, to compare the corresponding photophysical properties, photoreactivity, water solubility, cellular uptake, and phototoxicity. Depending on the bidentate ligand these complexes can be considered either for photocaging, or for PACT and/or PDT. Compound [8a]Cl is not suitable for photocaging or phototherapy because the azo group of the azpy spectator ligand stabilizes the ³MLCT state too much and prevents thermal population of the ³MC state, thereby quenching photosubstitution. Singlet oxygen generation was also fully quenched in [8a]Cl and [8b](PF₆)₂, emphasizing the poor photosensitizing properties of this compound. The five complexes [1a]Cl – [3a]Cl, [6a]Cl, and [7a]Cl, are non-toxic, and once substituted by thioethers they form complexes with similar photosubstitution quantum yields ($\Phi_{450} \sim 0.01$) and low ¹O₂ production quantum yields ($\Phi_{\Delta} < 0.10$). As a consequence, they are excellent candidates for the photocaging of thioether-based biologically active compounds such as the antibiotics amoxicillin and clindamycin. The exceptionally high cellular uptake measured for [6a]Cl is worth noticing (5220 ± 737 ng Ru per million cells), considering that this compound did not show any measurable cytotoxicity at concentrations lower than 25 μM. It can even turn highly hydrophilic compounds such as R into species such as [6b](PF₆)₂ that are still lipophilic enough to enter into cancer cells. Finally, [4a]Cl and [5a]Cl show similar lipophilicity compared to [6a]Cl and comparably high cellular uptake, but they also showed some toxicity both in the dark and after light activation. They are therefore less interesting as PACT carriers and instead have better potential as either a cytotoxic PACT agent or for PDT as we have recently demonstrated for [5b](PF₆)₂.^[13b] Overall, this work demonstrates that complexes based upon the [Ru(tpy)(N-N)(L)]ⁿ⁺ scaffold are good photocaging agents

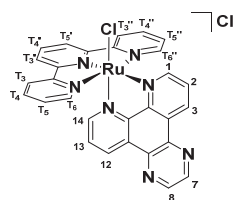
but poorly (photo)cytotoxic unless DNA intercalators such as dppz and dppn are chosen as a bidentate ligand, in which case they could serve as phototoxic agents.

4.5 Experimental

4.5.1 General

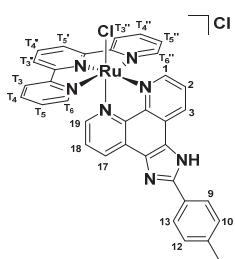
Reagents were purchased from Sigma-Aldrich and used without further purification. Dpq,^[30] dppz,^[30] dppn,^[31] pmip,^[32] azpy^[33] and pyimi^[34] were synthesized according to reported procedures. 2-(2-(2-(methylthio)ethoxy)ethoxy)ethyl-β-D-glucopyranoside and **[1b]**(PF₆)₂ were synthesized as described in Chapter 2. [Ru(tpy)Cl₃],^[35] [Ru(tpy)(bpy)Cl]Cl,^[16] [Ru(tpy)(phen)Cl]Cl,^[17] [Ru(tpy)(azpy)Cl]Cl,^[20] [Ru(tpy)(pyimi)Cl]Cl,^[19] [Ru(tpy)(dppz)Cl]Cl,^[18] and [Ru(tpy)(dppn)Cl]Cl,^[13b] were synthesized according to known literature procedures. 2,2':6',2''-Terpyridine (tpy) was obtained from ABCR GmbH & Co. Dry solvents were collected from a Pure Solve MD5 solvent dispenser from Demaco Holland BV. Solvents were deoxygenated by bubbling argon through the solution for 30 minutes and all inorganic reactions and were carried out under an inert atmosphere in the dark, unless stated otherwise. Solvents were removed under vacuum with a rotary evaporator in the dark at 30 °C, unless stated otherwise. Flash chromatography was performed on silica gel (Screening devices B.V.) with a particle size of 40 - 64 μM and a pore size of 60 Å. TLC analysis was conducted on TLC aluminium foils with silica gel matrix (Supelco, silica gel 60, 56524) with detection by UV-absorption (254 nm), by spraying with 10% H₂SO₄ in ethanol or with a solution of NH₄Mo₇O₂₄·4H₂O 25 g/L, NH₄CeSO₄·H₂O 10 g/L, 10% H₂SO₄ in H₂O, followed by charring at ~250 °C on a heating plate. NMR spectra were recorded on a Bruker AV-400, AV-500 or AV-850. ¹H NMR and ¹³C NMR were recorded in CD₃OD and (CD₃)₂CO with chemical shift (δ) relative to the solvent peak. High resolution mass spectra were recorded by direct injection (2 μl of 2 μM solution in water/acetonitrile; 50/50; v/v and 0.1% formic acid) in a mass spectrometer (Thermo Finnigan LTQ Orbitrap) equipped with an electrospray 250 °C) with resolution R = 60000 at m/z 400 (mass range m/z = 150 – 2000) and dioctylphtalate (m/z = 391.28428) as a lock mass. The high-resolution mass spectrometer was calibrated prior to measurements with a calibration mixture (Thermo Finnigan).

4.5.2 Synthesis



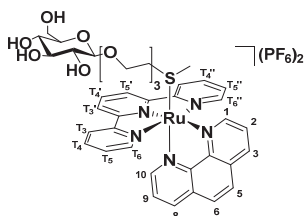
[Ru(tpy)(dpq)Cl]Cl, [3a]Cl: [Ru(tpy)Cl₃] (103 mg, 0.234 mmol) and dpq (54.0 mg, 0.233 mmol) were dissolved in deoxygenated EtOH/H₂O (4 mL, 4:1), Et₃N (35 μL, 0.25 mmol) was added and the mixture was heated at reflux for 4 h. The mixture was filtered over Celite®, the volume reduced by ~50% and the filtrate was allowed to cool overnight at 4 °C. The resulting precipitate was collected on a glas frit, washed with water (3 x 50 mL), and 1M HCl (3 x 50 mL), which, after drying

under high vacuum, afforded the title compound as a purple solid. (146 mg, 0.229, 98%). $R_f = 0.61$ (10% MeOH in DCM); $^1\text{H NMR}$ (400 MHz, CD_3OD) $\delta = 10.53$ (d, $J = 5.4$ Hz, 1H, 1), 9.85 (d, $J = 8.3$ Hz, 1H, 3), 9.27 (m, 2H, 8, 12), 9.19 (d, $J = 2.6$ Hz, 1H, 7), 8.72 (d, $J = 8.2$ Hz, 2H, T_3' , T_5'), 8.56 (d, $J = 8.0$ Hz, 2H, T_6''), 8.51 (dd, $J = 8.5, 5.1$ Hz, 1H, 2), 8.23 (t, $J = 8.1$ Hz, 1H, T_4'), 7.95 – 7.84 (m, 3H, T_5'' , T_5 , 14), 7.67 (d, $J = 5.5$ Hz, 2H, T_3 , T_3''), 7.54 (dd, $J = 8.5, 5.1$ Hz, 1H, 13), 7.27 – 7.17 (m, 2H, T_4'' , T_4). $^{13}\text{C NMR}$ (101 MHz, CD_3OD) $\delta = 160.2$ (C_q Arom), 159.7 (C_q Arom), 155.4 (C_H 1), 154.9 (C_H 14), 153.7 (C_H T_3 , T_3''), 152.2 (C_q Arom), 150.3 (C_q Arom), 147.8 (C_H 8), 147.6 (C_H 7), 141.5 (C_q Arom), 141.1 (C_q Arom), 138.5 (C_H T_5'' , T_4), 135.8 (C_H T_4'), 133.6 (C_H 3), 132.4 (C_H 12), 131.2 (C_q Arom), 130.9 (C_q Arom), 128.5 (C_H 2), 127.9 (C_H T_4' , T_4), 127.1 (C_H 13), 124.9 (C_H T_6'' , T_6), 123.8 (C_H T_3' , T_5'). HRMS: m/z calcd for $[\text{C}_{29}\text{H}_{19}\text{N}_7\text{RuCl}_2 - \text{Cl}]^+$: 602.04285, found: 602.04531; Elemental analysis calcd (%) for **[3b](PF₆)₂·4H₂O**: C, 49.09; H, 3.84; N, 13.82; found: C, 50.58; H, 3.96; N, 13.86.



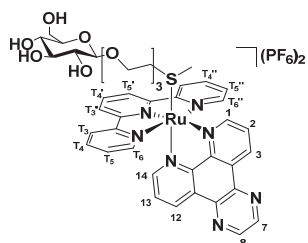
[Ru(tpy)(pmip)Cl]Cl, [6a]Cl: A mixture of $[\text{Ru}(\text{tpy})\text{Cl}_3]$ (0.252 g, 0.571 mmol), the ligand pmip (0.276 g, 0.888 mmol), and LiCl (0.216 g, 5.10 mmol) in EtOH/ H_2O (3:1, 40 mL), was refluxed for 5 minutes under an inert atmosphere, after which Et_3N (80.0 μL , 0.571 mmol) was added. The reaction was allowed to stir for an additional 10 minutes at reflux after which it was filtered hot over Celite[®]. The volume of the filtrate was then reduced by $\sim 50\%$ and

cooled at 4 °C overnight, which allowed the formation of a precipitate which was collected by filtration. After washing with H_2O (4 x 30 mL) the crude precipitate was further purified using a silica column (20% MeOH in DCM), which afforded **[6a]Cl** as a brown powder. (211 mg, 0.295 mmol, 52%). $R_f = 0.64$ (10% MeOH in DCM); $^1\text{H NMR}$ (850 MHz, CD_3OD) $\delta = 10.39$ (d, $J = 5.1$ Hz, 1H, 1), 9.33 (d, $J = 8.3$ Hz, 1H, 3), 8.75 (d, $J = 8.0$ Hz, 1H, 19), 8.70 (d, $J = 8.2$ Hz, 2H, T_3' , T_5'), 8.54 (d, $J = 8.1$ Hz, 2H, T_6'' , T_6), 8.40 (dd, $J = 8.3, 5.0$ Hz, 1H, 2), 8.20 (dd, $J = 21.9, 8.1$ Hz, 3H, T_4' , 9, 13), 7.89 (t, $J = 7.7$ Hz, 2H, T_5'' , T_5), 7.64 (d, $J = 5.4$ Hz, 1H, 17), 7.60 (d, $J = 5.6$ Hz, 2H, T_3'' , T_3), 7.45 (d, $J = 8.1$ Hz, 2H, 10, 12), 7.41 (dd, $J = 8.1, 5.4$ Hz, 1H, 18), 7.20 (t, $J = 6.6$ Hz, 2H, T_4 , T_4''), 2.47 (s, 3H, CH_3). $^{13}\text{C NMR}$ (214 MHz, CD_3OD) $\delta = 160.3$ (C_q Arom), 159.8 (C_q Arom), 153.5 (C_H T_3'' , T_3), 152.0 (C_H 1), 151.0 (C_H 17), 148.6 (C_q Arom), 146.7 (C_q Arom), 142.1 (C_q Arom), 138.3 (C_H T_5'' , T_5), 135.5 (C_H T_4), 130.9 (C_H 10, 12), 130.6 (C_H 3), 129.5 (C_H 19), 128.5 (C_H T_4 , T_4''), 128.0 (C_H 9, 13), 126.7 (C_H 2), 125.9 (C_H 18), 124.8 (C_H T_6'' , T_6), 123.7 (C_H T_5' , T_3'), 21.5 (CH_3). HRMS: m/z calcd for $[\text{C}_{35}\text{H}_{25}\text{N}_7\text{RuCl}_2 - \text{Cl}]^+$: 680.08980, found: 680.09151; Elemental analysis calcd (%) for **[6a]Cl·2.5H₂O**: C, 55.27; H, 3.98; N, 12.89; found: C, 55.57; H, 3.97; N, 12.57.



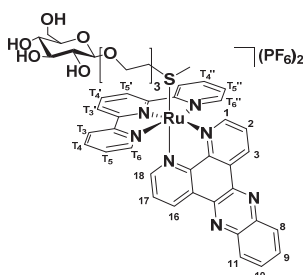
[Ru(tpy)(phen)(R)](PF₆)₂, [2b](PF₆)₂: A mixture of $[\text{Ru}(\text{tpy})(\text{phen})\text{Cl}]$ (54.0 mg, 0.0992 mmol) and 2-(2-(2-(methylthio)ethoxy)ethoxy)ethyl- β -D-glucopyranoside (94.0 mg, 0.275 mmol) in deoxygenated H_2O (15 mL) was allowed

to stir at 80 °C for 16 h, after which ~200 mg NH_4PF_6 was added. Concentration *in vacuo* was followed by purification of the crude over a Sephadex LH-20 column (MeOH), by collection of the orange fraction. Removal of the solvents under vacuum afforded **[2b](PF₆)₂** as a red solid. (80.3 mg, 0.0767, 83%). $R_f = 0.64$ (acetone/water/sat. KPF_6 100/80/20); ^1H NMR (400 MHz, CD_3OD) $\delta = 10.17$ (d, $J = 5.1$ Hz, 1H, 1), 8.99 (d, $J = 7.8$ Hz, 1H, 3), 8.83 (d, $J = 8.2$ Hz, 2H, T_3' , T_5'), 8.64 (d, $J = 8.1$ Hz, 2H, T_6 , T_6''), 8.51 (d, $J = 8.3$ Hz, 1H, 10), 8.48 – 8.43 (m, 2H, T_4' , 2), 8.40 (d, $J = 8.9$ Hz, 1H, 5), 8.21 (d, $J = 8.9$ Hz, 1H, 6), 8.05 (td, $J = 8.0$, 1.9 Hz, 2H, T_5'' , T_5), 7.73 – 7.68 (m, 1H, 8), 7.65 (d, $J = 5.4$ Hz, 2H, T_3'' , T_3), 7.58 (dd, $J = 8.2$, 5.3 Hz, 1H, 9), 7.35 – 7.28 (m, 2H, T_4 , T_4''), 4.29 (d, $J = 7.7$ Hz, 1H, H-1), 4.04 – 3.96 (m, 1H, *CHH* H-6), 3.90 – 3.83 (m, 1H, *CHH* OCH_2), 3.74 – 3.47 (m, 10H, *CHH* H-6, *CHH* OCH_2 , 4 x OCH_2), 3.37 (m, 1H, H-5), 3.30 – 3.25 (m, 2H, H-3, H-4), 3.14 (dd, $J = 9.0$, 7.9 Hz, 1H, H-2), 2.02 (t, $J = 5.5$ Hz, 2H, OCH_2SMe), 1.51 (s, 3H, OCH_2SMe). ^{13}C NMR (101 MHz, CD_3OD) $\delta = 159.4$ (C_q Arom), 158.9 (C_q Arom), 154.5 (C_H T_3'' , T_3), 154.3 (C_H 1), 151.7 (C_H 8), 148.6 (C_q Arom), 148.2 (C_q Arom), 140.0 (C_H T_5'' , T_5), 138.6 (C_H 3), 138.4 (C_H 10, 2), 132.9 (C_q Arom), 132.0 (C_q Arom), 129.7 (C_H 5, T_4 , T_4''), 128.9 (C_H 6), 127.9 (C_H T_4'), 126.8 (C_H 9), 126.2 (C_H 10, T_6 , T_6''), 125.5 (C_H T_3' , T_5'), 104.4 (C-1), 77.8 (C-3, C-5), 75.1 (C-2), 71.6 (C-4), 71.4 (OCH_2), 71.3 (OCH_2), 71.1 (OCH_2), 69.7 (C-6), 68.4 (OCH_2), 62.7 (OCH_2), 35.7 (OCH_2SMe), 15.6 (OCH_2SMe). HRMS: m/z calcd for $[\text{C}_{40}\text{H}_{45}\text{O}_8\text{N}_5\text{RuS P}_2\text{F}_{12} - 2\text{PF}_6]^{2+}$: 428.60107, found: 428.60248. Elemental analysis calcd (%) for **[2b](PF₆)₂**: C, 41.89; H, 3.96; N, 6.11; found: C, 41.81; H, 4.03; N, 6.07.



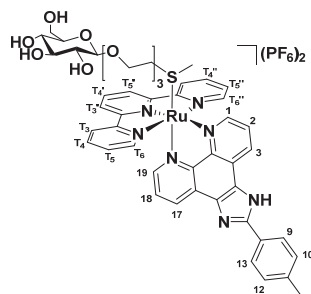
[Ru(tpy)(dpq)(R)](PF₆)₂, [3b](PF₆)₂: A mixture of **[Ru(tpy)(dpq)Cl]Cl** (75.0 mg, 0.118 mmol) and 2-(2-(2-(methylthio)ethoxy)ethoxy)ethyl-β-D-glucopyranoside (63 mg, 0.184) in deoxygenated H_2O (20 mL) were stirred at 80 °C for 48 h and concentrated *in vacuo*. The crude was redissolved in H_2O (20 mL) and AgPF_6 (71 mg, 0.281 mmol) and 2-(2-(2-(methylthio)ethoxy)ethoxy)ethyl-β-D-glucopyranoside (63 mg, 0.184 mmol) were added. After stirring for another 16 h at 80 °C, the mixture was hot filtered over Celite® and concentrated *in vacuo*. The crude was further purified over silica (acetone/water/sat. KPF_6 , 100/0/0 - 100/80/20) by collection of the orange fraction. Excess KPF_6 was then removed using a Sephadex LH-20 column (MeOH), yielding **[3b](PF₆)₂** as a dark orange solid. (33.0 mg, 0.0301 mmol, 25%). $R_f = 0.55$ (acetone/water/sat. KPF_6 , 100/80/20); ^1H NMR (400 MHz, CD_3OD) $\delta = 10.26$ (d, $J = 5.2$ Hz, 1H, 1), 9.97 (d, $J = 8.3$ Hz, 1H, 3), 9.50 (d, $J = 8.2$ Hz, 1H, 14), 9.29 (d, $J = 2.4$ Hz, 1H, 7), 9.22 (d, $J = 2.4$ Hz, 1H, 8), 8.86 (d, $J = 8.2$ Hz, 2H, T_3' , T_5'), 8.68 (d, $J = 8.1$ Hz, 2H, T_6 , T_6''), 8.60 (dd, $J = 8.5$, 5.1 Hz, 1H, 2), 8.48 (t, $J = 8.1$ Hz, 1H, T_4'), 8.07 (t, $J = 7.9$ Hz, 2H, T_5'' , T_5), 7.81 (d, $J = 5.7$ Hz, 1H, 12), 7.77 (d, $J = 5.5$ Hz, 2H, T_3 , T_3''), 7.72 (dd, $J = 8.5$, 5.2 Hz, 1H, 13), 7.34 (t, $J = 6.6$ Hz, 2H, T_4 , T_4''), 4.26 (d, $J = 7.8$ Hz, 1H, H-1), 4.06 – 3.94 (m, 1H, *CHH* H-6), 3.85 (d, $J = 11.8$ Hz, 1H, *CHH* OCH_2), 3.76 – 3.46 (m, 10H, *CHH* H-6, *CHH* OCH_2 , 4 x OCH_2), 3.35

(m, 1H, H-5), 3.27 – 3.18 (m, 2H, H-3, H-4), 3.08 (t, $J = 8.5$ Hz, 1H, H-2), 2.03 (t, $J = 5.4$ Hz, 2H, OCH_2SMe), 1.51 (s, 3H, OCH_2SMe). ^{13}C NMR (101 MHz, CD_3OD) $\delta = 159.3$ (C_q Arom), 158.9 (C_q Arom), 155.3 (C_H 1), 154.8 (C_H T_3 , T_3''), 152.9 (C_H 12), 150.3 (C_q Arom), 150.0 (C_q Arom), 148.0 (C_H 7), 147.9 (C_H 8), 141.2 (C_q Arom), 140.8 (C_q Arom), 140.2 (C_H T_5'' , T_5), 138.5 (C_H T_4'), 135.2 (C_H 3), 135.0 (C_H 14), 132.0 (C_q Arom), 131.1 (C_q Arom), 129.8 (C_H T_4 , T_4''), 128.8 (C_H 2), 127.7 (C_H T_3 , T_3''), 126.3 (C_H T_6 , T_6''), 125.5 (C_H T_3' , T_5), 111.8 (C_q Arom), 111.4 (C_q Arom), 104.5 (C-1), 78.0 (C-3, C-5), 75.1 (C-2), 71.6 (C-4), 71.4 (OCH_2), 71.3 (OCH_2), 71.2 (OCH_2), 69.7 (C-6), 68.4 (OCH_2), 62.7 (OCH_2), 35.8 (OCH_2SMe), 15.5 (OCH_2SMe). HRMS: m/z calcd for $[\text{C}_{40}\text{H}_{45}\text{O}_8\text{N}_5\text{RuSP}_2\text{F}_{12} - 2\text{PF}_6]^{2+}$: 454.60414, found: 454.60602; Elemental analysis calcd (%) for $[\mathbf{3b}](\text{PF}_6)_2 \cdot 5\text{H}_2\text{O}$: C, 39.14; H, 4.30; N, 7.61; found: C, 40.32; H, 4.28; N, 7.20.



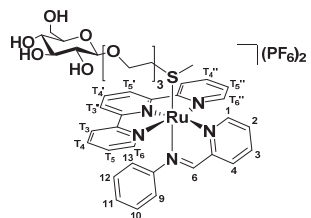
[Ru(tpy)(dppz)(R)](PF₆)₂, [4b](PF₆)₂: [Ru(tpy)(dppz)Cl]Cl (67 mg, 0.097 mmol) and 2-(2-(2-(methylthio)ethoxy)ethoxy)ethyl-β-D-glucopyranoside (50.0 mg, 0.146 mmol) were dissolved in deoxygenated H₂O (16 mL) and the reaction was heated at 80 °C under an inert atmosphere overnight. KPF₆ (~200 mg) was added, the mixture was concentrated *in vacuo* at 37 °C in the dark, followed by purification of the crude over silica

(acetone/water/sat. KP₆, 100% - 50/50/0 - 100/80/20). The orange band was collected, and excess KPF₆ was removed *via* Sephadex LH-20 (MeOH) purification. Removal of the solvent under reduced pressure yielded the title compound as a dark red solid (32.0 mg, 0.026 mmol, 26%). $R_f = 0.56$ (100/80/20 acetone/water/sat. KPF₆); ^1H NMR (400 MHz, CD_3OD) $\delta = 10.25$ (d, $J = 1.3$ Hz, 1H, 1), 10.08 (d, $J = 8.2$ Hz, 1H, 3), 9.60 (d, $J = 6.7$ Hz, 1H, 18), 8.86 (d, $J = 8.1$ Hz, 2H, T_3' , T_5'), 8.68 (d, $J = 8.0$ Hz, 2H, T_6'' , T_6), 8.63 – 8.54 (m, 2H, 2, 11), 8.52 – 8.40 (m, 2H, T_4' , 8), 8.19 – 8.03 (m, 4H, 9, 10, T_5 , T_5''), 7.86 – 7.80 (m, 2H, T_3 , T_3''), 7.78 (dd, $J = 5.4$, 1.5 Hz, 2H, 16), 7.71 (dd, $J = 8.1$, 5.4 Hz, 2H, 17), 7.36 (t, $J = 6.6$ Hz, 2H, T_4 , T_4''), 4.26 (d, $J = 7.7$ Hz, 1H, H-1), 4.07 – 3.94 (m, 1H, CHH H-6), 3.85 (d, $J = 11.7$ Hz, 1H, CHH OCH_2), 3.74 – 3.48 (m, 10H, CHH H-6, CHH OCH_2 , 4 x OCH_2), 3.25 – 3.21 (m, 2H, H-3, H-4), 3.17 (d, $J = 3.0$ Hz, 1H, H-5), 3.10 (dd, $J = 9.0$, 7.8 Hz, 1H, H-2), 2.03 (t, $J = 5.4$ Hz, 2H, OCH_2SMe), 1.50 (s, 3H, OCH_2SMe). ^{13}C NMR (101 MHz, CD_3OD) $\delta = 159.3$ (C_q Arom), 158.9 (C_q Arom), 155.2 (C_H 1), 154.9 (C_H T_3 , T_3''), 152.8 (C_H 17), 151.4 (C_q Arom), 144.4 (C_q Arom), 144.0 (C_q Arom), 141.4 (C_q Arom), 141.0 (C_q Arom), 140.2 (C_H T_5 , T_5''), 138.5 (C_H 8), 135.5 (C_H 3), 135.3 (C_H 18), 133.5 (C_H 9), 133.5 (C_H 10), 130.9 (C_H T_4'), 130.8 (C_H 2), 129.8 (C_H T_4 , T_4''), 129.0 (C_H 11), 128.0 (C_H 17), 126.3 (C_H T_6'' , T_6), 125.5 (C_H T_3' , T_5'), 104.5 (C-1), 78.0 (C-3, C-5), 75.1 (C-2), 71.6 (C-4), 71.4 (OCH_2), 71.4 (OCH_2), 71.2 (OCH_2), 69.7 (C-6), 68.4 (OCH_2), 62.7 (OCH_2), 35.8 (OCH_2SMe), 15.5 (OCH_2SMe). HRMS: m/z calcd for $[\text{C}_{46}\text{H}_{47}\text{O}_8\text{N}_7\text{RuSP}_2\text{F}_{12} - 2\text{PF}_6]^{2+}$: 479.61197; found: 479.61362; Elemental analysis calcd (%) for $[\mathbf{4b}](\text{PF}_6)_2 \cdot 6\text{H}_2\text{O}$: C, 40.71; H, 4.38; N, 7.23; found: C, 40.32; H, 4.28; N, 7.20.



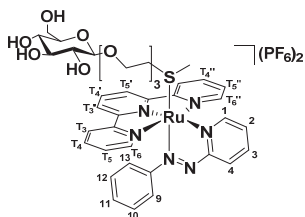
[Ru(tpy)(pmip)(R)](PF₆)₂, [6b](PF₆)₂: AgNO₃ (0.152 g, 0.895 mmol) was added to a solution of [Ru(tpy)(pmip)Cl]Cl (0.251 g, 0.351 mmol) in acetone/H₂O (60 mL, 3:1). The resulting mixture was heated overnight at 50 °C under an inert atmosphere and then hot-filtered over Celite®. The volume was reduced (~10%), 2 mL saturated aqueous NH₄PF₆ was added, and the resulting brown precipitate was collected on a glass frit, washed with H₂O (3 x 50 mL) and

Et₂O (3 x 50 mL) affording the title compound as a brown powder which was used without further purification. (0.275 g, 0.215 mmol, 95%). An aliquot (60.0 mg, 0.0630 mmol) was then, together with 2-(2-(2-(methylthio)ethoxy)ethoxy)ethyl-β-L-glucopyranoside (40.0 g, 0.117 mmol) dissolved in deoxygenated acetone (11 mL) and stirred at 50 °C under an inert atmosphere overnight in the dark, followed by concentration under vacuum at 30 °C in the dark and purification over a Sephadex LH-20 column (MeOH). The orange fraction was collected and the volume was reduced to ~10% then Et₂O was added. The resulting precipitate was collected by filtration on a Whatman® RC60 membrane filter, then washed with EtOAc (3 x 50 mL), Et₂O (3 x 50 mL) and heptane (3 x 50 mL) affording [6b](PF₆)₂ as an orange powder (60 mg, 0.047 mmol, 75%). *R_f* = 0.48 (100/80/20 acetone/water/sat. KPF₆); ¹H NMR (500 MHz, [D₆]acetone) δ = 10.21 (d, *J* = 5.2 Hz, 1H, 1), 9.44 (d, *J* = 8.2 Hz, 1H, 2), 8.99 (d, *J* = 8.2 Hz, 2H, T₃', T₅'), 8.90 (d, *J* = 8.2 Hz, 1H, 21), 8.79 (d, *J* = 8.0 Hz, 2H, T₃, T₃''), 8.60 – 8.52 (m, 2H, 2, T₄'), 8.22 (d, *J* = 8.2 Hz, 2H, 9, 13), 8.18 – 8.09 (m, 2H, T₄, T₄''), 7.97 (d, *J* = 5.4 Hz, 2H, T₆, T₆''), 7.83 (d, *J* = 5.4 Hz, 1H, 19), 7.61 (dd, *J* = 8.2, 5.2 Hz, 1H, 20), 7.46 – 7.35 (m, 4H, T₃, T₃'', 10, 12), 4.31 (d, *J* = 7.7 Hz, 1H, H-1), 3.99 – 3.89 (m, 1H, CHH H-5), 3.84 (dd, *J* = 11.7, 2.7 Hz, 1H, CHH OCH₂), 3.72 – 3.48 (m, 10H, CHH H-6, CHH OCH₂, 4 x OCH₂), 3.43 – 3.22 (m, 2H, H-3, H-4, H-5), 3.13 (t, *J* = 8.3 Hz, 1H, H-2), 2.42 (s, 3H, CH₃ Tol), 2.21 (t, *J* = 5.4 Hz, 2H), 1.63 (s, 3H, OCH₂SMe). ¹³C NMR (126 MHz, (CD₃)₂CO) δ = 159.0 (C_q Arom), 158.6 (C_q Arom), 154.8 (C_H T₆, T₆''), 154.4 (C_q Arom), 151.8 (C_H 1), 149.3 (C_H 19), 146.3 (C_q Arom), 146.0 (C_q Arom), 141.5 (C_q Arom), 139.7 (C_H T₄, T₄''), 137.9 (C_H 2), 131.9 (C_H 3), 131.6 (C_H 21), 130.6 (C_H T₅, T₅''), 129.5 (C_H 10, 12), 127.9 (C_q Arom), 127.5 (C_H 9, 13, T₄'), 126.3 (C_H 20), 125.9 (C_H T₃, T₃''), 125.2 (C_H T₃', T₃'), 104.2 (C-1), 78.0 (C-3), 77.5 (C-5), 74.8 (C-2), 71.6 (C-4), 71.3 (OCH₂), 71.0 (OCH₂), 70.9 (OCH₂), 69.2 (C-6), 68.2 (OCH₂), 62.8 (OCH₂), 35.8 (OCH₂), 21.4 (CH₃ Tol), 15.6 (OCH₂SMe). HRMS: *m/z* calcd for [C₄₈H₅₁O₈N₇RuSP₂F₁₂ – 2PF₆]²⁺: 493.62762, found: 493.62791; Elemental analysis calcd (%) for [6b](PF₆)₂: C, 45.15; H, 4.03; N, 7.68; found: C, 45.35; H, 4.23; N, 7.53.



[Ru(tpy)(pyimi)(R)](PF₆)₂, [7b](PF₆)₂: [Ru(tpy)(pyimi)Cl]Cl (30.0 mg, 0.0429 mmol) and 2-(2-(2-(methylthio)ethoxy)ethoxy)ethyl-β-D-glucopyranoside (83.0 mg, 0.242 mmol) were dissolved in acetone/H₂O (1:1, 7 mL) and to this mixture was added AgPF₆ (31 mg, 0.123 mmol).

After stirring for 72 h at reflux under inert atmosphere in the dark, the mixture was filtered over Celite® and concentrated *in vacuo* in the dark at 30 °C. The crude was then purified over silica (acetone/water/sat. KPF₆ 100/0/0 - 100/80/20) collecting the orange fraction. Subsequent purification over Sephadex LH-20 (MeOH) afforded, after concentrating *in vacuo* the title compound as an orange paste (19 mg, 0.016 mmol, 37%). $R_f = 0.64$ (100/80/20 acetone/water/sat. KPF₆). ¹H NMR (400 MHz, CD₃OD) $\delta = 9.85$ (d, $J = 5.5$ Hz, 1H, 1), 8.89 (s, 1H, 6), 8.59 – 8.51 (m, 3H, 3, T₃, T₃''), 8.45 (d, $J = 8.2$ Hz, 3H, T₃', T₅', 4), 8.21 (t, $J = 8.1$ Hz, 3H, 2, T₄, T₄''), 8.09 (t, $J = 8.1$ Hz, 1H, T₄'), 7.85 (d, $J = 5.4$ Hz, 2H, T₆'', T₆), 7.69 – 7.59 (m, 2H, T₅, T₅''), 7.11 (t, $J = 7.5$ Hz, 1H, 11), 6.96 (t, $J = 7.7$ Hz, 2H, 9, 13), 5.79 (d, $J = 7.9$ Hz, 2H, 10, 12), 4.25 (d, $J = 7.8$ Hz, 1H, H-1), 3.98 (m, 1H, CHH H-6), 3.86 (d, $J = 11.7$ Hz, 1H, CHH OCH₂), 3.73 – 3.38 (m, 10H, CHH H-6, CHH OCH₂, 4 x OCH₂), 3.34 (d, $J = 4.0$ Hz, 1H), 3.24 (d, $J = 6.6$ Hz, 1H), 3.12 – 3.04 (m, 1H, H-5), 1.94 (t, $J = 5.4$ Hz, 2H, OCH₂SMe), 1.42 (s, 3H, OCH₂SMe). ¹³C NMR (101 MHz, CD₃OD) $\delta = 170.9$ (C_q Arom), 159.3 (C_q Arom), 158.1 (C_q Arom), 157.9 (C_q Arom), 155.1 (C_H T₆'', T₆), 153.9 (C_H 1), 140.5 (C_H T₄, T₄''), 139.1 (C_H 4), 137.9 (C_H T₄'), 132.4 (C_H 3), 130.8 (C_H 2), 130.3 (C_H 9, 13), 130.2 (C_H T₅, T₅''), 129.2 (C_H 11), 125.9 (C_H T₃, T₃''), 124.8 (C_H T₃', T₅'), 120.9 (C_H 10, 12), 104.5 (C-1), 78.0 (C-3, C-5), 75.1 (C-2), 71.6 (C-4), 71.4 (OCH₂), 71.3 (OCH₂), 71.2 (OCH₂), 69.7 (C-6), 68.4 (OCH₂), 62.7 (OCH₂), 35.8 (OCH₂SMe), 15.7 (OCH₂SMe). HRMS: m/z calcd for [C₄₀H₄₇O₈N₅RuSp₂F₁₂ – 2PF₆]²⁺: 429.60889, found: 429.61047.



[Ru(tpy)(azpy)(R)](PF₆)₂, [8b](PF₆)₂: [Ru(tpy)(azpy)Cl]Cl (47.0 mg, 0.0849 mmol) and 2-(2-(2-(methylthio)ethoxy)ethoxy)ethyl-β-D-glucopyranoside (50.0 mg, 0.146 mmol) were dissolved in deoxygenated H₂O (5 mL, 0.02 M) and stirred at 80 °C for 48 h under an inert atmosphere after which solvents were removed under

reduced pressure at 30 °C in the dark. The crude was then purified over silica (acetone/water/sat. KPF₆ 100/0/0 - 100/80/20) by collection of the light purple fraction. Subsequent purification over Sephadex LH-20 (MeOH) afforded **[8b](PF₆)₂** as a purple solid (15 mg, 0.013 mmol, 15%). $R_f = 0.34$ (acetone/water/sat. KPF₆ 100/80/20); ¹H NMR (400 MHz, CD₃OD) $\delta = 9.75$ (d, $J = 5.6$ Hz, 1H, 1), 9.02 (d, $J = 8.0$ Hz, 1H, 4), 8.59 (d, $J = 8.1$ Hz, 5H, T₃', T₅', T₆, T₆''), 8.36 – 8.27 (m, 2H, 2, T₅''), 8.27 – 8.18 (m, 2H, T₅, T₄'), 7.63 – 7.57 (m, 4H, T₃'', T₃, T₄'', T₄), 7.28 (t, $J = 7.5$ Hz, 1H, 11), 7.07 (t, $J = 7.9$ Hz, 2H, 10, 12), 6.20 (d, $J = 7.5$ Hz, 2H, 9, 13), 4.26 (d, $J = 7.8$ Hz, 1H, H-1), 4.02 – 3.94 (m, 1H, CHH H-6), 3.89 – 3.82 (m, 1H, OCHH), 3.72 – 3.45 (m, 10H, CHH H-6, OCHH, 4 x OCH₂), 3.38 – 3.30 (m, 1H, H-5), 3.27 – 3.21 (m, 2H, H-3, H-4), 3.09 (t, $J = 8.4$ Hz, 1H, H-2), 2.02 (t, $J = 5.4$ Hz, 2H, OCH₂SMe), 1.50 (s, 3H, CH₃ OCH₂SMe). ¹³C NMR (101 MHz, CD₃OD) $\delta = 167.2$ (C_q Arom), 158.7 (C_q Arom), 156.9 (C_q Arom), 155.1 (C_H T₄'', T₄), 151.6 (C_H 1), 141.7 (C_H T₄', T₅), 141.1 (C_H 3), 139.7 (C_H 2), 131.4 (C_H 11), 130.8 (C_H 4), 130.5 (C_H 10, 2), 130.3 (C_H T₃'', T₃), 126.6 (C_H T₆, T₆''), 125.7 (C_H T₃', T₅'), 121.4 (C_H 9, 13), 111.4 (C_q Arom), 104.4 (C-1), 78.0 (C-3, C-5), 75.1

(C-2), 71.6 (C-4), 71.4 (OCH₂), 71.3 (OCH₂), 71.2 (OCH₂), 69.7 (C-6), 68.2 (OCH₂), 62.7 (OCH₂), 36.1 (OCH₂SMe), 15.7 (OCH₂SMe). HRMS: m/z calcd for [C₃₉H₄₆O₈N₆RuSP₂F₁₂ – 2PF₆]: 430.10652, found: 430.10721. Elemental analysis calcd (%) for **[8b]**(PF₆)₂: C, 40.74; H 4.03; N, 7.31; found: C, 40.53; H, 3.99; N, 7.15.

4.5.3 Photochemistry

4.5.3.1 General

Irradiation experiments were performed using a quartz fluorescence cuvette (1 cm path length) irradiated from the top (3 cm optical pathlength) with a custom-built LED light source equipped with either a Roithner LaserTechnik H2A1-H450 LED (λ_{exc} 450 nm, FWHM 35 nm) or H2A1-H470 LED (λ_{exc} 470 nm, FWHM 35 nm). UV-vis spectra were recorded on an Agilent Cary® 50 UV-vis spectrometer equipped with a Cary Single Cell Peltier and accessory for temperature control. Photon fluxes for both LEDs were determined using standard ferrioxalate actinometry.^[36]

4.5.3.2 Photosubstitution quantum yield measurements

General procedure: 3.00 mL of a solution of **[1b]**(PF₆)₂ ($1.38 \cdot 10^{-4}$ M) in H₂O was deoxygenated for 15 minutes with dinitrogen gas, after which it was irradiated at constant temperature (25 °C). During irradiation UV-vis spectra were recorded on a Varian Inc. Cary 50 UV-vis spectrometer with intervals of 30 seconds until t = 3600 seconds. ESI-MS spectra were recorded after the irradiation experiment to confirm the formation of the aqua species [Ru(tpy)(bpy)(OH₂)]²⁺ (m/z 254.5 calculated, 254.6 found). The quantum yield for the photosubstitution of the thioether ligand was calculated according to the method described earlier.^[37] Reference molar absorption coefficients used to calculate concentrations during irradiation are provided in table 4.4.

Table 4.4. Reference wavelengths (λ_{ref}) and molar absorption coefficients (ϵ_{ref}) for photosubstitution quantum yield calculations. RuSRR' = [Ru(tpy)(NN)(2-(2-(2-(methylthio)ethoxy)ethoxy)ethyl- β -D-glucopyranoside)](PF₆)₂ RuOH₂ = [Ru(tpy)(N-N)H₂O](PF₆)₂.

Compound	λ_{ref} in nm	ϵ_{ref} RuSRR' (M ⁻¹ cm ⁻¹)	ϵ_{ref} RuOH ₂ (M ⁻¹ cm ⁻¹)	N-N
[1b] (PF ₆) ₂	490	8.5×10^3	3.0×10^3	bpy
	410	3.1×10^3	5.0×10^3	
[2b] (PF ₆) ₂	490	2.1×10^3	8.3×10^3	phen
	410	5.2×10^3	5.7×10^3	
[3b] (PF ₆) ₂	490	3.9×10^3	6.7×10^3	dpq
	410	7.0×10^3	3.6×10^3	
[4b] (PF ₆) ₂	490	7.5×10^3	4.4×10^3	dppz
	420	4.8×10^3	7.2×10^3	
[5b] (PF ₆) ₂	490	7.4×10^3	12.4×10^3	dppn
	430	10.5×10^3	10.8×10^3	
[6b] (PF ₆) ₂	490	4.5×10^3	14.1×10^3	pmip
	430	8.9×10^3	6.6×10^3	
[7b] (PF ₆) ₂	490	8.7×10^3	14.0×10^3	pymi
	410	4.1×10^3	2.7×10^3	

4.5.3.3 Singlet oxygen and phosphorescence quantum yield

Emission measurements were carried out as described in appendix I.1.1.

4.5.4 Cytotoxicity Assay

The cytotoxicity assay was carried out as described in appendix I.2.1 with compounds [1a]Cl – [8a]Cl and [1b](PF₆)₂ – [8a](PF₆)₂. All compounds were dissolved in OMEM with the exception of [4a]Cl, [5a]Cl and [6a]Cl for which (a maximum of 0.5%) DMSO was used.

4.5.6 Cellular uptake

A549 cells were seeded (3×10^5) in a volume of 3 mL OptiMEM in 6-well plates. After 24 h 1 mL of a 100 μ M stock solution of [1a]Cl-[8a]Cl and [1b](PF₆)₂-[8b](PF₆)₂ in OMEM was added and incubated for 24 h. After 24 h incubation, the media was removed and the wells were washed with PBS (2 x 2 mL). Cells were trypsinized (1 mL) at 37 °C and transferred to a 14 mL corning tube with OMEM (2 x 2 mL). Corning tubes were centrifuged (1.2 RCF, 4 minutes). Media was aspirated and pellets were re-suspended in 1 mL PBS, and cells were counted. Samples were then centrifuged again, and the resulting pellets transferred to 10 mL glass vials with MilliQ (2 x 100 μ L), followed by overnight digestion with 2 mL 65% HNO₃. Aliquots of 1 mL were then diluted to 14 mL using MilliQ in 15 mL corning tubes. Ruthenium concentrations in each sample were then determined using ICP-MS. ICP-MS measurements were carried out on a i-CAP-Q ICP-MS (Thermo Scientific, Waltham, Massachusetts, USA). The system was optimized with a ruthenium-platinum solution which was calibrated within the range 0 - 25 μ g/L, with a detection limit of 0.01 μ g/L for all isotopes. Silver and Indium were used as an internal standard, to correct for sample dependent matrix effects. No reference sample was available; therefore several samples were spiked with a known concentration. The recovery of the spiked concentrations were all within a 10% deviation.

4.5.7 Log P_{o/w} determination

The partition coefficient between *n*-octanol and water (Log P_{o/w}) were determined according to the procedure described in appendix I.1.2.3: Stock solutions of complexes [1a]Cl - [8a]Cl and [1b](PF₆)₂ - [8b](PF₆)₂ (1×10^{-3} M) were prepared by dissolving the compounds in *n*-octanol saturated MilliQ water and [4a]Cl, [5a]Cl, [6a]Cl were dissolved in MilliQ saturated *n*-octanol water. For [4a] – [6a]Cl stock solution concentrations could not be determined *via* ICP-OES. These concentrations were calculated.

Log P values for [1a/b-8a/b]Cl/(PF₆)₂. SD = Standard deviation. Experiments were carried out in triplicate.

Compound	Mean	SD
[1a]Cl	-1.12	0.15
[2a]Cl	-1.08	0.16
[3a]Cl	-0.81	0.07
[4a]Cl	-0.02	0.01
[5a]Cl	1.01	0.04
[6a]Cl	-0.10	0.04
[7a]Cl	-1.61	0.19
[8a]Cl	-1.81	0.24
[1b](PF ₆) ₂	-0.23	0.08
[2b](PF ₆) ₂	-0.12	0.04
[3b](PF ₆) ₂	-0.51	0.02
[4b](PF ₆) ₂	-0.84	0.08
[5b](PF ₆) ₂	-0.50	0.13
[6b](PF ₆) ₂	-0.84	0.19
[7b](PF ₆) ₂	-0.20	0.02
[8b](PF ₆) ₂	-0.18	0.01

4.5.8 Crystals

Single crystals of [3a](PF₆)₂, [4a](PF₆)₂ and [5a]Cl were obtained as follows: [3a]Cl and [4a]Cl were converted to their corresponding PF₆ salts by dissolving them in a minimum amount of MeOH and adding a saturated solution of NH₄PF₆ in H₂O, the resulting precipitates were washed with H₂O (3x) and Et₂O (3x) and dissolved in 0.5 mL acetone in a small mass vial (~1 mg · mL⁻¹) and placed in a larger vial containing ~3 mL Et₂O (for [3b](PF₆)₂) or ~3 mL EtOAc (for [4b](PF₆)₂). A similar approach, but without the counter-anion exchange, was used for [5a]Cl with diisopropylether in acetonitrile. Detailed crystallographic data is provided in appendix III.1.

References

- [1] a). Z. Adhireksan, G. E. Davey, P. Campomanes, M. Groessl, C. M. Clavel, H. Yu, A. A. Nazarov, C. H. Yeo, W. H. Ang, P. Droge, U. Rothlisberger, P. J. Dyson, C. A. Davey, *Nat Commun* **2014**, *5*, 3462; b). M. H. Seelig, M. R. Berger, B. K. Keppler, *J Cancer Res Clin Oncol* **1992**, *118*, 195-200; c). M. Colucci, M. Coluccia, P. Montemurro, M. Conese, A. Nassi, F. Loseto, E. Alessio, G. Mestroni, N. Semeraro, *Int J Oncol* **1993**, *2*, 527-529; d). O. Novakova, J. Kasparkova, O. Vrana, P. M. Vanvliet, J. Reedijk, V. Brabec, *Biochemistry* **1995**, *34*, 12369-12378; e). A. C. G. Hotze, H. Kooijman, A. L. Spek, J. G. Haasnoot, J. Reedijk, *New J Chem* **2004**, *28*, 565-569.
- [2] A.-M. Florea, D. Büsselberg, *Cancers* **2011**, *3*, 1351-1371.
- [3] a). S. Leijen, S. A. Burgers, P. Baas, D. Pluim, M. Tibben, E. van Werkhoven, E. Alessio, G. Sava, J. H. Beijnen, J. H. Schellens, *Invest New Drugs* **2015**, *33*, 201-214; b). C. Mari, V. Pierroz, S. Ferrari, G. Gasser, *Chem Sci* **2015**, *6*, 2660-2686.
- [4] G. Subramanian, P. Parakh, H. Prakash, *Photobiol Sci* **2013**, *12*, 456-466.
- [5] K. Davia, D. King, Y. L. Hong, S. Swavey, *Inorg Chem Commun* **2008**, *11*, 584-586.

- [6] J. Fong, K. Kasimova, Y. Arenas, P. Kaspler, S. Lazic, A. Mandel, L. Lilge, *Photobiol Sci* **2015**, *14*, 2014-2023.
- [7] L. M. Loftus, J. K. White, B. A. Albani, L. Kohler, J. J. Kodanko, R. P. Thummel, K. R. Dunbar, C. Turro, *Chem Eur J* **2016**.
- [8] L. Zayat, C. Calero, P. Albores, L. Baraldo, R. Etchenique, *J Am Chem Soc* **2003**, *125*, 882-883.
- [9] a). M. A. Sgambellone, A. David, R. N. Garner, K. R. Dunbar, C. Turro, *J Am Chem Soc* **2013**, *135*, 11274-11282; b). R. N. Garner, J. C. Gallucci, K. R. Dunbar, C. Turro, *Inorg Chem* **2011**, *50*, 9213-9215.
- [10] T. Joshi, V. Pierroz, C. Mari, L. Gemperle, S. Ferrari, G. Gasser, *Angew Chem Int Ed* **2014**, *53*, 2960-2963.
- [11] E. Wachter, D. K. Heidary, B. S. Howerton, S. Parkin, E. C. Glazer, *Chem Commun* **2012**, *48*, 9649-9651.
- [12] a). M. K. Herroon, R. Sharma, E. Rajagurubandara, C. Turro, J. J. Kodanko, I. Podgorski, *Biol Chem* **2016**, *397*, 571-582; b). A. Li, R. Yadav, J. K. White, M. K. Herroon, B. P. Callahan, I. Podgorski, C. Turro, E. E. Scott, J. J. Kodanko, *Chem Commun* **2017**, *53*, 3673-3676.
- [13] a). V. H. S. van Rixel, B. Siewert, S. L. Hopkins, S. H. C. Askes, A. Busemann, M. A. Siegler, S. Bonnet, *Chem Sci* **2016**, *7*, 4922-4929; b). L. N. Lameijer, S. L. Hopkins, T. G. Breve, S. H. Askes, S. Bonnet, *Chem Eur J* **2016**, *22*, 18484-18491.
- [14] a). B. Siewert, V. H. van Rixel, E. J. van Rooden, S. L. Hopkins, M. J. Moester, F. Ariese, M. A. Siegler, S. Bonnet, *Chem Eur J* **2016**, *22*, 10960-10968; b). R. E. Goldbach, I. Rodriguez-Garcia, J. H. van Lenthe, M. A. Siegler, S. Bonnet, *Chem Eur J* **2011**, *17*, 9924-9929.
- [15] O. Novakova, J. Kasparkova, O. Vrana, P. M. van Vliet, J. Reedijk, V. Brabec, *Biochemistry* **1995**, *34*, 12369-12378.
- [16] A. Mijatovic, B. Smit, A. Rilak, B. Petrovic, D. Canovic, Z. D. Bugarcic, *Inorg Chim Acta* **2013**, *394*, 552-557.
- [17] S. Bonnet, J. P. Collin, N. Gruber, J. P. Sauvage, E. R. Schofield, *Dalton Trans* **2003**, 4654-4662.
- [18] A. K. Martensson, P. Lincoln, *Dalton Trans* **2015**, *44*, 3604-3613.
- [19] A. C. Hotze, J. A. Faiz, N. Mourtzis, G. I. Pascu, P. R. Webber, G. J. Clarkson, K. Yannakopoulou, Z. Pikramenou, M. J. Hannon, *Dalton Trans* **2006**, 3025-3034.
- [20] A. E. M. Boelrijk, A. M. J. Jorna, J. Reedijk, *J Mol Catal Chem* **1995**, *103*, 73-85.
- [21] A. Bahreman, B. Limburg, M. A. Siegler, E. Bouwman, S. Bonnet, *Inorg Chem* **2013**, *52*, 9456-9469.
- [22] a). K. Hansongnorn, U. Saeteaw, G. Mostafa, Y. C. Jiang, T. H. Lu, *Anal Sci* **2001**, *17*, 683-684; b). F. N. Rein, W. Chen, B. L. Scott, R. C. Rocha, *Acta Crystallogr E Crystallogr Commun* **2015**, *71*, 1017-1021.
- [23] a). B. A. Albani, C. B. Durr, C. Turro, *J Phys Chem A* **2013**, *117*, 13885-13892; b). J. D. Knoll, B. A. Albani, C. Turro, *Chem Commun* **2015**, *51*, 8777-8780.
- [24] V. Vichai, K. Kirtikara, *Nat Protocols* **2006**, *1*, 1112-1116.

- [25] E. Corral, A. C. Hotze, H. den Dulk, A. Leczkowska, A. Rodger, M. J. Hannon, J. Reedijk, *J Biol Inorg Chem* **2009**, *14*, 439-448.
- [26] U. Schatzschneider, J. Niesel, I. Ott, R. Gust, H. Alborzina, S. Wolf, *ChemMedChem* **2008**, *3*, 1104-1109.
- [27] A. P. Castano, T. N. Demidova, M. R. Hamblin, *Photodiagnosis Photodyn Ther* **2004**, *1*, 279-293.
- [28] Oecd, *OECD Guidelines for the Testing of Chemicals*, The Organisation for Economic Co-operation and Development, **1994**.
- [29] M. Frasconi, Z. Liu, J. Lei, Y. Wu, E. Strelakova, D. Malin, M. W. Ambrogio, X. Chen, Y. Y. Botros, V. L. Cryns, J.-P. Sauvage, J. F. Stoddart, *J Am Chem Soc* **2013**, *135*, 11603-11613.
- [30] E. B. van der Tol, H. J. van Ramesdonk, J. W. Verhoeven, F. J. Steemers, E. G. Kerver, W. Verboom, D. N. Reinhoudt, *Chem Eur J* **1998**, *4*, 2315-2323.
- [31] Z. Molphy, A. Prisecaru, C. Slator, N. Barron, M. McCann, J. Colleran, D. Chandran, N. Gathergood, A. Kellett, *Inorg Chem* **2014**, *53*, 5392-5404.
- [32] H. Xu, K. C. Zheng, H. Deng, L. J. Lin, Q. L. Zhang, L. N. Ji, *New J Chem* **2003**, *27*, 1255-1263.
- [33] R. A. Krause, K. Krause, *Inorg Chem* **1982**, *21*, 1714-1720.
- [34] C. H. Chien, S. Fujita, S. Yamoto, T. Hara, T. Yamagata, M. Watanabe, K. Mashima, *Dalton Trans* **2008**, 916-923.
- [35] K. A. Maghacut, A. B. Wood, W. J. Boyko, T. J. Dudley, J. J. Paul, *Polyhedron* **2014**, *67*, 329-337.
- [36] S. P. Pitre, C. D. McTiernan, W. Vine, R. DiPucchio, M. Grenier, J. C. Scaiano, *Sci Rep* **2015**, *5*, 16397.
- [37] A. Bahreman, J. A. Cuello-Garibo, S. Bonnet, *Dalton Trans* **2014**, *43*, 4494-4505.

Chapter 5:

$[\text{Ru}(\text{phbpy})(\text{N-N})(\text{dmsO}-\kappa\text{S})]^+$

A new photo-active chiral cyclometalated analogue of the $\text{Ru}(\text{tpy})(\text{N-N})(\text{dmsO}-\kappa\text{S})^{2+}$ scaffold

Abstract: Herein the synthesis of five new cyclometalated complexes with the general formula $[\text{Ru}(\text{phbpy})(\text{N-N})(\text{dmsO}-\kappa\text{S})]^+$ is described, where Hphbpy = 6'-phenyl-2,2'-bipyridyl, N-N = bpy (2,2'-bipyridine), phen (1,10-phenanthroline), dpq (pyrazino[2,3-f][1,10]phenanthroline), dppz (dipyrido[3,2- α :2',3'-c]phenazine or dppn (benzo[*l*]dipyrido[3,2- α :2',3'-c]phenazine). The thermal and photophysical properties of these complexes is investigated. The photosubstitution of dmsO ($\Phi_{450} = 4.1 \times 10^{-5}$ for $[\text{Ru}(\text{phbpy})(\text{bpy})(\text{dmsO}-\kappa\text{S})]^+$ and $\Phi_{450} = 1.6 \times 10^{-2}$ $[\text{Ru}(\text{phbpy})(\text{bpy})(\text{dmsO}-\kappa\text{S})]^+$) or the absence of photodissociation ($[\text{Ru}(\text{phbpy})(\text{dppz})(\text{dmsO}-\kappa\text{S})]^+$ and $[\text{Ru}(\text{phbpy})(\text{dppn})(\text{dmsO}-\kappa\text{S})]^+$) is explained in comparison to their polypyridyl analogues using electrochemistry and density functional theory (DFT) calculations. Their photoreactivity further translates to their cytotoxic properties against two different cancer cells lines (A549, lung cancer and MCF-7, breast cancer): Depending on the structure of the bidentate ligand, the complexes are photocytotoxic towards cancer cells using green light (11 μM before and 2 μM after irradiation when N-N = dpq) or highly cytotoxic in the dark (0.51 μM when N-N = dppn). Furthermore, by exploiting the photolability of $[\text{Ru}(\text{phbpy})(\text{phen})(\text{dmsO}-\kappa\text{S})]\text{PF}_6$ it was possible to separate the two enantiomers of this chiral molecule by coordination of a chiral sulfoxide followed by chiral HPLC purification. Therefore providing a new approach towards the synthesis of chiral cyclometalated ruthenium(II) complexes.

This chapter will be submitted for publication: L. N. Lameijer, C. J. van de Griend, A. G. Volbeda, M. A. Siegler, S. Bonnet; *Manuscript in preparation*.

5.1 Introduction

Since the clinical approval of cisplatin a great leap forward has been made in the field of bio-inorganic chemistry leading to the discovery of many new ruthenium complexes with anticancer properties. Two of the most thoroughly investigated anti-cancer agents are NAMI-A and KP1339 for which the latter clinical research is still ongoing. Currently, most research is focused on either compounds based upon the piano-stool Ru(II) η^6 -arene scaffold pioneered by the groups of Dyson and Sadler,^[1] or ruthenium(II) polypyridyl complexes, of which several (photoactive) candidates have been developed by the groups of Dunbar,^[2] Gasser,^[3] Glazer,^[4] Renfrew^[5] and Turro.^[6] More recently cyclometalated analogues of these complexes have emerged as a new subclass of light-activatable anticancer complexes.^[2] Typically, in this type of compounds one nitrogen atom in a polypyridyl ligand has been replaced by a carbon atom, resulting in an organometallic metallacycle.^[7] As a consequence, cyclometalated compounds often have better properties for chemotherapy or photodynamic therapy (PDT) than their non-cyclometalated analogons.^[7] In particular, cyclometalation leads to an increase in lipophilicity due to the decrease in the charge of the complex, which in turn increases uptake in cancer cells^[8] and often leads to higher cytotoxicity^[9] towards cancer cells. In addition, cycloruthenated polypyridyl complexes demonstrate to have more interesting properties for phototherapy compared to their non-cyclometalated analogons. Whereas the latter class of compounds typically absorb between 400 and 600 nm,^[10] a bathochromic shift is often observed for cyclometalated compounds due to the destabilization of t_{2g} orbitals by the π -donating cyclometalated carbanionic ligand, potentially allowing activation of these compounds with red light.^[11] The group of Turro has previously reported two cyclometalated complexes, *cis*-[Ru(phpy)(phen)(MeCN)₂]PF₆ and *cis*-[Ru(phpy)(bpy)(MeCN)₂]PF₆, (phpy = 2-phenylpyridine) that are capable of photosubstituting their acetonitrile ligand, and are phototoxic in cancer cells.^[12] Inspired by this work and following up on our investigation of caged ruthenium complexes with the general formula [Ru(tpy)(N-N)(L)]²⁺ in which L is a sulfur-based ligand, we herein investigate the synthesis, photochemistry, and biological properties of these complexes in which a carbanion is introduced in the tridentate ligand. Complexes **[1]**PF₆-**[5]**PF₆ have the general formula [Ru(phbpy)(N-N)(dmsO- κ S)]PF₆ with Hphbpy = 6'-phenyl-2,2'-bipyridyl and N-N = bpy (2,2'-bipyridine, **[1]**PF₆), phen (1,10-phenanthroline, **[2]**PF₆), dpq (pyrazino[2,3-*f*][1,10]phenanthroline, **[3]**PF₆), dppz (dipyrido[3,2-*a*:2',3'-*c*]phenazine), **[4]**PF₆), and dppn (benzo[*i*]dipyrido[3,2-*a*:2',3'-*c*]phenazine, **[5]**PF₆). An interesting property of these complexes is their chirality: By replacing one nitrogen atom in the tridentate ligand the plane of symmetry of these complexes is lost, effectively resulting in a chiral scaffold. In this chapter we elaborate on this new class of compounds, by providing insight in their synthesis, photophysical properties and compare their photoreactivity with that of the [Ru(tpy)(N-N)(L)]²⁺ complexes described in chapter 4. Furthermore, we demonstrate the

different ligand exchange properties of these complexes and answer the question whether these chiral complexes can be resolved, i.e., if their enantiomers can be separated.

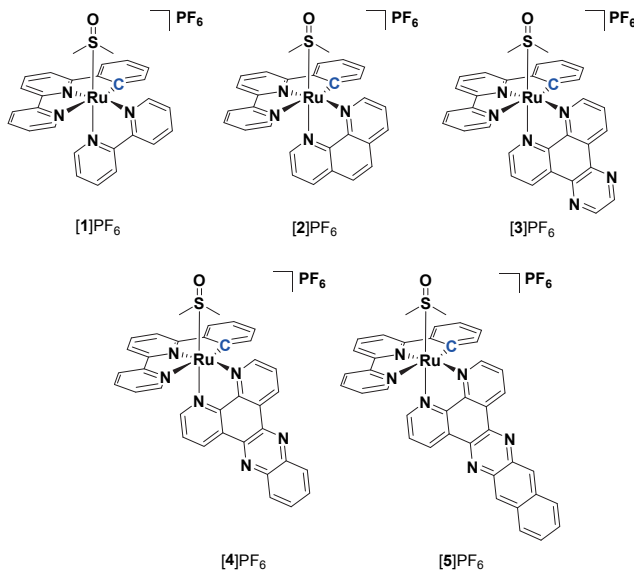
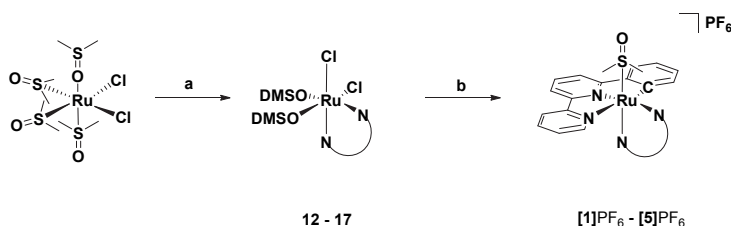


Figure 5.1. Chemical structures of the complexes presented in this study. $[\text{Ru}(\text{phbpy})(\text{NN})(\text{dmsO}-\kappa\text{S})]^+$, where N-N = bpy, phen, dpq, dppz or dpnp.

5.2 Results

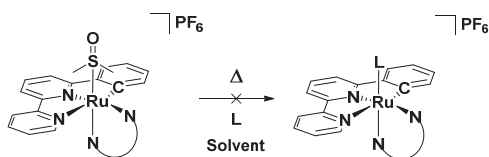
5.2.1 Synthesis

The first attempted route towards the synthesis of compounds $[\mathbf{1}]\text{PF}_6$ – $[\mathbf{5}]\text{PF}_6$ (Figure 5.1), inspired by the report of Ryabov and coworkers,^[13] consisted in the coordination of the terpyridine analogon Hphbpy to the ruthenium benzene dimer $[(\eta^6\text{-C}_6\text{H}_6)\text{RuCl}(\mu\text{-Cl})]_2$. However, this approach afforded the intermediate species $[\text{Ru}(\text{phbpy})(\text{MeCN})_3]\text{PF}_6$ in a maximum yield of only 32% and proved to be difficult to scale up. Therefore triggering the search for an alternative route depicted in Scheme 1. Starting from *cis*- $[\text{RuCl}_2(\text{dmsO}-\kappa\text{S})_3(\text{dmsO}-\kappa\text{O})]$, the reaction of the bidentate ligand N-N = bpy, phen, dpq, dppz, or dpnp, was realized first, followed by cyclometalation using Hphbpy in the presence of a catalytic amount of *N*-methylmorpholine, affording the five compounds $[\text{Ru}(\text{phbpy})(\text{N-N})(\text{dmsO}-\kappa\text{S})]\text{PF}_6$ ($[\mathbf{1}]\text{PF}_6$ – $[\mathbf{5}]\text{PF}_6$) as a racemic mixture of enantiomers in good yield (65 – 74%).



Scheme 5.1. Reagents and conditions. a). N-N = bpy in EtOH/DMSO (1:15), reflux, 86%; b). Phbpy, cat. *N*-methylmorpholine in MeOH/H₂O (5:1), reflux, 65%. For N-N = phen = 77% and 68%, N-N = dpq = 95% and 74%, NN = dpdz = 87% and 73%, NN = dppn = 96% and 65%.

With these compounds in hand, we attempted to obtain diastereomers by the thermal reaction of several chiral ligands as shown in Scheme 2 and summarized in Table 5.1 (entry 1 – 6). Heating [1]PF₆ and (*R*)-methyl *p*-tolylsulfoxide at increased temperatures (120 °C) in DMF resulted in the formation of ruthenium(III) species, as observed by a green color, whereas lower temperatures only led to the recovery of starting materials. Further attempts to substitute the monodentate ligand with non-chiral ligands (entry 7 – 8) such as LiCl, pyridine and acetonitrile also proved unsuccessful. This inertness is exceptional, as the terpyridine analogues of these complexes are known to thermally engage into selective exchange of the monodentate ligand in similar or milder conditions.^[14] The only thermal substitution observed with [4](PF₆)₂ was achieved in acetic acid, which resulted in the partial formation of [Ru(phbpy)(dppz)(AcOH)]⁺ as proven by mass spectrometry (found *m/z* 675.1, calcd. *m/z* 675.1), although this compound could not be isolated.



Scheme 5.2. General approach for the thermal conversion of complexes [1]PF₆, [2]PF₆ and [4]PF₆ with different monodentate ligands L.

Table 5.1. Attempts of ligand exchange for [1]PF₆, [2]PF₆ and [4]PF₆.

Entry	Complex	Ligand (L)	Solvent	T (°C)	Substitution
1	[1]PF ₆	(<i>R</i>)-Methyl <i>p</i> -tolylsulfoxide (5 eq.)	DMF	120	-
2	[1]PF ₆	(<i>R</i>)-Methyl <i>p</i> -tolylsulfoxide (5 eq.)	DMF	80	-
3	[1]PF ₆	(<i>R</i>)-Methyl <i>p</i> -tolylsulfoxide (5 eq.)	EtOH 3:1 H ₂ O	80	-
4	[4]PF ₆	Biotin (20 eq.)	EtOH 3:1 H ₂ O	80	-
5	[4]PF ₆	N-acetyl-L-methionine (20 eq.)	EtOH 3:1 H ₂ O	80	-
6	[4]PF ₆	N-Acetyl-L-cysteine methyl ester (20 eq.)	EtOH 3:1 H ₂ O	80	-
7	[4]PF ₆	L-Histidine methyl ester 2HCl (20 eq.)	EtOH 3:1 H ₂ O	80	-
8	[2]PF ₆	LiCl (20 eq.)	EtOH 3:1 H ₂ O	80	-
9	[4]PF ₆	-	MeCN	80	-
10	[4]PF ₆	-	Pyridine	80	-
11	[4]PF ₆	-	Acetic acid	80	Yes

5.2.2 Crystal structures

Single crystals suitable for crystal structure determination were obtained by slow vapor diffusion of ethyl acetate in dichloromethane for **[1]**PF₆, hexane in DCM for **[2]**PF₆ and **[3]**PF₆, or slow evaporation of a solution of **[4]**PF₆ in toluene. All compounds crystallized in space groups having an inversion center, thus containing a (1:1) mixture of enantiomers. A selection of bond lengths and angles is shown in Table 5.2. As expected, the ruthenium centers in these compounds have a distorted octahedral geometry similar to that of their terpyridyl analogues (described in chapter 4). Compared to [Ru(tpy)(bpy)(dmsO-κS)](OTf)₂ replacing the nitrogen within this scaffold with an anionic carbon atom has only a modest effect on the bond length of Ru1-C1 (2.043 Å) in **[1]**PF₆ compared to Ru1-N1 (2.079 Å).^[15] Furthermore, compared to its non-cyclometalated analogon the *trans*-influence of the carbon atom in phbpy⁻ results in an elongation of the Ru1-N2 bond length in [Ru(phbpy)(bpy)(dmsO-κS)]²⁺ (2.173(2) Å), whereas in [Ru(tpy)(bpy)(dmsO-κS)]²⁺ the Ru1-N3 length is 2.079(2) Å.^[16] In contrast, the ruthenium-sulfur bond length is shorter in **[1]**PF₆ (2.2558(7) Å) than in [Ru(tpy)(bpy)(dmsO-κS)]²⁺ (2.282(1) Å) as a result of the increased electron density on ruthenium, leading to stronger backbonding into the π* orbital of the S-bound dmsO ligand. Overall, this electronic effect barely affects the angles between C1-Ru1-N3 for **[1]**PF₆ (158.67(12) Å) and N1-Ru1-N3 for [Ru(tpy)(bpy)(dmsO-κS)]²⁺ (157.92(8) Å), confirming their high structural similarity.

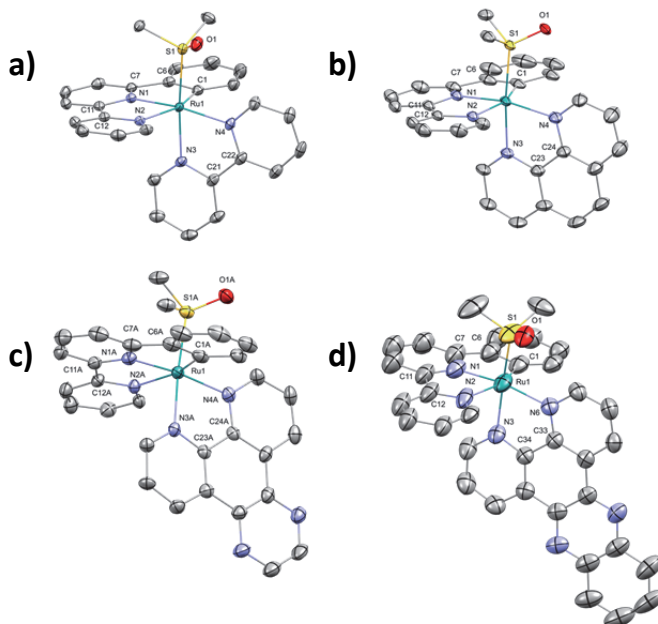


Table 5.2. Selected bond distances (Å) and bond angles (°) for complexes [1]PF₆, [2]PF₆, [3]PF₆ and [4]PF₆.

	[1]PF ₆	[2]PF ₆	[3]PF ₆	[4]PF ₆
Ru1-S1	2.2558(7)	2.2359(4)	2.2405(9)	2.210(3)
Ru1-C1	2.043(2)	2.041(3)	2.029(5)	2.030(1)
Ru1-N1	2.002(2)	2.004(2)	2.005(5)	2.019(7)
Ru1-N2	2.173(2)	2.164(2)	2.176(3)	2.180(1)
Ru1-N3	2.088(2)	2.110(2)	2.089(3)	2.094(3)
Ru1-N4	2.079(2)	2.091(2)	2.083(4)	2.071(4)
S1-O1	1.486(2)	1.489(2)	1.485(3)	1.501(6)
C1-Ru1-N2	157.92(8)	158.45(9)	158.5(2)	155.6(7)
N3-Ru1-N4	78.07(7)	78.67(7)	78.9(1)	78.2(1)
S1-Ru1-N4	96.25(5)	97.29(5)	96.6(1)	96.0(1)

5.2.3 Electronic absorption, emission and singlet oxygen

Electronic absorption spectra were recorded in acetonitrile for complexes [1]PF₆ – [5]PF₆ (Figure 5.3a) and the acetonitrile substituted [Ru(phbpy)(N-N)(CD₃CN)]²⁺ derivatives [6]PF₆, [7]PF₆ and [8]PF₆ (Figure 5.3b, for synthesis, see below). [Ru(tpy)(bpy)(dmsO-KS)](PF₆)₂, [9](PF₆)₂ and [Ru(tpy)(bpy)(MeCN)](PF₆)₂, [10](PF₆)₂ are included to demonstrate the effect of the phbpy⁻ ligand on the absorption spectra of the cyclometalated complexes. Compounds [1]PF₆ – [5]PF₆ showed a considerable bathochromic shift (~40 nm, Table 5.3) and have a broader ¹MLCT band compared to [9](PF₆)₂ (411 nm, Table 5.3). Similarly, the photoproducts for [1]PF₆ – [3]PF₆ in acetonitrile show a comparable shift of approximately 50 nm compared to [10](PF₆)₂. Such a bathochromic shift is common for cyclometalated ruthenium analogues as reported in literature,^[16-17] and it is mostly ascribed to an increase in the energy of the highest occupied molecular orbital (HOMO) since the lowest unoccupied molecular orbital (LUMO) remains relatively unchanged.^[16] Furthermore, for [4]PF₆ and [5]PF₆ near-UV and visible ligand-based π-π* transitions are also observed around 370 nm and 410 nm respectively, due to the increased conjugation of the dpz and dppn ligands.

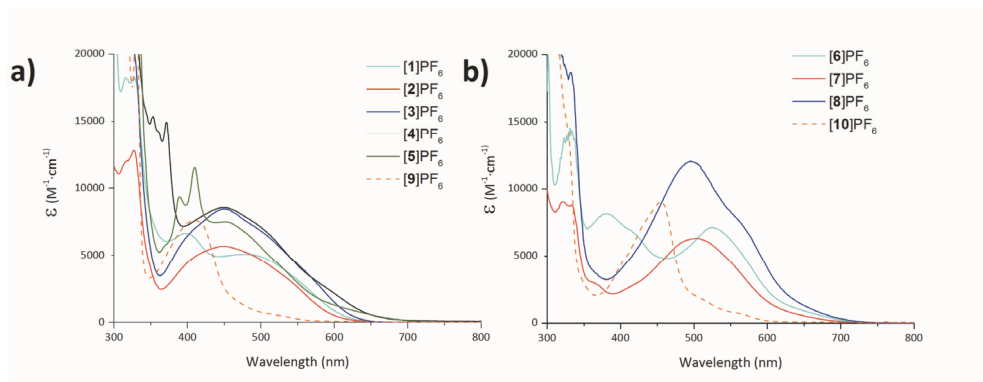


Figure 5.3 a). Electronic absorption spectra for [1]PF₆ – [5]PF₆ and b). [6]PF₆ – [8]PF₆ in acetonitrile. Dashed lines are for non-cyclometalated analogs [9](PF₆)₂ and [10](PF₆)₂ respectively.

Emission was measured for complexes [1]PF₆ – [5]PF₆ in acetonitrile. The maxima are reported in Table 5.3. All compounds are very weakly emissive with a slightly higher phosphorescence quantum yield (Φ_p) compared to the cyclometalated analogon [Ru(phbpy)(tpy)]⁺ ($\Phi_p = 5 \cdot 10^{-6}$).^[18] The emission wavelengths[†] for [1]PF₆ – [3]PF₆ are

comparable to those of $[\text{Ru}(\text{phbpy})(\text{tpy})]^+$ (786 – 800 nm versus 797 nm)^[18] and are similar to complexes reported by the group of Turro and Sauvage.^[16, 18] For complexes $[\mathbf{4}]\text{PF}_6$ and $[\mathbf{5}]\text{PF}_6$ a blue-shifted emission (618 and 672 nm) was observed compared to $[\text{Ru}(\text{phbpy})(\text{tpy})]^+$. Singlet oxygen quantum yields (Φ_Δ) were also determined in deuterated methanol by direct detection of the emission of $^1\text{O}_2$ at 1270 nm. Φ_Δ values lower than 0.04 were found for all complexes with the exception of $[\mathbf{3}]\text{PF}_6$, which produced $^1\text{O}_2$ with a photoefficiency (Φ_Δ) of 0.11. Interestingly, $[\text{Ru}(\text{phbpy})(\text{dppn})(\text{dmsO}-\kappa\text{S})]^+$ did not show any singlet oxygen production, whereas its non-cyclometalated analogue $[\text{Ru}(\text{tpy})(\text{dppn})(\text{CD}_3\text{OD})]^{2+}$ and $[\text{Ru}(\text{tpy})(\text{dppn})(\text{py})]^{2+}$ both have been demonstrated to be excellent PDT photosensitizers.^[19]

Table 5.3. Lowest-energy absorption maxima (λ_{max}), molar absorption coefficients at λ_{max} (ϵ in $\text{M}^{-1} \times \text{cm}^{-1}$), photosubstitution quantum yields (Φ_{450}) at 298 K, $^1\text{O}_2$ quantum yields (Φ_Δ) at 293 K and phosphorescence quantum yield (Φ_P) for $[\mathbf{1}]\text{PF}_6$ – $[\mathbf{11}]\text{PF}_6$.

Complex		λ_{max} (ϵ_{max} in $\text{M}^{-1} \text{cm}^{-1}$) ^[a]	λ_{em} (nm)	Φ_Δ ^[b]	Φ_P ^[b]
$[\mathbf{1}]\text{PF}_6$	$[\text{Ru}(\text{phbpy})(\text{bpy})(\text{dmsO}-\kappa\text{S})]\text{PF}_6$	476 ($50 \cdot 10^2$)	786	$3.2 \cdot 10^{-2}$	$1.6 \cdot 10^{-4}$
$[\mathbf{2}]\text{PF}_6$	$[\text{Ru}(\text{phbpy})(\text{phen})(\text{dmsO}-\kappa\text{S})]\text{PF}_6$	450 ($57 \cdot 10^2$)	800	$3.9 \cdot 10^{-2}$	$2.1 \cdot 10^{-4}$
$[\mathbf{3}]\text{PF}_6$	$[\text{Ru}(\text{phbpy})(\text{dpq})(\text{dmsO}-\kappa\text{S})]\text{PF}_6$	451 ($83 \cdot 10^2$)	787	$1.1 \cdot 10^{-1}$	$2.1 \cdot 10^{-4}$
$[\mathbf{4}]\text{PF}_6$	$[\text{Ru}(\text{phbpy})(\text{dppz})(\text{dmsO}-\kappa\text{S})]\text{PF}_6$	450 ($84 \cdot 10^2$)	618	$7.0 \cdot 10^{-3}$	$2.6 \cdot 10^{-4}$
$[\mathbf{5}]\text{PF}_6$	$[\text{Ru}(\text{phbpy})(\text{dppn})(\text{dmsO}-\kappa\text{S})]\text{PF}_6$	450 ($75 \cdot 10^2$)	672	-	$8.4 \cdot 10^{-5}$
$[\mathbf{6}]\text{PF}_6$	$[\text{Ru}(\text{phbpy})(\text{bpy})(\text{CD}_3\text{CN})]\text{PF}_6$	525 ($71 \cdot 10^2$)			
$[\mathbf{7}]\text{PF}_6$	$[\text{Ru}(\text{phbpy})(\text{phen})(\text{CD}_3\text{CN})]\text{PF}_6$	503 ($63 \cdot 10^2$)			
$[\mathbf{8}]\text{PF}_6$	$[\text{Ru}(\text{phbpy})(\text{dpq})(\text{CD}_3\text{CN})]\text{PF}_6$	495 ($119 \cdot 10^2$)			
$[\mathbf{9}]\text{PF}_6$	$[\text{Ru}(\text{tpy})(\text{bpy})(\text{dmsO}-\kappa\text{S})](\text{PF}_6)_2$	411 ($75 \cdot 10^2$)			
$[\mathbf{10}]\text{PF}_6$	$[\text{Ru}(\text{tpy})(\text{bpy})(\text{MeCN})](\text{PF}_6)_2$	455 ($91 \cdot 10^2$)			

[a] In MeCN. [b] In CD_3OD .

5.2.4 Photochemistry

Due to the exceptional thermal inertness of complexes $[\mathbf{1}]\text{PF}_6$ – $[\mathbf{5}]\text{PF}_6$ we attempted to substitute the dmsO ligands using visible light irradiation while reactions were monitored with ^1H NMR. When a sample of $[\mathbf{1}]\text{PF}_6$ was irradiated in acetonitrile with the white light ($h\nu \geq 410$ nm, Scheme 5.3) of a 1000 W Xenon Arc lamp fitted with a 400 nm cutoff filter, a photoproduct was formed which was later confirmed to be the acetonitrile adduct (see below). As shown in Figure 5.4, the ^1H NMR spectra clearly demonstrate the formation of a single species with a doublet appearing at 9.88 ppm and a doublet disappearing at 10.49 ppm. This photochemical behavior is very similar to the photosubstitution of $[\text{Ru}(\text{tpy})(\text{N}-\text{N})(\text{X})]^{2+}$, where the monodentate ligand is replaced by a solvent molecule.^[20] In a similar fashion the dmsO ligand in $[\mathbf{2}]\text{PF}_6$ and $[\mathbf{3}]\text{PF}_6$ could also be substituted with acetonitrile. However, $[\mathbf{4}]\text{PF}_6$ and $[\mathbf{5}]\text{PF}_6$ were not able to exchange their ligand. This is odd, given that their non-cyclometalated analogons $[\text{Ru}(\text{tpy})(\text{dppz})(\text{SRR}')]^+$ and $[\text{Ru}(\text{tpy})(\text{dppn})(\text{SRR}')]^+$ ($\text{SRR}' = 2-(2-(2-(\text{methylthio})\text{ethoxy})\text{ethoxy})\text{ethyl}-\beta\text{-D-glucopyranoside}$) described in Chapter 3 both have been demonstrated to be photo-active.

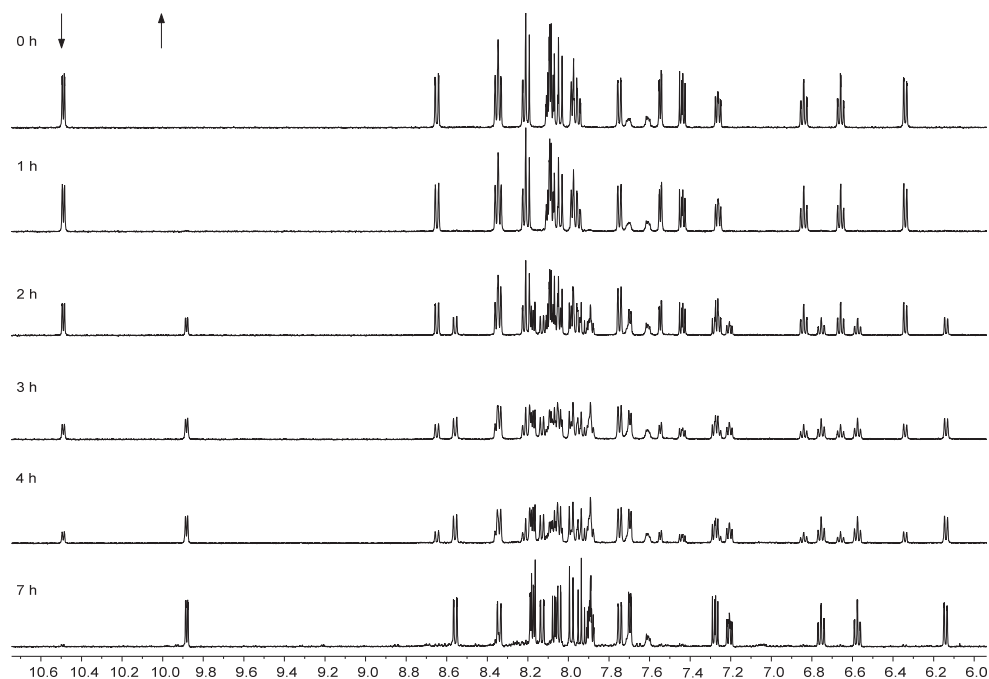


Figure 5.4 Evolution of the ^1H NMR spectra of $[\mathbf{2}]\text{PF}_6$ in CD_3CN (3.0 mg in 0.6 mL) upon irradiation with white light (>410 nm) from a 1000 W Xenon Arc lamp fitted with 400 nm cutoff filter 1 cm from the light source at $T = 298$ K. Spectra were taken every 1 h, with $t_{\text{irr}} = 7$ h.

To further investigate the ability of complexes $[\mathbf{1}]\text{PF}_6 - [\mathbf{5}]\text{PF}_6$ to exchange their monodentate ligand for a solvent molecule we studied them more thoroughly using UV-vis spectroscopy (Figure 5.5). Both $[\mathbf{4}]\text{PF}_6$ and $[\mathbf{5}]\text{PF}_6$ were confirmed to be photochemically inert, while complex $[\mathbf{1}]\text{PF}_6 - [\mathbf{3}]\text{PF}_6$ were all found to convert to their acetonitrile counterparts with clear isobestic points for $[\mathbf{1}]\text{PF}_6$ (441 and 490 nm), $[\mathbf{2}]\text{PF}_6$ (470 nm) and $[\mathbf{3}]\text{PF}_6$ (455 nm), confirming the formation of a single species for each photoconversion. After each reaction, ESI-MS spectra were taken to confirm the formation of the acetonitrile photoproduct. The photosubstitution quantum yields (Φ_{450}) for the complexes were found to be 4.1×10^{-5} for $[\mathbf{1}]\text{PF}_6$, 1.3×10^{-5} for $[\mathbf{2}]\text{PF}_6$ and 2.2×10^{-5} for $[\mathbf{3}]\text{PF}_6$. These values are a thousand-fold lower than those determined for $[\text{Ru}(\text{tpy})(\text{bpy})(\text{dmsO}-\kappa\text{S})]^{2+}$ ($\Phi_{450} = 1.6 \times 10^{-2}$). This is most likely caused due to the destabilization of the ^3MC state due to the increased electron density at the metal center brought by the strong σ -donor C-atom, and stabilization of the $^3\text{MLCT}$, which leads to a larger energy gap between the $^3\text{MLCT}$ and ^3MC state and makes thermal population of the latter rather unlikely.^[17] This interpretation is supported by previous work of the group of Turro, who have demonstrated that the efficiency of the photosubstitution in sterically congested cyclometalated complexes are much lower or absent, compared to their polypyridyl analogues.^[12, 16] Overall, the modest but very selective photosubstitution

properties of [1]PF₆ - [3]PF₆ open new doors towards the synthesis of photo-active, chiral cyclometalated complexes.

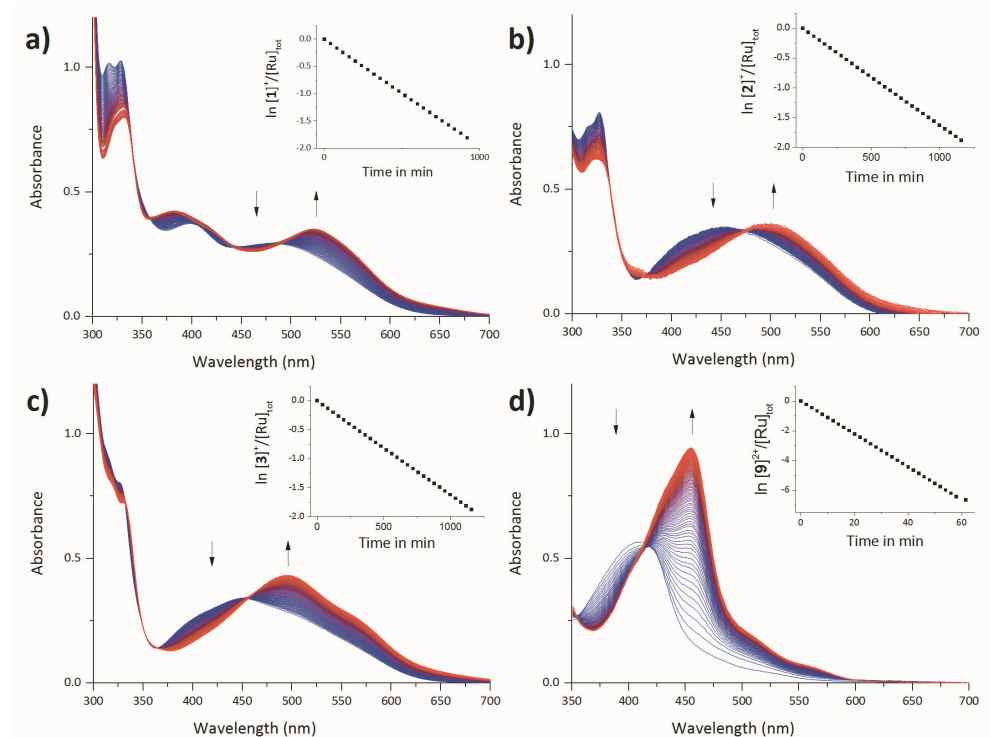


Figure 5.5 Electronic absorption spectra of [1]PF₆ – [3]PF₆ and [9](PF₆)₂ in deoxygenated MeCN upon irradiation at 450 nm at T = 298 K. Spectra measured every 30 min (every 0.5 min for [9]PF₆). a. [1](PF₆)₂, $t_{irr} = 16$ h, $[Ru]_{tot} = 5.78 \times 10^{-5}$ M, photon flux = 1.68×10^{-7} mol s⁻¹. b. [2](PF₆)₂, $t_{irr} = 23$ h, $[Ru]_{tot} = 6.08 \times 10^{-5}$ M, photon flux = 1.67×10^{-7} mol s⁻¹. c. [3]PF₆, $t_{irr} = 16$ h, $[Ru]_{tot} = 4.06 \times 10^{-5}$ M, photon flux = 1.68×10^{-7} mol s⁻¹. d. [9](PF₆)₂, $t_{irr} = 1$ h, $[Ru]_{tot} = 6.52 \times 10^{-5}$ M, photon flux = 5.54×10^{-8} mol s⁻¹.

5.2.5 Electrochemistry and DFT

The electrochemical properties of complexes [1]PF₆ – [9]PF₆ were determined with cyclic voltammetry (Figure 5.6 and Table 5.4) to provide insight in the frontier orbitals of the complexes.^[21] As summarized in Table 5.4, the cyclometalated dmsol complexes [1]PF₆ – [5]PF₆ show semi-reversible oxidation processes ($I_{pa}/I_{pc} \approx 1$) with Ru^{II}/Ru^{III} couples near ~0.30 V vs. Fc^{0/+} whereas its non-cyclometalated analogon [9](PF₆)₂ showed an irreversible Ru^{II} → Ru^{III} oxidation at 1.23 V vs. Fc^{0/+}. This indicates that the HOMO of the cyclometalated complexes is destabilized due to the π-donating instead of π-accepting character from the phbpy⁻ ligand. The irreversible oxidation for [9](PF₆)₂ is attributed to linkage isomerization of DMSO from being S bound to O-bound to the ruthenium center,^[22] indicating that cyclometalation prevents redox-induced linkage isomerization, due to the increased electron density on ruthenium. When acetonitrile complex [10]PF₆ was used for comparison with the cyclometalated complexes instead, a similar destabilization on the HOMO energy levels was found. For the dmsol complexes [1]PF₆ - [5]PF₆ the HOMO appeared at a higher potential (0.30 V vs. Fc^{0/+}) than for acetonitrile compounds [6]PF₆ -

[7]PF₆ (0.00 V vs. Fc^{0/+}) which can be explained by the origin of the monodentate ligand; S-dmsso is a stronger π-acceptor than CD₃CN and therefore has a stronger electron withdrawing effect on ruthenium(II), which in turn leads to stabilization of the HOMO.^[23] The LUMO for [1]PF₆ – [3]PF₆ was found to have very similar energy, with quasi-reversible reductions around -2.0 V vs. Fc^{0/+}, suggesting that these are phbpy-based. For [4]PF₆ and [5]PF₆ the LUMO appears to be lower in energy (-1.4 V vs. Fc^{0/+} for [4]PF₆ and -1.2 V vs. Fc^{0/+} for [5]PF₆) due to the strong electron-accepting properties of the dipyrrophenazine moieties.^[24]

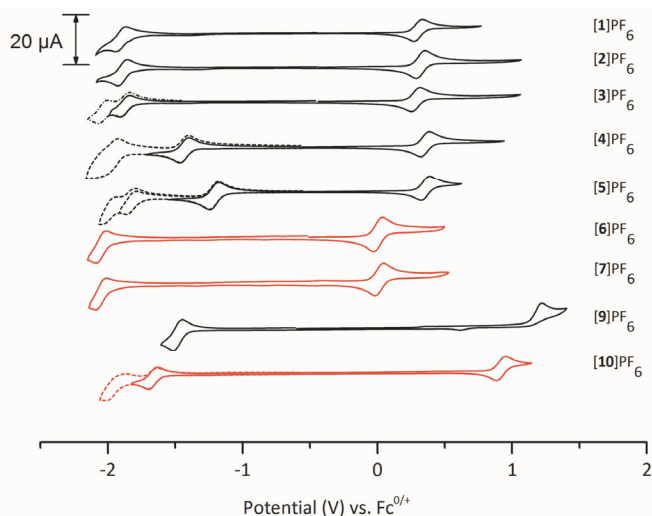


Figure 5.6 Cyclic voltammograms of cyclometalated complexes [1]PF₆ – [7]PF₆ and non-cyclometalated complexes [9](PF₆)₂ and [10](PF₆)₂. Scan rate 100 mV s⁻¹, with the exception of [4]PF₆, [6]PF₆, [7]PF₆ and [9]PF₆ which were measured at 200 mV s⁻¹. L = dmsso-κS or CD₃CN.

Table 5.4. Redox potentials measured with cyclic voltammetry (vs Fc^{0/Fc⁺}) in MeCN with [Bu₄N]PF₆ as supporting electrolyte. Complexes were measured at 298 K with a scan rate of 100 mV.s⁻¹, with the exception of [4]PF₆, [6]PF₆, [7]PF₆ and [8]PF₆ which were measured at 200 mV.s⁻¹.

		$E_{1/2}$ (V)	i_{pa}/i_{pc}	$E_{1/2}$ (V)	i_{pc}/i_{pa}
[Ru(phbpy)(bpy)(dmsso-κS)]PF ₆	[1]PF ₆	+0.30	0.99	-1.90	1.47
[Ru(phbpy)(phen)(dmsso-κS)]PF ₆	[2]PF ₆	+0.32	1.02	-1.89	1.11
[Ru(phbpy)(dpq)(dmsso-κS)]PF ₆	[3]PF ₆	+0.29	1.01	-1.87, -1.95	0.66, 2.23
[Ru(phbpy)(dppz)(dmsso-κS)]PF ₆	[4]PF ₆	+0.35	1.04	-1.43, -2.00	1.03, -
[Ru(phbpy)(dppn)(dmsso-κS)]PF ₆	[5]PF ₆	+0.36	1.05	-1.21, -1.82, -2.01	1.07, 1.52
[Ru(phbpy)(bpy)(CD ₃ CN)]PF ₆	[6]PF ₆	0.00	1.00	-2.05	1.34
[Ru(phbpy)(phen)(CD ₃ CN)]PF ₆	[7]PF ₆	+0.02	1.04	-2.05	-1.38
[Ru(tpy)(bpy)(DMSO)](PF ₆) ₂	[9](PF ₆) ₂	+1.23 ^[a]	-	-1.48	1.00
[Ru(tpy)(bpy)(MeCN)](PF ₆) ₂	[10](PF ₆) ₂	+0.92	0.95	-1.67	1.06

[a] E_{pa}

To provide further insight on the frontier orbitals of these complexes, their HOMO – LUMO gap was plotted in an energy diagram (Figure 5.7, left). This plot revealed that the HOMO-LUMO gap between complexes [1]PF₆ – [3]PF₆ is very similar, with ΔE (ΔE_{pa}-E_{pc}) ~ 2.2 V vs. Fc^{0/+}. This value is significantly lower than that of the tpy analogues [Ru(tpy)(bpy)(L)]²⁺ with L = S-dmsso and MeCN (ΔE = 2.6 and 2.7 V vs. Fc^{0/+}), which is

explained by an increase of the energy of the HOMO due to the π -donating properties of the phbpy⁻ ligand.^[16] Surprisingly, for [4]PF₆ and [5]PF₆ however, the ΔE values found (ΔE - 1.6 V for [4]PF₆ and ΔE 1.8 V for [5]PF₆) are much lower than those found for complexes [1]PF₆ – [3]PF₆, suggesting that the dppz and dppn ligands have a stabilizing effect on the ¹MLCT level.

To further elaborate that hypothesis, we then performed density functional theory (DFT) calculations at the BPE0/TZP level using the conductor-like screening model (COSMO) to simulate solvent effects. The calculated HOMO and LUMO energy levels show a trend (Figure 5.7, right), that fitted very well with the results acquired from cyclic voltammetry. Furthermore, these calculations revealed that for complex [3]⁺, [4]⁺ and [5]⁺ the LUMO is located on the bidentate ligand dpq, dppz, and dppn, respectively (Figure S.IV.3-5), whereas for [1]PF₆ and [2]PF₆ it is located on the phbpy⁻ ligand. Like for [Ru(tpy)(dppz)(L)]²⁺, for which the LUMO was also found on the dppz ligand,^[24] for complexes [4]PF₆ and [5]PF₆ extending the conjugation of the bidentate ligand results in a shift of the LUMO from the tridentate to the bidentate ligand. For the more conjugated complexes [4]PF₆ and [5]PF₆ this does not affect the main ¹MLCT band (Figure 3). However, assuming that the photochemistry occurs from the lowest excited ¹MLCT, this would lead to a ³MLCT state for [4]PF₆ and [5]PF₆ too low in energy to allow thermal population of ³MC state. Therefore making alternative pathways, such as non-radiative decay a preferred pathway over photo-dissociation.^[25]

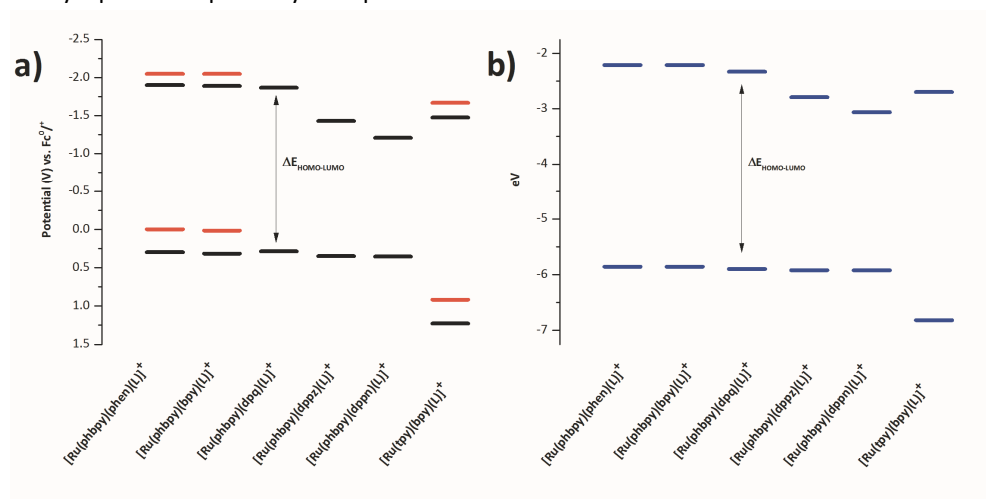
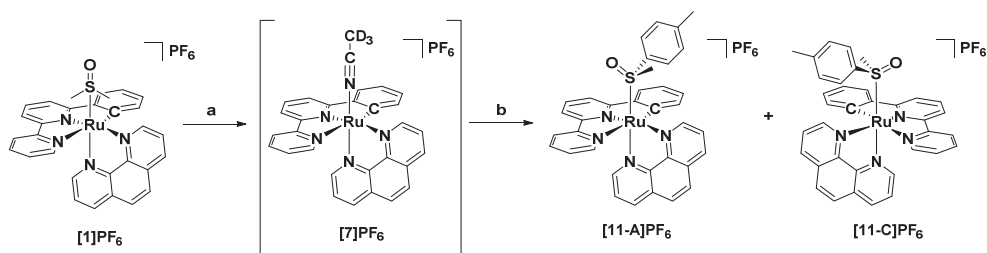


Figure 5.7 a). HOMO and LUMO orbital energy diagram derived from cyclic voltammetry data for complexes with general formula [Ru(phenbpy)(N-N)L]⁺ with N-N = phen, bpy, dpq, dppz and dppn or [Ru(tpy)(bpy)L]⁺. Red lines L = S-dmsol. Black lines L = MeCN/CD₃CN. **b).** HOMO and LUMO orbital energy diagram derived from DFT calculations, L = dmsol-xS.

5.2.6 Resolving diastereomers

The photochemical lability of the complexes [1]PF₆ – [3]PF₆ allowed us to investigate whether separation of their respected enantiomers was possible. Similar to the approach

described in the previous section (§ 5.2.4), compound **[2]PF₆** was converted to photoproduct **[7]PF₆** using white light in deuterated acetonitrile, which allowed the reaction to be monitored with ¹H NMR spectroscopy. After completion of the reaction (~7 h) an attempt was made to resolve this intermediate **[7]PF₆** with either a chiral HPLC column or by crystallization using sodium (+)-tartrate, however without success. An alternative procedure was therefore used: **[7]PF₆** was allowed to react with an excess of enantiomerically pure (*R*)-methyl *p*-tolylsulfoxide in MeOH, affording a (1:1) mixture of diastereomers of (anticlockwise/clockwise) A/C-[Ru(phbpy)(phen)(*R*)-Methyl *p*-tolylsulfoxide]]PF₆, **[11-A/C]PF₆** (Scheme 5.3). Subsequent purification over a chiral HPLC column, afforded **[11-A]PF₆** and **[11-C]PF₆** as their respective diastereomers in 9% yield (6% over two steps for **[11-A]PF₆** and 3% over two steps for **[11-C]PF₆** (Figure S.IV.6).



Scheme 5.3. Reagents and conditions for the synthesis of **[11-A/C]PF₆**. a. $h\nu, \geq 410 \text{ nm}$. b. (*R*)-Methyl *p*-tolylsulfoxide in MeOH, reflux, 16 h. (6% over two steps for **[10-A]PF₆**, 3% over two steps for **[10-C]PF₆**).

¹H NMR confirmed that fraction 1 corresponded to the R-C diastereomer, which is most apparent because of its more shielded α -proton of phen appearing at 10.64 ppm (Figure 5.8). Fraction 2 contained the R-A diastereomer, with a doublet appearing at 10.74 ppm (Figure 8). This deshielding effect on the α -proton on phen is most likely attributed to the interaction of the tolyl group with the bidentate ligand, which is supported by NOESY experiments (Figure S.IV.6), which show the absence of interaction between the methyl of the sulfoxide and phen, whereas this interaction is weakly observed for **[11-A]PF₆** (Figure S.IV.7). However, crystal structures are needed to confirm the stereochemistry of these complexes.

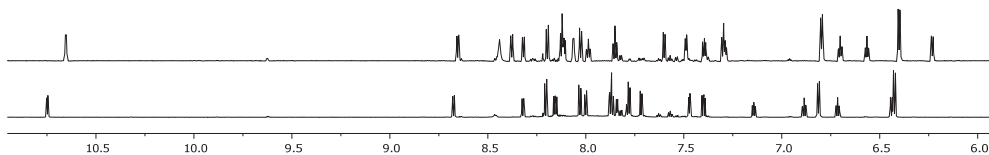


Figure 5.8. ¹H NMR spectrum (850 MHz) of **[11-C]PF₆** (top) and **[11-A]PF₆** (bottom).

Since both complexes **[11-A]PF₆** and **[11-C]PF₆** were isolated as diastereomers and were not resolved as their respective enantiomers **[7-A]PF₆** and **[7-C]PF₆**, determining their specific rotation would not provide any useful information about their chirality. Circular dichroism (CD) was used instead. The CD spectra (Figure 5.9) displayed symmetrical curves

typical for enantiomers, except in the region below 250 nm where the contribution of the chiral (*R*)-tolylsulfoxide becomes non-negligible.^[26] At higher wavelengths (260 – 600 nm), either positive or negative Cotton effects were observed for **[11-A]**PF₆ or **[11-C]**PF₆ complex, which are most likely only originating from metal-based transitions. Theoretically, resolution of these complexes by performing blue light irradiation in acetonitrile may be tempting. However, photosubstitution is usually accompanied by racemization of the coordination sphere, so that thermal ligand substitution would be preferred.^[27] The exceptional thermal stability of the sulfoxide cyclometalated complexes prevented us from obtaining isolated enantiomers. However, CD of the diastereoisomers **[11-A]**PF₆ and **[11-C]**PF₆ provided a clear proof of the chirality of these complexes.

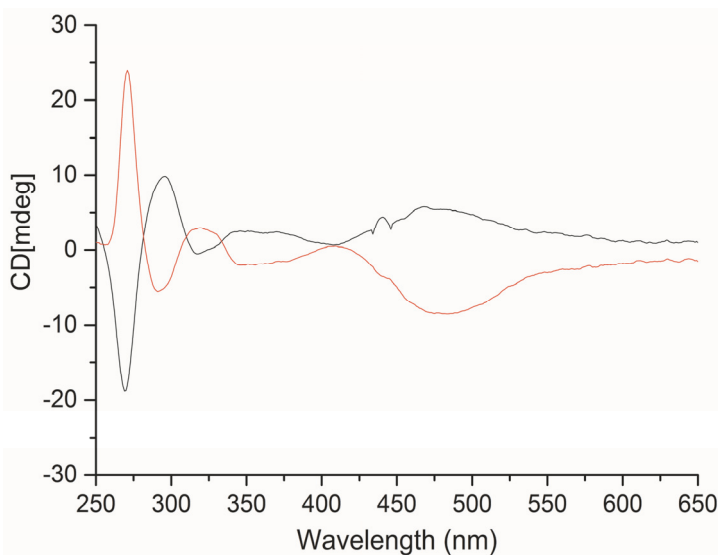


Figure 5.9. Superposition of CD spectra of first fraction (**[11-C]**PF₆) and second fraction (**[11-A]**PF₆) eluted diastereoisomers. T = 293 K, c = 5 × 10⁻⁵ M in MeCN.

5.2.7 DNA interaction and cytotoxicity

The cytotoxic properties of **[1]**PF₆ – **[3]**PF₆ were investigated in the dark as well under green light irradiation ($\lambda = 520\text{nm}$, 10 min, 25.0 ± 1.9 mW, 15 ± 1.1 J cm⁻²) against two different human cancer cell lines, A549 (lung cancer) and MCF-7 (breast cancer). Considering the poor photosensitizing and photodissociation properties of **[4]**PF₆ and **[5]**PF₆, these complexes were only tested in the dark after a high-throughput screening confirmed that there are no differences in EC₅₀ for these complexes before and after light irradiation. Cells were seeded, treated with a concentration series of **[1]**PF₆ – **[5]**PF₆ at t = 24 h, irradiated or maintained in the dark after media refreshment (t = 48 h), followed by cell viability determination at t = 96 h using the sulforhodamine B (SRB) assay.^[28] The cell-growth inhibition concentrations (EC₅₀) are reported in Table 5.5. In the dark complexes

[1]PF₆ – [3]PF₆ are moderately to non-cytotoxic with EC₅₀ values between 43 and >100 μM. However, upon green light irradiation complex [1]PF₆ and [3]PF₆ showed an increase in cytotoxicity resulting in photo-indices ranging from 1.4 to 9.3 reaching low micromolar (<10 μM) cytotoxicity values. This effect might be ascribed to the generation of reactive oxygen species since these three complexes have been demonstrated to be poor to moderate singlet oxygen sensitizers (Φ_{Δ} = 0.032 - 0.11). However, as shown in Figure S.IV.8, our DNA studies in the presence of green light did not show the formation of any DNA adducts or open circular DNA, which suggests that these compounds have another target than nuclear DNA. This result is in contrast to that of reported analogues, such as the D-glucose conjugated [Ru(tpy)(dppn)(SRR')]²⁺ complex reported in chapter 3, which was demonstrated to have a very high affinity for (mitochondrial) DNA in the dark and cleaved DNA.^[19a] On the other hand, complexes [4]PF₆ and [5]PF₆ were demonstrated to be very cytotoxic to both cell lines, approaching EC₅₀ values in the low micromolar to sub-micromolar range against both A549 and MCF-7 cells. This result is in accordance with other cyclometalated complexes reported by Fetzer et. al. who have shown that more lipophilic cyclometalated complexes often have an increased cytotoxic effect on cancer cells, compared to polypyridyl analogues.^[29] However, even for [4]PF₆ and [5]PF₆ complexes, which contain the well-known intercalators dppz and dppn,^[3, 19a, 30] no DNA interaction was observed, even at high MC:BP ratios of 5:1, therefore suggesting an alternative mode of action, such as disturbance of oxido-reductase enzymes.^[29]

Table 5.5. (Photo)cytotoxicity for [1]PF₆ - [5]PF₆ expressed as effective concentrations (EC₅₀ in μM) in the dark and after irradiation with green light (520 ± 38 nm, 25.0 mW ± 1.9 · cm⁻², 10 minutes, 15 · J cm⁻² ± 1.14) in A549 and MCF-7 cells. Values are reported in μM with ±95% confidence intervals (CI). Photocytotoxicity index (PI = EC_{50, dark}/EC_{50, 520 nm}).

Complex	Light dose (J cm ⁻²)	A549			MCF-7		
		EC ₅₀ (μM)	±CI (95%)	PI	EC ₅₀ (μM)	±CI (95%)	PI
[1]PF ₆	0	>100	-		67	+14	
	15	69	+6.8 -6.1	>1.4	21	+5.5 -4.2	
[2]PF ₆	0	43	+13 -9.5	5.7	18	+3.9 -3.2	5.8
	15	7.6	+2.0 -1.7		3.1	+0.49 -0.44	
[3]PF ₆	0	62	+20 -14	9.3	11	+3.6 -2.8	5.5
	15	6.7	+1.5 -1.2		2.0	+0.72 -0.56	
[4]PF ₆	0	2.6	+0.37 -0.32	-	1.5	+0.28 -0.24	-
	15	n.d.	-	-	n.d.	-	-
[5]PF ₆	0	1.2	+0.17 -0.14	-	0.51	+0.059 -0.055	-
	15	n.d.	-	-	n.d.	-	-

5.3 Discussion

Three of the presented cycloruthenated complexes ($[1]PF_6 - [3]PF_6$) have been demonstrated to have photodissociative properties in the presence of acetonitrile. Recent examples of the group of Turro have shown that complexes such as *cis*- $[Ru(phpy)(phen)(CH_3CN)_2]PF_6$ are as photoactive as their non-cyclometalated counterparts, with a reported photosubstitution quantum yield (Φ_p) of 0.25.^[12] However, this value was obtained by irradiation in dichloromethane in the presence of 2 mM tetrabutyl ammonium chloride. It has been a well-established fact that more polar solvents have a stabilizing effect on 3MLCT states, without affecting the 3MC states, thereby increasing the 3MC - 3MLCT energy gap. Therefore providing an explanation for the high photosubstitution quantum yield for $[Ru(phpy)(phen)(CH_3CN)_2]PF_6$ in dichloromethane. A more recent report by Albani et. al. has shown that for $[Ru(biq)_2(phpy)]PF_6$ the *phpy* ligand increases the energy of the 3MC state, which in their case completely prevents photodissociation.^[16] Our findings show that the ligand exchange efficiency upon irradiation of complexes $[1]PF_6 - [5]PF_6$ is mostly determined by the cyclometalated ligand, which seems to have a great effect on the energy of both the HOMO and LUMO. However, when phenazine based ligands are introduced in the $[Ru(phbpy)(N-N)(dmsO-\kappa S)]^+$ scaffold, the LUMO is shifted from the tridentate ligand to the bidentate ligand. This has multiple consequences. First, $[3]PF_6$ both generates modest amounts of 1O_2 ($\Phi_\Delta = 0.11$) due to competition with a $^3\pi\pi^*$ state and is able to substitute its monodentate ligand with a solvent molecule. Second, the photo-reactivity of these complexes seems to be diminished due to the stabilized 1MLCT state, which makes population of the 3MC from the lowered 3MLCT state very unlikely for both complex $[4]PF_6$ and $[5]PF_6$. This effect is in great contrast to the photochemical behavior of the non-cyclometalated compounds, which undergo efficient photosubstitution. For example, compared to $[4]PF_6$, $[Ru(tpy)(dppz)(SRR')]^{2+}$ -reported in chapter 4- has a photosubstitution quantum yield of ~ 0.02 , whereas $[Ru(tpy)(dppn)(SRR')]^{2+}$ is able to exchange its monodentate ligand upon light irradiation and a good 1O_2 sensitizer ($\Phi_\Delta = 0.71$).^[19a] Therefore demonstrating that modifications on the bidentate ligand in the $[Ru(phbpy)(N-N)(dmsO-\kappa S)]^+$ scaffold have a major effect on its photo-reactivity.

5.4 Conclusion

In this work we have presented five new cycloruthenated complexes ($[1]PF_6 - [5]PF_6$) based on the $[Ru(phbpy)(N-N)(L)]^+$ architecture. We have demonstrated the exceptional thermal stability of these complexes towards thermal substitution, and provided a thorough description of their photophysical behavior. In spite of their low 1O_2 generation quantum yields, complexes $[1]PF_6 - [3]PF_6$ were found to be photocytotoxic, while $[4]PF_6$ and $[5]PF_6$ were not photocytotoxicity but very cytotoxic in the dark. The submicromolar

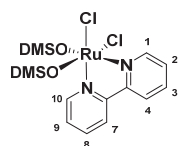
EC₅₀ values found for these complexes provide an incentive to study them in more detail, since they have an unexpected poor binding affinity for DNA. Finally, we have demonstrated that we can synthesize and separate a set of specific diastereomers (**[11-A]**PF₆ and **[11-C]**PF₆) from **[2]**PF₆ using a two-step photochemical and thermal approach. To conclude, these results open interesting new prospects in the field of photo-active chiral anticancer drugs.

5.5 Experimental

5.5.1 General

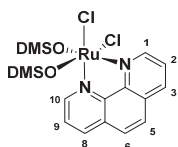
Reagents were purchased from Sigma-Aldrich and used without further purification. Dpq,^[31] dpbz,^[31] dpbn,^[32] Hphbpy,^[33] (*R*)-(+)-methyl *p*-tolyl sulfoxide^[34] and *cis*-Ru(dmsO)₄Cl₂^[35] were synthesized according to reported procedures. Dry solvents were collected from a Pure Solve MD5 solvent dispenser from Demaco Holland BV. For all inorganic reactions solvents were deoxygenated by bubbling argon through the solution for 30 minutes and carried out under an inert atmosphere in the dark, unless stated otherwise. Solvents were removed under vacuum with a rotary evaporator in the dark at 30 °C, unless stated otherwise. Flash chromatography was performed on silica gel (Screening devices B.V.) with a particle size of 40 - 64 μm and a pore size of 60 Å. Chiral HPLC was performed on a Jupiter® 4μm Proteo 90 Å 3000 UHPLC (250 x 21.2 mm, flow rate 14 mL·min⁻¹). TLC analysis was conducted on TLC aluminium foils with silica gel matrix (Supelco, silica gel 60, 56524) with detection by UV-absorption (254 nm). NMR spectra were recorded on a Bruker AV-400 or AV-500. ¹H NMR and ¹³C NMR spectra were recorded in [D₆]acetone, [D₃]acetonitrile and [D₆]DMSO with chemical shifts (δ) relative to the solvent peak. High resolution mass spectra were recorded by direct injection (2 μl of 2 μM solution in water/acetonitrile; 50/50; v/v and 0.1% formic acid) in a mass spectrometer (Thermo Finnigan LTQ Orbitrap) equipped with an electrospray ion source in positive mode (source voltage 3.5 kV, sheath gas flow 10, capillary temperature 250 °C) with resolution R = 60000 at m/z 400 (mass range m/z = 150 – 2000) and dioctylphthalate (m/z = 391.28428) as a lock mass. The high-resolution mass spectrometer was calibrated prior to measurements with a calibration mixture (Thermo Finnigan).

5.5.2 Synthesis

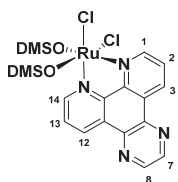


[Ru(bpy)(dmsO)₂Cl₂], [12]: *cis*-[Ru(dmsO)₄Cl₂] (200 mg, 0.410 mmol) and bpy (64.0 mg, 0.410 mmol) were dissolved in deoxygenated EtOH/DMSO (3.2 mL, 16:1) and heated at reflux for 2 h. After cooling to rt, the resulting precipitate was filtered, washed with cold ethanol (5 mL), diethyl ether (15 mL) and dried *in vacuo* affording the title compound as an orange powder (168 mg, 0.350 mmol, 86%). ¹H NMR (400 MHz,

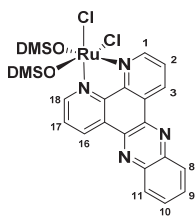
[D₆]DMSO) δ = 9.66 (d, J = 4.5 Hz, 1H, 1), 9.55 (d, J = 4.5 Hz, 1H, 10), 8.66 (d, J = 8.1 Hz, 1H, 7), 8.61 (d, J = 8.2 Hz, 1H, 4), 8.22 (td, J = 7.8, 1.6 Hz, 1H, 8), 8.10 (td, J = 7.8, 1.5 Hz, 1H, 3), 7.77 (dd, J = 7.2, 5.6 Hz, 1H, 9), 7.61 (dd, J = 7.4, 5.7 Hz, 1H, 2), 3.40 (s, 3H, CH₃), 3.36 (s, 3H, CH₃), 2.98 (s, 3H, CH₃), 2.28 (s, 3H, CH₃); HRMS: m/z calcd for [C₁₄H₂₀Cl₂N₂O₂RuS₂ - Cl]⁺: 448.96982; found: 489.96900; elemental analysis calcd (%) for [12]: C 34.71, H 4.16, N 5.78; found: C 34.82, H 4.31, N 5.53.



[Ru(phen)(dmsO)₂Cl₂], [13]: The procedure described for [12] was followed using *cis*-Ru(dmsO)₄Cl₂ (100 mg, 0.210 mmol) and phen (38.0 mg, 0.210 mmol) yielding the product as an orange powder (82.0 mg, 0.160 mmol, 77%). ¹H NMR (400 MHz, [D₆]DMSO) δ = 9.96 (d, J = 5.4 Hz, 1H, 1), 9.83 (d, J = 5.2 Hz, 10), 8.87 (d, J = 8.2 Hz, 1H, 8), 8.74 (d, J = 8.3 Hz, 3), 8.34 – 8.22 (m, 2H, 5, 6), 8.17 (dd, 1H, J = 8.2, 5.4 Hz, 9), 8.01 (dd, J = 8.2, 5.4 Hz, 1H, 2), 3.48 (s, 3H, CH₃), 3.43 (s, 3H, CH₃), 2.94 (s, 3H, CH₃), 2.15 (s, 3H, CH₃); HRMS: m/z calcd for [C₁₆H₂₀Cl₂N₂O₂RuS₂ - Cl]⁺: 472.96962; found: 472.96904; elemental analysis calcd (%) for [13]: C 37.80, H 3.97, N 5.51; found: C 37.64, H 4.03, N 5.58.

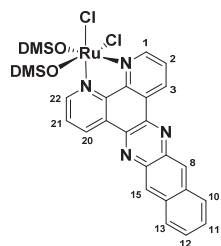


[Ru(dpq)(dmsO)₂Cl₂], [14]: The procedure described for [12] was followed using *cis*-Ru(dmsO)₄Cl₂ (200 mg, 0.410 mmol) and dpq (95.0 mg, 0.410 mmol) yielding the product as an orange brown powder (220 mg, 0.390 mmol, 95%). ¹H NMR (400 MHz, [D₆]DMSO) δ = 10.13 (d, J = 5.5 Hz, 1H, 1), 10.00 (d, J = 6.5 Hz, 1H, 14), 9.66 (d, J = 6.9 Hz, 1H, 12), 9.53 (d, J = 8.2 Hz, 1H, 3), 9.35 (m, 2H, 7, 8), 8.33 (dd, J = 8.2, 5.3 Hz, 1H, 13), 8.17 (dd, J = 8.2, 5.5 Hz, 1H, 2), 3.50 (s, 3H, CH₃), 3.45 (s, 3H, CH₃), 2.95 (s, 3H, CH₃), 2.28 (s, 3H, CH₃); HRMS: m/z calcd for [C₁₈H₂₀Cl₂N₄O₂RuS₂ - Cl]⁺: 524.975969; found: 524.97535; elemental analysis calcd (%) for [14]: C 38.57, H 3.60, N 10.00; found: C 37.73; found: H 4.12, N 9.50.

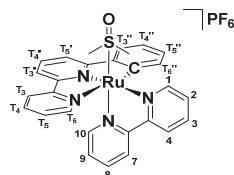


[Ru(dppz)(dmsO)₂Cl₂], [15]: *cis*-[Ru(dmsO)₄Cl₂] (100 mg, 0.210 mmol) and dppz (60.0 mg, 0.210 mmol) in ethanol (3 mL) and DMSO (0.2 mL) were refluxed for 2 h. The reaction was cooled down to room temperature and the resulting precipitate was filtered, washed with cold ethanol (5 mL) and diethyl ether (15 mL). The crude was then redissolved in a minimal amount of acetone, and precipitated with Et₂O to afford the title compound as a light brown powder (110 mg, 0.18 mmol, 87%). ¹H NMR (400 MHz, [D₆]DMSO) δ = 10.10 (d, J = 4.2 Hz, 1H, 1), 9.98 (d, J = 3.9 Hz, 1H, 18), 9.73 (d, J = 8.0 Hz, 1H, 16), 9.61 (d, J = 7.7 Hz, 1H, 3), 8.54 – 8.46 (m, 2H, 8, 11), 8.36 – 8.29 (m, 1H, 17), 8.20 – 8.12 (m, 3H, 2, 9, 10), 3.49 (s, 3H, CH₃), 3.46 (s, 3H, CH₃), 2.95 (s, 3H, CH₃), 2.32 (s, 3H, CH₃); HRMS: m/z calcd for [C₂₂H₂₂Cl₂N₄O₂RuS₂ - Cl]⁺:

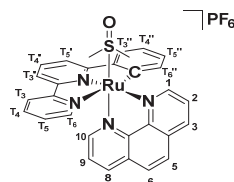
574.99162; found: 574.99119; elemental analysis calcd (%) for [15].2H₂O: C 49.49, H 3.58, N 9.62; found: C 48.69, H 3.43, N 9.35.



[Ru(dppn)(dmsO)₂Cl₂], [16]: The same procedure was followed as described for [15] using *cis*-[Ru(dmsO)₄Cl₂] (100 mg, 0.206 mmol) and dppn (70.0 mg, 0.211 mmol) to afford the product as an light brown powder (131 mg, 0.198 mmol, 96%). ¹H NMR (400 MHz, [D₆]DMSO) δ = 10.09 (d, *J* = 5.5 Hz, 1H, 1), 9.96 (d, *J* = 4.3 Hz, 1H, 22), 9.72 (d, *J* = 6.9 Hz, 1H, 21), 9.60 (d, *J* = 7.9 Hz, 1H, 3), 9.23 (d, *J* = 2.4 Hz, 2H, 8, 15), 8.49 – 8.39 (m, 2H, 10, 13), 8.37 – 8.27 (m, 1H, 21), 8.19 – 8.10 (m, 1H, 2), 7.85 – 7.71 (m, 2H, 11, 12), 3.50 (s, 3H, CH₃), 3.46 (s, 3H, CH₃), 2.96 (s, 3H, CH₃), 2.35 (s, 3H, CH₃); HRMS: *m/z* calcd for [C₂₆H₂₄Cl₂N₄O₂RuS₂ – Cl]⁺: 625.00727; found: 625.00679; elemental analysis calcd (%) for [16]: C 47.27, H 3.66, N 8.48; found: C 47.47, H 3.79, N 8.36.

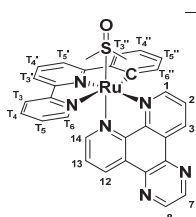


[Ru(phbpy)(bpy)(dmsO)]PF₆, [1]PF₆: [Ru(bpy)(dmsO)₂Cl₂] (122 mg, 0.250 mmol) and Hphbpy (58 mg 0.25 mmol) were dissolved in a mixture of MeOH/H₂O (15 mL, 5:1) and to this mixture were added 4 drops of *N*-ethylmorpholine. After heating at reflux for 16 h, solvents were removed *in vacuo*, followed by purification over silica (0 – 15% MeOH in DCM) and salt metathesis using aqueous KPF₆. The resulting precipitate was filtered and washed with water (3x) affording the title compound as a red powder (116 mg, 0.16 mmol, 65%). *R_f* = 0.30 (10% MeOH in DCM); ¹H NMR (400 MHz, [D₆]acetone) δ = 10.32 (d, *J* = 5.9 Hz, 1H, 1), 8.72 (d, *J* = 8.2 Hz, 1H, 4), 8.64 (d, *J* = 8.2 Hz, 1H, T₅'), 8.58 (d, *J* = 8.2 Hz, 1H, 7), 8.46 (d, *J* = 7.9 Hz, 1H, T₃'), 8.30 (d, *J* = 5.4 Hz, 1H, T₆), 8.26 – 8.10 (m, 4H, 3, T₅', T₄' T₃), 7.90 (t, *J* = 7.9 Hz, 1H, 1H, 8), 7.84 (t, *J* = 7.5 Hz, 2H, 2, T₃'), 7.59 – 7.50 (m, 1H, T₅), 7.39 (d, *J* = 5.6 Hz, 1H, 10), 7.25 (t, *J* = 6.6 Hz, 1H, 9), 6.89 (t, *J* = 7.5 Hz, 1H, T₄'), 6.81 (t, *J* = 7.3 Hz, 1H, T₅'), 6.61 (d, *J* = 7.4 Hz, 1H, T₆'), 2.41 (s, 3H, CH₃), 2.25 (s, 3H, CH₃); ¹³C NMR (101 MHz, [D₆]acetone) δ = 181.9 (C_q), 168.4 (C_q), 157.9 (C_q), 156.8 (C_q), 156.0 (C_q), 154.9 (C_H, 1), 153.1 (C_H, T₆), 149.0 (CH, 10), 148.0 (C_q), 139.7 (C_H, T₄), 138.4 (C_H, T₆'), 138.2 (C_H, T₄'), 137.7 (C_H, 8), 136.0 (C_H, 3), 130.9 (C_H, T₅'), 128.7 (C_H, T₅), 127.3 (C_H, 9), 127.2 (C_H, 2), 126.2 (C_H, T₃'), 124.9 (C_H, T₃), 124.7 (C_H, 4), 123.8 (C_H, 7), 123.2 (C_H, T₄'), 121.1 (C_H, T₃'), 120.4 (C_H, T₅'), 45.6 (CH₃), 43.5 (CH₃); HRMS: *m/z* calcd for [C₂₈H₂₅N₄ORuS – PF₆]: 567.07926; found: 567.07885; elemental analysis calcd (%) for [1]PF₆: C 47.26, H 3.54, N 7.87; found: C 46.54, H 4.19, N 7.35.



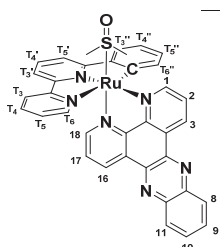
[Ru(phbpy)(phen)(dmsO)]PF₆, [2]PF₆: The same procedure was followed as described for [6]PF₆ using [Ru(phen)(dmsO)₂Cl₂] (114 mg, 0.22 mmol) and Hphbpy (51 mg, 0.22 mmol) to afford the product as a red powder (113 mg, 0.15 mmol, 68%). ¹H NMR (400

MHz, [D₆]acetone) δ = 10.67 (d, J = 5.4 Hz, 1H, 1), 8.82 (d, J = 8.2 Hz, 1H, 3), 8.64 (d, J = 8.1 Hz, 1H, T₃), 8.51 (dd, J = 8.2, 4.7 Hz, 2H, 8, T₅), 8.35 (d, J = 8.9 Hz, 1H, 5), 8.28 (d, J = 8.1 Hz, 1H, T_{5'}), 8.26 – 8.15 (m, 3H, 2, 6, T₆, T_{4'}), 8.11 (t, J = 7.9 Hz, 1H, T₄), 7.84 (d, J = 7.7 Hz, 1H, T_{3''}), 7.76 (d, J = 5.2 Hz, 1H, 10), 7.62 (dd, J = 8.3, 5.1 Hz, 1H, 9), 7.46 – 7.36 (m, 1H, T₅), 6.83 (t, J = 7.5 Hz, 1H, T_{4''}), 6.66 (t, J = 7.3 Hz, 1H, T_{5''}), 6.41 (d, J = 7.5 Hz, 1H, T_{6''}), 2.47 (s, 3H, CH₃), 2.35 (s, 3H, CH₃); ¹³C NMR (101 MHz, [D₆]acetone) δ = 180.9 (C_q), 167.6 (C_q), 157.2 (C_q), 157.1 (C_q), 154.3 (CH, 1), 152.4 (C_H, T_{4'}), 148.6 (C_H, 10), 147.3 (C_q), 147.2 (C_q), 145.5 (C_q), 138.8 (C_H, T₄), 137.6 (CH, T_{6''}), 137.5 (C_H, T₆), 136.0 (C_H, T₅), 134.3 (C_H, 3), 131.3 (C_q), 130.2 (C_q), 129.8 (C_H, T_{5''}), 128.5 (C_H, 5), 127.7 (C_H, T₅), 127.4 (C_H, 6), 125.6 (C_H, 2), 125.3 (CH, T_{3''}), 125.0 (C_H, 9), 124.0 (C_H, T₂), 122.3 (C_H, T_{4''}), 120.3 (C_H, 8), 119.6 (C_H, T_{5'}), 44.7 (CH₃), 43.2 (CH₃). HRMS: m/z calcd for [C₃₀H₂₅N₄ORuS – PF₆]⁺: 591.07926; found: 591.07887; elemental analysis calcd (%) for [2]PF₆: C 48.98, H 3.43, N 7.62; found: C 48.46, H 3.57, N 7.47.



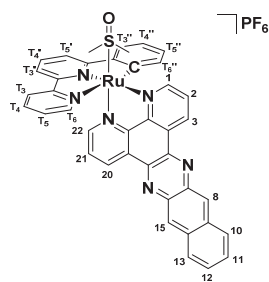
[Ru(phbpy)(dpq)(dmsO)]PF₆, [3]PF₆: The same procedure was followed as described for [6]PF₆ using [Ru(dpq)(dmsO)₂Cl₂] (115 mg, 0.210 mmol) and Hphbpy (49.0 mg, 0.220 mmol) to afford the product as a red powder (120 mg 0.150 mmol 74%). ¹H NMR (400 MHz, [D₆]acetone) δ = 10.80 (d, J = 4.3 Hz, 1H, 1), 9.66 (d, J = 6.9 Hz, 1H, 3), 9.32 – 9.22 (m, 2H, 7, 12), 9.16 (d, J = 2.1 Hz, 1H, 8),

8.64 (d, J = 8.2 Hz, 1H, T₃), 8.50 (d, J = 6.9 Hz, 1H, T_{3'}), 8.38 – 8.26 (m, 3H, 2, T_{5'}, T₆), 8.22 (t, J = 8.0 Hz, 1H, T_{4'}), 8.10 (t, J = 8.0 Hz, 1H, T₄), 7.96 – 7.82 (m, 2H, 14, T_{3''}), 7.72 – 7.57 (m, 1H, 13), 7.42 (t, J = 6.4 Hz, 1H, T₅), 6.84 (t, J = 6.8 Hz, 1H, T_{4''}), 6.68 (t, J = 6.7 Hz, 1H, T_{5''}), 6.55 (d, J = 6.3 Hz, 1H, T_{6''}), 2.48 (s, 3H, CH₃), 2.38 (s, 3H, CH₃). ¹³C NMR (101 MHz, [D₆]acetone) δ = 181.1 (C_q), 168.0 (C_q), 157.7 (C_q), 157.5 (C_q), 156.1 (CH, 1), 153.1 (C_H, T₆), 150.6 (C_H, 14), 149.2 (C_q), 147.8 (C_q), 147.7 (C_q), 147.4 (C_H, 7), 147.1 (C_H, 8), 140.8 (C_q), 140.1 (C_q), 139.5 (CH, T₄), 138.3 (CH, T_{4'}), 138.3 (C_H, T_{6''}), 132.8 (C_H, 12), 131.2 (C_H, 3), 130.7 (C_q), 130.5 (C_H, T_{5''}), 129.3 (C_q), 128.3 (C_H, T₅), 127.0 (C_H, 2), 126.6 (C_H, 13), 126.0 (C_H, T_{3''}), 124.7 (C_H, T₃), 123.0 (C_H, T_{4''}), 121.0 (C_H, T_{3'}), 120.3 (C_H, T_{5'}), 45.1 (CH₃), 43.7 (CH₃). ESI-MS: m/z calcd for [C₃₂H₂₅N₆ORuS – PF₆]⁺: 643.1; found: 643.1; elemental analysis calcd (%) for [3]PF₆·4H₂O: C 44.71, H 3.87, N 9.78; found: C 43.90, H 3.48, N 9.40.



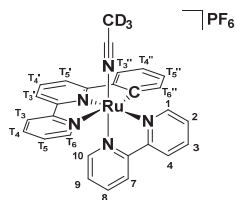
[Ru(phbpy)(dppz)(dmsO)]PF₆, [4]PF₆: The same procedure was followed as described for [6]PF₆ using [Ru(dppz)(dmsO)₂Cl₂] (160 mg, 0.26 mmol) and Hphbpy (60 mg, 0.26 mmol) to afford the product as a dark red powder (161 mg, 0.190 mmol, 73%). A racemic mixture was obtained but only one enantiomer is shown. ¹H NMR (400 MHz, [D₆]acetone) δ = 10.79 (d, J = 6.3 Hz, 1H, 1), 9.75 (d, J = 8.1 Hz, 1H, 3), 9.37 (d, J = 8.1 Hz, 1H, 16), 8.67 (d, J = 8.1 Hz, 1H, T₃), 8.53 (d, J = 7.9 Hz, 1H, 8), 8.48 (d, J = 8.3 Hz, 1H, T_{3'}), 8.41 – 8.29 (m,

4H, 7, 2, T₅', T₆), 8.24 (t, *J* = 8.1 Hz, 1H, T₄'), 8.20 – 8.08 (m, 3H, T₄, 9, 10), 7.87 (dd, *J* = 14.5, 6.9 Hz, 2H, 18, T₃'), 7.68 (t, *J* = 7.1 Hz, 1H, 17), 7.46 (t, *J* = 6.8 Hz, 1H, T₅), 6.88 (t, *J* = 7.5 Hz, 1H, T₄'), 6.74 (t, *J* = 7.4 Hz, 1H, T₅'), 6.66 (d, *J* = 7.5 Hz, 1H, T₆'), 2.50 (s, 3H, CH₃), 2.39 (s, 3H, CH₃). ¹³C NMR (101 MHz, [D₆]acetone) δ = 180.3 (C_q), 167.2 (C_q), 156.8 (C_q), 156.8 (C_q), 155.4 (C_H, 1), 152.3 (C_H, T₆), 149.9 (C_H, 18), 149.4 (C_q), 148.0 (C_q), 147.1 (C_q), 142.6 (C_q), 142.4 (C_q), 140.1 (C_q), 139.5 (C_q), 138.7 (C_H, T₄), 137.7 (C_H, T₄'), 137.4 (C_H, T₆'), 132.2 (C_H, 16), 132.1 (C_H, 10), 132.1 (C_H, 11), 130.7 (C_H, 3), 130.3 (C_q), 129.8 (C_H, T₅'), 129.6 (C_H, 8), 129.5 (C_H, 9), 128.9 (C_q), 127.5 (CH, T₄), 126.3 (C_H, 2), 125.9 (C_H, 17), 125.2 (C_H, T₃'), 123.9 (C_H, T₂), 122.3 (C_H, 8), 120.2 (C_H, T₃'), 119.6 (C_H, 2), 44.3 (CH₃), 42.9 (CH₃). HRMS: *m/z* calcd for [C₃₆H₂₇N₆ORuS – PF₆]⁺: 693.10105; found: 693.10113; elemental analysis calcd (%) for [4]PF₆: C 51.61, H 3.25, N 10.03; found: C 48.86, H 3.52, N 9.05.



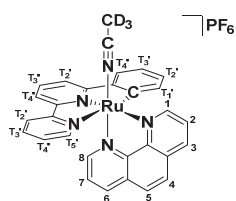
[Ru(phbpy)(dppn)(dmsO)]PF₆, [5]PF₆: The same procedure was followed as described for [6]PF₆ using [Ru(dppn)(dmsO)₂Cl₂] (100 mg, 0.15 mmol) and Hphbpy (35 mg, 0.15 mmol) to afford the product as a dark red powder (88 mg 0.10 mmol 65%). A racemic mixture was obtained but only one enantiomer is shown. ¹H NMR (500 MHz, [D₆]acetone) δ = 10.80 (d, *J* = 5.5 Hz, 1H, 1), 9.53 (d, *J* = 8.0 Hz, 1H, 3), 9.00 (d, *J* = 8.0 Hz, 1H, 20), 8.87 (s, 1H, 3), 8.71 (s, 1H, 15), 8.68 (d, *J* = 8.2 Hz, 1H, T₃), 8.54

(d, *J* = 8.0 Hz, 1H, T₃'), 8.37 (d, *J* = 7.4 Hz, 2H, T₅', T₆), 8.35 – 8.23 (m, 3H, 2, 10, T₄'), 8.14 (t, *J* = 7.9 Hz, 1H, T₄), 8.05 (d, *J* = 8.5 Hz, 1H, 13), 7.97 (d, *J* = 7.7 Hz, 1H, 3), 7.72 (d, *J* = 5.5 Hz, 1H, 22), 7.67 (t, *J* = 7.4 Hz, 1H, 12), 7.64 – 7.58 (m, 1H, 11), 7.51 – 7.44 (m, 1H, T₅), 7.38 (dd, *J* = 8.0, 5.4 Hz, 1H, 21), 6.95 (t, *J* = 7.3 Hz, 1H, T₄'), 6.87 (dt, *J* = 14.3, 7.3 Hz, 2H, T₆'), T₅'), 2.52 (s, 3H, CH₃), 2.41 (s, 3H, CH₃). ¹³C NMR (126 MHz, [D-6]acetone) δ 181.3 (C_q), 168.2 (C_q), 157.8 (C_q), 157.8 (C_q), 156.5 (C_H, 1), 153.3 (C_H, 21), 150.9 (C_q), 150.8 (C_H, 22), 149.5 (C_q), 148.1 (C_q), 141.9 (C_q), 141.3 (C_q), 139.7 (C_H, T₄), 139.3 (C_q), 139.3 (C_q), 138.9 (C_H, T₆'), 138.4 (C_H, 1), 135.9 (C_q), 135.8 (C_q), 133.0 (C_H, 20), 131.8 (C_H, 3), 131.6 (C_q), 130.9 (C_H, T₅'), 130.1 (C_q), 129.6 (C_H, 10), 129.6 (C_H, 13), 129.0 (C_H, 8), 129.0 (C_H, 15), 128.8 (C_H, 12), 128.7 (C_H, 11), 128.5 (C_H, T₅), 127.3 (C_H, 2), 126.8 (C_H, 21), 126.3 (C_H, T₃'), 124.9 (C_H, T₃), 123.4 (C_H, T₄'), 121.2 (C_H, T₃'), 120.6 (C_H, T₅'), 45.2 (CH₃), 43.9 (CH₃). HRMS: *m/z* calcd for [C₄₀H₂₉N₆ORuS – PF₆]⁺: 743.11670; found: 743.11680; elemental analysis calcd (%) for [5]PF₆: C 54.12, H 3.29, N 9.47; found: C 52.67, H 3.82, N 8.78.

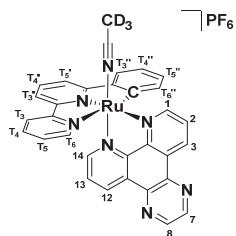


[Ru(phbpy)(bpy)(CD₃CN)]PF₆ [6]PF₆: [1]PF₆ (3.0 mg, 4.0 μmol) was dissolved in 0.6 mL deoxygenated CD₃CN and irradiated for 7 h at 1 cm from a Xenon Arc (1000 W) lamp fitted with IR (> 700 nm) and UV-cutoff (< 400 nm) filter at 298 K, while maintaining the temperature at 25 °C. After completion of the reaction, the sample was concentrated *in vacuo* to afford the title compound as a dark

purple solid (2.7 mg, 4.0 μmol , quant.). ^1H NMR (500 MHz, $[\text{D}_3]$ acetonitrile) δ = 9.55 (d, J = 5.8 Hz, 1H, 1), 8.40 (d, J = 8.2 Hz, 1H, 4), 8.33 (d, J = 8.1 Hz, 1H, T_3), 8.18 (d, J = 8.1 Hz, 1H, T_3'), 8.14 (d, J = 8.0 Hz, 1H, T_4'), 8.03 – 7.96 (m, 3H, 3, T_6), 7.95 – 7.87 (m, 2H, T_4 , T_5'), 7.74 (dd, J = 7.6, 1.4 Hz, 1H, T_3''), 7.68 (ddd, J = 7.3, 5.7, 1.4 Hz, 1H, 2), 7.58 (ddd, J = 8.2, 7.4, 1.5 Hz, 1H, 8), 7.36 (ddd, J = 5.8, 1.5, 0.8 Hz, 1H, 10), 7.32 (ddd, J = 7.5, 5.3, 1.2 Hz, 1H, T_5), 6.91 (ddd, J = 7.3, 5.8, 1.4 Hz, 1H, 9), 6.81 (td, J = 7.5, 1.3 Hz, 1H, T_4''), 6.73 (td, J = 7.3, 1.4 Hz, 1H, T_5''), 6.36 (ddd, J = 7.4, 1.4, 0.6 Hz, 1H, T_6''). ^{13}C NMR (126 MHz, $[\text{D}_3]$ acetonitrile) δ = 184.8 (C_q), 167.0 (C_q), 157.2 (C_q), 156.7 (C_q), 156.7 (C_q), 154.9 (C_q), 151.0 (C_H , 1), 150.6 (C_H , T_6), 149.6 (C_H , 10), 147.8 (C_q), 137.6 (C_H , T_4), 136.3 (C_H , T_6''), 135.0 (C_H , 1), 133.4 (C_H , 8), 132.5 (C_H , 3), 128.9 (C_H , T_5''), 126.7 (C_H , T_5), 125.9 (C_H , 2), 125.2 (C_H , 9), 124.4 (C_H , T_3''), 123.2 (C_H , 3), 122.8 (C_H , T_3), 122.2 (C_H , 7), 121.2 (C_H , T_4''), 118.7 (C_H , T_3'), 117.8 (C_H , 2). ESI-MS m/z calcd for $[\text{C}_{28}\text{H}_{22}\text{N}_5\text{Ru}_6 - \text{PF}_6]^+$: 530.1; found: 530.0.

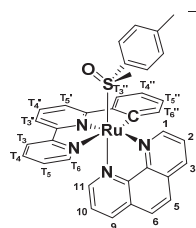


[Ru(phbpy)(phen)(CD_3CN)] PF_6 , [7] PF_6 : The same procedure was followed as described for [6] PF_6 using $[\text{Ru}(\text{phbpy})(\text{bpy})(\text{dmsO})]\text{PF}_6$ (1.9 mg, 3.0 μmol) to afford the product as a dark red solid (1.8 mg, 3.0 μmol , quant.). A racemic mixture was obtained but only one enantiomer is shown. ^1H NMR (500 MHz, $[\text{D}_3]$ acetonitrile) δ 9.91 (d, J = 4.2 Hz, 1H, 1), 8.58 (d, J = 7.0 Hz, 1H, 3), 8.37 (d, J = 7.4 Hz, 1H, T_3), 8.22 – 8.17 (m, 2H, 5, T_3'), 8.15 (d, J = 6.8 Hz, 1H, 8), 8.11 – 8.05 (m, 2H, 2, T_5'), 8.02 – 7.95 (m, 2H, 6, T_4'), 7.94 – 7.89 (m, 2H, T_4 , T_6), 7.77 (d, J = 6.4 Hz, 1H, T_3''), 7.72 (d, J = 4.1 Hz, 1H, 10), 7.30 (dd, J = 8.1, 5.4 Hz, 1H, 9), 7.23 (t, J = 7.8, 1H, T_5), 6.78 (t, J = 6.8 Hz, 1H, T_4''), 6.60 (t, J = 7.3 Hz, 1H, T_5''), 6.17 (d, J = 6.2 Hz, 1H, T_6''). ^{13}C NMR (126 MHz, $[\text{D}_3]$ acetonitrile) δ = 184.7 (C_q), 167.2 (C_q), 157.2 (C_q), 156.9 (C_q), 151.2 (C_H , 1), 150.7 (C_H , T_6), 150.1 (C_H , 10), 147.8 (C_q), 147.4 (C_q), 146.7 (C_q), 137.6 (C_H , T_4), 136.3 (C_H , T_6''), 135.1 (C_H , T_4'), 132.5 (C_H , 8), 131.5 (C_H , 3), 130.8 (C_q), 129.7 (C_q), 128.7 (C_H , T_5''), 127.7 (C_H , 5), 127.2 (C_H , 6), 126.6 (C_H , T_5), 125.2 (C_H , 2), 124.4 (C_H , T_3''), 124.1 (C_H , 9), 122.8 (C_H , T_3), 121.2 (C_H , T_4''), 118.7 (C_H , T_3'), 117.9 (C_H , 2). ESI-MS $[\text{C}_{30}\text{H}_{19}\text{D}_3\text{N}_5\text{Ru}_6 - \text{PF}_6]^+$: 559.1; found: 559.1.



[Ru(phbpy)(dpq)(CD_3CN)] PF_6 , [8] PF_6 : The same procedure was followed as described for [6] PF_6 using $[\text{Ru}(\text{dpq})(\text{dmsO})_2\text{Cl}_2]$ (2.4 mg, 3.0 μmol , quant.). A racemic mixture was obtained but only one enantiomer is shown. ^1H NMR (500 MHz, $[\text{D}_3]$ acetonitrile) δ = 9.99 (d, J = 4.2 Hz, 1H, 1), 9.47 (d, J = 8.1 Hz, 1H, 3), 9.16 (d, J = 2.1 Hz, 1H, 7), 9.08 (d, J = 2.1 Hz, 1H, 8), 9.05 (d, J = 8.0 Hz, 1H, 12), 8.36 (d, J = 8.1 Hz, 1H, T_3), 8.22 – 8.15 (m, 2H, 2, T_3), 8.07 (d, J = 7.2 Hz, 1H, T_5'), 7.99 – 7.94 (m, 2H, 1, T_6), 7.91 (ddd, J = 8.1, 7.5, 1.6 Hz, 1H, T_4), 7.82 (d, J = 6.8 Hz, 1H, 14), 7.77 (d, J = 6.4 Hz, 1H, 3), 7.39 (dd, J = 8.1, 5.5 Hz, 1H, 13), 7.22 (ddd, J = 7.5, 5.3, 1.2 Hz, 1H, T_5), 6.77 (t, J = 7.3 Hz, 1H, T_4''), 6.60 (t, J = 7.3 Hz, 1H, T_5''), 6.28 (d, J = 7.4 Hz, 1H, T_6''). ^{13}C NMR (126

MHz, [D₃]acetonitrile) δ = 184.1 (C_q), 167.0 (C_q), 157.2 (C_q), 156.8 (C_q), 152.0 (C_H, 1), 151.5 (CH, T₆), 151.3 (C_H, 14), 149.1 (C_q), 148.1 (C_q), 147.8 (C_q), 146.2 (C_H, 7), 146.0 (C_H, 8), 140.4 (C_q), 140.0 (C_q), 137.8 (C_H, T₄), 136.5 (C_H, T₆''), 135.4 (C_H, T₄'), 129.8 (C_q), 129.0 (C_H, 12), 128.8 (C_H, T₅''), 128.6 (C_q), 127.9 (C_H, 3), 126.6 (C_H, T₅), 126.0 (C_H, 2), 125.1 (C_H, 13), 124.5 (C_H, T₃''), 122.9 (C_H, T₃), 121.4 (C_H, T₄''), 118.8 (C_H, T₃'), 118.0 (C_H, T₅'). ESI-MS *m/z* calcd for [C₃₂H₂₂N₇Ru₆ – PF₆]⁺: 606.1; found: 606.1.



A and C-[Ru(phbpy)(phen)(*R*-methyl *p*-tolylsulfoxide)]PF₆, [11-A]PF₆ and [11-A]PF₆: [2]PF₆ (13.6 mg, 18.5 μ mol) was dissolved in deoxygenated MeCN (3 mL) and irradiated for 3 h in a custom built photo-cell 1 cm from a Xenon Arc (1000 W) lamp fitted with IR (>700 nm) and UV-cutoff (<410 nm) filter, while maintaining the temperature at 25 °C. After concentrating the reaction *in vacuo*, the resulting solid was redissolved in deoxygenated MeOH (10

mL), followed by the addition of (*R*)-(+)-methyl *p*-tolyl sulfoxide (10.3 mg, 66.8 μ mol). The mixture was allowed to stir at reflux for 16 h, after it was purified over a chiral HPLC (0.1% HCO₂H, 30 to 35% MeCN in H₂O, 20 min) affording both [11-C]PF₆ (*R_f* = 12.184 min, 0.8 mg, 0.99 μ mol, 5%) and [11-A]PF₆ (*R_f* = 12.984 min, 0.5 mg, 0.62 μ mol, 3%) as their respective diastereomers, [11-A]PF₆: ¹H NMR (850 MHz, [D₃]acetonitrile) δ = 10.75 (d, *J* = 5.3 Hz, 1H, 1), 8.67 (d, *J* = 8.2 Hz, 1H, 3), 8.32 (d, *J* = 7.9 Hz, 1H, T₂'), 8.20 (d, *J* = 8.8 Hz, 1H, 5), 8.16 (dd, *J* = 8.2, 5.2 Hz, 1H, 2), 8.03 (d, *J* = 8.8 Hz, 1H, 6), 8.00 (d, *J* = 8.1 Hz, 1H, 11), 7.89 – 7.86 (m, 2H, 10, T₅), 7.84 (d, *J* = 5.3 Hz, 1H, T₂), 7.80 – 7.75 (m, 2H, T₄'', T₄), 7.72 (d, *J* = 8.0 Hz, 1H, 9), 7.47 (d, *J* = 5.4 Hz, 1H, T₄'), 7.40 (dd, *J* = 8.1, 5.2 Hz, 1H, T₃'), 7.14 (dd, *J* = 7.3, 5.4 Hz, 1H, T₃), 6.89 (t, *J* = 7.3 Hz, 1H, T₃''), 6.81 (d, *J* = 8.1 Hz, 2H, 2 x CH *m*-tolyl), 6.71 (t, *J* = 7.2 Hz, 1H, T₂''), 6.44 (d, *J* = 7.5 Hz, 1H, T₁''), 6.43 (d, *J* = 12.9, 7.8 Hz, 2H, 2 x CH *o*-tolyl), 2.77 (s, 3H). ESI-MS *m/z* calcd for [C₃₆H₂₉N₄ORuS – PF₆]⁺: 667.1; found: 667.1.

5.5.3 Photochemistry

5.5.3.1 Photosubstitution quantum yield

3.00 mL of [1]PF₆ (6.83 x 10⁻⁵ M), [2]PF₆ (4.10 x 10⁻⁵ M), [3]PF₆ (4.10 x 10⁻⁵ M) or [9](PF₆)₂ (6.52 x 10⁻⁵ M) in acetonitrile was transferred to a 1 cm wide quartz fluorescence cuvette with stirring bar and deoxygenated for 15 minutes with dinitrogen after which it was irradiated with a Roithner LaserTechnik H2A1-H450 LED (λ_{exc} 450 nm, FWHM 35 nm) with photon flux Φ = 1.86 · mol photons · s⁻¹ (or Φ = 1.86 · mol photons · s⁻¹ for [9](PF₆)₂) while the solution was kept at constant temperature (25 °C). During this period UV-vis spectra were recorded on a Varian Inc. Cary 50 UV-vis spectrometer with an interval of 10 minutes for 24 h and ESI-MS spectra were recorded after the irradiation experiment to confirm the formation of the solvent species [Ru(phbpy)(N-N)(MeCN)]⁺. Photosubstitution quantum yields were determined as described earlier.^[36]

5.5.3.2 NMR irradiation experiments

^1H NMR irradiation experiments were carried out as follows: 2.0 mg of either [1]PF₆, [2]PF₆ or [3]PF₆ were dissolved in 0.6 mL [D₃]acetonitrile and irradiated 1 cm from a Xenon-Arc 1000 W fitted with IR (>700 nm) and UV-cutoff (<410 nm) filters, while maintaining the temperature at 25 °C during the irradiation period spectra were recorded every h on a Bruker AV-400 until completion.

5.5.3.3 Singlet oxygen quantum yield

Singlet oxygen measurements were carried out as described in the appendix (II.1).

5.5.4 Electrochemistry

Cyclic voltammetry experiments were performed using a cell with a platinum working electrode, a silver wire as pseudo-reference electrode, and a platinum wire as auxiliary electrode. 0.1 M Bu₄NPF₆ in MeCN was used as the supporting electrolyte. 1 mM solutions of each complex were purged with argon prior to the experiment, and was measured at room temperature using Autolab PGSTAT10 and GPES 4.9 by Eco Chemie. Each experiment was calibrated against ferrocene with a scan rate of 100 mV s⁻¹. For [4]PF₆, [6]PF₆, [7]PF₆, [8]PF₆ a scan rate of 200 mV s⁻¹ was used.

5.5.5 DNA-interactions

Agarose gel electrophoresis was carried out as described in appendix II.2.2 according to the following table for compound [1]PF₆ – [3]PF₆:

Lane	Description	Time of irradiation (min)	Light dose (Jcm ⁻²)
1	λ MW marker	0	0
2	DNA control, 37 °C, dark	0	0
3	DNA control, 37 °C, irradiated	15	22.5
4	5:1 BP:MC, 37 °C, dark	0	0
5	5:1 BP:MC, 37 °C, irradiated 1 min	1	1.5
6	5:1 BP:MC, 37 °C, irradiated 3 min	3	4.5
7	5:1 BP:MC, 37 °C, irradiated 5 min	5	7.5
8	5:1 BP:MC, 37 °C, irradiated 10 min	10	15
9	5:1 BP:MC, 37 °C, irradiated 15 min	15	22.5
10	λ MW marker	0	0

For compound [5]PF₆ the following table was used:

Lane	BP:MC
1	Cisplatin control
2	DNA control
3	5
4	10
5	15
6	25
7	50
8	100
9	λ MW marker

5.5.6 Cytotoxicity Assay

The cytotoxicity assay was carried out as described in appendix II.2.1 with the following modifications: Compounds [1]PF₆ – [3]PF₆ were directly diluted in OptiMEM medium. For compounds [4]PF₆ and [5]PF₆ DMSO needed to be added, but final DMSO concentrations did not exceed 0.5%. Compounds [1]PF₆ – [3]PF₆ were irradiated for 10 minutes with green light (520 ± 38 nm, 25.0 ± 1.9 mW cm⁻², 10 minutes, $15 \cdot \pm 1.2$ J cm⁻²).

5.5.7 Circular Dichroism

Measurements were performed on a BioLogic Science Instruments MOS-500 Circular Dichroism Spectrometer, using stock solutions of 4.9×10^{-5} M for both [11-A] and [11-C] in acetonitrile.

References

- [1] a). B. S. Murray, M. V. Babak, C. G. Hartinger, P. J. Dyson, *Coord Chem Rev* **2016**, *306*, 86-114; b). S. J. Dougan, P. J. Sadler, *Chimia* **2007**, *61*, 704-715.
- [2] B. Pena, A. David, C. Pavani, M. S. Baptista, J. P. Pellois, C. Turro, K. R. Dunbar, *Organometallics* **2014**, *33*, 1100-1103.
- [3] C. Mari, V. Pierroz, R. Rubbiani, M. Patra, J. Hess, B. Spingler, L. Oehninger, J. Schur, I. Ott, L. Salassa, S. Ferrari, G. Gasser, *Chem Eur J* **2014**, *20*, 14421-14436.
- [4] E. Wachter, D. K. Heidary, B. S. Howerton, S. Parkin, E. C. Glazer, *Chem Commun* **2012**, *48*, 9649-9651.
- [5] H. Chan, J. B. Ghrayche, J. Wei, A. K. Renfrew, *Eur J Inorg Chem* **2017**, *2017*, 1679-1686.
- [6] B. A. Albani, B. Pena, N. A. Leed, N. A. de Paula, C. Pavani, M. S. Baptista, K. R. Dunbar, C. Turro, *J Am Chem Soc* **2014**, *136*, 17095-17101.
- [7] J. Liu, L. N. Ji, W. J. Mei, *Prog Chem* **2004**, *16*, 969-974.
- [8] H. Y. Huang, P. Y. Zhang, H. M. Chen, L. N. Ji, H. Chao, *Chem Eur J* **2015**, *21*, 715-725.
- [9] U. Schatzschneider, J. Niesel, I. Ott, R. Gust, H. Alborzina, S. Wolf, *ChemMedChem* **2008**, *3*, 1104-1109.
- [10] C. Mari, V. Pierroz, S. Ferrari, G. Gasser, *Chem Sci* **2015**, *6*, 2660-2686.
- [11] T. Funaki, M. Yanagida, N. Onozawa-Komatsuzaki, K. Kasuga, Y. Kawanishi, M. Kurashige, K. Sayama, H. Sugihara, *Inorg Chem Commun* **2009**, *12*, 842-845.
- [12] A. M. Palmer, B. Pena, R. B. Sears, O. Chen, M. El Ojaimi, R. P. Thummel, K. R. Dunbar, C. Turro, *Philos T R Soc A* **2013**, *371*, 20120135.
- [13] A. D. Ryabov, R. Le Lagadec, H. Estevez, R. A. Toscano, S. Hernandez, L. Alexandrova, V. S. Kurova, A. Fischer, C. Sirlin, M. Pfeffer, *Inorg Chem* **2005**, *44*, 1626-1634.
- [14] S. Bonnet, J. P. Collin, N. Gruber, J. P. Sauvage, E. R. Schofield, *Dalton Trans* **2003**, 4654-4662.
- [15] J. J. Rack, J. R. Winkler, H. B. Gray, *J Am Chem Soc* **2001**, *123*, 2432-2433.

- [16] B. A. Albani, B. Pena, K. R. Dunbar, C. Turro, *Photobiol Sci* **2014**, *13*, 272-280.
- [17] F. Barigelletti, B. Ventura, J. P. Collin, R. Kayhanian, P. Gavina, J. P. Sauvage, *Eur J Inorg Chem* **2000**, 113-119.
- [18] J. P. Collin, M. Beley, J. P. Sauvage, F. Barigelletti, *Inorg Chim Acta* **1991**, *186*, 91-93.
- [19] a). L. N. Lameijer, S. L. Hopkins, T. G. Breve, S. H. Askes, S. Bonnet, *Chem Eur J* **2016**, *22*, 18484-18491; b). J. D. Knoll, B. A. Albani, C. B. Durr, C. Turro, *J Phys Chem A* **2014**, *118*, 10603-10610.
- [20] R. E. Goldbach, I. Rodriguez-Garcia, J. H. van Lenthe, M. A. Siegler, S. Bonnet, *Chem Eur J* **2011**, *17*, 9924-9929.
- [21] H. J. Jang, S. L. Hopkins, M. A. Siegler, S. Bonnet, *Dalton Trans* **2017**, *46*, 9969-9980.
- [22] J. J. Rack, A. A. Rachford, A. M. Shelker, *Inorg Chem* **2003**, *42*, 7357-7359.
- [23] S. P. Foxon, C. Metcalfe, H. Adams, M. Webb, J. A. Thomas, *Inorg Chem* **2007**, *46*, 409-416.
- [24] T. A. White, S. Maji, S. Ott, *Dalton Trans* **2014**, *43*, 15028-15037.
- [25] J. D. Knoll, B. A. Albani, C. Turro, *Acc Chem Res* **2015**, *48*, 2280-2287.
- [26] B. Laleu, P. Mobian, C. Herse, B. W. Laursen, G. Hopfgartner, G. Bernardinelli, J. Lacour, *Angew Chem Int Ed* **2005**, *44*, 1879-1883.
- [27] A. J. Gottle, F. Alary, M. Boggio-Pasqua, I. M. Dixon, J. L. Heully, A. Bahreman, S. H. Askes, S. Bonnet, *Inorg Chem* **2016**, *55*, 4448-4456.
- [28] V. Vichai, K. Kirtikara, *Nat Protocols* **2006**, *1*, 1112-1116.
- [29] L. Fetzter, B. Boff, M. Ali, M. Xiangjun, J. P. Collin, C. Sirlin, C. Gaiddon, M. Pfeffer, *Dalton Trans* **2011**, *40*, 8869-8878.
- [30] a). V. Pierroz, R. Rubbiani, C. Gentili, M. Patra, C. Mari, G. Gasser, S. Ferrari, *Chem Sci* **2016**, *7*, 6115-6124; b). H. Song, J. T. Kaiser, J. K. Barton, *Nat Chem* **2012**, *4*, 615-620; c). Y. Sun, L. E. Joyce, N. M. Dickson, C. Turro, *Chem Commun* **2010**, *46*, 2426-2428; d). H. Huang, P. Zhang, B. Yu, Y. Chen, J. Wang, L. Ji, H. Chao, *J Med Chem* **2014**, *57*, 8971-8983.
- [31] E. B. van der Tol, H. J. van Ramesdonk, J. W. Verhoeven, F. J. Steemers, E. G. Kerver, W. Verboom, D. N. Reinhoudt, *Chem Eur J* **1998**, *4*, 2315-2323.
- [32] Z. Molphy, A. Prisecaru, C. Slator, N. Barron, M. McCann, J. Colleran, D. Chandran, N. Gathergood, A. Kellett, *Inorg Chem* **2014**, *53*, 5392-5404.
- [33] E. C. Constable, R. P. Henney, T. A. Leese, D. A. Tocher, *Dalton Trans* **1990**, 443-449.
- [34] M. L. Bode, P. J. Gates, S. Y. Gebretnsae, R. Vleggaar, *Tetrahedron* **2010**, *66*, 2026-2036.
- [35] I. P. Evans, A. Spencer, W. G., *J Chem Soc Dalton* **1973**, 204-209.
- [36] A. Bahreman, J. A. Cuello-Garibo, S. Bonnet, *Dalton Trans* **2014**, *43*, 4494-4505.

Chapter 6:

Efficient red light-activation of a NAMPT inhibitor under hypoxia using water-soluble ruthenium complexes

Abstract: Two water-soluble ruthenium complexes [1]Cl₂ and [2]Cl₂ are described that release a cytotoxic nicotinamide phosphoribosyltransferase (NAMPT) inhibitor upon irradiation with a low dose (21 J cm⁻²) of red light. Up to an 18-fold increase in inhibition of NAMPT activity was measured upon red-light activation of [2]Cl₂, while no differences between activity in the dark and after irradiation were observed for [1]Cl₂. For the first time the dark and red light-induced cytotoxicity of these photocaged compounds could be tested on cells grown under hypoxic conditions (1% O₂). In skin (A431) and lung (A549) cancer cells a 3- to 4-fold increase in cytotoxicity was found upon red light irradiation for [2]Cl₂, when the cells were cultured and irradiated under normoxic conditions (21% O₂) or hypoxic conditions (1.0%). These results demonstrate the potential of photoactivated chemotherapy for hypoxic cancer cells where classical photodynamic therapy, which relies on oxygen activation, is poorly efficient.

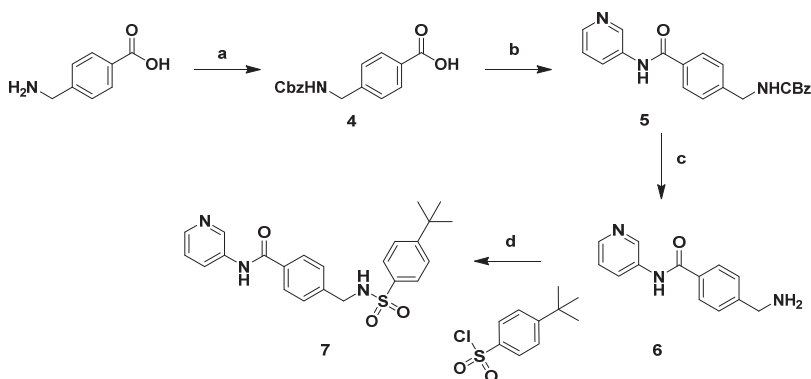
This work has been published as a communication: L. N. Lameijer, D. Ernst, S. L. Hopkins, M. S. Meijer, S. H. C. Askes, S. E. Le Devedec, S. Bonnet, *Angew Chem Int Ed* **2017**, *56*, 11549-11553.

6.1 Introduction

Nicotinamide phosphoribosyltransferase (NAMPT) is a key enzyme in the salvage pathway of nicotinamide adenine dinucleotide (NAD⁺) biosynthesis that is abnormally up regulated in cancer cells.^[1] Importantly, high NAMPT expression in different types of cancer has been associated with poor prognosis in cancer patients, which makes NAMPT a potential therapeutic target.^[2] It has been shown that NAMPT inhibition leads to reduction of intracellular NAD⁺ levels, which can induce apoptosis in cancer cells.^[2a, 3] However, it has also been reported that targeting of NAMPT might lead to side effects such as blindness.^[4] A strategy called PhotoActivated ChemoTherapy (PACT) might solve selectivity issues.^[5] PACT consists in hiding the toxicity of the compound with a caging agent that is released upon irradiation with light together with the free drug.^[5b, 6] Ruthenium polypyridyl complexes are particularly promising photocaging groups as they can be activated using visible light,^[7] whereas most organic caging groups require UV light for activation.^[8] Unlike photodynamic therapy (PDT), a clinically approved therapy that relies on the photocatalytic activation of ³O₂ into ¹O₂ by a photosensitizer,^[9] PACT is oxygen independent^[5b, 9] which makes it a promising and complementary therapeutic strategy for targeting hypoxic tumors. However, proof of efficacy of PACT under hypoxia is still lacking. Herein we describe a setup that can shine monochromatic red light on living cells under hypoxia (1%), allowing the study of PACT compounds [1]Cl₂ and [2]Cl₂ (Scheme 6.2). Red light is superior to previously reported blue- or green-light activation of PACT compounds due to deeper tissue penetration (0.5-1.0 cm),^[10] and can be used with higher doses without significant light-induced cytotoxicity.^[11] Two sterically hindered ruthenium photocaging scaffolds were chosen based upon earlier work by the groups of Turro and Kodanko:^[12] [Ru(tpy)(dmbpy)(L)]²⁺ (tpy = 2,2',6'-2"-terpyridine; dmbpy = 6,6'-dimethyl-2,2'-bipyridine) and [Ru(tpy)(biq)(L)]²⁺ (biq = 2,2'-biquinoline). Both types of complexes have an absorption band that extends in the red region of the phototherapeutic window,^[13] and photodissociate their ligand when the monodentate ligand L is a thioether or a pyridine moiety.^[12a, 14] These scaffold were used to cage STF-31, a known cytotoxic organic compound containing a pyridine moiety, for which the toxicity was reported to originate from inhibition of both NAMPT enzyme activity^[15] and glucose transporter 1 (GLUT1).^[16] We synthesized the two STF-31-containing compounds [1]Cl₂ and [2]Cl₂ (Scheme 6.2), demonstrated that red light can release STF-31, and show that photorelease leads to efficient PACT under both normoxic (21% O₂), and hypoxic (1% O₂) conditions.

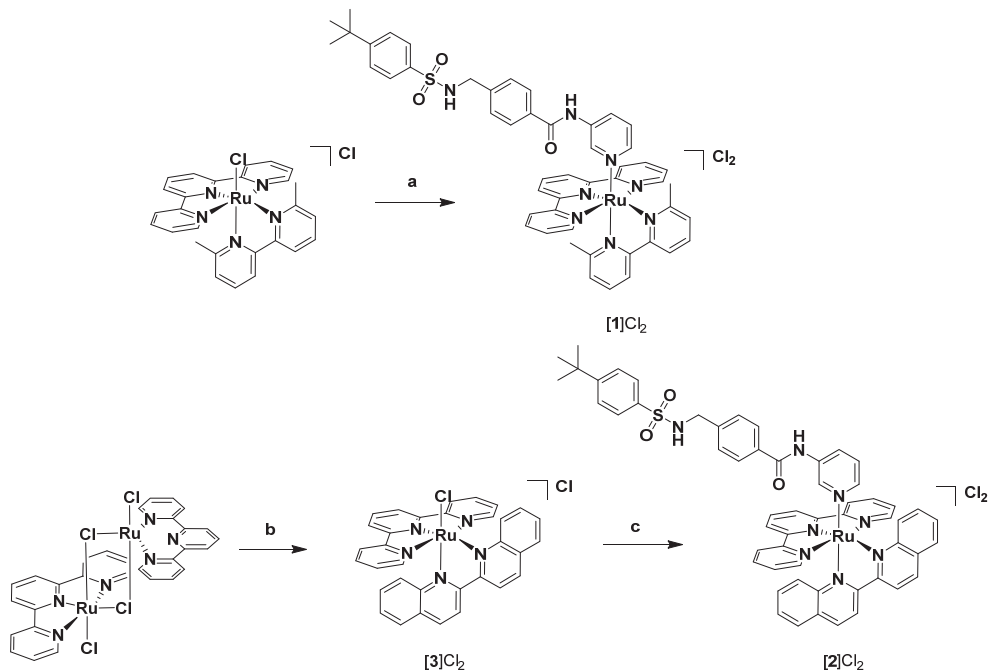
6.2 Results and discussion

STF-31 was synthesized according to a reported procedure^[16b] using *t*-butylphenylsulfonyl chloride in the last step to install the *t*-butyl moiety (Scheme 6.1).



Scheme 6.1. a). Cbz-Cl in water/dioxane/aq. NaHCO₃, 16 h, rt, 83%; b). i). cat. DMF, 1.65 eq. (COCl)₂ in THF, 5 h, rt – 50 °C ii). 1.06 eq. 3-aminopyridine in pyridine, 16 h, rt, 81%; c). 33% HBr in AcOH, 3 h, rt, 98%; d). 4-(*t*-butyl)benzenesulfonyl chloride in MeCN/pyridine, 16 h, rt, 54%.

Compounds [1]Cl₂ and [2]Cl₂ were then synthesized by reacting STF-31 with the precursors [Ru(tpy)(dmbpy)(Cl)]Cl^[14] and [Ru(tpy)(biq)(Cl)]Cl, respectively (Scheme 6.2). The latter precursor was synthesized in high yield (90%), starting from ruthenium dimer [{Ru(tpy)Cl₂}]₂·H₂O.^[17] Both caged inhibitors were isolated as PF₆ salts, purified over Sephadex LH-20 and converted to their chloride salt by salt metathesis, to afford [1]Cl₂ and [2]Cl₂ as red or purple solids in 50% and 44% yield, respectively.



Scheme 6.2. a). i). STF-31 (2.0 eq.), AgPF₆ (2.2 eq.) in acetone/H₂O (2:1), 50 °C, 2 h ii). NBu₄Cl in acetone, 44%; b). biq (1.0 eq.) in (CH₂OH)₂, 1 hr, 180 °C, 90%; c). i). STF-31 (1.2 eq.), AgPF₆ (2.1 eq.) in EtOH/H₂O (2:1), 80 °C, 4 h; ii). NBu₄Cl in acetone, 50%

One of the challenges in PACT is to find the ideal balance between thermal stability and photoactivation efficiency, expressed as the photosubstitution quantum yield (Φ_p). Previous research has shown that $[\text{Ru}(\text{tpy})(\text{dmbpy})(\text{SRR}')^{2+}]$ complexes are less stable and more photoreactive than the corresponding $[\text{Ru}(\text{tpy})(\text{biq})(\text{SRR}')^{2+}]$ compounds in water,^[18] therefore preventing their application in PACT.^[19] In contrast, Turro et al. have demonstrated that complexes with L=pyridine are stable enough to be isolated while retaining photosubstitution properties under low-energy visible light ($\lambda_{\text{irr}} > 590 \text{ nm}$).^[12b] The photoreactivity of $[\mathbf{1}]\text{Cl}_2$ and $[\mathbf{2}]\text{Cl}_2$ in water was tested under red light irradiation. Figure 6.1 shows the evolution of the electronic absorption spectrum of $[\mathbf{1}]^{2+}$ upon activation at 625 nm under deoxygenated conditions in H_2O . The initial metal-to-ligand charge transfer ($^1\text{MLCT}$) band at 473 nm was gradually replaced by a new $^1\text{MLCT}$ band at 484 nm with a clear isosbestic point at 477 nm, due to the formation of $[\text{Ru}(\text{tpy})(\text{dmbpy})(\text{H}_2\text{O})]^{2+}$ (m/z found 536.1, calc m/z 536.1 for $[\text{Ru}(\text{tpy})(\text{dmbpy})(\text{OH})]^+$).

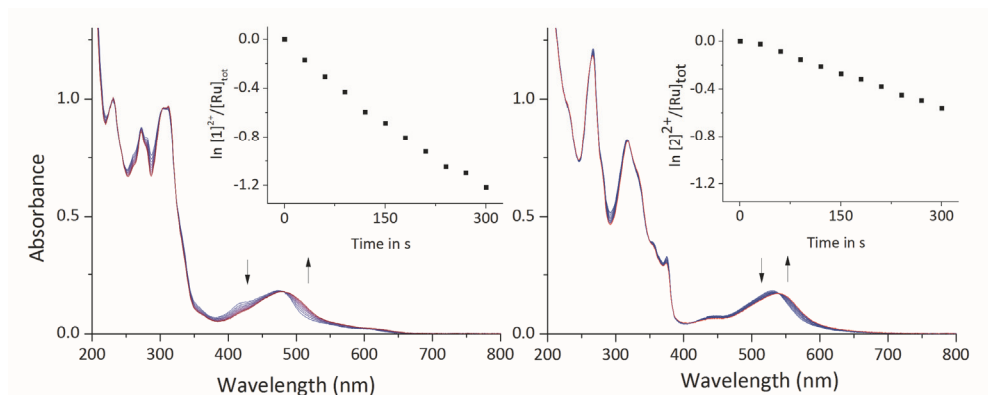


Figure 6.1. UV-vis spectra of $[\mathbf{1}]\text{Cl}_2$ (left) and $[\mathbf{2}]\text{Cl}_2$ (right) in deoxygenated H_2O under red light irradiation (625 nm, photon flux $1.30 \times 10^{-7} \text{ mol}\cdot\text{s}^{-1}$). Spectra were taken for 5 min each 30 s. $T = 298 \text{ K}$.

In a parallel experiment using ^1H NMR spectroscopy a solution of $[\mathbf{1}]\text{Cl}_2$ in D_2O was irradiated using white light ($> 610 \text{ nm}$). During irradiation the doublet of at 6.89 ppm was replaced by two doublets at 6.80 and 7.78 ppm, while the characteristic ^tBu singlet at 0.94 ppm disappeared, confirming photodissociation of STF-31 (Figure S.V.1). The photosubstitution quantum yields (Φ_{625}) were determined to be 0.057 at rt and 0.080 at 37 °C. Where the higher quantum yield for photosubstitution at increased temperature is consistent with thermal population of the triplet metal-centred states (^3MC) via the photochemically generated $^3\text{MLCT}$ states.^[12b] For $[\mathbf{2}]\text{Cl}_2$, irradiation at 625 nm resulted in a shift of the MLCT band at 531 nm to 549 nm, and the formation of the photoproduct $[\text{Ru}(\text{tpy})(\text{biq})(\text{H}_2\text{O})]^{2+}$ (found $m/z = 607.8$, calcd $m/z = 608.1$ for $[\text{Ru}(\text{tpy})(\text{biq})(\text{OH})]^+$). When a solution of $[\mathbf{2}]\text{Cl}_2$ in D_2O was irradiated using white light ($>610 \text{ nm}$) the ^1H NMR spectrum (Figure S.V.2) showed a new, distinctive quartet at 8.86 ppm, and a decrease of the doublet at 6.69 ppm and singlet at 0.90 ppm. Photosubstitution occurred with a quantum

yield Φ_{625} of 0.013 and 0.019 at rt and 37 °C, respectively (Table 6.1). The lower photoreactivity of [2]Cl₂ compared to [1]Cl₂ is consistent with previous work.^[12b] Both [1]Cl₂ (log P_{ow} = -0.63 ± 0.04) and [2]Cl₂ (log P_{ow} = -0.08 ± 0.04) are water-soluble, but STF-31 is not (log P_{ow} = +3.92), resulting in ligand precipitation during photosubstitution of STF-31 in the NMR tube. Hence the caging Ru complexes significantly increase water solubility of the inhibitor.

Table 6.1. Absorption maxima (λ_{\max}), molar absorption coefficients at λ_{\max} (ϵ) and at 625 nm (ϵ_{625}), photosubstitution quantum yields (Φ_{625}) at 298 and 310 K in water, ¹O₂ generation quantum yields (Φ_{Δ}) at 293 K, and photosubstitution reactivity ($\xi = \Phi_{625} \cdot \epsilon_{625}$).

Complex	λ_{\max} in nm ^[a] (ϵ in M ⁻¹ cm ⁻¹)	ϵ_{625} ^[a] in M ⁻¹ cm ⁻¹	Φ_{625} ^[a] (Φ_{625} at 310 K)	Φ_{Δ} ^[b]	ξ ^[20] (ξ at 310 K)
[1]Cl ₂	473 (8.1 × 10 ³)	379	0.057 (0.080)	<0.005	2.2 (3.0)
[2]Cl ₂	531 (9.3 × 10 ³)	609	0.013 (0.019)	0.036	0.79 (1.2)

[a] in H₂O. [b] in CD₃OD.

Before testing these compounds in cancer cells the dose of red light necessary to obtain full activation in the cell irradiation setup was evaluated to be 20.6 J.cm⁻², which corresponds to 10 minutes irradiation under normoxia (Figure 6.2).^[11]

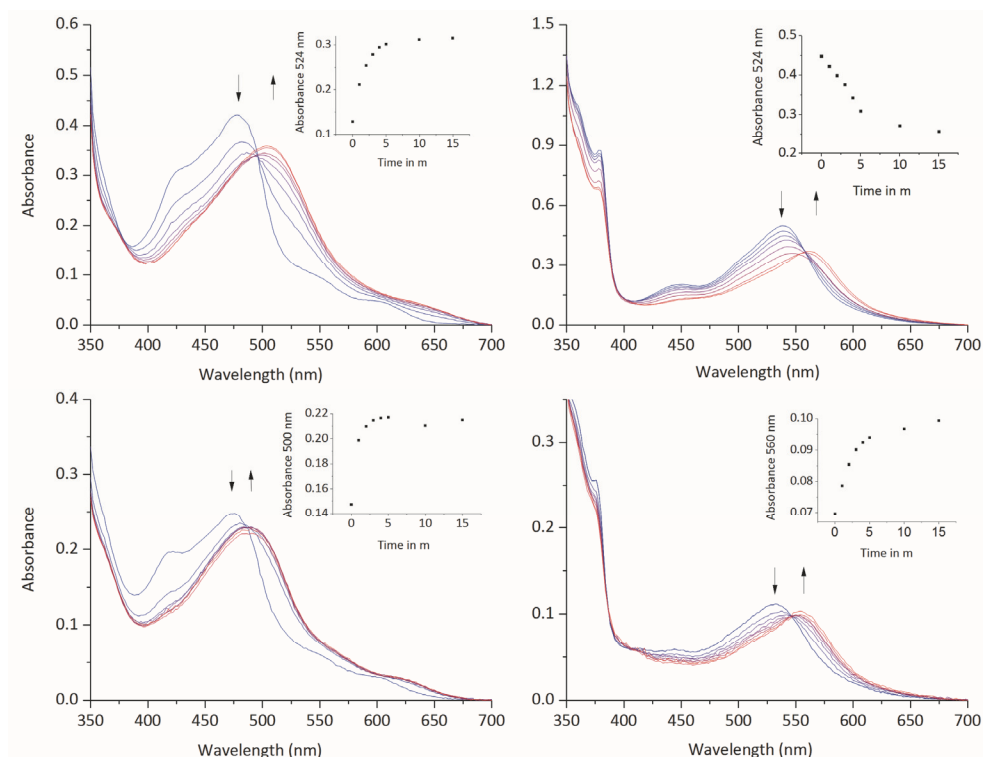


Figure 6.2. Irradiation of 1×10^{-4} M ($v = 200 \mu\text{L}$) [1]Cl₂ and [2]Cl₂ using the red light array for 15 minutes in the normoxia setup. Top left: [1]Cl₂ in DMSO. Top right: [2]Cl₂ in DMSO. Bottom left: [1]Cl₂ in OptiMEM media + 10% DMSO. Bottom right: [2]Cl₂ in OptiMEM media + 10% DMSO. Irradiations were carried out over fifteen minutes. Spectra were plotted using Origin Pro 9.1 and the baseline was subtracted.

The cytotoxicity of STF-31 and of its caged analogues [1]Cl₂ and [2]Cl₂ was first tested in normoxic conditions (21% O₂) against three human cancer cell lines (A549, MCF-7, and A431) and a non-cancerous cell-line (MRC-5).^[11] two plates were treated with STF-31, [1]Cl₂ or [2]Cl₂, and after 6 hours incubation one plate was irradiated with red light (628 nm, 20.6 J·cm⁻²) while the other was left in the dark. At t = 48 h medium was replaced. Cell viability was then assayed by using sulforhodamine B (SRB) 96 h after seeding.^[21] Cell growth inhibition effective concentrations (EC₅₀) were calculated from the dose-response curves of treated vs. non-treated wells (Figure 6.3 and Table S.V.1).

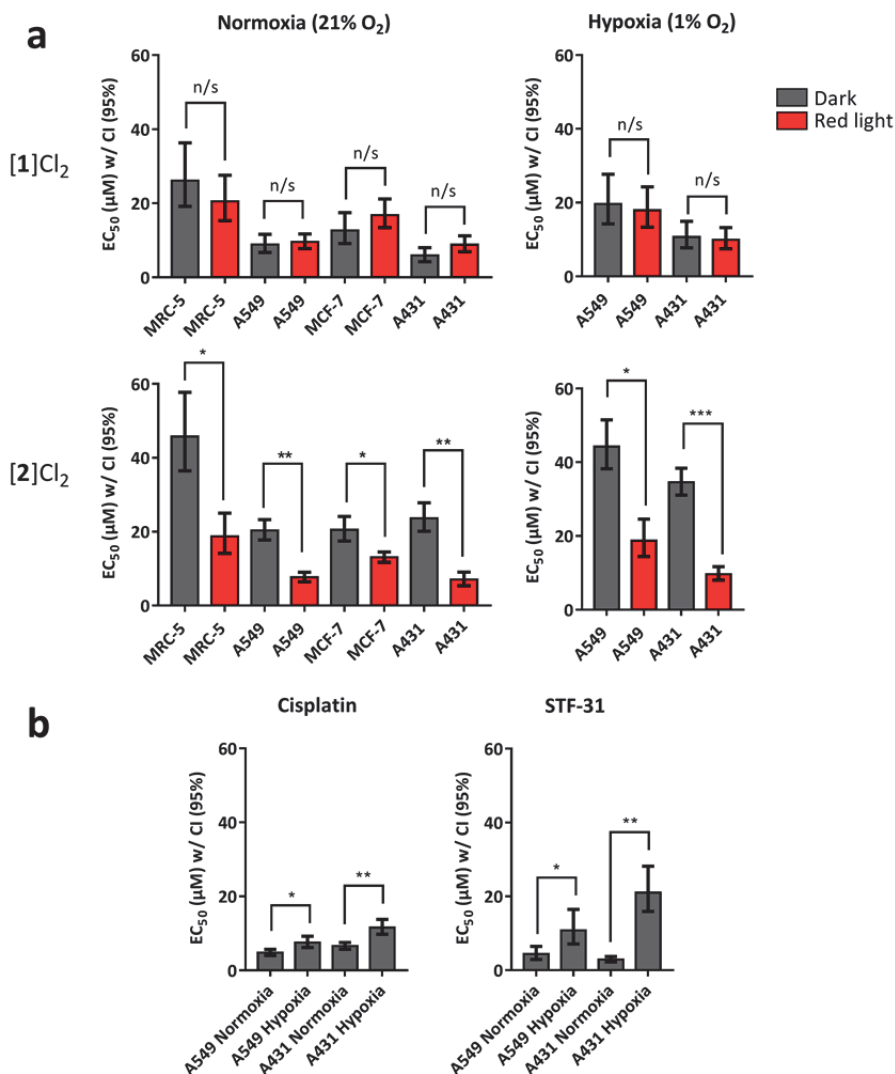


Figure 6.3. a). Cell growth inhibition effective concentrations (EC₅₀ in μM) for [1]Cl₂, [2]Cl₂ in the dark and under red light irradiation in human cancer cells under normoxia (21.0% O₂, 7.0% CO₂) and hypoxia (1.0% O₂, 7.0% CO₂). **b).** EC₅₀ for STF-31 and cisplatin under normoxia and hypoxia. Data points are the mean of three independent experiments; error bars show 95% confidence intervals (in μM). * = p < 0.05, ** ≤ 0.01, *** ≤ 0.001. n/s = Not significant. See Table S.V.1 for all EC₅₀ values.

Under normoxia (Figure 6.3a), STF-31 appeared to be highly cytotoxic in all cell lines, including MRC-5. Compound [1]Cl₂ also caused a great cytotoxic effect on all cancerous cell lines, but its effect was limited on the non-cancerous MRC-5 cell line (EC₅₀ > 20 μM). Importantly, a negligible difference was found between the irradiated and non-irradiated wells. This result was in great contrast to [2]Cl₂, which was less cytotoxic against the non-cancerous MRC-5 cells in the dark (EC₅₀ > 40 μM) and highly toxic (EC₅₀ < 10 μM) to cancerous cells after irradiation, with a marked difference in cytotoxicity between dark and irradiated cells for both A549 and A431. Considering the minimal ¹O₂ production (3.6%, Table 6.1), this effect is most likely attributed to the anti-proliferative effect of the photoreleased STF-31.

To validate whether the photocytotoxicity could be ascribed to photorelease of STF-31, instead of PDT, [1]Cl₂, [2]Cl₂, and SFT-31, were tested under hypoxia, in which ¹O₂ generation is impaired. We therefore modified our LED-based irradiation setup^[11] allowing irradiation on living cells while controlling O₂ concentrations (1 - 21%, Figure S.V.4). We then repeated the cytotoxicity assay using the same protocol and light dose of 20.6 J.cm⁻², but now at 1.0% O₂ (see Figure S.V.4, lower left). As shown in Figure 6.2 and Table S.V.1, the EC₅₀ values for all compounds were found to be higher than under normoxia, which is consistent with earlier reports on the higher resistance of hypoxic cells to chemotherapy.^[22] No photocytotoxicity was observed for [1]Cl₂. However, the photoindices found for [2]Cl₂ under hypoxia (3.6 and 2.4 for A431 and A549 respectively) were identical to those found under normoxic conditions (3.3 and 2.6 for A431 and A549 respectively), demonstrating the observed photocytotoxicity for [2]Cl₂ is independent of the O₂ concentration.

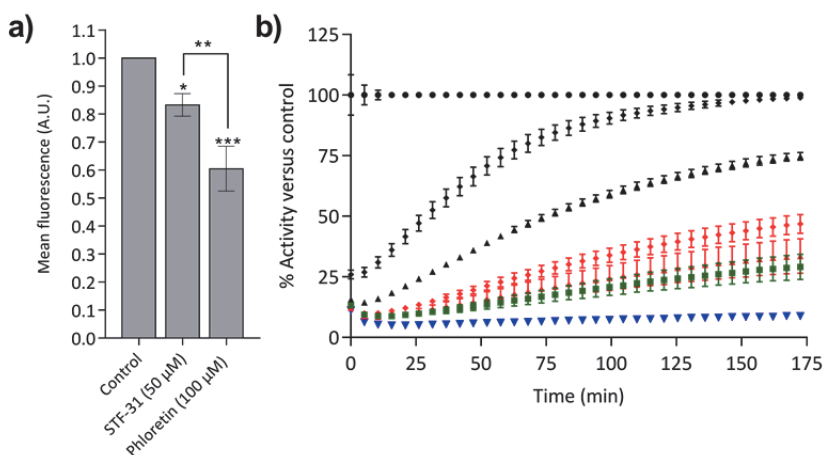


Figure 6.4. a). Normalized mean fluorescence intensity (MFI) of 2-[N-(7-nitrobenz-2-oxa-1,3-diazol-4-yl)amino]-2-deoxy-D-glucose (NBDG) in A549 cells treated with 2% DMSO, STF-31, or phloretin. Error bars are the mean of three independent experiments with \pm standard deviation (SD). * = $p \leq 0.05$, ** = $p \leq 0.01$, *** = $p \leq 0.001$. **b).** Representative plot of the percentage (%) of NAMPT activity observed for different compounds vs. control (2% DMSO) after 1 h incubation. Data points represent the mean of at least two replicates, and error bars represent standard error of the mean (SEM). • = Vehicle control, ♦ = [2]Cl₂ dark (2 μM), ▲ = [1]Cl₂ dark (2 μM), ◆ = [2]Cl₂ light (2 μM), ▲ = [1]Cl₂ light (2 μM), ■ = STF-31 (2 μM), ▼ = FK866 (20 μM).

We then investigated the enzyme inhibition properties of STF-31, which is both a reported GLUT-1 and NAMPT inhibitor.^[15a, 16a, 23] GLUT-1 overexpressing A549 cells^[24] were starved using glucose-free medium, followed by incubation of 2 h with a vehicle control (2% DMSO), 50 μM STF-31, or 100 μM phloretin, a well-known GLUT-1 inhibitor.^[25] Cells were then treated with the fluorescent D-glucose analogue NBDG,^[26] and analyzed by flow cytometry (Figure S.V.6). STF-31 showed a minimal glucose-uptake inhibition compared to phloretin.^[27] Therefore the observed cytotoxicity of STF-31 is most likely not related to impaired glucose uptake and GLUT-1 inhibition. The NAMPT enzyme activity inhibition of STF-31, [1]Cl₂, and [2]Cl₂, was therefore determined using the commercial Cyclex® assay after 1 h incubation of A549 cells with the irradiated or non-irradiated compounds (Figure 6.4b). At 2 μM concentration STF-31 showed the largest effect on NAMPT activity, confirming that it is a NAMPT inhibitor.^[15a] Use of [2]Cl₂ resulted in a dramatic reduction in NAMPT activity after red light activation, whereas the non-irradiated sample suffered much less inhibition. A similar effect was observed for [1]Cl₂, although the dark activity was found to be much higher than that of [2]Cl₂. The dark inhibitory concentrations (IC₅₀) of 4.8 μM for [2]Cl₂ was lowered by a factor 18 down to 0.26 μM after irradiation, which is similar to the value obtained for STF-31 (0.25 μM). The NAMPT inhibitory effect of STF-31 is thus fully recovered upon red-light activation of [2]Cl₂.

Table 6.2. NAMPT activity inhibitory concentration (IC₅₀ with 95% confidence intervals, in μM) obtained for STF-31, [2]Cl₂ in the dark and [2]Cl₂ after red light irradiation. Photoindex (PI) = IC_{50,dark}/IC_{50,light}.

STF-31		[2]Cl ₂			
IC ₅₀ in μM (Dark)	CI	IC ₅₀ in μM (Dark)	CI	IC ₅₀ in μM	PI
0.25	+0.027	4.8	+0.89	0.26	+0.079
	-0.027		-0.75		-0.094

[a] Samples were irradiated for 10 minutes at 37 °C. See appendix V.

The almost identical EC₅₀ values found for [1]Cl₂ in the dark and after light irradiation, and its high NAMPT inhibition in the dark, suggested that [1]Cl is thermally unstable: Monitoring for 48 hours at 37 °C in the dark in OptiMEM® (Figure 6.5), showed that [1]²⁺ slowly decomposes to [Ru(tpy)(dmbpy)(OH₂)]²⁺ while [2]²⁺ remains stable (Figure S.V.7, left and right). This result is in contrast to the report of Kodanko et al. who used [Ru(tpy)(dmbpy)]²⁺ to cage a steroidal CYP17A1 inhibitor.^[12a] According to our results, [Ru(tpy)(N-N)(L)]²⁺ complexes are only stable enough for PACT when the bidentate ligand is 2,2'-biquinoline, whereas ligands which induce increased steric strain, such as 6,6'-dimethyl-2,2'-bipyridine increase the photoreactivity but also the thermal lability.^[14]

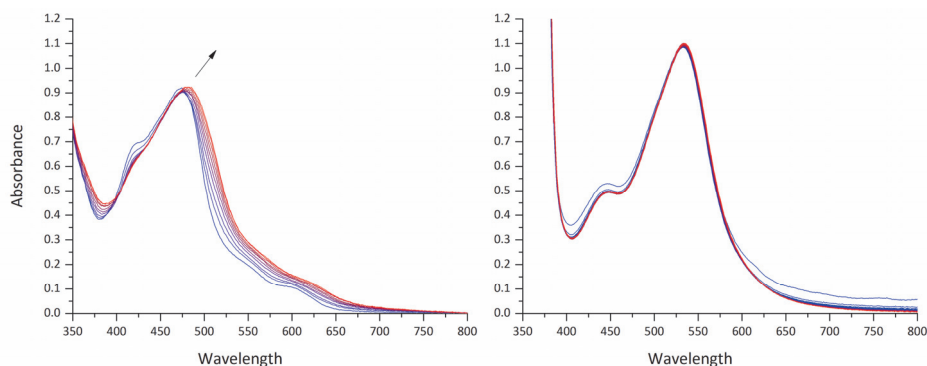


Figure 6.5. Stability of $[1]Cl_2$ (left) and $[2]Cl_2$ (right) in OptiMEM media + 2.5% FCS at 37 °C over 48 hours in the dark. Spectra measured each hour, gradient indicates intervals from blue to red. Arrow (left) indicates a shift of the MLCT absorption maximum due to formation of the chlorido species.

6.3 Conclusion

In conclusion, we have demonstrated for the first time the potential of PACT in hypoxic cancer cells using a photocaged NAMPT inhibitor. Whereas under hypoxic conditions classical PDT type II would not be effective because of the absence of dioxygen, $[2]Cl_2$ represents a promising form of photocaged drug, with a similar photoindex under hypoxia (1% O_2) as in normoxia (21% O_2). Also, this compound is soluble in water and can be activated using red light, whereas most PACT compounds reported to date require UV, blue or green light. The steric hindrance of $[2]Cl_2$ is high enough to obtain activation using clinically relevant light doses ($21 J \cdot cm^{-2}$),^[28] but low enough to acquire thermal stability. In contrast, $[1]Cl_2$ is too labile in the dark, which make it unsuitable for PACT. Altogether this study represents the first example of PACT where the phototoxicity index measured in hypoxic cancer cells with red light can be explained altogether by a low 1O_2 quantum yield, an efficient oxygen-independent photosubstitution reaction, and an enzyme inhibition assay.

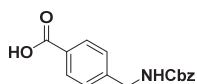
6.4 Experimental

6.4.1 General

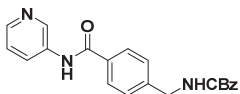
Reagents were purchased from Sigma-Aldrich and used without further purification. Dry solvents were collected from a Pure Solve MD5 solvent dispenser from Demaco. For all inorganic reactions solvents were deoxygenated by bubbling argon through the solution for 30 minutes. Flash chromatography was performed on silica gel (Screening devices B.V.) with a particle size of 40 - 64 μm and a pore size of 60 Å. TLC analysis was conducted on TLC aluminium foils with silica gel matrix (Supelco, silica gel 60, 56524) with detection by UV-absorption (254 nm). Infrared spectra were recorded on a Perkin Elmer UATR (Single Reflection Diamond) Spectrum Two device ($4000-700 cm^{-1}$; resolution $4 cm^{-1}$). 1H NMR and ^{13}C NMR were recorded in $[D_6]DMSO$ and CD_3OD with chemical shift (δ) relative to the

solvent peak on a Bruker AV-500. High resolution mass spectra were recorded by direct injection (2 μ l of 2 μ M solution in water/acetonitrile; 50/50; v/v and 0.1% formic acid) in a mass spectrometer (Thermo Finnigan LTQ Orbitrap) equipped with an electrospray ion source in positive mode (source voltage 3.5 kV, sheath gas flow 10, capillary temperature 250 °C) with resolution $R = 60000$ at m/z 400 (mass range $m/z = 150 - 2000$) and dioctylphthalate ($m/z = 391.28428$) as a lock mass. The high-resolution mass spectrometer was calibrated prior to measurements with a calibration mixture (Thermo Finnigan). Elemental analysis was performed at Kolbe Mikrolab Germany to confirm the purity of STF-31, **[1]**Cl₂ and **[2]**Cl₂ $\geq 95\%$.

6.4.2 Ligand synthesis

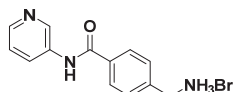


4-[(Benzyloxycarbonyl)amino]methyl benzoic acid, 4: To a cooled mixture (0 °C) of 4-(aminomethyl)benzoic acid (10.0 g, 66.2 mmol) in water/dioxane/aq. NaHCO₃ (700 ml, 5:1:1, 0.09 M) was added dropwise benzyl chloroformate (11.3 mL, 79.2 mmol). The reaction was allowed to reach room temperature and stirred overnight after which 1 M HCl was added until a pH of ~ 3 was reached. The resulting suspension was filtered, washed with water (3 x 100 mL) and Et₂O (3 x 100 mL) affording the title compound as a white powder (15.7 g, 55.0 mmol, 83%). $R_f = 0.85$ (10% H₂O in EtOAc); IR (neat): 3310, 3032, 2948, 2676, 1683, 1611; ¹H NMR: (500 MHz, [D₆]DMSO) $\delta = 12.89$ (s, 1H, COOH), 7.90 (t, $J = 7.1$ Hz, 3H, H_{arom}), 7.37 (d, $J = 4.7$ Hz, 6H, H_{arom}), 5.05 (s, 2H, CH₂ Cbz), 4.27 (d, $J = 6.4$ Hz, 2H, CH₂ Arom). ¹³C NMR (126 MHz, [D₆]DMSO) $\delta = 167.7$ (C=O COOH), 157.0 (C=O CBz), 145.4 (C_q Arom), 137.6 (C_q Arom), 129.9 (C_q Arom), 129.9 (C_H Arom), 128.9 (C_H Arom), 128.4 (C_H Arom), 128.3 (C_H Arom), 127.5 (C_H Arom), 66.0 (CH₂ CBz), 44.2 (CH₂ Arom); HRMS: m/z calcd for [C₁₆H₁₅NO₄ + H⁺]: 286.10738; found: 286.10756.



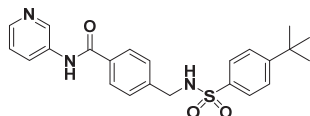
Benzyl (4-(pyridin-3-ylcarbamoyl)benzyl)carbamate, 5: To a solution of **4** (10.7 g, 37.5 mmol) in dry THF (150 mL, 0.25 M) at rt was added a catalytic amount of DMF (five drops) followed by the dropwise addition of (COCl)₂ (5.30 mL, 61.8 mmol). The reaction was stirred until bubbling ceased (~ 15 minutes) after which the mixture was heated at 50 °C for five h. The reaction mixture was concentrated *in vacuo* and the residue was redissolved in dry pyridine (80 mL, 0.47 M) followed by addition of 3-aminopyridine (3.75 g, 39.8 mmol) in portions. The pale pink suspension was stirred overnight at room temperature upon which the reaction was quenched with demi-water (200 mL). The resulting precipitate was filtered off, washed with water (3 x 50 mL) and Et₂O (3 x 50 mL) affording **5** as an off-white solid (10.9 g, 30.2 mmol, 81%). $R_f = 0.50$ (10% MeOH in DCM); IR (neat): 3359, 3221, 3035, 1710, 1670, 1531; ¹H NMR: (500 MHz, [D₆]DMSO) $\delta = 10.42$ (s, 1H, H_{arom}), 8.94 (s, 1H, H_{arom}), 8.32 (d, $J = 5.4$ Hz, 1H, H_{arom}), 8.20 (d, $J = 8.6$ Hz, 1H, H_{arom}), 7.94 (d, $J = 7.9$ Hz, 3H, H_{arom}), 7.45 – 7.25

(m, 6H, H_{arom}), 5.06 (s, 2H, CH_2 Cbz), 4.30 (d, $J = 6.7$ Hz, 2H, CH_2 Arom); ^{13}C NMR: (126 MHz, $[\text{D}_6]\text{DMSO}$) $\delta = 166.2$ (C=O CONH), 157.0 (C=O Cbz), 145.0 (C_H Arom), 144.4 (C_q Arom), 142.4 (C_H Arom), 137.7 (C_q Arom), 136.4 (C_q Arom), 133.4 (C_q Arom), 128.9 (C_H Arom), 128.4 (C_H Arom), 127.9 (C_H Arom), 127.4 (C_H Arom), 124.1 (C_H Arom), 66.0 (CH_2 Cbz), 44.1 (CH_2 Arom); HRMS: m/z calcd for $[\text{C}_{21}\text{H}_{19}\text{N}_3\text{O}_3 + \text{H}^+]$: 362.14992; found: 362.15013.



4-(aminomethyl)-*N*-(pyridin-3-yl)benzamide (bromide salt), 6:

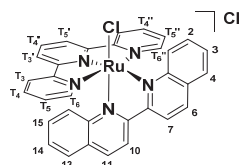
Compound **5** (6.03 g, 16.7 mmol) was suspended in 33% HBr in acetic acid (90 mL, 0.19 M) and stirred under a dry atmosphere at room temperature for 3 h, after which the precipitate was filtered off and washed with Et_2O (3 x 50 mL), yielding **6** as a white solid (6.36 g, 16.3 mmol, 98%). $R_f = 0.20$ (20% MeOH, 0.1% Et_3N in DCM); IR (neat): 3121, 3008, 2934, 1681, 1585, 1534; ^1H NMR: (500 MHz, CD_3OD) $\delta = 9.62$ (s, 1H, H_{arom}), 8.82 (d, $J = 8.8$ Hz, 1H, H_{arom}), 8.64 (d, $J = 5.8$ Hz, 1H, H_{arom}), 8.14 (m, 3H, H_{arom}), 7.68 (d, $J = 7.9$ Hz, 2H, H_{arom}), 4.26 (s, 2H, CH_2 Arom); ^{13}C NMR: (126 MHz, CD_3OD) $\delta = 168.0$ (C=O CONH_2), 140.9 (C_q Arom), 139.2 (C_q Arom), 137.7 (C_H Arom), 135.1 (C_q Arom), 134.1 (C_H Arom), 130.4 (C_H Arom), 129.9 (C_H Arom), 129.9 (C_H Arom), 43.8 (CH_2 Arom); HRMS: m/z calcd for $[\text{C}_{13}\text{H}_{13}\text{N}_3\text{O} + \text{H}^+]$: 228.11314; found: 228.11323.



4-((4-(*t*-butyl)phenylsulfonamido)methyl)-*N*-(pyridin-3-yl)benzamide, 7 (STF-31):

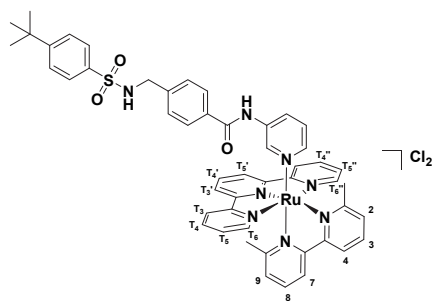
To a suspension of **6** (632 mg, 1.62 mmol) in dry pyridine (10 mL, 0.16 M) was added dropwise a solution of 4-(*t*-butyl)benzenesulfonyl chloride (393 mg, 1.69 mmol) in dry MeCN (5 mL, 0.34 M). The bright yellow mixture was stirred overnight under a dinitrogen atmosphere after which it was diluted with EtOAc (100 mL) and transferred to a separatory funnel. The organic layer was washed with 1 M HCl (3 x 25 mL), sat. NaHCO_3 (3 x 25 mL) and water (3 x 25 mL) after which it was dried (MgSO_4) and concentrated *in vacuo*. Recrystallization from EtOAc/PE afforded the title compound as a fine beige powder (367 mg, 0.87 mmol, 54%). $R_f = 0.61$ (10% MeOH in DCM); IR (neat): 3121, 2934, 3008, 1681, 1611, 1586, 1534; ^1H NMR (500 MHz, $[\text{D}_6]\text{DMSO}$) $\delta = 10.38$ (s, 1H, CONH), 8.91 (s, 1H, H_{arom}), 8.31 (d, $J = 5.0$ Hz, 1H, H_{arom}), 8.23 (s, 1H, SO_2NH), 8.17 (d, $J = 8.4$ Hz, 1H, H_{arom}), 7.86 (d, $J = 7.9$ Hz, 2H, H_{arom}), 7.69 (d, $J = 8.1$ Hz, 2H, H_{arom}), 7.55 (d, $J = 8.2$ Hz, 2H, H_{arom}), 7.43 – 7.35 (m, 4H, H_{arom}), 4.09 (s, 2H, CH_2 Arom), 1.28 (s, 9H, 3 x CH_3 *t*Bu); ^{13}C NMR (126 MHz, DMSO) $\delta = 165.5$ (C=O CONH_2), 155.3 (C_q Arom), 142.0 (C_H Arom), 141.8 (C_q Arom), 137.9 (C_q Arom), 135.8 (C_q Arom), 132.9 (C_q Arom), 127.6 (C_H Arom), 127.5 (C_H Arom), 127.3 (C_H Arom), 126.3 (C_H Arom), 125.9 (C_H Arom), 123.5 (C_H Arom), 45.8 (CH_2 Arom), 30.8 (3 x CH_3 *t*Bu); HRMS: m/z calcd for $[\text{C}_{23}\text{H}_{25}\text{N}_3\text{O}_3\text{S} + \text{H}^+]$: 424.16894; found: 424.16987; elemental analysis *calcd* (%): C, 65.23; H, 5.95; N, 9.92; found: C 65.52, H 6.32, N 9.73.

6.4.3 Complex synthesis



[Ru(tpy)(biq)Cl]Cl, [3]Cl₂: To a solution of Ruthenium dimer $[\{\text{Ru}(\text{tpy})\text{Cl}_2\}_2]\cdot\text{H}_2\text{O}$ (199 mg, 0.230 mmol) in 1,2-ethanediol (3 mL, 0.08 M) was added 2,2'-biquinoline (biq) (119 mg, 0.462 mmol) and the mixture was heated at 180 °C for 1 hr after which the solution was allowed to cool down to rt, diluted with EtOH (10 mL)

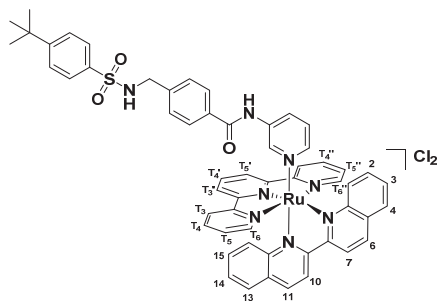
and filtered over Celite to remove any insoluble material. Ethanol was removed *in vacuo* and Et₂O was added to the residue, resulting in a precipitate which was washed with Et₂O (3 x 50 mL) and dried under high vacuum affording a violet microcrystalline solid. (275 mg, 0.416 mmol, 90%). $R_f = 0.85$ (100/80/20 acetone/water/aq. KPF₆); ¹H NMR (500 MHz, CD₃OD) $\delta = 9.65$ (d, $J = 9.5$ Hz, 1H, 1), 8.97 (d, $J = 8.9$ Hz, 1H, 6), 8.91 (d, $J = 9.3$ Hz, 1H, 7), 8.65 (dd, $J = 14.2, 8.4$ Hz, 3H, 10, T₃', T₅'), 8.47 (d, $J = 8.0$ Hz, 1H, T₃, T₃'), 8.30 (dd, $J = 8.0, 1.8$ Hz, 1H, 4), 8.24 (d, $J = 9.3$ Hz, 1H, 11), 8.19 (t, $J = 8.1$ Hz, 1H, T₄'), 7.96 – 7.77 (m, 7H, T₄, T₄'', T₆, T₆'', 2, 3, 16), 7.44 (ddd, $J = 8.2, 6.9, 1.3$ Hz, 1H, 15), 7.32 (ddd, $J = 7.3, 5.6, 1.4$ Hz, 2H, T₅, T₅''), 7.20 (ddd, $J = 8.6, 6.9, 1.5$ Hz, 1H, 14), 6.80 (d, $J = 9.0$ Hz, 1H, 13); ¹³C NMR (126 MHz, CD₃OD) $\delta = 163.2$ (C_q Arom), 160.7 (C_q Arom), 160.4 (C_q Arom), 160.0 (C_q Arom), 153.9 (2 x C_H 3, 16) 153.2 (C_q Arom), 152.5 (C_q Arom), 139.8 (C_H 7), 138.8 (C_H T₄, T₄''), 137.7 (C_H 11), 136.8 (C_H T₄'), 132.1 (C_H 14), 131.8 (2 x C_H T₆, T₆''), 131.8 (2 x C_H T₄, T₄''), 130.8 (C_q Arom), 130.4 (2 x C_H 2, 3), 129.9 (1 x C_H 4), 129.7 (C_q Arom), 129.6 (C_H 15), 128.4 (2 x CH T₅, T₅''), 124.9 (C_H 13), 124.9 (2 x C_H T₃, T₃''), 123.9 (2 x CH T₃', T₅'), 121.7 (C_H 10), 121.7 (C_H 6). ¹³C NMR (126 MHz, CD₃OD) $\delta = 161.9, 159.4, 159.0, 158.6, 152.5, 151.8, 151.2, 138.4, 137.5, 136.4, 135.5, 130.7, 130.5, 130.4, 129.4, 129.1, 128.6, 128.4, 128.3, 127.0, 123.6, 123.5, 122.6, 120.4, 120.4$; HRMS: m/z calcd for [C₃₃H₂₃N₅Cl₂Ru – Cl]: 626.06800; found: 626.06891.



[Ru(tpy)(dmbpy)(STF-31)]Cl₂, [1]Cl₂: To a solution of [Ru(tpy)(dmbpy)Cl]Cl^[14] (204 mg, 0.346 mmol) in deoxygenated EtOH/H₂O (10 mL, 2:1, 0.035 M) was added STF-31 (178 mg, 0.420 mmol) and AgPF₆ (180 mg, 0.712 mmol) the mixture was stirred at 80 °C for 4 h, after which it was filtered over Celite and concentrated *in vacuo* at 30 °C. The crude product was directly purified over Sephadex LH-20 (acetone). The

orange band was collected, the volume reduced to ~10% and a saturated solution of NBu₄Cl in acetone (1 mL) was added. The resulting precipitate was collected by filtration over a Whatman® RC60 membrane filter and subsequently washed with acetone (3 x 50 mL) and Et₂O (3 x 50 mL). Reprecipitation from EtOH/Et₂O afforded the title compound as a microcrystalline red solid (176 mg, 0.174 mmol, 50%). $R_f = 0.53$ (100/80/20

acetone/water/aq. KPF₆); ¹H NMR: (500 MHz, CD₃OD) δ = 8.83 – 8.74 (m, 3H, H_{arom}), 8.72 – 8.64 (m, 2H, H_{arom}), 8.59 (d, J = 8.0 Hz, 1H, H_{arom}), 8.51 (d, J = 8.0 Hz, 1H, H_{arom}), 8.37 – 8.29 (m, 2H, H_{arom}), 8.27 – 8.18 (m, 3H, H_{arom}), 8.14 (t, J = 7.9 Hz, 1H, H_{arom}), 7.83 (d, J = 7.9 Hz, 1H, H_{arom}), 7.81 – 7.69 (m, 5H, H_{arom}), 7.65 (dt, J = 13.7, 6.6 Hz, 2H, H_{arom}), 7.53 (dd, J = 19.4, 7.1 Hz, 3H, H_{arom}), 7.36 (d, J = 8.2 Hz, 2H, H_{arom}), 7.12 (dd, J = 8.5, 5.5 Hz, 1H, H_{arom}), 7.05 (d, J = 7.6 Hz, 1H, H_{arom}), 4.13 (s, 2H, CH₂ Arom), 2.18 (s, 3H, 1 x CH₃ Arom), 1.56 (s, 3H, 1 x CH₃ Arom), 1.33 (s, 9H, 3 x CH₃ tBu); ¹³C NMR: (126 MHz, CD₃OD) δ 166.7 (C=O CONH), 165.0 (C_q Arom), 159.3 (C_q Arom), 159.1 (C_q Arom), 158.9 (C_q Arom), 158.8 (C_q Arom), 158.7 (C_q Arom), 158.0 (C_q Arom), 156.1 (C_q Arom), 153.8 (C_H Arom), 152.8 (C_H Arom), 146.6 (C_H Arom), 142.3 (C_q Arom), 142.3 (C_H Arom), 138.8 (C_H Arom), 138.7 (C_H Arom), 138.2 (C_H Arom), 137.9 (C_H Arom), 137.8 (C_q Arom), 132.4 (C_q Arom), 128.7 (C_H Arom), 128.7 (C_H Arom), 128.6 (C_H Arom), 128.4 (C_H Arom), 127.6 (C_H Arom), 127.5 (C_H Arom), 126.9 (C_H Arom), 126.6 (C_H Arom), 125.8 (C_H Arom), 125.6 (C_H Arom), 125.2 (C_H Arom), 124.5 (C_H Arom), 124.2 (C_H Arom), 123.6 (C_H Arom), 122.0 (C_H Arom), 121.7 (C_H Arom), 46.0 (CH₂ Arom), 30.2 (3 x CH₃ tBu), 24.0 (CH₃ Arom), 22.3 (CH₃ Arom); HRMS: *m/z* calcd (%) for [C₅₀H₄₈N₈O₃RuS₂Cl₂ – 2Cl]: 471.13013; found: 471.13089; elemental analysis *calcd* (%) for [1]Cl₂·4H₂O: C, 55.35; H, 5.20; N, 10.33; found: C, 55.59 H, 5.24 N, 10.28.



[Ru(tpy)(biq)(STF-31)]Cl₂, [2]Cl₂: To a solution of [Ru(tpy)(biq)Cl]Cl (59.8 mg, 0.0904 mmol) in deoxygenated acetone/H₂O (10 mL, 1:1, 0.009 M) was added STF-31 (75 mg, 0.177 mmol) and AgPF₆ (50 mg, 0.198 mmol) and the mixture was heated at 50 °C for 2 h. The purple mixture was filtered hot over Celite, and concentrated *in vacuo* at 30 °C. The crude product was purified over Sephadex LH-20 (methanol). The

pink/purple band was collected, concentrated, redissolved in a minimal amount of acetone and precipitated by the addition of 1 mL saturated NBu₄Cl in acetone. The resulting precipitate was collected by filtration over a Whatman® RC60 membrane filter and subsequently washed with acetone (3 x 5 mL) and Et₂O (3 x 5 mL). The precipitate was recovered with MeOH and concentrated, affording the title compound as a purple solid. (43.5 mg, 0.0400 mmol, 44%). *R_f* = 0.61 (100/80/20 acetone/water/aq. KPF₆); ¹H NMR: (500 MHz, CD₃OD) δ = 9.19 (d, J = 8.8 Hz, 1H, H_{arom}), 9.07 (d, J = 8.8 Hz, 1H, H_{arom}), 8.93 (dd, J = 12.7, 8.6 Hz, 2H, H_{arom}), 8.83 – 8.78 (m, 2H, H_{arom}), 8.70 (d, J = 8.0 Hz, 1H, H_{arom}), 8.48 (t, J = 7.1 Hz, 2H, H_{arom}), 8.40 – 8.32 (m, 2H, H_{arom}), 8.21 – 8.08 (m, 2H, H_{arom}), 8.05 – 7.95 (m, 2H, H_{arom}), 7.89 (d, J = 8.0 Hz, 1H, H_{arom}), 7.81 – 7.69 (m, 4H, H_{arom}), 7.67 (d, J = 8.4 Hz, 2H, H_{arom}), 7.59 – 7.48 (m, 4H, H_{arom}), 7.45 (dd, J = 24.4, 6.1 Hz, 2H, H_{arom}), 7.41 – 7.28 (m, 5H, H_{arom}), 6.99 (dd, J = 8.5, 5.7 Hz, 1H, H_{arom}), 6.82 (d, J = 8.8 Hz, 1H, H_{arom}), 4.12 (s, 2H, CH₂ Arom), 1.33 (s, 9H, 3 x CH₃ tBu); ¹³C NMR: (126 MHz, CD₃OD) δ = 168.0 (C=O CONH), 161.8

(C_q Arom), 160.7 (C_q Arom), 160.1 (C_q Arom), 160.0 (C_q Arom), 159.6 (C_q Arom), 157.5 (C_q Arom), 152.2 (C_q Arom), 151.2 (C_q Arom), 148.2 (C_H Arom), 143.9 (C_H Arom), 143.2 (C_H Arom), 141.0 (C_H Arom), 140.3 (C_H Arom), 140.2 (C_H Arom), 140.0 (C_H Arom), 139.4 (C_q Arom), 139.1 (C_q Arom), 138.3 (C_H Arom), 133.8 (C_q Arom), 132.7 (C_H Arom), 132.4 (C_H Arom), 131.7 (C_q Arom), 131.4 (C_H Arom), 130.8 (C_H Arom), 130.4 (C_H Arom), 130.0 (C_H Arom), 130.0 (C_q Arom), 129.8 (C_H Arom), 129.8 (C_H Arom), 129.0 (C_H Arom), 128.8 (C_H Arom), 127.9 (C_H Arom), 127.5 (C_H Arom), 126.0 (C_H Arom), 125.8 (C_H Arom), 125.2 (C_H Arom), 124.7 (C_H Arom), 122.5 (C_H Arom), 122.3 (C_H Arom), 47.3 (CH₂ Arom), 31.5 (3 x CH₃ Arom); HRMS: *m/z* calcd for [C₅₆H₄₈N₈O₃RuSCl₂ – 2Cl]: 507.13013; found: 507.13098; elemental analysis *calcd* (%) for [2]Cl₂.4H₂O: C, 58.13; H, 4.88; N, 9.68; found: C, 58.14 H, 4.78 N, 9.53.

6.4.4 Photosubstitution quantum yield determination

3.00 mL of [1]Cl₂ (6.83 x 10⁻⁵ M) or [2]Cl₂ (4.10 x 10⁻⁵ M) in demiwater was deoxygenated for 15 minutes with nitrogen after which it was irradiated while the solution was kept at constant temperature (25 or 37 °C). During this period UV-vis spectra were recorded on a Varian Inc. Cary 50 UV-vis spectrometer with an interval of 30 seconds until 630 seconds. ESI-MS spectra were recorded after the irradiation experiment to confirm the formation of the aqua species [Ru(tpy)(dmbpy)(OH₂)]²⁺ and [Ru(tpy)(biq)(OH₂)]²⁺. The quantum yield of photosubstitution was calculated as described before^[20] with the following modification: The photon flux was extrapolated from the average ratio between the photon flux determined by ferrioxalate actinometry^[29] and the theoretical photon flux of the same family of LEDs (413, 450 and 490) at a given power density and was calculated 1.32 x 10⁻⁷ mol s⁻¹ at 625 nm. For the photosubstitution of [1]Cl₂ 500 and 410 nm were used as reference wavelengths, with ε₅₀₀ = 2.2 x 10³ M cm⁻¹ and ε₄₁₀ = 6.2 x 10³ M cm⁻¹ with ε₅₀₀ = 5.4 x 10³ M cm⁻¹ and ε₅₀₀ = 3578 M cm⁻¹ for [Ru(tpy)(dmbpy)(H₂O)]Cl₂. For the photosubstitution of [2]Cl₂ 550 and 500 nm were used as reference wavelengths, with ε₅₅₀ = 6.9 x 10³ M cm⁻¹ and ε₅₀₀ = 7.1 x 10³ M cm⁻¹ with ε₅₅₀ = 9.9 x 10³ M cm⁻¹ and ε₅₀₀ = 5.8 x 10³ M cm⁻¹ for [Ru(tpy)(biq)(H₂O)]Cl₂.

6.4.5 Singlet oxygen (¹O₂) quantum yield measurements

The setup, measurement and calculation were carried out as described in general appendix I.1.1 with the following modifications: Irradiation was carried out using a red laser (635 nm) with methylene blue as a reference in CD₃OD (Φ_Δ = 0.52)^[30] at 293 K.

6.4.6 UV-vis evolution spectrum in a 96-well plate in DMSO and OptiMEM® media

Compounds [1]Cl₂ and [2]Cl₂ were dissolved in OMEM (OptiMEM® without phenol red, supplemented with 0.2% (P/S), 0.9% v/v Glutamine-S and 2.0% FCS) + 10% DMSO and pure DMSO. In order to prevent light-scattering occurring from the precipitation of STF-31 a higher concentration of DMSO was used. Compounds were transferred to a 96-well plate,

irradiated at different intervals ($t = 0, 1, 2, 3, 4, 5, 10$ and 15 minutes) with red light (628 ± 19 nm, 34.4 ± 1.7 mW \cdot cm⁻²), followed by a read-out at a M1000 Tecan® reader. Spectra were plotted using Origin Pro 9.1 and the baseline was subtracted to correct for baseline drifting.

6.4.7 Log $P_{o/w}$ determination

The partition coefficient between *n*-octanol and water (log $P_{o/w}$) were determined following to the method described in appendix I.2.3.

6.4.8 Stability in OptiMEM® media 48 hours

Compound [1]Cl₂ and [2]Cl₂ ($c = 1.0 \times 10^{-4}$ and 1.1×10^{-4} M respectively) were dissolved in OMEM complete (OptiMEM without phenol red, supplemented with 0.2% (P/S), 0.9% v/v Glutamine-S and 2.0% FCS). Absorption spectra were recorded in Varian Inc. Cary 50 UV-vis spectrometer over 48 hours with an interval of 15 minutes while maintaining the temperature at 37 °C. After this time period samples were frozen solid using liquid nitrogen, lyophilized and redissolved in methanol. ESI-MS spectra were recorded to confirm the major species to be [Ru(tpy)(dmbpy)Cl]⁺ (554.1 calcd, 554.1 found) and [2]²⁺ (507.1 calcd., 506.9 found) for [1]Cl₂ and [2]Cl₂ respectively.

6.4.9 Biology

Experimental details of cell culturing, cytotoxicity and cell irradiation under normoxia and hypoxia, NBDG-uptake, and NAMPT inhibition can be found in the appendix (V.2).

References

- [1] A. D. Gujar, S. Le, D. D. Mao, D. Y. Dadey, A. Turski, Y. Sasaki, D. Aum, J. Luo, S. Dahiya, L. Yuan, K. M. Rich, J. Milbrandt, D. E. Hallahan, H. Yano, D. D. Tran, A. H. Kim, *P Natl Acad Sci USA* **2016**, *113*, E8247-E8256.
- [2] a). J. A. Khan, X. Tao, L. Tong, *Nat Struct Mol Biol* **2006**, *13*, 582-588; b). C. A. Lyssiotis, L. C. Cantley, *Clin Cancer Res* **2014**, *20*, 6-8.
- [3] B. Tan, D. A. Young, Z. H. Lu, T. Wang, T. I. Meier, R. L. Shepard, K. Roth, Y. Zhai, K. Huss, M. S. Kuo, J. Gillig, S. Parthasarathy, T. P. Burkholder, M. C. Smith, S. Geeganage, G. Zhao, *J Biol Chem* **2013**, *288*, 3500-3511.
- [4] T. S. Zabka, J. Singh, P. Dhawan, B. M. Liederer, J. Oeh, M. A. Kauss, Y. Xiao, M. Zak, T. Lin, B. McCray, N. La, T. Nguyen, J. Beyer, C. Farman, H. Uppal, P. S. Dragovich, T. O'Brien, D. Sampath, D. L. Misner, *Toxicol Sci* **2015**, *144*, 163-172.
- [5] a). D. Crespy, K. Landfester, U. S. Schubert, A. Schiller, *Chem Commun* **2010**, *46*, 6651-6662; b). C. Mari, V. Pierroz, S. Ferrari, G. Gasser, *Chem Sci* **2015**, *6*, 2660-2686; c). U. Schatzschneider, *Eur J Inorg Chem* **2010**, *2010*, 1451-1467; d). N. J. Farrer, L. Salassa, P. J. Sadler, *Dalton Trans* **2009**, 10690-10701; e). A. Presa, R. F. Brissos, A. B. Caballero, I. Borilovic, L. Korrodi-Gregorio, R. Perez-Tomas, O. Roubeau, P. Gamez, *Angew Chem Int Ed* **2015**, *54*, 4561-4565.

- [6] T. Respondek, R. Sharma, M. K. Herroon, R. N. Garner, J. D. Knoll, E. Cueny, C. Turro, I. Podgorski, J. J. Kodanko, *ChemMedChem* **2014**, *9*, 1306-1315.
- [7] a). E. M. Rial Verde, L. Zayat, R. Etchenique, R. Yuste, *Front Neural Circuits* **2008**, *2*, 2; b). B. S. Howerton, D. K. Heidary, E. C. Glazer, *J Am Chem Soc* **2012**, *134*, 8324-8327; c). S. Betanzos-Lara, L. Salassa, A. Habtemariam, O. Novakova, A. M. Pizarro, G. J. Clarkson, B. Liskova, V. Brabec, P. J. Sadler, *Organometallics* **2012**, *31*, 3466-3479; d). A. Habtemariam, C. Garino, E. Ruggiero, S. Alonso-de Castro, J. Mareque Rivas, L. Salassa, *Molecules* **2015**, *20*, 7276-7291.
- [8] a). P. Anstaett, V. Pierroz, S. Ferrari, G. Gasser, *Photobiol Sci* **2015**, *14*, 1821-1825; b). L. Zayat, M. G. Noval, J. Campi, C. I. Calero, D. J. Calvo, R. Etchenique, *ChemBiochem* **2007**, *8*, 2035-2038; c). T. Joshi, V. Pierroz, C. Mari, L. Gemperle, S. Ferrari, G. Gasser, *Angew Chem Int Ed* **2014**, *53*, 2960-2963.
- [9] D. E. Dolmans, D. Fukumura, R. K. Jain, *Nat Rev Cancer* **2003**, *3*, 380-387.
- [10] P. Avci, A. Gupta, M. Sadasivam, D. Vecchio, Z. Pam, N. Pam, M. R. Hamblin, *Semin Cutan Med Surg* **2013**, *32*, 41-52.
- [11] S. L. Hopkins, B. Siewert, S. H. Askes, P. Veldhuizen, R. Zwier, M. Heger, S. Bonnet, *Photobiol Sci* **2016**, *15*, 644-653.
- [12] a). A. Li, R. Yadav, J. K. White, M. K. Herroon, B. P. Callahan, I. Podgorski, C. Turro, E. E. Scott, J. J. Kodanko, *Chem Commun* **2017**, *53*, 3673-3676; b). J. D. Knoll, B. A. Albani, C. B. Durr, C. Turro, *J Phys Chem A* **2014**, *118*, 10603-10610.
- [13] H. Yin, M. Stephenson, J. Gibson, E. Sampson, G. Shi, T. Sainuddin, S. Monroe, S. A. McFarland, *Inorg Chem* **2014**, *53*, 4548-4559.
- [14] A. Bahreman, B. Limburg, M. A. Siegler, E. Bouwman, S. Bonnet, *Inorg Chem* **2013**, *52*, 9456-9469.
- [15] a). D. J. Adams, D. Ito, M. G. Rees, B. Seashore-Ludlow, X. Puyang, A. H. Ramos, J. H. Cheah, P. A. Clemons, M. Warmuth, P. Zhu, A. F. Shamji, S. L. Schreiber, *Acs Chem Biol* **2014**, *9*, 2247-2254; b). P. S. Dragovich, K. W. Bair, T. Baumeister, Y. C. Ho, B. M. Liederer, X. Liu, Y. Liu, T. O'Brien, J. Oeh, D. Sampath, N. Skelton, L. Wang, W. Wang, H. Wu, Y. Xiao, P. W. Yuen, M. Zak, L. Zhang, X. Zheng, *Bioorg Med Chem Lett* **2013**, *23*, 4875-4885; c). E. M. Kropp, B. J. Oleson, K. A. Broniowska, S. Bhattacharya, A. C. Chadwick, A. R. Diers, Q. Hu, D. Sahoo, N. Hogg, K. R. Boheler, J. A. Corbett, R. L. Gundry, *Stem Cell Transl Med* **2015**, *4*, 483-493.
- [16] a). D. A. Chan, P. D. Sutphin, P. Nguyen, S. Turcotte, E. W. Lai, A. Banh, G. E. Reynolds, J. T. Chi, J. Wu, D. E. Solow-Cordero, M. Bonnet, J. U. Flanagan, D. M. Bouley, E. E. Graves, W. A. Denny, M. P. Hay, A. J. Giaccia, *Sci Transl Med* **2011**, *3*, 1-9; b). M. Bonnet, J. U. Flanagan, D. A. Chan, A. J. Giaccia, M. P. Hay, *Bioorg Med Chem* **2014**, *22*, 711-720; c). D. Kraus, J. Reckenbeil, M. Wenghoefer, H. Stark, M. Frentzen, J. P. Allam, N. Novak, S. Frede, W. Gotz, R. Probstmeier, R. Meyer, J. Winter, *Cell Mol Life Sci* **2016**, *73*, 1287-1299.
- [17] D. C. Marelus, S. Bhagan, D. J. Charboneau, K. M. Schroeder, J. M. Kamdar, A. R. McGettigan, B. J. Freeman, C. E. Moore, A. L. Rheingold, A. L. Cooksy, D. K. Smith, J. J. Paul, E. T. Papish, D. B. Grotjahn, *Eur J Inorg Chem* **2014**, 676-689.

- [18] A. J. Gottle, F. Alary, M. Boggio-Pasqua, I. M. Dixon, J. L. Heully, A. Bahreman, S. H. Askes, S. Bonnet, *Inorg Chem* **2016**, *55*, 4448-4456.
- [19] A. Bahreman, B. Limburg, M. A. Siegler, E. Bouwman, S. Bonnet, *Inorg Chem* **2013**, *52*, 9456-9469.
- [20] A. Bahreman, J. A. Cuello-Garibo, S. Bonnet, *Dalton Trans* **2014**, *43*, 4494-4505.
- [21] V. Vichai, K. Kirtikara, *Nat Protocols* **2006**, *1*, 1112-1116.
- [22] J. P. Cosse, C. Michiels, *Anti-cancer agents in medicinal chemistry* **2008**, *8*, 790-797.
- [23] a). C. Xintaropoulou, C. Ward, A. Wise, H. Marston, A. Turnbull, S. P. Langdon, *Oncotarget* **2015**, *6*, 25677-25695; b). T. Matsumoto, S. Jimi, K. Migita, Y. Takamatsu, S. Hara, *Leukemia Res* **2016**, *41*, 103-110.
- [24] J. Park, H. Y. Lee, M. H. Cho, S. B. Park, *Angew Chem Int Ed* **2007**, *46*, 2018-2022.
- [25] S. C. Hsu, R. S. Molday, *J Biol Chem* **1991**, *266*, 21745-21752.
- [26] C. Zou, Y. Wang, Z. Shen, *J Biochem Bioph Meth* **2005**, *64*, 207-215.
- [27] L. Ma, R. Wang, Y. Nan, W. Li, Q. Wang, F. Jin, *Int J Oncol* **2016**, *48*, 843-853.
- [28] S. S. Dhillon, T. L. Demmy, S. Yendamuri, G. Loewen, C. Nwogu, M. Cooper, B. W. Henderson, *J Thorac Oncol* **2016**, *11*, 234-241.
- [29] C. G. Hatchard, C. A. Parker, *Proc R Soc A* **1956**, *235*, 518-536.
- [30] C. Tanielian, C. Wolff, *J Phys Chem* **1995**, *99*, 9825-9830.

Chapter 7:

Summary, conclusions and outlook

7.1 Summary

7.1.1 General introduction

Conventional chemotherapy suffers from poor selectivity leading to adverse side-effects in patients using these drugs. A possible solution to overcome these selectivity issues is by local activation of a drug with light, providing spatio-temporal control over drug activity. In the field of bioinorganic chemistry, ruthenium(II) polypyridyl prodrugs Ru-L have been investigated as potential light-induced drug delivery devices where photo-activation leads to bond-cleavage and the release of an aquated metal species Ru-OH₂ and a ligand L (Figure 7.1 left) or as PDT sensitizer (Figure 7.1 right). In theory, the aquated metal complex, for example [Ru(tpy)(bpy)(H₂O)]²⁺, is thermally reactive towards species bearing donor atoms such as amines, thioethers or aromatic imines, present in amino acids, RNA, and DNA. Under physiological conditions, the reactivity of these substrates towards [Ru(tpy)(bpy)H₂O]²⁺ may lead to similar adducts as observed for cisplatin, potentially leading to cell toxicity. However, not all ruthenium compounds are toxic and the nature of the spectator ligands remaining bound to the metal after photosubstitution, play a critical role on toxicity of the metal-based photoproduct. Simultaneously, an organic ligand L is released as well, which can be a drug with a defined target and known biological mode of action.

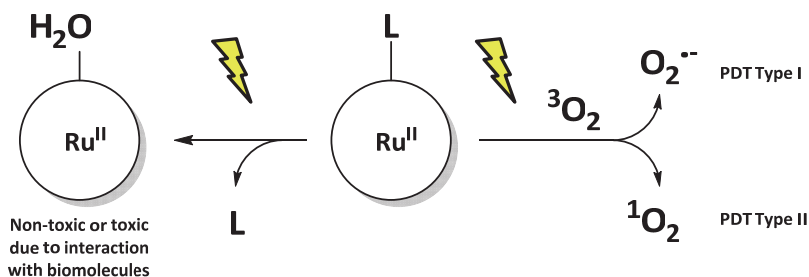


Figure 7.1. Simplified diagram with principle of photoactivated chemotherapy (PACT) in inorganic systems based on ruthenium(II). Two dominant mechanisms are illustrated: Left: Upon light irradiation, a ligand or drug (L) is released resulting in an aquated ruthenium species which is either non-toxic (PACT carrier) or toxic (PACT drug). Right: The ruthenium(II) polypyridyl species act as a PDT type I or II photosensitizer.

The research described in this thesis aimed at the development of new photoactivated chemotherapy (PACT) drugs against cancer based on the [Ru(tpy)(NN)(L)]²⁺ scaffold, which has well-defined photosubstitution properties.^[1]

7.1.2 Ruthenium polypyridyl D-glucose glycoconjugates

In Chapter 2 we described a synthetic approach towards every positional isomer of D-glucose bearing a methylthioether functional group. These compounds were used as ligands and conjugated to a non-toxic photosubstitutionally active ruthenium complexes

with the formula $[\text{Ru}(\text{tpy})(\text{bpy})(\text{L})]^{2+}$, $[\text{Ru}(\text{S-tpy})(\text{bpy})(\text{L})]^+$ (S-tpy = [2,2':6',2''-terpyridine]-4'-sulfonic acid) and $[\text{Ru}(\text{bpy})_2(\text{L})]^{2+}$. The idea behind this work was to determine which modifications of D-glucose are tolerated by glucose transporters without impairing active uptake. Most challenging was the synthesis of 2-O and 4-O alkylated derivatives, since the use of the benzyl(idene) protecting group(s) was unfavored due to the presence of sulfur donor atoms in ligand L.

7.1.3 D- versus L glucose conjugation

Conventional methods to determine glucose uptake via glucose transporters (GLUTs) use competitive inhibition with GLUT inhibitors such as phloretin, which often require conditions that are very different from those used in cytotoxicity assays. In Chapter 3 we describe a new method to investigate whether or not a glycosylated compound is taken up by GLUT transporters, which consists in comparing two conjugates bearing either a D- or an L-glucose moiety. The synthesis of two D/L enantiomers of a thioether-functionalized glucose ligand and their coordination to the highly lipophilic ruthenium complex $[\text{Ru}(\text{tpy})(\text{dppn})(\text{OH}_2)]^{2+}$ ($[1]^{2+}$, tpy = 2,2':6',2''-terpyridine, dppn = benzo[*i*]dipyrido-[3,2- α :2',3'-c]phenazine) is presented, together with toxicity, uptake, and intracellular localization studies. The use of enantiomers allowed for an unbiased comparison between cytotoxicity of the conjugates, while comparing a glycon versus an aglycon would not account for their different physical properties and in particular their different Log $P_{o/w}$ values. Submicromolar cytotoxicity values were found for $[\text{Ru}(\text{tpy})(\text{dppn})(\text{L})]^{2+}$ after blue light irradiation, which was attributed to the photorelease of $[\text{Ru}(\text{tpy})(\text{dppn})(\text{OH}_2)]^{2+}$. This activated species showed a remarkably high affinity for DNA while generating high amounts of ROS under light irradiation. Interestingly, the D- or an L-glucose-ruthenium conjugates showed different cytotoxicity in the dark, but this difference could not be attributed to GLUT-mediated uptake. The DNA light switch properties of these compounds revealed identical localization in the mitochondria for both enantiomers. Independent of the cell confluence, of the addition of an ATP-blocker (sodium azide), or of incubation time, both compounds were taken up in a similar manner. Therefore, uptake occurs *via* passive diffusion for these compounds, while the difference in cytotoxicity is most likely related to an enantioselective, post-uptake enzymatic process, such as active efflux or enzymatic breakdown of the β -glycosidic bond of the ligand by a β -glucosidase. Although the ruthenium-glucose conjugates in this chapter were not taken up by GLUT transporters, the selective localization of the prodrug, the very high affinity for mitochondrial DNA (400:1 bp:Ru), and their high singlet oxygen quantum yield (0.71) make them excellent candidates for PDT.

7.1.4 Photodynamic therapy or photoactivated chemotherapy?

The findings described in the previous chapter provided an incentive for a thorough investigation of sixteen different complexes based upon the $[\text{Ru}(\text{tpy})(\text{NN})(\text{L})]^{2+}$ scaffold.

The difference between photodynamic therapy and photo-activated therapy is often unclearly defined in the literature or poorly demonstrated. By measuring both the $^1\text{O}_2$ generation quantum yield and the photosubstitution quantum yield of glycoconjugates of this series of complexes, some insight is provided in this chapter between these two different modes of action. Structural modifications of the bidentate spectator ligands NN in $[\text{Ru}(\text{tpy})(\text{NN})(\text{L})]^{2+}$ lead to completely different photochemical and biological activity. One of the most important findings described Chapter 4 is that highly similar analogues $[\text{Ru}(\text{tpy})(\text{dppz})(\text{L})]^{2+}$ and $[\text{Ru}(\text{tpy})(\text{dppn})(\text{L})]^{2+}$ induce photocytotoxicity *via* PACT and PDT, respectively. Also, the compound $[\text{Ru}(\text{tpy})(\text{dppn})\text{Cl}]\text{Cl}$, was found to be very cytotoxic against A549 and MCF-7 cancer cells after blue light activation, which, given the low singlet oxygen quantum yield of this compound is most likely due to its hydrolysis *in vitro*, since we have demonstrated in Chapter 3 that the aqua compound $[\text{Ru}(\text{tpy})(\text{dppn})(\text{OH}_2)]^{2+}$ is an excellent PDT sensitizer. Other findings of Chapter 4 are that only one of the analogues $[\text{Ru}(\text{tpy})(\text{azpy})(\text{L})]^{2+}$ and $[\text{Ru}(\text{tpy})(\text{pymi})(\text{L})]^{2+}$ is photoactive, and that increased cellular uptake due to increased lipophilicity does not necessarily warrant (photo)cytotoxicity in A549 and MCF-7 cancer cells. Overall, this study emphasizes that $[\text{Ru}(\text{tpy})(\text{dppn})(\text{SRR}')](\text{PF}_6)_2$ (described in Chapter 3) is a unique prodrug characterized by two modes of action, i.e. PACT and PDT.

7.1.5 Cyclometalated complexes based upon $[\text{Ru}(\text{tpy})(\text{bpy})(\text{L})]^{2+}$

Due to the poor cytotoxicity of most complexes described in Chapter 4, cyclometalated complexes derived from the $[\text{Ru}(\text{tpy})(\text{NN})(\text{L})]^{2+}$ scaffold were designed as alternative, monocationic PACT agents. Cyclometalated complexes often absorb at higher wavelengths than their non-cyclometalated analogues, and they are often more cytotoxic. The plane of symmetry in $[\text{Ru}(\text{tpy})(\text{NN})(\text{L})]^{2+}$ complexes, which includes the bidentate ligand, is lost when replacing one nitrogen atom of the terpyridine with a carbon atom. Such replacement induces hence chirality, which was confirmed by the synthesis and separation of the two diastereoisomers of $[\text{Ru}(\text{phbpy})(\text{phen})(\text{SORR}')]^+$ (Hphbpy = 6'-phenyl-2,2'-bipyridyl, SORR' = (*R*)-methyl *p*-tolylsulfoxide), where the chiral cyclometalated complex is bound to an enantiomerically pure chiral sulfoxide ligand. Meanwhile, the thermal and photophysical properties were investigated of racemic complexes $[\text{Ru}(\text{phpy})(\text{NN})(\text{dmsO-kS})]^+$ with increasing annulated bidentate ligands (NN = bpy, dpq, phen, dppz and dppn). Compared to the non-cyclometalated analogons described in Chapter 4, these cyclometalated complexes showed a much lower ligand photosubstitution efficiency, and the ones bearing the dppz or dppn ligand even completely lacked the ability to photorelease the monodentate ligand. Density functional theory calculations and cyclic voltammetry further revealed that the diminished photoreactivity of these complexes is most likely the result of a larger gap between the $^3\text{MLCT}$ and ^3MC states, making thermal population of the ^3MC state from the photogenerated $^3\text{MLCT}$ state more unlikely. The broader absorption bands of these

complexes allowed three of them to be activated using green light (520 nm) in A549 and MCF-7 cells, reaching photocytotoxicity at sub-micromolar concentrations. Since both the $^1\text{O}_2$ production and ligand photosubstitution quantum yields were found to be very low, the photocytotoxicity of these compounds is attributed to a PDT type I mechanism, although the localization, target, and mode of action of these compounds remains largely unknown.

7.1.6 Red light and hypoxia

A current drawback of light-activated ruthenium(II) polypyridyl prodrugs are that these drugs are usually activated with wavelengths that fall outside the range of phototherapeutic window (600 – 850 nm). In Chapter 3 – 5 it is demonstrated that non-sterically hindered complexes based upon the $[\text{Ru}(\text{tpy})(\text{NN})(\text{L})]^{2+}$ or $[\text{Ru}(\text{phbpy})(\text{NN})(\text{L})]^+$ architecture can be activated with blue to green light. Still, these wavelengths do not penetrate through biological tissues very well. Although upconverting drug delivery systems are currently being developed to overcome this problem,^[2] they often have very low overall efficiency, making them complicated to use for therapy. In the past, Bonnet's group has studied series of sterically congested ruthenium complexes $[\text{Ru}(\text{tpy})(\text{NN})(\text{L})]^{2+}$ using *dmpby* or *biq* as bidentate ligand NN.^[3] When L is a thioether ligand, very high ligand photosubstitution quantum yields were observed. However, these complexes were also thermally unstable, which prevents their use as photoactivated prodrugs. Sterically non-hindered pyridine ligands L offer lower photosubstitution quantum yields than thioether ligands, but much higher stability in the dark. In Chapter 6, two complexes $[\text{Ru}(\text{tpy})(\text{dmbpy})(\text{L})]^{2+}$ and $[\text{Ru}(\text{tpy})(\text{biq})(\text{L})]^{2+}$ were used as PACT carriers to photocage the pyridine-containing ligand STF-31, a known NAMPT inhibitor. Pyridine binding to the ruthenium center generated new MLCT bands in the red region, which allowed for activating these complexes using red light. We demonstrated that the molar absorption coefficients and photosubstitution quantum yield at body temperature (37 °C) is high enough for these compounds to be fully activated within 10 min irradiation. Most importantly, for the first time a demonstration of PACT under hypoxia is given. $[\text{Ru}(\text{tpy})(\text{biq})(\text{STF-31})]^{2+}$ was tested under low dioxygen concentration (1%) using a specific irradiation setup for hypoxic cells recently developed in the group. The caged STF-31 compound had a photocytotoxic effect both under hypoxia and normoxia, whereas in the latter condition traditional PDT would not work.

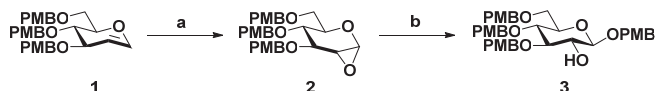
7.2 General conclusions

In this thesis new light-activated compounds based upon the $[\text{Ru}(\text{tpy})(\text{NN})(\text{L})]^{2+}$ or $[\text{Ru}(\text{phbpy})(\text{NN})(\text{L})]^+$ scaffold are described, which were tested against human cancer cell lines. The use of a number of bidentate ligands led to essentially non-toxic compounds, but improving lipophilicity of the complexes either by cyclometalation, or by extension of

the aromatic backbone of the NN ligand, led to cytotoxic and/or phototoxic species. New synthetic routes were developed towards positional isomers of a thioether-functionalized D-glucose ligand, after coordination to ruthenium, leading to the corresponding ruthenium(II) polypyridyl glycoconjugates. GLUT-mediated uptake was not detected for any of these complexes, which may be due either to a too short or too long linker between the thioether donor atom and the glucose moieties, or to the charge and overall hindrance of the ruthenium fragment that may prevent, in the conjugate, interaction of glucose with the GLUT transporter. Notwithstanding, the glucose moiety significantly improved the water solubility of these compounds, allowing for the study of the photoreactivity of these complexes independent of the lipophilicity of the bidentate ligand. By studying a wide variety of ligands, we found that complexes based upon the $[\text{Ru}(\text{NNX})(\text{NN})(\text{L})]^{2+/1+}$ ($\text{X}=\text{N}$ or C) scaffold can act either as a PACT drug, or as a PACT carrier, or as a PDT drug, while apparent minor modifications of these complexes had major impact on their photoreactivity and (photo)cytotoxicity. Last but not least, we provided the first demonstration that PACT is applicable under hypoxic conditions in which traditional PDT does not work.

7.3 Outlook

A major drawback of the synthetic route presented for the liberation of the 2-O position in D-glucose in Chapter 2 is the use of freshly prepared dimethyldioxirane (DMDO). The synthesis of this compound is arduous and only relatively small quantities can be made safely at a laboratory scale, therefore preventing the synthesis of this compound on a large scale. A proposed alternative route would proceed via the stereospecific *in situ* epoxidation of protected D-glucal **1** (Scheme 7.1), allowing access to larger amounts of **3** (Scheme 7.1).



Scheme 7.1. Alternative 2-O modification: a). Oxone, aq. NaHCO_3 , DCM, 0° to rt; b). PMB-OH, ZnCl_2 in THF, -78°C to rt.

We have demonstrated in Chapter 3 that glycoconjugates based upon the $[\text{Ru}(\text{tpy})(\text{dppn})(\text{SRR}')^{2+}]$ scaffold where SRR' bears a triethyleneglycol bridge between the thioether ligand and the glucose moiety are not transported *via* GLUT. However, the D- and L-glucose derivatives showed different cytotoxicity in the dark. These findings implicate that a post-uptake process such as hydrolysis by a β -glucosidase is responsible for this difference in cytotoxicity. This observation opens up new routes towards the use of glucosidase inhibitors in PACT. For example, the cyanogenic glycoside D-amygdalin could be coordinated via its nitrile group to $[\text{Ru}(\text{tpy})(\text{bpy})\text{Cl}]\text{Cl}$ or to one of the PACT

carriers described in Chapter 4. One of the fundamental reasons this cytotoxic compound (**6**, Figure 2) is not used in chemotherapy is the ubiquitous expression of glucosidases in both normal and cancer cells. An idea is proposed here, where modification of this structure by coordination to ruthenium would prevent enzymatic processing by a β -glucosidase in the dark, whereas release of this 'prodrug' with light would release the β -1,6-linked D-glucose disaccharide (Figure 2), where enzymatic breakdown of this molecule would lead to the release of hydrogen cyanide, the latter inducing cell-death.

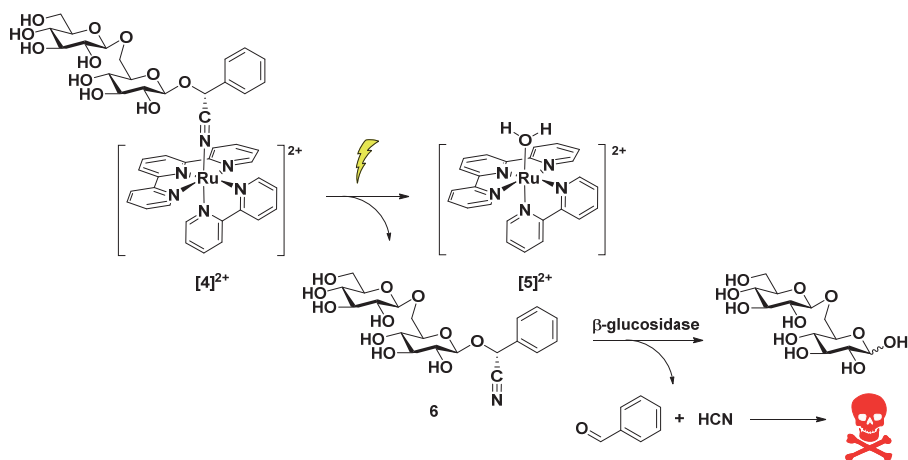


Figure 2. Proposed two-step mechanism for controlled release of D-amygdalin cell-death using a β -glucosidase.

The observed photocytotoxicity for cyclometalated compounds **[1]PF₆** – **[3]PF₆** in Chapter 5 are promising for future use in PACT. However, a current drawback of these compounds is their low ligand photosubstitution quantum yield. A proposed improvement would be to introduce a substituted bidentate ligand that leads to a more sterically congested complex, as demonstrated for polypyridyl complexes bearing biq and dmbpy in Chapter 6. As depicted in Figure 3, introducing steric hindrance in cyclometalated complexes **[7]⁺** and **[8]⁺** may reduce the ligand field splitting and hence lower the ³MC state, making the latter more easily (thermally) accessible from the photochemically generated ³MLCT state and leading to higher ligand exchange efficiency. The observed (photo)cytotoxicity for these complexes could not be attributed to DNA interaction and/or ¹O₂ generation. Future fractionation experiments to determine the location of these complexes *in cellulo* combined with experiments to prove the generation of reactive oxygen species of these complexes, could provide insight in the mode of action of these drugs.

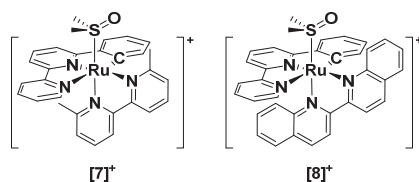


Figure 3. Proposed sterically hindered ruthenium(II) cyclometalated PACT compounds.

As described in Chapter 6 one of the observed disadvantages of the compound $[\text{Ru}(\text{tpy})(\text{biq})(\text{STF-31})]^{2+}$ was its relatively low photocytotoxicity index. Although the cytotoxicity under irradiation cannot be improved, the high cytotoxicity in the dark could possibly be reduced by further lowering the $\log P_{o/w}$ of the prodrug. A general trend observed throughout this thesis is that more lipophilic ruthenium drugs usually induce higher cytotoxicity in the dark. Therefore, a modification on the lead PACT drug described in Chapter 6 is proposed, where a sulfonate group is introduced on the 4' position (Figure 4) of the terpyridine, which should increase the overall water solubility, possibly reducing the dark cytotoxicity, and thereby increasing the photoindex.

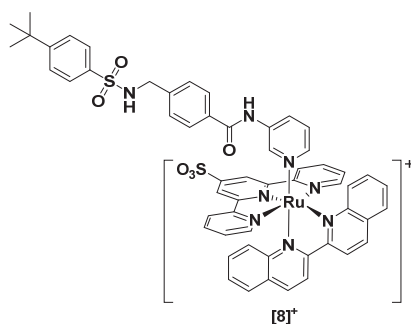


Figure 4. Proposed modification of ruthenium-photocaged NAMPT inhibitor.

Overall, the suggestions in this chapter may contribute to the advancement of photo-activated chemotherapy. This might make future clinical application of this new potential therapy possible.

References

- [1] R. E. Goldbach, I. Rodriguez-Garcia, J. H. van Lenthe, M. A. Siegler, S. Bonnet, *Chem Eur J* **2011**, *17*, 9924-9929.
- [2] S. H. Askes, W. Pomp, S. L. Hopkins, A. Kros, S. Wu, T. Schmidt, S. Bonnet, *Small* **2016**, *12*, 5579-5590.
- [3] A. Bahreman, B. Limburg, M. A. Siegler, E. Bouwman, S. Bonnet, *Inorg Chem* **2013**, *52*, 9456-9469.

Appendix I: General procedures

I.1.1 Singlet oxygen ($^1\text{O}_2$) and phosphorescence quantum yield measurements

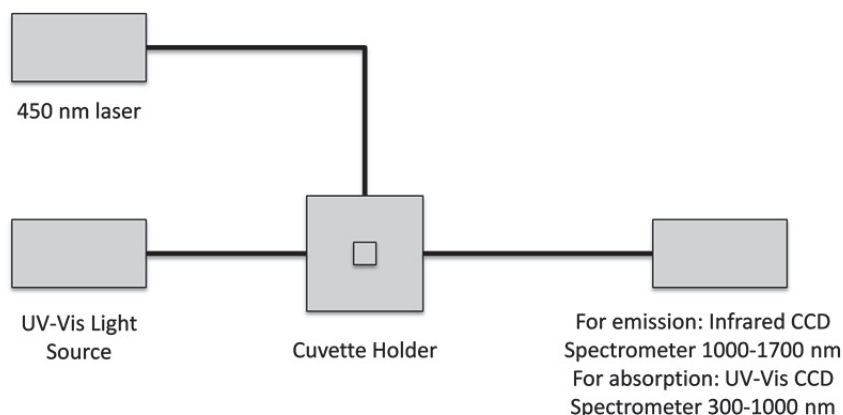


Figure S.I.1 Setup for $^1\text{O}_2$ quantum yield measurement and emission spectroscopy.

The quantum yield of singlet oxygen generation was determined in a custom-built setup (Figure S.I.1), in which both UV-VIS absorption and infrared emission spectroscopy could be performed. Emission experiments were carried out in the same setup. All optical parts were connected with optical fibers from Avantes (Apeldoorn, The Netherlands), with a diameter of 200–600 μm . For each measurement, 2 mL of sample, consisting of the compound in CD_3OD , was placed in a stirred 111-OS macro fluorescence cuvette from Hellma in a CUV-UV/VIS-TC temperature-controlled cuvette holder from Avantes. The sample was allowed to equilibrate at 293 K for 5 minutes. Emission spectroscopy was performed with a 450 nm fiber-coupled laser (Laser system LRD-0450 from Laserglow, Toronto, Canada), which was set to 50 mW at the cuvette (4 mm beam diameter; $0.4 \text{ W}\cdot\text{cm}^{-2}$) at a 90° angle with respect to the spectrometer. The excitation power was measured using a S310C thermal sensor connected to a PM100USB power meter (Thorlabs). The infrared emission spectrum was visualized from 1000 nm to 1700 nm with an Avantes NIR256-1.7TEC spectrometer, for the phosphorescence experiment the emission spectrum was visualized from 300 to 900 nm with an Avantes 2048L StarLine spectrometer with a Thorlabs FEL0500 500 nm long pass filter. The infrared emission spectrum was acquired within 9 seconds, after which the laser was turned off directly. UV-

Vis absorption spectra before and after emission spectroscopy were measured using an Avalight-DHc halogen-deuterium lamp (Avantes) as light source (turned off during emission spectroscopy) and an Avantes 2048L StarLine UV-Vis spectrometer as detector, both connected to the cuvette holder at a 180° angle. No difference in UV-Vis absorption spectrum was found due to exposure to the blue laser, showing that the singlet oxygen emission is that of the starting compound. All spectra were recorded with Avasoft software from Avantes and further processed with Microsoft Office Excel 2010 and Origin Pro software.

The quantum yield of singlet oxygen production was calculated using the relative method with [Ru(bpy)₃]Cl₂ as the standard (0.73 in CD₃OD)^[1], according to equation 1:

$$\Phi_{sam}^{\Delta} = \Phi_{std}^{\Delta} \times \frac{A_{std}^{450}}{A_{sam}^{450}} \times \frac{E_{sam}}{E_{std}}$$

Equation S.I.1

where Φ^{Δ} is the quantum yield of singlet oxygen generation, A^{450} is the absorbance at 450 nm (always kept below 0.1 for a 1 cm path length), E is the integrated emission peak of singlet oxygen at 1270 nm, and sam and std denote the sample and standard, respectively.

The quantum yield of phosphorescence was calculated using the relative method with [Ru(bpy)₃]Cl₂ as the standard (0.042 in water)^[2] according to equation 2:

$$\Phi_{sam}^{em} = \Phi_{std}^{em} \times \frac{A_{std}^{450}}{A_{sam}^{450}} \times \frac{E_{sam}}{E_{std}}$$

Equation S.I.2

where Φ^{em} is the quantum yield of phosphorescence, A^{450} is the absorbance at 450 nm (always kept below 0.1 for a 1 cm path length), E is the integrated emission range from 550 to 850 nm, and sam and std denote the sample and standard, respectively.

I.2.1 Cell culturing and cytotoxicity assay

I.2.1.1 General

Human cancer cell lines (A549, human lung carcinoma; MCF-7, human breast adenocarcinoma) were distributed by the European Collection of Cell Cultures (ECACC), and purchased through Sigma Aldrich. Dulbecco's Minimal Essential Medium (DMEM, with

and without phenol red, without glutamine), 200 mM Glutamine-S (GM), trichloroacetic acid (TCA), glacial acetic acid, sulforhodamine B (SRB), tris(hydroxymethyl)aminomethane (tris base), were purchased from Sigma Aldrich. Fetal calf serum (FCS) was purchased from Hyclone. Penicillin and streptomycin were purchased from Duchefa and were diluted to a 100 mg/mL penicillin/streptomycin solution (P/S). Trypsin and Opti-MEM[®] (without phenol red) were purchased from Gibco[®] Life Technologies. Trypan blue (0.4% in 0.81% sodium chloride and 0.06% potassium phosphate dibasic solution) was purchased from BioRad. Plastic disposable flasks and 96-well plates were purchased from Sarstedt. Cells were counted using a BioRad TC10 automated cell counter with Biorad Cell Counting Slides. UV-vis measurements for analysis of 96-well plates were performed on a M1000 Tecan Reader. Cells were inspected with an Olympus IX81 microscope.

1.2.1.2 Cell culturing

Cells were cultured in DMEM complete (Dulbecco's Modified Eagle Medium (DMEM) with phenol red, supplemented with 8.0% v/v fetal calf serum (FCS), 0.2% v/v penicillin/streptomycin (P/S), and 0.9% v/v Glutamine-S (GM)). Cells were cultured under humidified conditions, 37 °C atmosphere containing 7.0% CO₂ in 75 cm² flasks and sub-cultured (1:3 to 1:6 ratio) upon reaching 70-80% confluency (approximately once per week). Media was refreshed every second day. Cells were passaged for 4 - 8 weeks.

1.2.1.3 Cell irradiation setup

Cell irradiation setup. The cell irradiation system consists of a Dtabis thermostat (980923001) fitted with two flat-bottom microplate thermoblocks (800010600) and a 96.-LED array fitted to a standard 96-well plate. The 450 nm LED (OVL-3324), fans (40 mm, 24 V DC, 9714839), and power supply (EA-PS 2042-06B) were ordered from Farnell. Full description of the cell irradiation setup is given in Hopkins et al.^[3]

1.2.1.4 Cytotoxicity Assay

Cells were seeded at $t = 0$ in 96-well plates at a density of 5×10^3 (A549) and 8×10^3 (MCF7) cells/well in a volume of 100 μ L of Opti-MEM[®] complete without phenol red and incubated for 24 h at 37 °C and 7% CO₂. After this period, 100 μ L of six different concentrations (1 – 100 μ M for dark plates, 0.1 – 10 μ M for irradiated plates) of freshly prepared stock solutions of [D-2](PF₆)₂ and [L-2](PF₆)₂ in Opti-MEM were added to the wells in triplicate. Plates were incubated in the dark for an additional 24 h. After this period the media in each well was refreshed, and half of the plates were irradiated for 5 minutes with blue light (454 ± 11 nm, 10.5 ± 0.7 mW · cm⁻², $3.2 \cdot \text{J cm}^{-2} \pm 0.2$), while the other half was kept in the dark under otherwise identical conditions. After irradiation all plates were placed back in the incubator and incubated for an additional 48 hours. Then the cells were fixed by adding 100 μ L of cold trichloroacetic acid (TCA, 10% w/v) in each well. Next, TCA was removed from the wells, plates were gently washed five times with

water, air-dried, stained using 100 μL sulforhodamine B (0.6% w/v SRB in 1% v/v acetic acid) for 30-45 minutes, washed five times with ~ 300 μL acetic acid (1% v/v), and air-dried. The SRB dye was then solubilized using 200 μL of tris base (10 mM), and the absorbance in each well was read at 510 nm using a M1000 Tecan Reader.

The SRB absorbance data were used to calculate the fraction of viable cells in each well using Excel and GraphPad Prism[®] as follows. The absorbance data from three technical triplicate wells per concentration were averaged. Relative cell viabilities were calculated by dividing the average absorbance of treated wells by the average absorbance of the untreated wells. Three independent biological replicates were completed for each cell line (three different passage numbers per cell line). The average cell viability of the three biological replicates was plotted versus the logarithm of the concentration in μM , with standard deviation error of each point. Using the dose-response curve for each cell line in dark and irradiated conditions, the effective concentration EC_{50} (defined as the concentration of drug that gives a half-maximum effect) was calculated by fitting the curves using a non-linear regression function with fixed Y maximum (100%) and minimum (0%) (relative cell viability), and a variable Hill-slope, resulting in the simplified two-parameter Hill-slope equation 1.

$$\frac{100}{(1 + 10^{((\log_{10} EC_{50} - X) \times Hill\ Slope)})}$$

Equation S.I.3

1.2.3 Log P_{ow} determination

The partition coefficient between *n*-octanol and water (Log P_{ow}) were determined according to OECD guidelines^[4] according to the following method: Stock solutions of complexes (1×10^{-3} M) were prepared by dissolving the compounds in *n*-octanol saturated MilliQ water (MilliQ saturated *n*-octanol for complexes insoluble in water). Three aliquots (0.200 ml) of these stock solutions were transferred to 15 mL corning tubes and diluted with *n*-octanol saturated MilliQ to 1.00 ml resulting in $c_{final} = 0.20 \times 10^{-3}$ M. Then, 1.00 ml of MilliQ-saturated *n*-octanol (*n*-octanol saturated MilliQ for complexes insoluble in water) was added. The mixture was shaken in a GFL 3016 reciprocating shaker at 60 rpm for 1 h while protecting the compounds from light and then centrifuged for 10 minutes at 2000 rpm. 0.500 mL aliquots from each technical replicate were then transferred to 15 mL corning tubes and diluted with 5% HNO_3 until $V_{final} = 5.00$ mL. Ruthenium concentrations in the water phase (from both the stock solution and the dilution) were determined using a Varian Inc. Vista MPX Simultaneous ICP-OES. Partition coefficients were calculated using equation S.I.4.

$$\log P_{ow} = \log \frac{[\text{Ru}]_{\text{oct}}}{[\text{Ru}]_{\text{aq}}}$$

Equation S.I.4

Where $[Ru]_{\text{oct}}$ and $[Ru]_{\text{aq}}$ are the concentrations of Ru in the n-octanol and aqueous layers respectively and represent the mean \pm SD of three technical replicates.

References

- [1] D. Garcia-Fresnadillo, Y. Georgiadou, G. Orellana, A. M. Braun, E. Oliveros, *Helv Chim Acta* **1996**, *79*, 1222-1238.
- [2] J. Van Houten, R. J. Watts, *J Am Chem Soc* **1976**, *98*, 4853-4858.
- [3] S. L. Hopkins, B. Siewert, S. H. Askes, P. Veldhuizen, R. Zwier, M. Heger, S. Bonnet, *Photobiol Sci* **2016**, *15*, 644-653.
- [4] Oecd, *OECD Guidelines for the Testing of Chemicals*, The Organisation for Economic Co-operation and Development, **1994**.

Appendix II: Supporting information for Chapter 3

II.1 Photochemistry

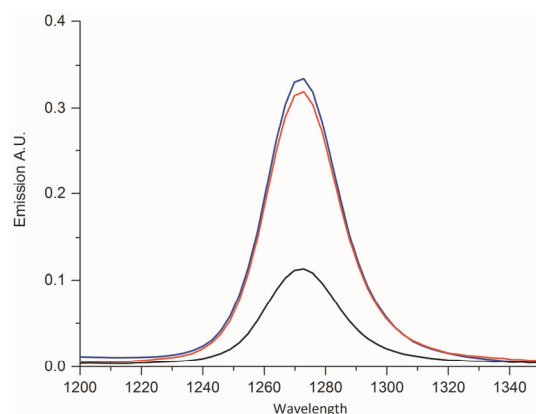


Figure S.II.2. Time-integrated emission spectra of $[\text{Ru}(\text{bpy})_3]\text{Cl}_2$ (black), $[\text{D-2}](\text{PF}_6)_2$ (red) and the photoproduct of $[\text{D-2}](\text{PF}_6)_2 + 1$ eq. of ligand (black) in CD_3OD irradiated with blue light ($\lambda_{\text{exc}} = 450$ nm, 50 mW), stirred under air in CD_3OD at 298 K.

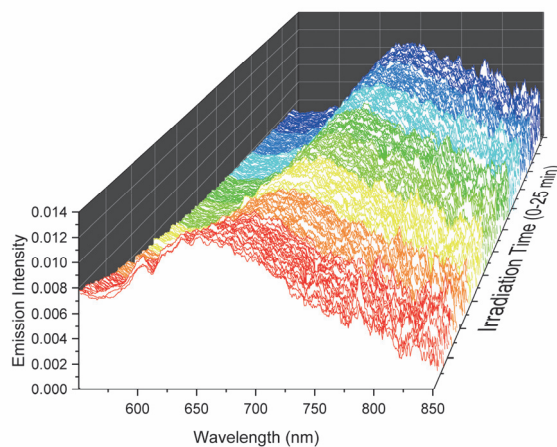


Figure S.II.3. Time evolution of the emission spectra of $[\text{D-2}](\text{PF}_6)_2$ (red, $\lambda_{\text{exc}} = 450$ nm, $\lambda_{\text{em}} = 648$ nm) irradiated with blue light (450 nm) to form $[\text{1}](\text{PF}_6)_2$ (blue, $\lambda_{\text{exc}} = 450$ nm, $\lambda_{\text{em}} = 690$ nm) in PBS.

II.2 Biology

II.2.2 DNA photointeraction studies

Agarose gel electrophoresis was used to assay the photoinduced binding and photocleavage of pUC19 plasmid using [D-2](PF₆)₂. A 5X tris-boric acid (TBA) buffer (45 mM tris(hydroxymethyl)aminomethane and 45 mM boric acid, pH = 7.4) was used in the gel and for the running buffer. Phosphate buffer (PB, 100 mM NaH₂PO₄, pH = 7.0) was used for DNA-MC interactions. A 0.8% w/w agarose gel (0.24 g agarose, 24 g DI H₂O, and 6 mL TBA) was made using the OWL B1A Easycast system. Each sample was prepared. The irradiated sample consisted of 20 μL pUC19 plasmid (20 μg, [DNA bp]_{final} = 1.9 × 10⁻³ M), 2 μL of 0.5 mM solution of complex [D-2](PF₆)₂ in PB ([[D-2](PF₆)₂]_{final} = 4.9 × 10⁻⁶ M) and 178 μL PB, for a total volume of 200 μL of a 400:1 base pair to metal complex ratio. A dark metal complex control was prepared using 4 μL pUC19 DNA, 0.4 μL of 0.5 mM solution of complex [D-2](PF₆)₂ in PB, and 35.6 μL PB. Dark and irradiated DNA controls were prepared using 4 μL pUC19 DNA and 36 μL PB. The dark and irradiated samples were run in parallel using the same LED irradiation setup above. Each sample was loaded into separate wells of two 96-well plates (dark and 455 nm irradiated). For the irradiated sample, 20 μL aliquots were removed at 1, 3, 5, 10, and 15 minutes correlating to doses of 0.6, 1.9, 3.2, 6.3, and 9.5 Jcm⁻², respectively. At the end of the experiment, 20 μL of the dark DNA control, irradiated DNA control, and dark DNA-metal complex control (t = 0 min irr) were removed. To each of the 20 μL aliquots, 4 μL of 6X loading dye was added. The λ DNA-*Hind*III digest molecular weight (MW) marker was prepared by adding 2 μL (1 μg) of the DNA MW marker, 18 μL PB, and 4 μL 6X loading dye. The gel electrophoresis chamber was filled with 50 mL TBA and 210 mL DI H₂O. To each well in the gel 12 μL (1 μg of DNA) of each sample were loaded according to the Table S.II.1. The gel was run at 105 V for 90 min. The gel was stained using 10 μL (10 mg/mL) ethidium bromide in 200 mL DI H₂O for 30 min with slight shaking and then destained in 200 mL DI H₂O for 20 min. Immediately following destaining, the gel was imaged on a BioRad ChemiDoc imaging system using the ethidium bromide setting. Using Image Lab, the volume of the OC and SC bands in each lane was determined for time 0-15 min irradiation of the 400:1 BP:MC ratio samples, Figure S.II.4.

Table S.II.1. Agarose gel electrophoresis loading description with irradiation times (min) and corresponding light doses (J x cm⁻²).

Lane	Description	Time of irradiation (min)	Light dose (Jcm ⁻²)
1	λ MW marker	0	0
2	DNA control, 37 °C, dark	0	0
3	DNA control, 37 °C, irradiated	15	9.5
4	400:1 BP:MC, 37 °C, dark	0	0
5	400:1 BP:MC, 37 °C, irradiated 1 min	1	0.6
6	400:1 BP:MC, 37 °C, irradiated 3 min	3	1.9
7	400:1 BP:MC, 37 °C, irradiated 5 min	5	3.2
8	400:1 BP:MC, 37 °C, irradiated 10 min	10	6.3
9	400:1 BP:MC, 37 °C, irradiated 15 min	15	9.5
10	λ MW marker	0	0

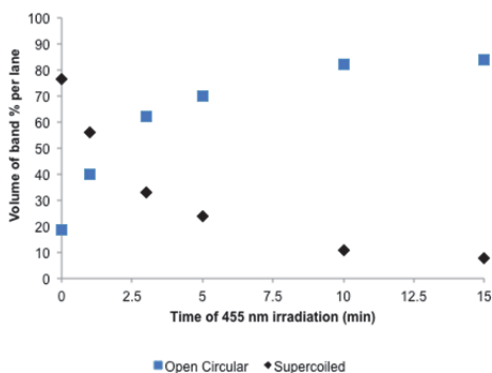


Figure S.II.4. Plot of volume of band per lane as a function of time of 455 nm irradiation (min).

II.2.3 Emission microscopy, 20x objective

All images using the 20x air objective were acquired using an Olympus IX81 inverted microscope system, Figures S.II.5-S.II.10. Fluorescence and emission imaging of the control cells and metal complex treated cells was performed using 488 nm excitation. Fluorescence imaging of DAPI stained cells was performed using the DAPI filter block (350 nm excitation/450 nm emission filter). The exposure time was 1 s, lamp intensity was 100% and gain was set to 100. For all images, cells were irradiated using 488 nm light for 30 s prior to capturing the image. Fiji ImageJ software was used to process images.^[1] The metal complex emission was visualized in yellow and DAPI in blue.

II.2.4 General preparation of cells samples for microscopy imaging

A549 cells were used for microscopy imaging experiments. Cells were seeded (100 μL OMEM-complete) at specified concentrations (see each experiment) in ibidi 1 $\mu\text{-slide}$ 8-well ibiTreat chamber. Cells were incubated for 24 h at 37 $^{\circ}\text{C}$ and 7% CO_2 . Following the 24 h incubation, cells were treated [D-2](PF₆)₂ and [L-2](PF₆)₂ (final concentration = 25 μM) and placed back in the incubator for a specified amount of time depending on experiment. Prior to imaging, media was removed from all wells, and refreshed with OMEM-complete.

II.2.5 Visualization (20x obj.) of the time-dependent incubation of [D-2](PF₆)₂ and [L-2](PF₆)₂

A549 cells were seeded at 1×10^5 cells/well in three ibidi 1 $\mu\text{-slide}$ 8-well ibiTreat chambers. Cells were incubated for 24 h (37 $^{\circ}\text{C}$, 7% CO_2) and then treated with a final concentration of 25 μM of [D-2](PF₆)₂ and [L-2](PF₆)₂. The cells were incubated in the presence of metal complexes for 4, 6, and 24 h, Figure S.II.5. Media was refreshed and cells were imaged. Control wells were imaged under the same conditions as the metal complex treated wells (30 s exposure to 488 nm irradiation, followed by imaging). For the

24 h metal complex treated samples, the nucleus was co-stained using DAPI. One well of [D-2](PF₆)₂ and [L-2](PF₆)₂ were stained with 2 μL of 0.1 mg/mL DAPI for one minute, Figure S.II.6.

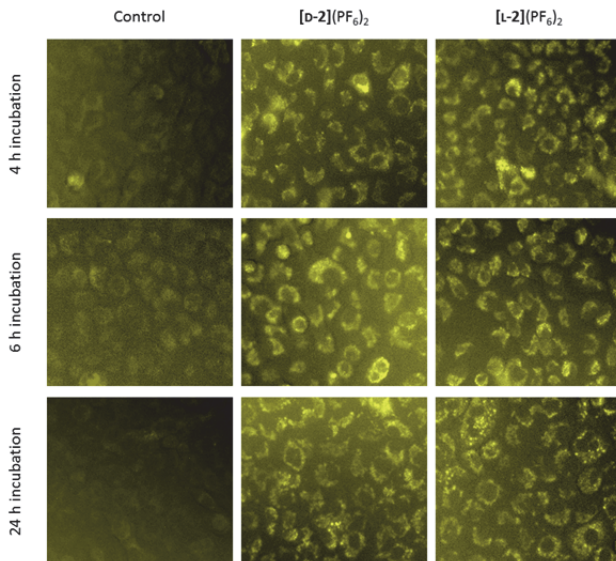


Figure S.II.5. Images of autofluorescence of A549 cells and emission of [D-2](PF₆)₂ and [L-2](PF₆)₂ treated A549 cells (20x obj.). Cells were treated at 25 μM final concentration for the metal complexes and then incubated for 4, 6, or 24 h at 37 °C and 7% CO₂. Images show that under the same conditions, the emission of the metal complexes is above the background autofluorescence observed in untreated cells.

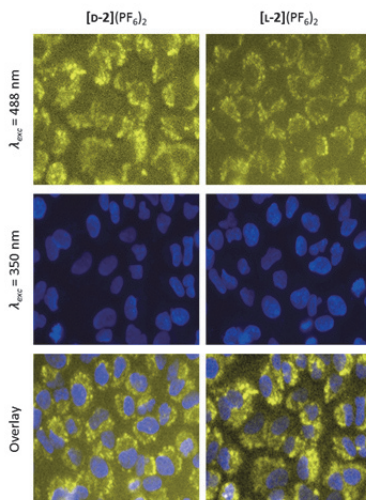


Figure S.II.6. Images of emission from [D-2](PF₆)₂ and [L-2](PF₆)₂ treated A549 cells, fluorescence of DAPI co-stained cells, and the overlay showing no nuclear co-localization of the metal complexes.

II.2.6 Visualization at 4 h incubation of [D-2](PF₆)₂ and [L-2](PF₆)₂ with lower seeding density

To determine if a higher ratio of metal complex to cell population influenced the localization of the complexes, A549 cells were seeded at 6×10^3 cells/well in an ibidi 1 μ -slide 8-well ibiTreat chamber. Cells were incubated for 24 h (37 °C, 7% CO₂) and then treated with a final concentration of 25 μ M of [D-2](PF₆)₂ and [L-2](PF₆)₂. The metal complexes for were incubated (37 °C, 7% CO₂) in the presence of the cells for 4 h, Figure S.II.7. Media was refreshed and cells were imaged. Control wells were imaged under the same conditions as the metal complex treated wells (30 s exposure to 488 nm irradiation, followed by imaging). Images were compared to those seeded at 1×10^5 cells/well, but no significant difference in localization was observed.

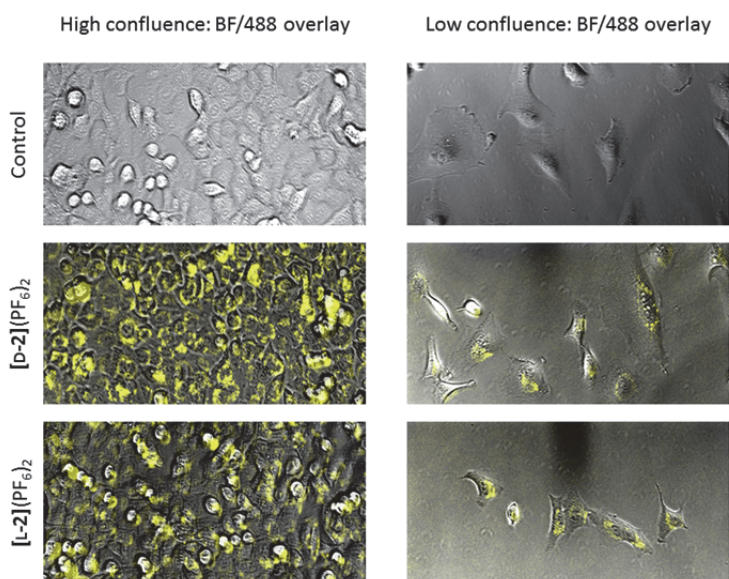


Figure S.II.7. Overlay images (BF and 488 nm excitation, 20x obj.) of cells only and [D-2](PF₆)₂ or [L-2](PF₆)₂ treated A549 cells after 4 h incubation at high and low seeding densities. The ratio of metal complex to cells does not influence metal complex localization.

II.2.7 Visualization at 4 h incubation of [D-2](PF₆)₂ and [L-2](PF₆)₂ in the presence of sodium azide

Sodium azide (NaN₃), an inhibitor of energy dependent uptake mechanisms, was used to determine whether the uptake of [D-2](PF₆)₂ or [L-2](PF₆)₂ was energy dependent. Cells were seeded at 6×10^3 cells/well in an ibidi 1 μ -slide 8-well ibiTreat chamber. Cells were incubated for 24 h (37 °C, 7% CO₂). Three wells were pretreated with NaN₃ (100 μ M final concentration) for one hour prior to treatment with media or [D-2](PF₆)₂ or [L-2](PF₆)₂. After one hour, control cells were incubated with 100 μ M NaN₃, and metal complex treated cells were incubated with 100 μ M NaN₃ and 25 μ M [D-2](PF₆)₂ or [L-2](PF₆)₂ for

four additional hours (37 °C, 7% CO₂). Media was refreshed and cells were imaged, Figure S.II.8. Control wells were imaged under the same conditions as the metal complex treated wells (30 s exposure to 488 nm irradiation, followed by imaging). All images were processed in the same fashion.

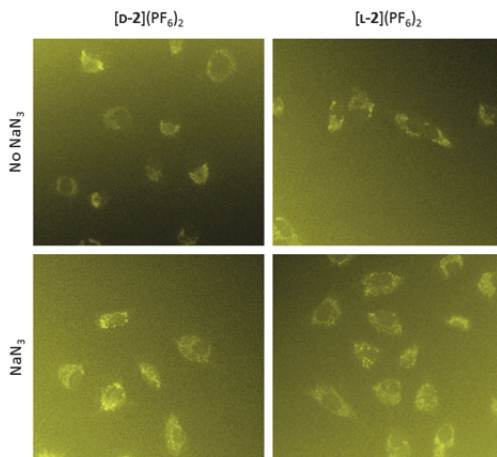


Figure S.II.8. A549 cells imaged (20x obj.) after no incubation or (pre)incubation with NaN₃ and [D-2](PF₆)₂ and [L-2](PF₆)₂. Images show negligible difference in the presence or absence of NaN₃ strongly supporting that the complexes utilize a facilitated diffusion uptake mechanism.

II.2.8 Emission microscopy, 100x objective

Emission and fluorescence imaging using a 100x objective was performed using a customized Zeiss Axiovert S100 Inverted Microscope setup. The microscope was fitted with a Zeiss 100 x Plan Apochromat 1.4 NA oil objective and an Orca Flash 4.0 V2 sCMOS camera from Hamamatsu, which together produced images with pixel size of 69 nm. The camera exposure time was 250 ms. For direct excitation and emission imaging of [D-2](PF₆)₂ and [L-2](PF₆)₂, a 488 nm laser was used. For fluorescence microscopy of MitoTracker Deep Red (MTDR), an LRD-0635-PFR-00200-01 LabSpec 635nm Collimated Diode Laser (Laserglow Technologies, Toronto, Canada) was used as excitation source, combined with a Chroma ZT405/532/635rpc dichroic beam splitter. All laser beam spots had a Gaussian intensity profile. Fiji ImageJ software was used to process images.^[1] The metal complex emission was visualized in yellow and MTDR in red.

II.2.9 Visualization (100x obj.) at 6 h incubation of [D-2](PF₆)₂ and [L-2](PF₆)₂ with MTDR

A549 cells were seeded at 3×10^3 cells/well in an ibidi 1 μ -slide 8-well ibiTreat chamber. Cells were incubated for 24 h (37 °C, 7% CO₂) and then treated with a final concentration of 25 μ M of [D-2](PF₆)₂ or [L-2](PF₆)₂. The metal complexes for were incubated for 6 h (37 °C, 7% CO₂). At 5.5 h cells were co-stained using MitoTracker Deep Red (1.1×10^{-3} M final concentration) and incubated for 30 min. Cells were washed 3 times with PBS buffer and

then 200 μL OMEM-complete was added to the wells for imaging. For each set of images, cells were initially imaged using the 635 nm channel, then 488 nm, and finally the 635 nm channel, Figure S.II.9.

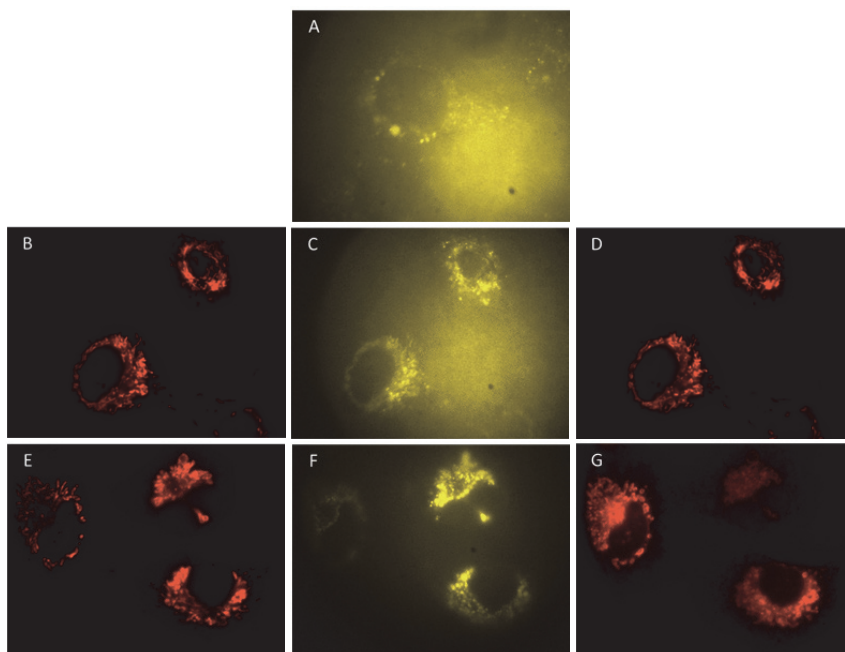


Figure S.II.9. A549 cells (A) untreated and unstained ($\lambda_{\text{exc}} = 488 \text{ nm}$), (B) untreated and stained with MitoTracker Deep Red (MTDR) before 488 nm excitation ($\lambda_{\text{exc}} = 639 \text{ nm}$), (C) untreated and stained with MTDR ($\lambda_{\text{exc}} = 488 \text{ nm}$), (D) untreated and stained with MTDR after 488 nm excitation ($\lambda_{\text{exc}} = 639 \text{ nm}$), (E) treated with $[\text{D-2}](\text{PF}_6)_2$ for 6 h and stained with MTDR before 488 nm excitation ($\lambda_{\text{exc}} = 639 \text{ nm}$), (F) treated with $[\text{D-2}](\text{PF}_6)_2$ for 6 h and stained with MTDR ($\lambda_{\text{exc}} = 488 \text{ nm}$), (G) treated with $[\text{D-2}](\text{PF}_6)_2$ for 6 h and stained with MTDR after 488 nm excitation ($\lambda_{\text{exc}} = 639 \text{ nm}$). Images B-D and E-G were taken consecutively.

II.2.10 Visualization (100x obj.) at 24 h incubation of $[\text{D-2}](\text{PF}_6)_2$ and $[\text{L-2}](\text{PF}_6)_2$

A549 cells were seeded at 6×10^4 cells/well in an ibidi 1 μ -slide 8-well ibiTreat chamber. Cells were incubated for 24 h (37 $^\circ\text{C}$, 7% CO_2) and then treated with a final concentration of 25 μM of $[\text{D-2}](\text{PF}_6)_2$ and $[\text{L-2}](\text{PF}_6)_2$. The metal complexes for were incubated for 24 h (37 $^\circ\text{C}$, 7% CO_2). Media was refreshed and cells were imaged. A selection of single cell images are shown for untreated and $[\text{D-2}](\text{PF}_6)_2$ or $[\text{L-2}](\text{PF}_6)_2$ treated cells, Figure S.II.10.

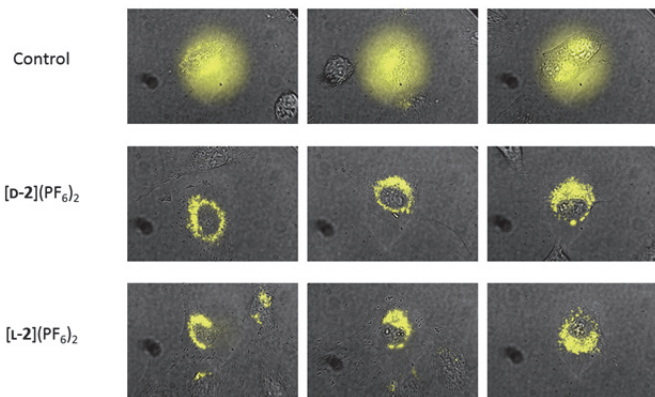


Figure S.II.10. Single cell examples of control images, [D-2](PF₆)₂ and [L-2](PF₆)₂ treated images at 488 nm.

II.2.11 Phase contrast microscopy images

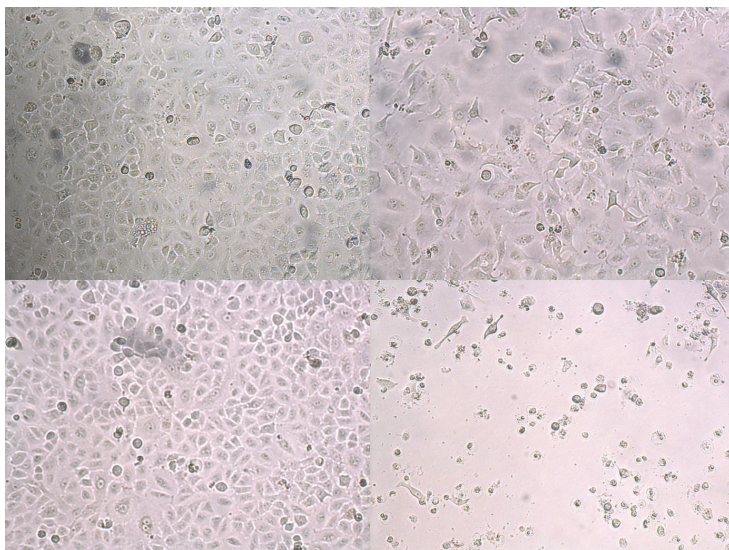


Figure S.II.11. A549 cells (10 x obj.). From top left to bottom right: A549 cells after 96 hours. Top left: A549 cells in the dark after 96 hours; Top right: A549 cells treated with 20 μM of [D-2](PF₆)₂ after 96 hours; Bottom left: A549 cells, irradiated with blue light (455 nm, 3.1 J.cm⁻²) after 96 hours; Bottom right: A549 cells treated with 1 μM of compound [D-2](PF₆)₂ and irradiated (455 nm, 3.1 J.cm⁻²), after 96 hours.

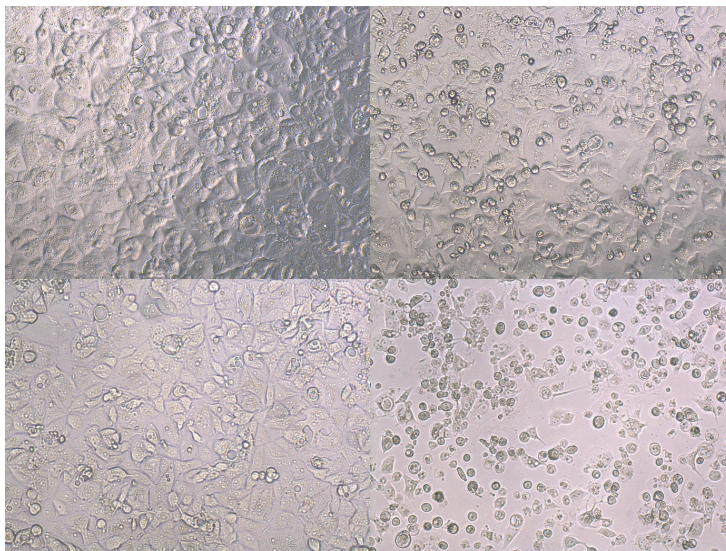


Figure S.II.12. MCF-7 cells (10 x obj.). From top left to bottom right: MCF-7 cells after 96 hours. Top left: MCF-7 cells in the dark after 96 hours; Top right: MCF-7 cells treated with 20 μM of [D-2](PF₆)₂ after 96 hours; Bottom left: MCF-7 cells, irradiated with blue light (455 nm, 3.1 J.cm⁻²) after 96 hours; Bottom right: MCF-7 cells treated with 1 μM of compound [D-2](PF₆)₂ and irradiated (455 nm, 3.1 J.cm⁻²), after 96 hours.

II.3 Chiral HPLC Traces of D-3 and L-3

Spectra were collected using an analytical Lux Cellulose-1 chiral HPLC column eluted with gradient: MeCN/MeOH from 0 to 30%.

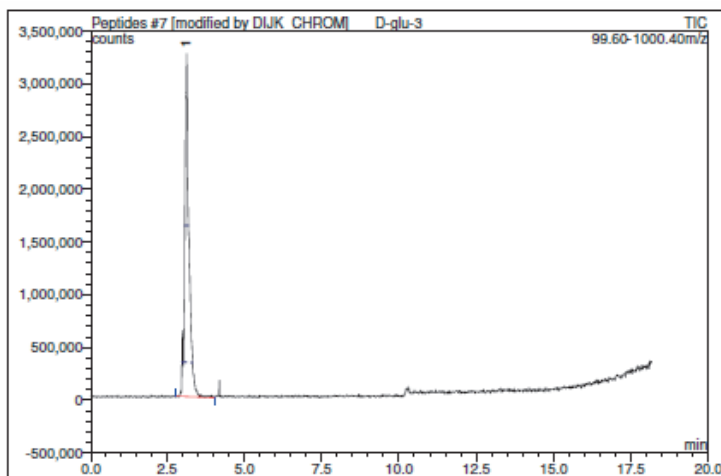


Figure S.II.13. Chiral HPLC trace of D-3. $R_t = 2.38$ min.

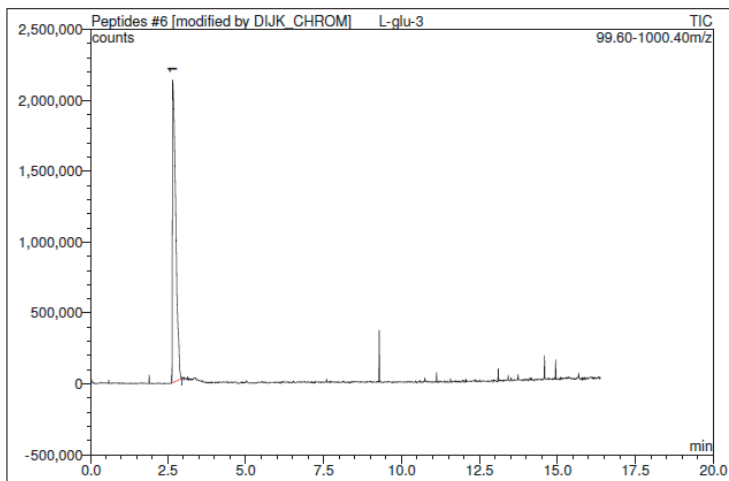


Figure S.II.14. Chiral HPLC trace of L-3. $R_t = 2.48$ min.

References

- [1] J. Schindelin, I. Arganda-Carreras, E. Frise, V. Kaynig, M. Longair, T. Pietzsch, S. Preibisch, C. Rueden, S. Saalfeld, B. Schmid, *Nat Methods* **2012**, *9*, 676-682.



Appendix III: Supporting information for Chapter 4

III.1 Single Crystal X-ray Crystallography

All reflection intensities were measured at 110(2) K using a SuperNova diffractometer (equipped with Atlas detector) with Cu $K\alpha$ radiation ($\lambda = 1.54178 \text{ \AA}$) for [3a]Cl and [5a]Cl and with Mo $K\alpha$ radiation ($\lambda = 0.71073 \text{ \AA}$) for [4a]Cl under the program CrysAlisPro (Versions 1.171.36.32 or 1.171.37.35, Agilent Technologies, 2013-2014). The same program was used to refine the cell dimensions and for data reduction. The structure was solved with the program SHELXS-2014/7^[1] and was refined on F^2 with SHELXL-2014/7.^[1] Analytical numeric absorption correction using a multifaceted crystal model was applied using CrysAlisPro. The temperature of the data collection was controlled using the system Cryojet (manufactured by Oxford Instruments). The H atoms were placed at calculated positions using the instructions AFIX 43 or AFIX 137 with isotropic displacement parameters having values 1.2 or 1.5 U_{eq} of the attached C atoms.

[3a]PF₆: The structure is mostly ordered. The contribution of a very disordered acetone lattice solvent molecule (at least 4 different orientations) has been removed from the final refinement using the Squeeze procedure in Platon.^[2]

[4a]PF₆: The structure is partly disordered. The PF₆⁻ counterion is found disordered over two orientations, and the occupancy factor of the major component of the disorder refines to 0.768(7).

[5a]Cl: The structure is mostly ordered. The crystal that was mounted on the diffractometer was twinned. The twin relationship corresponds to a twofold axis along the [0.9830 0.1273 0.1321] reciprocal axis. The BASF scale factor refines to 0.2154(6). The crystal lattice contains a fair amount of partially occupied and disordered lattice ethanol molecules. As the crystal is twinned and diffracted poorly, the contribution of those lattice solvent molecules was removed in the final refinement *via* the Squeeze procedure^[2] in order to keep the data-to-parameter ratio to an acceptable level.

Table SIII.1 Experimental details for [3a]PF₆

Crystal data	
Chemical formula	C ₂₉ H ₁₉ ClN ₇ Ru·F ₆ P
<i>M_r</i>	747.00
Crystal system, space group	Triclinic, <i>P</i> -1
Temperature (K)	110
<i>a</i> , <i>b</i> , <i>c</i> (Å)	11.6962 (3), 11.7752 (4), 13.0474 (4)
α , β , γ (°)	66.304 (3), 73.164 (2), 77.418 (3)
<i>V</i> (Å ³)	1564.34 (9)
<i>Z</i>	2
Radiation type	Cu <i>K</i> α
μ (mm ⁻¹)	5.94
Crystal size (mm)	0.12 × 0.07 × 0.03
Data collection	
Diffractometer	SuperNova, Dual, Cu at zero, Atlas
Absorption correction	Analytical <i>CrysAlis PRO</i> , Agilent Technologies, Version 1.171.36.32 (release 02-08-2013 <i>CrysAlis171</i> .NET) (compiled Aug 2 2013,16:46:58) Analytical numeric absorption correction using a multifaceted crystal model based on expressions derived by R.C. Clark & J.S. Reid. (Clark, R. C. & Reid, J. S. (1995). <i>Acta Cryst.</i> A51, 887-897)
<i>T</i> _{min} , <i>T</i> _{max}	0.630, 0.858
No. of measured, independent and observed [<i>I</i> > 2σ(<i>I</i>)] reflections	20417, 6125, 5665
<i>R</i> _{int}	0.032
(sin θ /λ) _{max} (Å ⁻¹)	0.616
	Refinement
<i>R</i> [<i>F</i> ² > 2σ(<i>F</i> ²)], <i>wR</i> [<i>F</i> ²], <i>S</i>	0.029, 0.074, 1.05
No. of reflections	6125
No. of parameters	406
H-atom treatment	H-atom parameters constrained
$\Delta\rho_{\max}$, $\Delta\rho_{\min}$ (e Å ⁻³)	0.49, -0.71

Table 2. Experimental details for [4a]PF₆

Crystal data	
Chemical formula	C ₂₃ H ₂₁ ClN ₇ Ru·F ₆ P·C ₃ H ₆ O
<i>M_r</i>	855.13
Crystal system, space group	Monoclinic, <i>C2/c</i>
Temperature (K)	110
<i>a</i> , <i>b</i> , <i>c</i> (Å)	32.2377 (8), 13.6587 (3), 15.3929 (4)
β (°)	94.373 (2)
<i>V</i> (Å ³)	6758.1 (3)
<i>Z</i>	8
Radiation type	Mo <i>K</i> α
μ (mm ⁻¹)	0.67
Crystal size (mm)	0.16 × 0.12 × 0.04
Data collection	
Diffractometer	SuperNova, Dual, Cu at zero, Atlas
Absorption correction	Gaussian <i>CrysAlis PRO</i> , Agilent Technologies, Version 1.171.36.32 (release 02-08-2013 <i>CrysAlis171</i> .NET) (compiled Aug 2 2013,16:46:58) Numerical absorption correction based on gaussian integration over a multifaceted crystal model
<i>T</i> _{min} , <i>T</i> _{max}	0.840, 1.000
No. of measured, independent and observed [<i>I</i> > 2σ(<i>I</i>)] reflections	22327, 6645, 5405
<i>R</i> _{int}	0.038
(sin θ /λ) _{max} (Å ⁻¹)	0.617

Refinement	
$R[F^2 > 2\sigma(F^2)], wR(F^2), S$	0.034, 0.080, 1.06
No. of reflections	6645
No. of parameters	532
No. of restraints	219
H-atom treatment	H-atom parameters constrained
	$w = 1/[\sigma^2(F_o^2) + (0.0273P)^2 + 16.154P]$ where $P = (F_o^2 + 2F_c^2)/3$
$\Delta\rho_{\max}, \Delta\rho_{\min}$ (e Å ⁻³)	0.56, -0.47

Table 3. Experimental details for [5a]Cl

Crystal data	
Chemical formula	C ₃₇ H ₂₃ ClN ₇ Ru-Cl
M_r	737.59
Crystal system, space group	Triclinic, <i>P</i> -1
Temperature (K)	110
a, b, c (Å)	13.6493 (4), 20.4870 (5), 28.9153 (8)
α, β, γ (°)	69.435 (2), 86.421 (2), 85.182 (2)
V (Å ³)	7539.0 (4)
Z	8
Radiation type	Cu K α
μ (mm ⁻¹)	4.94
Crystal size (mm)	0.17 × 0.07 × 0.02
Data collection	
Diffractometer	SuperNova, Dual, Cu at zero, Atlas
Absorption correction	Analytical CrysAlis PRO, Agilent Technologies, Version 1.171.37.35 (release 13-08-2014 CrysAlis171 .NET) (compiled Aug 13 2014, 18:06:01) Analytical numeric absorption correction using a multifaceted crystal model based on expressions derived by R.C. Clark & J.S. Reid. (Clark, R. C. & Reid, J. S. (1995). Acta Cryst. A51, 887-897) Empirical absorption correction using spherical harmonics, implemented in SCALE3 ABSPACK scaling algorithm.
T_{\min}, T_{\max}	0.643, 0.904
No. of measured, independent and observed [$I > 2\sigma(I)$] reflections	67801, 29948, 16371
R_{int}	0.071
$(\sin \theta/\lambda)_{\text{max}}$ (Å ⁻¹)	0.598
Refinement	
$R[F^2 > 2\sigma(F^2)], wR(F^2), S$	0.049, 0.099, 0.77
No. of reflections	29948
No. of parameters	1694
H-atom treatment	H-atom parameters constrained
$\Delta\rho_{\max}, \Delta\rho_{\min}$ (e Å ⁻³)	0.93, -0.77

References

- [1] G. M. Sheldrick, *Acta Crystallogr C Struct Chem* **2015**, *71*, 3-8.
- [2] A. L. Spek, *Acta Crystallogr C Struct Chem* **2015**, *71*, 9-18.

Appendix IV: Supporting information for Chapter 5

S.IV.1 Optimized structures of [1]PF₆ to [5]PF₆ by DFT (COSMO).

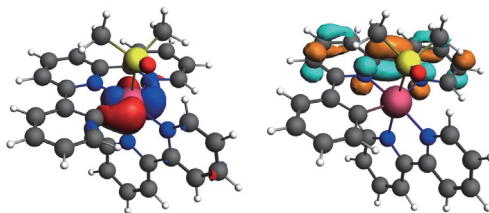


Figure S.IV.1. HOMO (left) and LUMO (right) of [1]PF₆ optimized by DFT (COSMO).

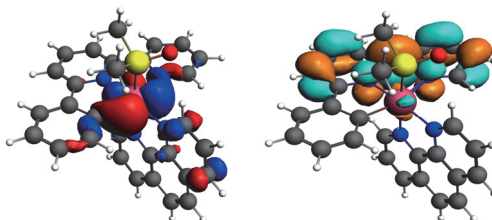


Figure S.IV.2. HOMO (left) and LUMO (right) of [2]PF₆ optimized by DFT (COSMO).

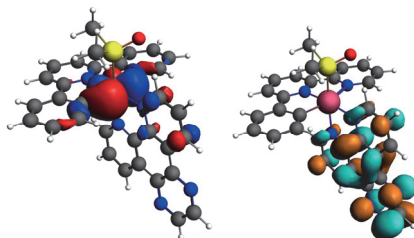


Figure S.IV.3. HOMO (left) and LUMO (right) of [3]PF₆ optimized by DFT (COSMO).

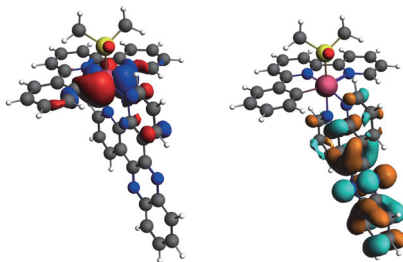


Figure S.IV.4. HOMO (left) and LUMO (right) of [4]PF₆ optimized by DFT (COSMO).

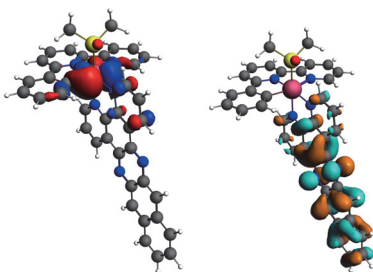


Figure S.IV.5. HOMO (left) and LUMO (right) of [5]PF₆ optimized by DFT (COSMO).

S.IV.2 Chiral HPLC trace of [11-C]PF₆ and [11-A]PF₆

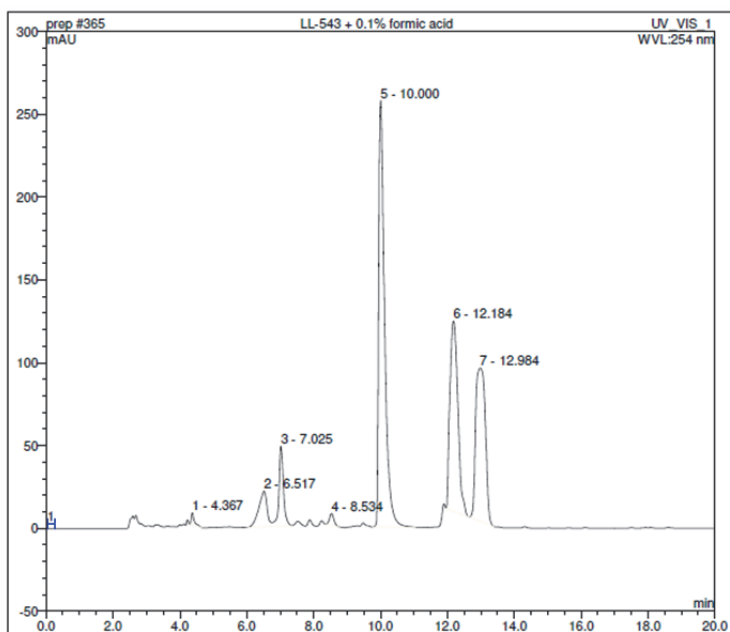
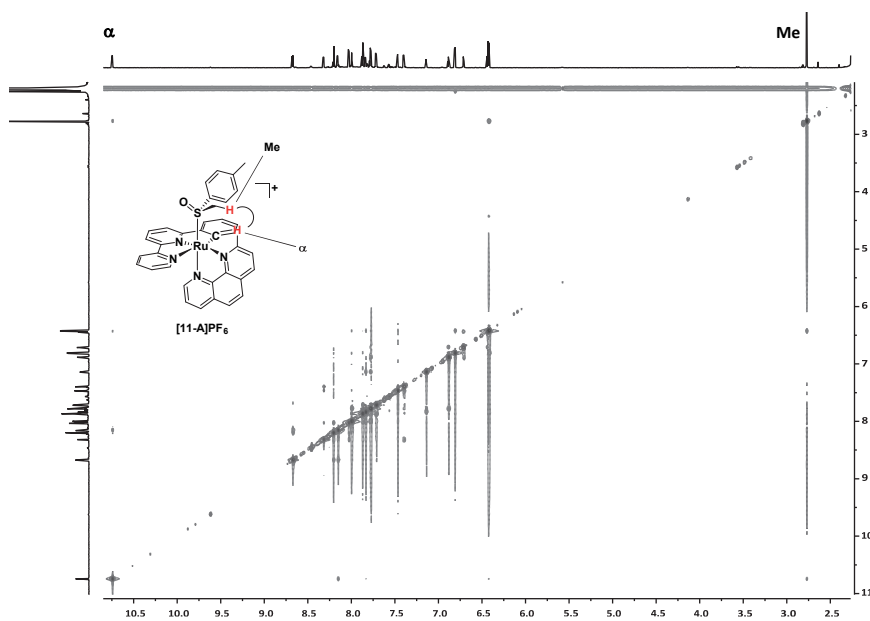
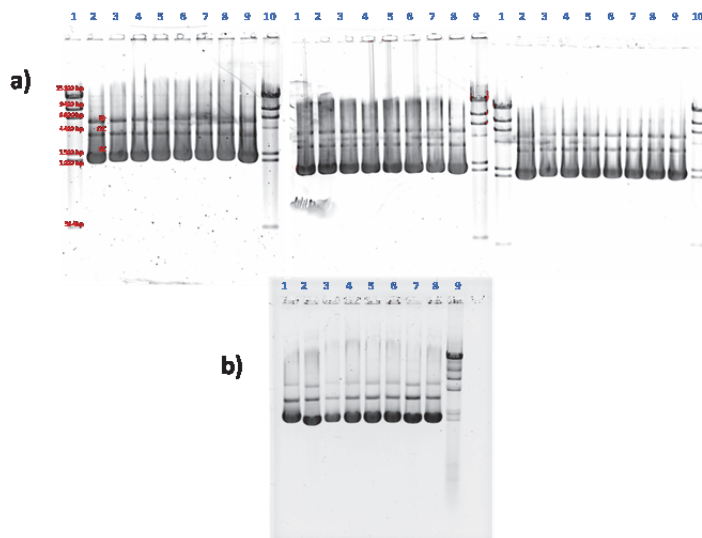


Figure S.IV.6. HPLC trace of [11-C]PF₆ (6, R_t = 12.184 min) and [11-A]PF₆ (7, R_t = 12.984 min).

S.IV.3 NOESY [11-A]PF₆

S.IV.4 Agarose DNA gels



Appendix V: Supporting information for Chapter 6

V.1 ^1H NMR evolution spectra in D_2O

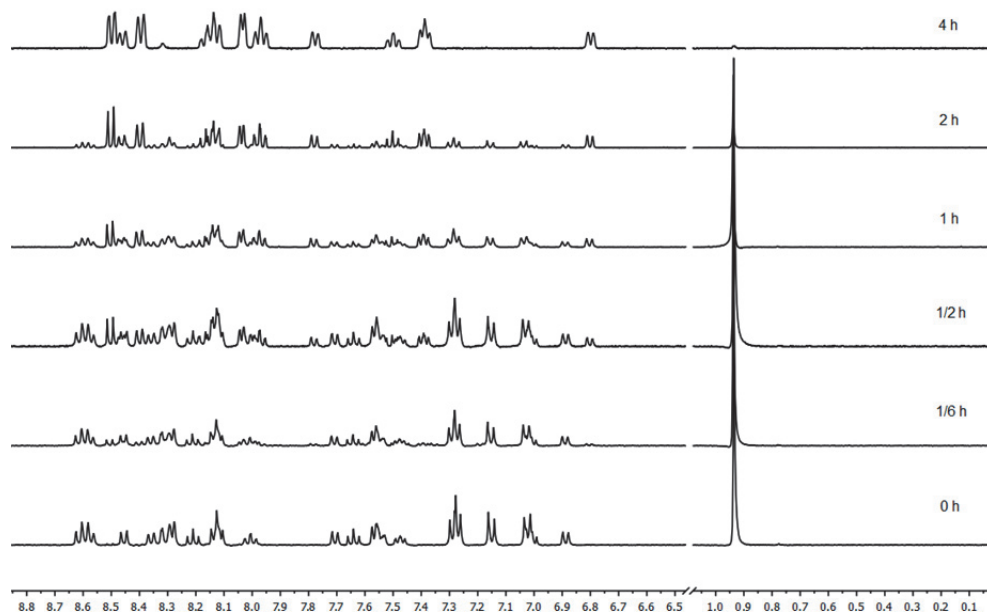


Figure S.V.1. ^1H NMR evolution spectrum of $[\text{1}]\text{Cl}_2$ in D_2O (1 mg in 0.6 mL) irradiated with white light using a 1000 W Xenon arc lamp fitted with a combined 400 nm cutoff filter, and a 610 nm long-pass filter 30 cm from the light source at $T = 298$ K. Spectra were taken at time 0, 10, 30, 60, 120 and 240 minutes on a Bruker 400 NMR.

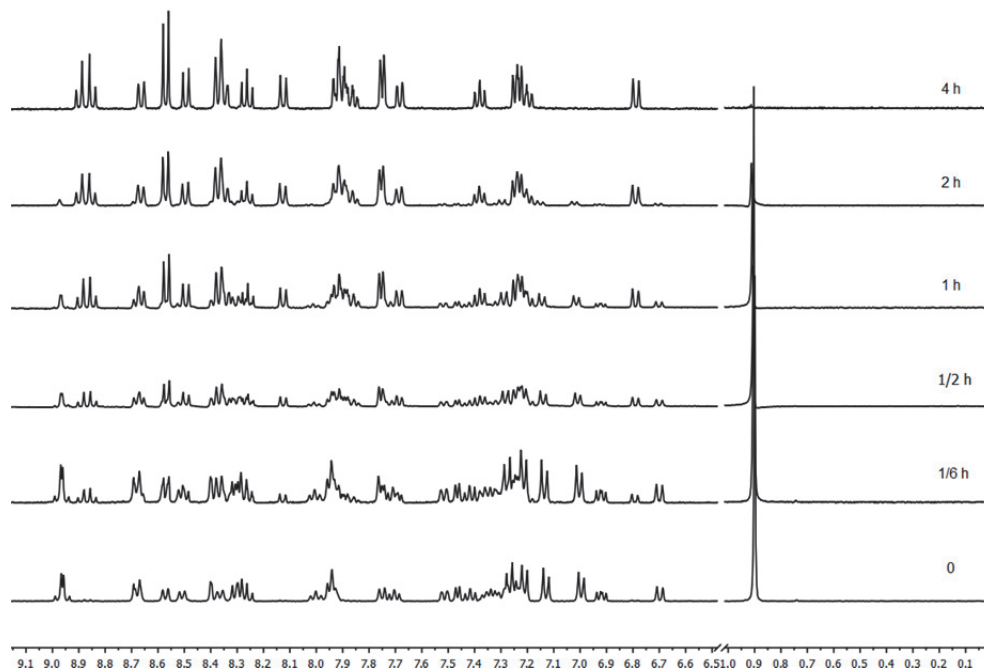


Figure S.V.2. ^1H NMR evolution spectrum of 1 mg of $[2]\text{Cl}_2$ in 0.6 mL D_2O irradiated using a Xenon arc lamp fitted with a combined 400 nm cutoff filter, and a 610 longpass filter 30 cm from the light source at $T = 298$ K. Spectra were taken at intervals $t = 0, 10, 30, 60, 120$ and 240 minutes on a Bruker 400 NMR.

V.2 Cell culturing

General

Human cancer cell lines (A549, human lung carcinoma; MCF-7, human breast adenocarcinoma, A431, human epidermoid) and the non-cancerous cell line MRC-5 (fetal lung fibroblasts) were distributed by the European Collection of Cell Cultures (ECACC), and purchased through Sigma Aldrich. Dulbecco's Minimal Essential Medium (DMEM, with and without phenol red, without glutamine), 200 mM Glutamine-S (GM), trichloroacetic acid (TCA), glacial acetic acid, sulforhodamine B (SRB), tris(hydroxymethyl)aminomethane (tris base), were purchased from Sigma Aldrich. Fetal calf serum (FCS) was purchased from Hyclone. Penicillin and streptomycin were purchased from Duchefa and were diluted to a 100 mg/mL penicillin/streptomycin solution (P/S). Trypsin and Opti-MEM® (without phenol red) were purchased from Gibco® Life Technologies. Trypan blue (0.4% in 0.81% sodium chloride and 0.06% potassium phosphate dibasic solution) was purchased from BioRad. Plastic disposable flasks and 96-well plates were purchased from Sarstedt. Cells were counted using a BioRad TC10 automated cell counter with Biorad Cell Counting Slides. UV-vis measurements for analysis of 96-well plates were performed on a M1000 Tecan Reader. Cells were inspected with an Olympus IX81 microscope.

Cell culturing under normoxia and hypoxia

Cells were cultured in DMEM complete (Dulbecco's Modified Eagle Medium (DMEM) with phenol red, supplemented with 8.0% v/v fetal calf serum (FCS), 0.2% v/v penicillin/streptomycin (P/S), and 0.9% v/v Glutamine-S (GM)). Cells were cultured under humidified conditions, 37 °C atmosphere, 21% O₂ and 7.0% CO₂ in 75 cm² flasks and sub-cultured (1:3 to 1:6 ratio) upon reaching 70-80% confluency (approximately once per week). Media was refreshed every second day. Cells were passaged for 4 - 8 weeks. Cells under hypoxia were cultured under similar conditions, but under an atmosphere of 1.0% O₂ with 7.0% CO₂ in a hypoxic incubator (New Brunswick Galaxy 170R).

V.3 Cell irradiation setup for normoxia and hypoxia

96-well plates were irradiated using the setup described in detail earlier.^[1] For irradiation under hypoxic conditions a Tokai Hit® stage top incubator (INUBG2ETFP-WSKM) with sensor lid for multi-well plate (W-200F) was coupled to a GM-8000 digital gas mixer (Figure S.V.4). 96-well plates were placed in the incubator and the red LED-array described earlier^[1] was placed on top of the sensor lid (give ref van the LEDs). The power-intensity of the red LED array was determined using a custom-built integrating sphere setup and was found to be 23.0 ± 1.5 mW cm⁻² using the setup under hypoxic conditions. Under normoxic conditions the same LED array was placed directly on top of the well plates (with lid), leading to slightly higher power density at the level of the cell monolayer, as reported earlier (34.4 ± 1.7 mW cm⁻²).^[1] In such conditions, 15 min of red light irradiation under hypoxia corresponded to the same dose as 10 min irradiation under normoxia (20.6 J.cm⁻²).

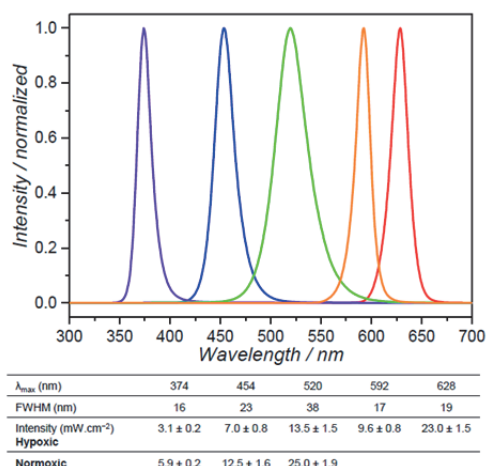


Figure SV.3. Spectroscopic characteristics and light intensities (mW cm⁻²) for each LED at normoxic and hypoxic conditions.

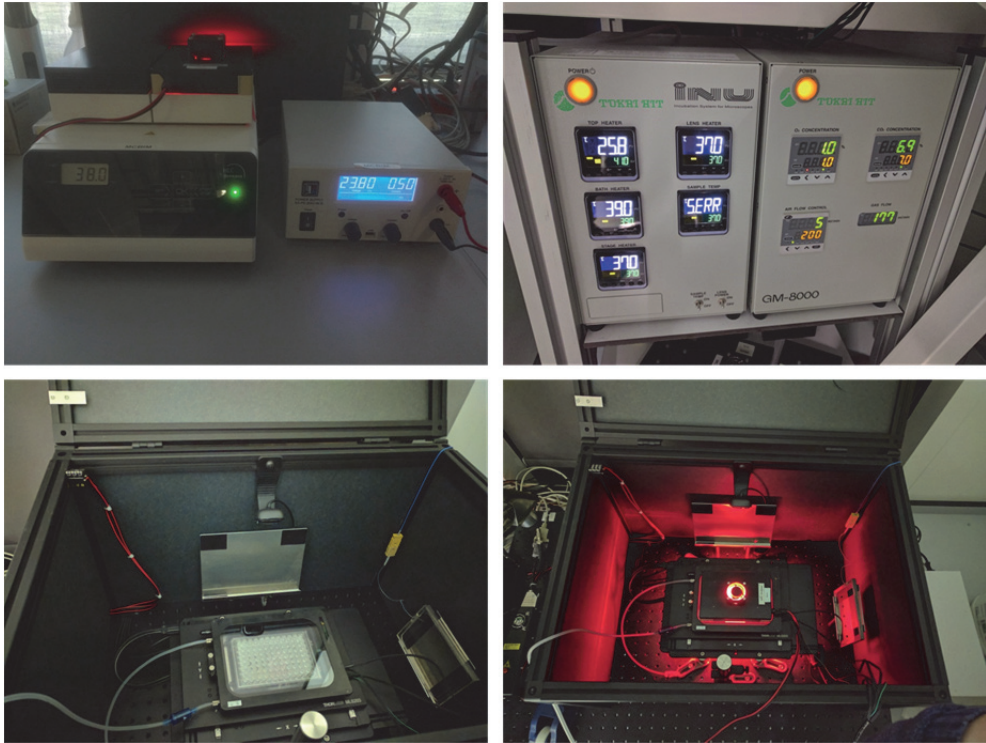


Figure S.V.4. Top left: LED irradiation system fitted with red LED array. Top right: Hypoxic digital gas mixer and stage top incubator temperature controller. Lower left: Stage top incubator with 96-well plate. Lower right: Stage top incubator with 96-well plate fitted with red LED array (on).

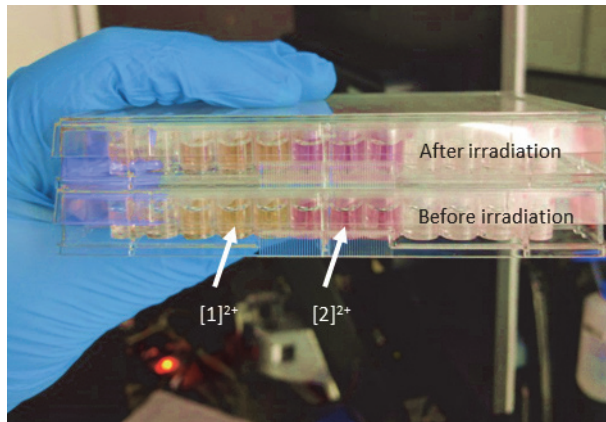


Figure S.V.5. $[1]Cl_2$ and $[2]Cl_2$ before (bottom, orange and pink) and after (top, brown and purple) red light irradiation. Top: $[1]Cl_2$ and $[2]Cl_2$ left in the dark. Bottom: $[2]Cl_2$ and $[2]Cl_2$ after irradiation with 625 nm for 10 minutes in the normoxia setup.

V.4. Cytotoxicity Assay

Treatment under normoxia and hypoxia

The treatment protocol was carried out as described in our previous paper^[2] with the following modifications: Cells were treated with aliquots of test compounds dissolved in OMEM with the exception of STF-31 which was dissolved in 1% DMSO in OMEM, with final concentration not exceeding 0.5% DMSO. Cells were incubated for 6 hours after which one plate was treated with red light (628 ± 19 nm, 34.4 mW $\pm 1.7 \cdot \text{cm}^{-2}$, 10 minutes, $20.6 \cdot \text{J cm}^{-2} \pm 1.02$), while the other was kept in the dark at 37 °C. For treatment under hypoxia, one plate was kept in the hypoxic incubator (New Brunswick Galaxy 170R, 1.0% O₂, 7.0% CO₂) while the other plate was transferred quickly from the hypoxic incubator to the stage top incubator allowing to settle for 15 minutes to reach 37 °C and an atmosphere of 1% O₂ and 7.0% CO₂, followed by irradiation with red light (628 ± 19 nm, 23.0 ± 1.5 mW $\cdot \text{cm}^{-2}$, 15 minutes, $20.6 \cdot \text{J cm}^{-2} \pm 2.03$). After 18 hours medium was replaced with OMEM, and after a total of 96 hours after seeding cells were fixed by adding cold TCA (10% w/v; 100 mL) in each well. The SRB assay was carried out as described before.^[2] All values were determined as the mean of three independent biological experiments, with three technical triplicates for each biological replicate. Results are summarized in table S.V.1.

Table S.V.1. (Photo)cytotoxicity of [1]Cl₂, [2]Cl₂ and STF-31 expressed as effective concentrations (EC₅₀ in μM) in the dark and after irradiation with red light (628 ± 19 nm, 34.4 mW $\pm 1.7 \cdot \text{cm}^{-2}$, 10 minutes, $20.6 \cdot \text{J cm}^{-2} \pm 1.02$) under normoxic (21% O₂) conditions versus A549, A431, MCF-7 and MRC-5 cells. And versus A549 and A431 cells under hypoxic (1.0% O₂) conditions with red light (628 ± 19 nm, 23.0 ± 1.5 mW $\cdot \text{cm}^{-2}$, 15 minutes, $20.6 \cdot \text{J cm}^{-2} \pm 2.03$).

Cell line	% O ₂	Light dose (J cm ²)	[1]Cl ₂			[2]Cl ₂			STF-31		Cisplatin	
			EC ₅₀	CI	PI	EC ₅₀	CI	PI	EC ₅₀	CI	EC ₅₀	CI
A549	20	0	8.9	+2.7	0.93	20.3	+2.9	2.6	4.4	+2.1	4.8	+0.89
				-2.1			-2.5			-1.5		-0.76
	1	20.6	9.6	+2.1		7.7	+1.4		4.2	+1.7	-	
				-1.8	1.2	45.6	+9.1	2.4	10.8	+5.7	7.5	+1.7
A431	20	0	20.6	+9.4		45.6	+9.1		10.8	+5.7	7.5	+1.7
				-6.0			-7.3			-3.7		-1.4
	1	20.6	17.9	+6.4		18.7	+5.8		-		-	
				-4.6			-4.3					
MCF-7	20	0	5.9	+2.1	0.67	23.6	+4.2	3.3	2.9	+0.79	6.6	+0.94
				-1.7			-3.5			-0.66		-0.81
	1	20.6	8.8	+2.4		7.1	+2.0		3.2	+0.73	-	
				-1.9	1.1	34.6	+3.8	3.6	21	+7.2	11.6	+2.2
MRC-5	20	0	10.7	+4.2		34.6	+3.8		21	+7.2	11.6	+2.2
				-3.0			-3.5			-5.1		-1.8
	1	20.6	9.9	+3.3		9.6	+2.1		-		-	
				-2.5	1.3	20.5	+3.6	1.6	4.8	+2.6	10.6	+1.9
MCF-7	20	0	12.7	+4.8		20.5	+3.6	1.6	4.8	+2.6	10.6	+1.9
				-3.6			-3.1			-1.8		-1.5
	1	20.6	16.8	+4.3		13.1	+1.5		6.2	+2.5	-	
				-3.4	1.3	45.8	+11.9	2.4	11.8	+4.0	5.9	+1.4
MRC-5	20	0	26.1	+10.2		45.8	+11.9	2.4	11.8	+4.0	5.9	+1.4
				-6.9			-9.3			-3.0		-1.1
	1	20.6	20.5	+7.1		18.8	+6.3		10.5	+3.4	-	
				-5.2			-4.7			-2.6		

V.5 NBDG uptake

A549 cells were seeded in 6.5 cm² dishes at a density of 2.5×10^5 per well in OMEM. After 24 hours, reaching a confluency of ~80%, the media was aspirated and the cells were washed 3 x times with 1 mL PBS. Vehicle control, STF-31 (50 μ M) and phloretin (250 μ M) dissolved in phenol-red and glucose-free DMEM[®] media were then added to each well (V = 1.0 mL). After incubating for one hour at 37 °C, 0.5 mL of a stock solution (300 μ g/mL) of 2-[N-(7-nitrobenz-2-oxa-1,3-diazol-4-yl) amino]-2-deoxy-D-glucose (2-NBDG, Cayman Chemical Company) in MilliQ was added. At t = 3 h, media was removed and each well was washed with cold PBS twice and cells were trypsinized (500 μ L), glucosefree medium with 2.5 % FCS was added (500 μ L) and the content of the well were transferred to 1.5 mL Smart-Lock Eppendorf[®] Cups. After centrifugation (5 min, 1200 RCF, rt), the supernatant was gently removed, cells were resuspended in 0.5 mL DMEM glucosefree medium and transferred to a 96-well plate with V = 200 μ L per well. One out of two groups were stained with prodium iodide (PI) with $c_{\text{final}} = 1 \mu\text{g/mL}$. Flow cytometry analysis was performed within 30 minutes on a FACSCanto II (Becton Dickinson, Franklin Lakes, NJ). The cells were examined on 4 different parameters: relative size (Forward Scatter), granularity or internal complexity (Side Scatter), and FITC-A ($\lambda_{\text{ex}} = 488 \text{ nm}$, $\lambda_{\text{em}} = 530 \pm 15 \text{ nm}$) and APC-A ($\lambda_{\text{ex}} = 633 \text{ nm}$, $\lambda_{\text{em}} = 660 \pm 10 \text{ nm}$) for 2-NBDG and PI, respectively. Ten thousand events were recorded in the gated region within 100 seconds, and data were analyzed using FlowJo software (Treestar, Ashland, OR). Healthy cells were defined as propidium iodide (PI)-negative, and necrotic cells were defined as PI-positive.

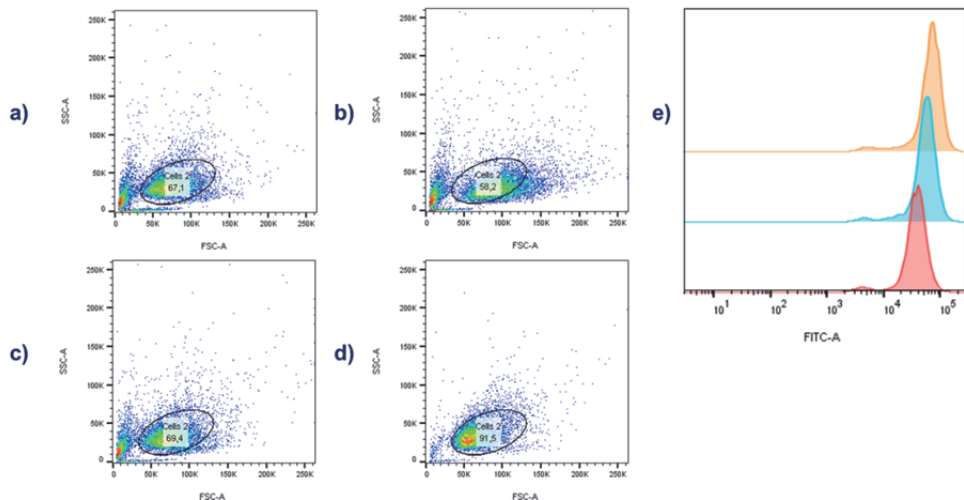


Figure S.V.6. Dot plots of a). Control with only NBDG. b). Phloretin (250 μ M). c). STF-31 (50 μ M) and negative control containing only medium (DMEM glucosefree). Dot plots are representative of three independent experiments. e). Histograms showing fluorescence of 2-NBDG ($\lambda_{\text{ex}} = 488 \text{ nm}$) after 3 hour treatment with control (top), 50 μ M STF-31 (middle) and 100 μ M phloretin (lower).

V.6 NAMPT assay

The Cyclex® NAMPT assay (Sanbio BV Biologicals) was carried out as described in the company manual using method II with the following modifications: Half the concentration of each component in the kit was used to allow measurements over a longer period of time and to prevent oversaturation of the absorbance for the control wells. The IC_{50} of compound **[2]**Cl₂ and STF-31 were determined by measuring the reaction rate for four different concentrations of compound. Stock solutions for STF-31 and **[2]**Cl₂ were diluted in DMSO to four different concentrations. For **[2]**Cl₂ an aliquot of the stock solution was irradiated for 10 minutes in the normoxia setup and further diluted in DMSO. Slopes were determined using linear regression during the linear range (0-10 minutes) and then the slope of regression lines was plotted against compound concentration. Using the dose-response curve the inhibition concentration IC_{50} (defined as the concentration of drug that inhibits the enzyme activity by 50%) was calculated by fitting the curves using a non-linear regression function with fixed Y maximum (100%) and minimum (0%) (relative cell viability), and a variable Hill-slope, resulting in the simplified two-parameter Hill-slope equation 2. All graphs were plotted using Graphpad Prism 7, Graphpad Software Inc.

$$\frac{100}{(1 + 10^{((\log_{10} IC_{50} - X) \times Hill\ Slope)})}$$

Equation V.1

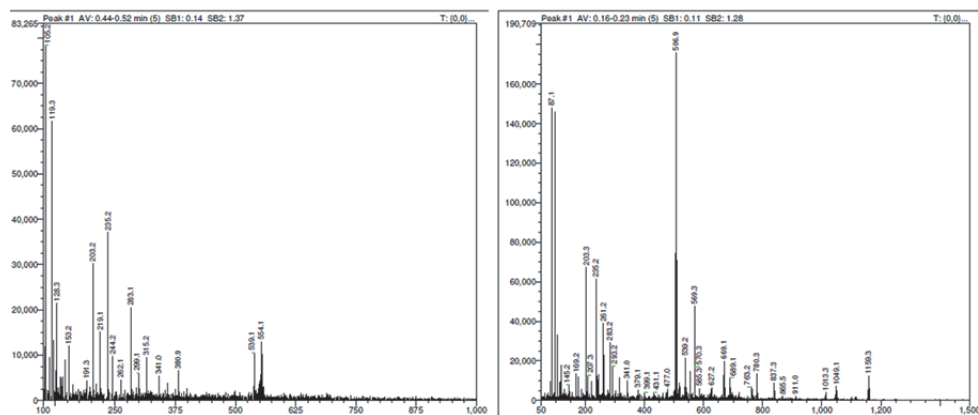


Figure S.V.7. Left: MS spectrum showing conversion of **[1]**Cl₂ to **[Ru(tpy)(dmbpy)Cl]⁺** after 48 hours exposure to OMEM. Right: **[2]**Cl₂ after 48 hours.

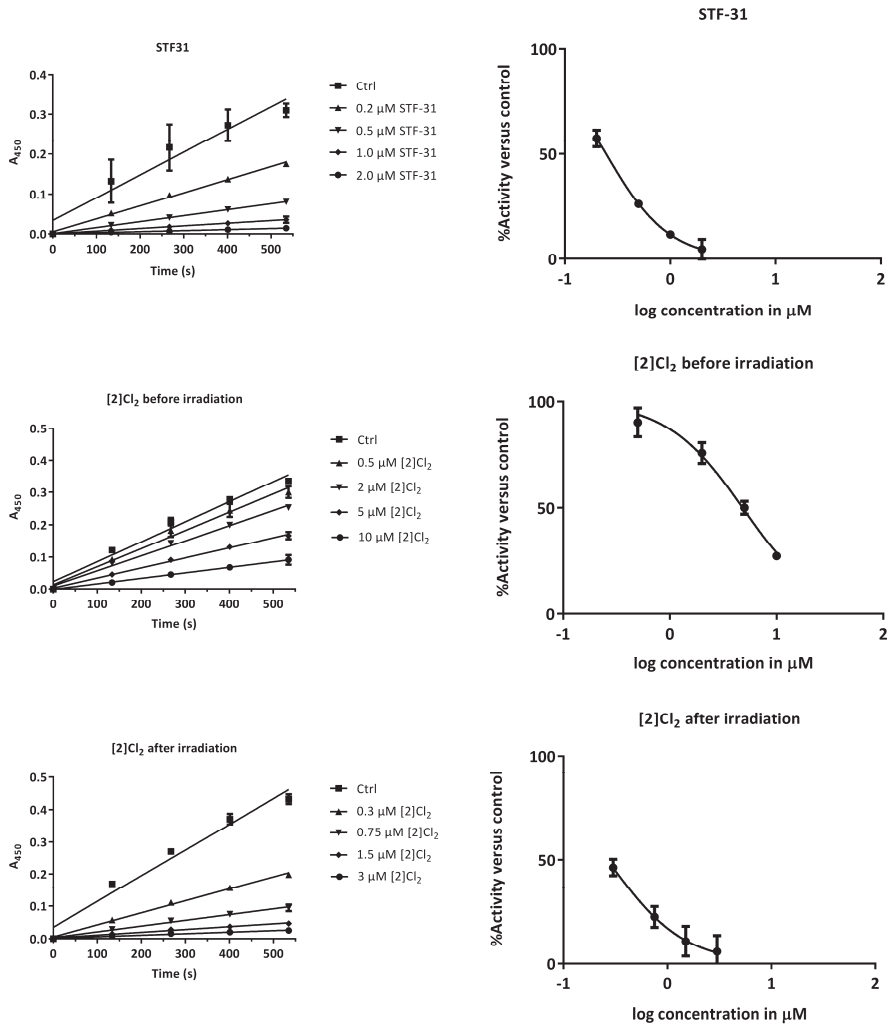


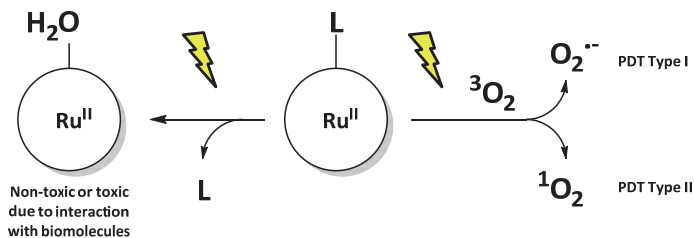
Figure S.V.8. Left: A_{450} of formazan against time (s) at different concentrations of STF-31, $[2]Cl_2$ -dark and $[2]Cl_2$ -light. $[2]Cl_2$ before and after irradiation with red light versus absorbance of formazan at 450 nm. Right: Dose response curves of %activity of enzyme versus the logarithm of concentration of substrate in μM .

References

- [1] S. L. Hopkins, B. Siewert, S. H. Askes, P. Veldhuizen, R. Zwier, M. Heger, S. Bonnet, *Photobiol Sci* **2016**, *15*, 644-653.
- [2] L. N. Lameijer, S. L. Hopkins, T. G. Breve, S. H. Askes, S. Bonnet, *Chem Eur J* **2016**, *22*, 18484-18491.

Samenvatting

Conventionele chemotherapie is naast chirurgie en bestraling een van de voornaamste therapieën om kanker te bestrijden. Een groot nadeel is echter dat deze vorm van therapie vele bijwerkingen veroorzaakt in kankerpatiënten, omdat de drugs die worden gebruikt niet alleen de kankercellen, maar ook gezonde cellen aanvallen. Een mogelijke oplossing voor dit probleem is het lokaal activeren van zogenoemde ‘prodrugs’ met een externe stimulus, zoals licht. Zichtbaar licht (400 – 650 nm) kan tot een centimeter door de huid doordringen, waardoor er kan worden gereguleerd waar en wanneer de drugs worden geactiveerd. Dit biedt mogelijkheden om vormen van kanker te behandelen waar conventionele therapieën geen uitkomst bieden. In het veld van bioorganische chemie worden ruthenium(II) polypyridyl prodrugs (Ru-L) bestudeerd als mogelijke licht-actieveerbare verbindingen waarbij fotoactivatie leidt tot het verbreken van de Ru-L band. Hierbij komt óf een organisch ligand L en een gesolvateerd Ru-OH₂ adduct vrij (Fig 1, links), óf wordt er een fotodynamisch effect bewerkstelligd via het genereren van superoxide of singlet zuurstof (Fig 1, rechts). In theorie kan het geactiveerde deeltje, zoals bijvoorbeeld [Ru(tpy)(bpy)(H₂O)]²⁺ (bpy = 2,2'-bipyridine, tpy = 2,2':6',2''-terpyridine), reageren met in het menselijke lichaam aanwezige verbindingen als amines, thioethers of purines en pyrimidines, die aanwezig zijn in aminozuren, RNA, en DNA. Onder fysiologische condities kan de reactiviteit van deze biologische moleculen met [Ru(tpy)(bpy)H₂O]²⁺ leiden tot adducten zoals deze worden gevormd met cisplatina, hetgeen mogelijk leidt tot celdood. Echter, niet alle rutheniumverbindingen zijn toxisch en de rol van de liganden die achterblijven na fotosubstitutie speelt een kritische rol in de cytotoxiciteit van het gesolvateerde rutheniumadduct. Tegelijkertijd wordt ook een organisch ligand vrijgemaakt, hetgeen een drug kan zijn met een gedefinieerd doelwit en bekende modus operandi.



Figuur 1. Versimpeld diagram van het principe van foto-geactiveerde chemotherapie (PACT) gebaseerd op ruthenium(II) verbindingen. Twee verschillende mechanismen zijn afgebeeld: Links: Na bestraling met licht wordt een ligand of drug (L) losgelaten waarbij een gesolvateerd ruthenium deeltje wordt gevormd (Ru-OH₂). Rechts: De ruthenium(II) prodrug gedraagt zich als een fotodynamisch agens via fotodynamisch therapie type I of type II.

Dit proefschrift beschrijft de synthese van nieuwe *foto-geactiveerde chemotherapie* (PACT) drugs gebaseerd op het $[\text{Ru}(\text{tpy})(\text{NN})\text{L}]^{n+}$ manifold en de mogelijke biologische toepassing hiervan als medicijn tegen kanker.

In hoofdstuk 2 is de synthese beschreven voor het onafhankelijk modificeren van elke positie (O1-O6) van D-glucose met een methylthioether groep. Deze verbindingen zijn vervolgens gebruikt als liganden voor niet-toxische, maar fotoactieve ruthenium complexen met de formules $[\text{Ru}(\text{tpy})(\text{bpy})(\text{L})]^{2+}$, $[\text{Ru}(\text{S-tpy})(\text{bpy})(\text{L})]^+$ (S-tpy = [2,2':6',2''-terpyridine]-4'-sulfonzuur) en $[\text{Ru}(\text{bpy})_2(\text{L})]^{2+}$. Het idee achter deze benadering was om te bepalen welke modificaties worden getolereerd door zogenoemde glucose-transporters (GLUTs). De belangrijkste uitdaging in dit werk was de synthese van respectievelijk de 2-O en de 4-O gemodificeerde suikers, omdat de geïntroduceerde functionele groep (methylthioether) het gebruik van benzyli(deen) beschermgroepen onmogelijk maakte.

Conventionele methoden om glucoseopname te bepalen via GLUTs maken gebruik van competitieve inhibitie met GLUT-inhibitoren zoals floretine. Bij deze benadering zijn de condities die worden gebruikt voor de analyse van cytotoxiciteit echter niet volledig nagebootst, wat de interpretatie van deze experimenten bemoeilijkt. In hoofdstuk 3 wordt een methode beschreven waarmee is onderzocht of een glucoseconjugaat actief wordt opgenomen door een glucose-transporter door de efficiëntie van de opname van twee chemisch equivalente glucose-enantiomeren (D/L) met elkaar te vergelijken. De synthese van de conjugaten wordt beschreven, waarbij de thioether gefunctionaliseerde glucoseliganden (D/L) zijn gecoördineerd aan het lipofiele $[\text{Ru}(\text{tpy})(\text{dppn})(\text{OH}_2)]^{2+}$ (dppn = benzo[*ij*]dipyrido-[3,2-*a*:2',3'-*c*]phenazine) complex. Tevens is de cytotoxiciteit, de opname in kankercellen en de lokalisatie van deze complexen in de cellen bepaald. Het gebruik van enantiomeren liet een eerlijke vergelijking van de cytotoxiciteit van beide conjugaten toe. Waarbij een vergelijking tussen het suikerconjugaat het 'normale' conjugaat niet zouden corrigeren voor het verschil in chemische structuur, polariteit en hydrofiliciteit. Submicromolaire waarden voor cytotoxiciteit zijn gevonden voor $[\text{Ru}(\text{tpy})(\text{dppn})(\text{L})]^{2+}$, welke zijn toegeschreven aan de fotodissociatie van L, resulterend in de verbinding $[\text{Ru}(\text{tpy})(\text{dppn})(\text{OH}_2)]^{2+}$. Dit geactiveerde deeltje heeft een bijzonder hoge affiniteit voor binding aan DNA, terwijl tegelijkertijd grote hoeveelheden reactieve zuurstofdeeltjes worden gegenereerd door bestraling met licht. Opmerkelijk genoeg is gevonden dat de D- en L-glucose-rutheniumconjugaten niet even cytotoxisch zijn in het donker, maar kan dit verschil niet worden toegeschreven aan opname via een glucose-transporter. Uit lokalisatiestudies bleek dat beide complexen aanwezig waren in de mitochondrieën. Onafhankelijk van het stadium van de groeifase, de toevoeging van een remmer van oxidatieve fosforylering (natrium azide) of de incubatietijd, werden beide verbindingen in dezelfde mate opgenomen. Dit duidt erop dat opname van deze complexen waarschijnlijk passief gebeurt, en kan het verschil in cytotoxiciteit worden toegeschreven aan een

enzymatisch proces na opname, zoals verschil in snelheid van uitscheiding of het enzymatische afbreken van de β -glycosidische band door een β -glucosidase. Hoewel de ruthenium-glucoseconjugaten die beschreven zijn in dit hoofdstuk niet worden opgenomen door glucose-transporters, maken de selectieve lokalisatie van de prodrugs, de hoge affiniteit die zij hebben voor mitochondriaal DNA en de efficiëntie voor de productie van singletzuurstof van deze complexen (0.71) hen bijzonder geschikte kandidaten voor fotodynamische therapie (PDT).

Op basis van de bevindingen beschreven in het hoofdstuk 3, wordt in hoofdstuk 4 gerapporteerd hoe zestien verschillende complexen gebaseerd op het $[\text{Ru}(\text{tpy})(\text{NN})(\text{L})]^{2+}$ manifold uitgebreid bestudeerd zijn op zowel hun biologische activiteit en opname in kankercellen als hun fotochemische eigenschappen. Hierbij is vooral gekeken naar het verschil tussen fotodynamische therapie en PACT. Door zowel de productie van singletzuurstof als de efficiëntie van fotosubstitutie te meten, is inzicht verkregen in de manier waarop deze metaalcomplexen werken. Structurele veranderingen van het bidentaat ligand NN in $[\text{Ru}(\text{tpy})(\text{NN})(\text{L})]^{2+}$ leiden tot verschillende fotochemische en biologische activiteit. Een van de belangrijkste bevindingen beschreven in hoofdstuk 4 is dat de structureel gelijkende analogons $[\text{Ru}(\text{tpy})(\text{dppz})(\text{L})]^{2+}$ (dppz = dipyrido[3,2- α :2',3'-c]phenazine) en $[\text{Ru}(\text{tpy})(\text{dppn})(\text{L})]^{2+}$ fotocytotoxiciteit veroorzaken door respectievelijk een PACT- en PDT-mechanisme. Ook bleek het complex $[\text{Ru}(\text{tpy})(\text{dppn})\text{Cl}]\text{Cl}$ sterk cytotoxisch tegen A549 and MCF-7 kankercellen na activatie met blauw licht. Dit is opmerkelijk, omdat de efficiëntie van singletzuurstofproductie voor deze verbinding erg laag is. Het is daarom aannemelijk dat deze verbinding hydrolyseert na opname waarbij $[\text{Ru}(\text{tpy})(\text{dppn})(\text{OH}_2)]^{2+}$ wordt verkregen, hetgeen een sterke PDT-verbinding is, zoals beschreven in hoofdstuk 3. Andere bevindingen beschreven in dit hoofdstuk zijn dat van de analogons $[\text{Ru}(\text{tpy})(\text{azpy})(\text{L})]^{2+}$ (azpy = 2-(phenylazo)pyridine) en $[\text{Ru}(\text{tpy})(\text{pymi})(\text{L})]^{2+}$ (pymi = ((*E*)-*N*-phenyl-1-(pyridin-2-yl)methanimine) alleen de laatste fotoreactief is en dat verhoogde intracellulaire opname in kankercellen niet per sé leidt tot verhoogde (foto)cytotoxiciteit. Een belangrijke bevinding is dat de verbinding $[\text{Ru}(\text{tpy})(\text{dppn})(\text{SRR}')](\text{PF}_6)_2$, beschreven in hoofdstuk 3, een unieke prodrug is welke volgens zowel het PACT- als PDT-mechanisme werkt.

De meeste metaalcomplexen beschreven in hoofdstuk 4 bleken niet cytotoxisch na activering met licht. Nieuwe metaalcomplexen gebaseerd op het in dit proefschrift beschreven $[\text{Ru}(\text{tpy})(\text{NN})(\text{L})]^{2+}$ manifold zijn daarom ontworpen als alternatieve, monokationische PACT-verbindingen. De gecyclometallegeerde complexen die in de literatuur zijn beschreven absorberen vaker bij een langere golflengte dan niet-gecyclometallegeerde verbindingen. Tevens zijn ze vaak meer cytotoxisch voor kankercellen. Omdat de symmetrie in het $[\text{Ru}(\text{tpy})(\text{NN})(\text{L})]^{2+}$ manifold vervalt wanneer een van de buitenste stikstofatomen in het tridentaat ligand wordt vervangen door een

koolstofatoom, ontstaat een chirale verbinding. In hoofdstuk 5 is beschreven hoe twee diastereoisomeren gebaseerd op $[\text{Ru}(\text{phbpy})(\text{phen})(\text{SORR}')^+]^+$ (Hphbpy = 6'-phenyl-2,2'-bipyridyl, SORR' = (R)-methyl *p*-tolylsulfoxide) zijn gesynthetiseerd en van elkaar zijn gescheiden op een chirale kolom. Tevens is er een uitgebreide studie gedaan naar de fotofysische eigenschappen van racemische mengsels van complexen gebaseerd op $[\text{Ru}(\text{phpy})(\text{NN})(\text{dmsO-kS})]^+$ met een toenemende grootte van het aromatisch systeem van de bidentaat liganden (NN = bpy, dpq, phen, dppz and dppn, dpq = pyrazino[2,3-*f*][1,10]phenanthroline, phen = 1,10-phenanthroline). In vergelijking tot de tpy analogons beschreven in hoofdstuk 4, hebben deze gecyclometalleerde complexen een veel lager fotosubstituerendement. Voor de complexen met het bidentaat ligand dppz of dppn is de mogelijkheid tot fotodissociatie zelfs volledig afwezig. Dichtheidsfunctionaaltheorieberekeningen en cyclische voltammetrie hebben verder laten zien dat de verminderde fotoreactiviteit van deze complexen het resultaat is van een groter verschil in energie tussen de $^3\text{MLCT}$ (triplet metaal-naar-ligand ladingsoverdrachttoestand) - en ^3MC -toestand (triplet metaalgecentreerde toestand), waardoor thermische populatie van de ^3MC -toestand vanuit de gegenereerde $^3\text{MLCT}$ aangeslagen toestand minder waarschijnlijk is. De bredere absorptieband van deze complexen stond toe dat drie van hen kunnen worden geactiveerd met groen licht (520 nm) in A549 and MCF-7 cellen, waarbij submicromolaire fotocytotoxiciteit kon worden bewerkstelligd. Dit moet waarschijnlijk worden toegeschreven aan een PDT type-I mechanisme, maar de lokalisatie, het doelwit en de modus operandi van deze verbindingen zal verder moeten worden onderzocht.

Een nadeel van de huidige lichtactiveerbare ruthenium(II)-polypyridyl prodrugs is dat deze meestal worden geactiveerd met golflengtes die ver buiten het fotherapeutische gebied vallen (600 – 850 nm). In hoofdstuk 3 – 5 is beschreven dat niet sterisch-gehinderde complexen gebaseerd op $[\text{Ru}(\text{tpy})(\text{NN})(\text{L})]^{2+}$ of $[\text{Ru}(\text{phbpy})(\text{NN})(\text{L})]^+$ kunnen worden geactiveerd met blauw of groen licht. Deze golflengten hebben echter een beperkte penetratiediepte in weefsel. Hoewel er systemen worden ontwikkeld om rood licht om te zetten naar blauw licht, is de efficiëntie van fotoactivering vaak laag waardoor toepassing in biologische systeem problematisch blijft. In het verleden heeft de groep van Bonnet sterisch-gehinderde rutheniumverbindingen gesynthetiseerd gebaseerd op $[\text{Ru}(\text{tpy})(\text{NN})(\text{L})]^{2+}$, met 6,6'-dimethyl-2,2'-dipyridyl (dmbpy) of 2,2'-biquinoline (biq) als bidentaat ligand. Hoewel een hoog kwantumrendement voor fotodissociatie kon worden verkregen wanneer een thioether als monodentaat ligand (L) werd gebruikt, bleken deze verbindingen erg instabiel en dus niet geschikt te zijn om te worden gebruikt als fotoactieve prodrugs. Sterische, niet gehinderde pyridine liganden (L) daarentegen, hebben een lager kwantumrendement voor fotodissociatie, maar zijn veel stabiel in het donker. In hoofdstuk 6 worden de twee complexen $[\text{Ru}(\text{tpy})(\text{dmbpy})(\text{STF-31})]^{2+}$ en $[\text{Ru}(\text{tpy})(\text{biq})(\text{STF-31})]^{2+}$ beschreven, welke de bekende NAMPT-remmer (NAMPT =

nicotinamide phosphoribosyltransferase) STF-31 als monodentaat ligand bevatten. De binding van de pyridinegroep van STF-31 aan het ruthenium(II)-centrum resulteerde in nieuwe ¹MLCT absorptiebanden, waardoor activatie met dieper doordringend rood licht mogelijk werd. Ondanks de relatieve lage molaire absorptiecoëfficiënt voor rood licht, kunnen deze verbindingen binnen tien minuten volledig geactiveerd worden door de hoge efficiëntie voor fotosubstitutie bij lichaamstemperatuur (37 °C). Er is gekeken naar het effect van [Ru(tpy)(biq)(STF-31)]²⁺ op cellen bij zowel normale (21%) als lage zuurstofconcentraties (1%); de resultaten laten zien dat het vrijmaken van de verbinding STF-31 leidt tot een fotocytotoxisch effect onder zowel hypoxische als normoxische condities. Het feit dat dit gebeurt zonder verlies van fotocytotoxiciteitindex, (de ratio tussen de celdood in het donker en in het licht) – hetgeen wel zou gebeuren bij zuurstofafhankelijke fotodynamische therapie - is de eerste demonstratie van de potentie van PACT ten opzichte van PDT, aangezien kankercellen vaak zuurstofarm zijn.



Curriculum Vitae

Lucien Lameijer was born in Nieuweschans on the 14th of August in 1985. After obtaining his high school diploma (HAVO) in 2005 at the ID College Gouda, he started studying chemistry at the Hogeschool Leiden. During this bachelor program he took courses from the BSc program Molecular Science & Technology at Leiden University and performed a research internship under the supervision of Dr. Wouter Hogendorf and Prof. Dr. Gijs van der Marel at the Biosyn group. During this internship he synthesized phosphoramidites based on *N*-acetyl glucosamine as precursors for teichoic acid fragments. He received his BSc degree in Applied Sciences (BASC) in May 2011, after which he continued his studies with a master Chemistry (Design & Synthesis) at Leiden University. A second research internship was carried out as part of his MSc curriculum on the synthesis of an orthogonally protected supernucleoside under the supervision of Dr. Hans Kistemaker and Dr. Dmitri Filippov at the Biosyn group. He obtained his MSc degree in May 2013.

In July 2013, he started as a PhD candidate in the research group “Metals in Catalysis, Biomimetics & Inorganic Materials” (MCBIM) at Leiden University. Under the supervision of Dr. Sylvestre Bonnet and Prof. Dr. Lies Bouwman he conducted the research presented in this thesis. Posters on parts of his work have been presented at the HRSMC symposium (2015 Amsterdam, ‘Best poster prize’), CHAINS conference (2015, Veldhoven) and Gordon Research Conference ‘Metals in Medicine’ (2016, Andover, NH, USA). At CHAINS 2016, Lucien gave an oral presentation on “*D- versus L-glucose conjugation: Mitochondrial Targeting of a Light-Activated Ruthenium-Based Anticancer Prodrug*”.

During the course of his graduate program he participated in the following courses:

- HRSMC summer school “Advanced Metal-Organic Chemistry and Catalysis”
- HRSMC Photochemistry school “Photochemistry, Fundamentals and Applications”
- HRSMC Physical Methods in Inorganic Chemistry
- Effective Communication
- Communication in Science
- On Being a Scientist
- Time Management



List of publications

- 1. A red light-activated ruthenium-caged NAMPT inhibitor remains phototoxic in hypoxic cancer cells**
L. N. Lameijer, D. Ernst, S. L. Hopkins, M. S. Meijer, S. H. C. Askes, S. E. Le Devedec, S. Bonnet, *Angew Chem Int Ed* **2017**, *56*, 11549-11553.
- 2. D- Versus L-Glucose Conjugation: Mitochondrial Targeting of a Light-Activated Dual-Mode-of-Action Ruthenium-Based Anticancer Prodrug**
L. N. Lameijer, S. L. Hopkins, T. G. Brevé, S. H. C. Askes, S. Bonnet, *Chem Eur J* **2016**, *22*, 18484-18491.
- 3. Synthesis of Well-Defined Adenosine Diphosphate Ribose Oligomers**
H. A. V. Kistemaker, L. N. Lameijer, N. J. Meeuwenoord, H. S. Overkleeft, G. A. van der Marel, D. V. Filippov, *Angew Chem Int Ed* **2015**, *54*, 4915-4918.
- 4. Fluorous linker facilitated synthesis of teichoic acid fragments**
W. F. Hogendorf, L. N. Lameijer, T. J. Beenakker, H. S. Overkleeft, D. V. Filippov, J. D. Codee, G. A. Van der Marel, *Org Lett* **2012**, *14*, 848-851.
- 5. Photodynamic therapy or photoactivated chemotherapy? A thorough study of glycoconjugates based upon the [Ru(tpy)(NN)(L)]²⁺ scaffold**
L. N. Lameijer, T. G. Brevé, V. H. S. van Rixel, S. H. C. Askes, M. Siegler, S. Bonnet.; *Manuscript in preparation*
- 6. [Ru(phbpy)(N-N)(dmsO-κS)]⁺: A new photo-active chiral cyclometalated analogue of the Ru(tpy)(N-N)(dmsO-κS)²⁺ scaffold**
L. N. Lameijer, C. J. van de Griend, A. G. Volbeda, M. A. Siegler, S. Bonnet; *Manuscript in preparation*
- 7. The synthesis of O-1 to O-6 substituted positional isomers of D-glucose-thioether ligands and their ruthenium polypyridyl conjugates**
L. N. Lameijer, S. Bonnet.; *Manuscript in preparation*.